INVESTIGATION OF DONOR, ACCEPTOR AND SUBSTITUENT EFFECT ON PHTHALIMIDE AND THIENO[3,4-*c*]PYRROLE-4,6-DIONE BASED DONOR-ACCEPTOR-DONOR TYPE MONOMERS AND POLYMERS

A THESIS SUBMITTED TO
THE GRADUATE SCHOOL OF NATURAL AND APPLIED SCIENCES
OF
MIDDLE EAST TECHNICAL UNIVERSITY

BY

DENİZ ÇAKAL

IN PARTIAL FULFILLMENT OF THE REQUIREMENTS
FOR
THE DEGREE OF DOCTOR OF PHILOSOPHY
IN
CHEMISTRY

NOVEMBER 2021

Approval of the thesis:

INVESTIGATION OF DONOR, ACCEPTOR AND SUBSTITUENT EFFECT ON PHTHALIMIDE AND THIENO[3,4-*c*]PYRROLE-4,6-DIONE BASED DONOR-ACCEPTOR-DONOR TYPE MONOMERS AND POLYMERS

submitted by **DENİZ ÇAKAL** in partial fulfillment of the requirements for the degree of **Doctor of Philosophy** in **Chemistry, Middle East Technical University** by,

Prof. Dr. Halil Kalıpçılar
Dean, Graduate School of **Natural and Applied Sciences** _____

Prof. Dr. Özdemir Doğan
Head of the Department, **Chemistry** _____

Prof. Dr. Ahmet M. Önal
Supervisor, **Chemistry, METU** _____

Prof. Dr. Atilla Cihaner
Co-Supervisor, **Chemical Engineering, Atılım University** _____

Examining Committee Members:

Prof. Dr. Ali Çırpan
Chemistry, METU _____

Prof. Dr. Ahmet M. Önal
Chemistry, METU _____

Prof. Dr. Seha Tirkeş
Chemical Engineering, Atılım University _____

Assoc. Prof. Dr. Emrullah Görkem Günbaş
Chemistry, METU _____

Assoc. Prof. Dr. Merve İçli Özkut
Chemistry, Ankara University _____

Date: 26.11.2021

I hereby declare that all information in this document has been obtained and presented in accordance with academic rules and ethical conduct. I also declare that, as required by these rules and conduct, I have fully cited and referenced all material and results that are not original to this work.

Name Last name : Deniz Çakal

Signature :

ABSTRACT

INVESTIGATION ON DONOR, ACCEPTOR AND SUBSTITUENT EFFECT ON PHTHALIMIDE AND THIENO[3,4-*c*]PYRROLE-4,6-DIONE BASED DONOR-ACCEPTOR-DONOR TYPE MONOMERS AND POLYMERS

Çakal, Deniz
Doctor of Philosophy, Chemistry
Supervisor : Prof. Dr. Ahmet M. Önal
Co-Supervisor: Prof. Dr. Atilla Cihaner

November 2021, 290 pages

Conjugated organic materials comprise a major field of material chemistry focused on the improvement of new building blocks for the synthesis of novel semiconducting materials with advanced functional properties. Such semiconducting systems have the advantage of low cost, solution processability and flexibility and find many applications in the field of plastic photovoltaics, electrochromics and display technologies. The electronic and optical features of these semiconducting organic materials can be tailored via molecular engineering. One of the most effective strategy for engineering at molecular level is utilizing donor-acceptor approach. This approach uses electron rich and electron deficient units to provide highly conductive and low band gap materials. Thiophene and its alkylenedioxythiophene derivatives are popular electron rich building blocks to construct donor units for conjugated semiconducting materials. Phthalimide (PI) and thieno[3,4-*c*]pyrrole-4,6-dione (TPD) compounds comprise two different classes of acceptor units having electron-withdrawing carbonyl groups. The pairing

of thiophene based donors with PI and TPD acceptor units in donor-acceptor-donor configuration generates a series of conjugated monomers with a reduced energy gap to be investigated in this thesis from different perspectives.

The first part of the thesis is dedicated to the modification of the electron deficient PI acceptor unit with two different side groups including polyhedral oligomeric silsesquioxane (POSS) and propyl functions and then the coupling of these novel PI acceptors with thiophene and 3,4-ethylenedioxythiophene (EDOT) donor units to obtain donor-acceptor-donor type monomers and their corresponding polymers. The final effort is dedicated to the investigation of the monomers and polymer within the donor-acceptor-donor configuration to provide an improved understanding of substituent and donor effect on optical and electronic properties of these conjugated materials.

The second part of the thesis focused on the modification of TPD unit through functionalization with four different side groups involving ethylhexyl, POSS, azobenzene and fluoerene. Three of these side groups were appended into TPD acceptor unit for the first time. These functionalized TPD acceptor units were combined with thiophene, EDOT and highly soluble didecyl-substituted 3,4-propylenedioxythiophene (ProDOT) donor units to construct donor-acceptor-donor type conjugated organic frameworks. The investigation of these conjugated systems in donor-acceptor-donor configuration has provided a deep insight on evaluating the role of different types of functional side groups on the acceptor unit. Furthermore, optoelectronic features of these systems were investigated to elucidate the effect of aforementioned functional side groups as well as donor units. Lastly, these TPD-based donor-acceptor-donor architectures were compared with the previously synthesized PI-based analogs to unveil the effect of the acceptor group on optoelectronic properties.

In the third and last part of the thesis, the formation of a new core unit was achieved by modifying PI acceptor unit within donor-acceptor-donor configuration.

This modification is achieved by converting imide functional group of the acceptor moiety into diimide. The obtained novel system was further investigated to shed light on the structural effects of both diimide functional group and benzene ring structure on the acceptor units. The chemiluminescence characteristics of the newly synthesized system was also investigated as well as its optoelectronic properties. The optoelectronic data obtained for the trimeric system with the modified core unit was reported together with the unmodified ones for comparision sake and all the results were also supported by computational calculations.

In this dissertation, it was found that donor and acceptor units play key roles on the electrochemical and optical behaviors such as band gap, neutral state color, and electrochromic performance while the substituent does not significantly change optoelectronic properties of polymers. Also, the effect of donor units on the electrochemical and optical band gap values of polymers were investigated, it was found that each series follow the same trend depending on the strength of donor unit (i.e. $E_{g,Thiophene} > E_{g,ProDOT} > E_{g,EDOT}$). A similar trend was also detected for the oxidation potentials of the monomers. When the effect of acceptor units on the optoelectronic properties were investigated, it was found that more improved results were observed for TPD-based polymers as compared to PI-based polymer. This study also shows that the acceptor such as PI and TPD can be modified by any functional group to impart new functionalities without altering their optoelectronic properties.

Keywords: Donor-Acceptor-Donor Type Monomers, Phthalimide and Thieno[3,4-*c*]pyrrole-4,6-dione Acceptors, New Substituents on Acceptors (POSS, Azobenzene, Fluorene), Chemiluminescence

ÖZ

VERİCİ, ALICI VE SÜBSTİTÜENT GRUPLARIN FTALİMİD VE TİYENO[3,4-*c*]PİROL-4,6-DİON ESASLI VERİCİ-ALICI-VERİCİ DÜZENİNDEKİ MONOMERLER VE POLİMERLER ÜZERİNDEKİ ETKİSİNİN ARAŞTIRILMASI

Çakal, Deniz
Doktora, Kimya
Tez Yöneticisi: Prof. Dr. Ahmet M. Önal
Ortak Tez Yöneticisi: Prof. Dr. Atilla Cihaner

Kasım 2021, 290 sayfa

Konjuge organik malzemeler, malzeme biliminin üstün fonksiyonel özelliklere sahip yarı iletkenlerin sentezi için gerekli yeni yapı bloklarının geliştirilmesine odaklanmış önemli bir dalını oluşturmaktadır. Bu yarı iletken sistemler sahip oldukları düşük maliyet, esneklik, ve işlenebilirlik gibi önemli özellikleriyle fotovoltaik, elektrokromik ve ekran teknolojisi gibi pek çok alanda uygulamaya sahiptir. Organik yarı iletkenlerin elektronik ve optik özelliklerini moleküler mühendislik ile değiştirmek mümkündür. Moleküler düzeyde uygulanabilecek en önemli stratejilerden biri alıcı-verici düzeninde yapılar oluşturmaktır. Bu yaklaşımla elektronca zengin ve fakir gruplar kullanılarak iletkenliği yüksek olan düşün bant aralıklı malzemeler elde etmek mümkündür. Tiyofen ve alkilendioksitiyofen türevleri, konjuge yarı iletkenlerin elde edilmesinde en çok kullanılan verici grupları oluşturan elektronca zengin yapılardır. Ftalimid (PI) ve tiyeno[3,4-*c*]pirol-4,6-dion (TPD) bileşikleri elektron çeken karbonil gruplarına sahip önemli iki farklı alıcı grubu oluşturmaktadır. Tiyofen bazlı verici grupların, PI ve TPD alıcı birimleriyle verici-alıcı-verici düzeninde eşleştirilmesi ile elde

edilen düşük bant aralıklı bir dizi konjuge monomer bu tezde pek çok açıdan incelenecektir.

Tezin ilk bölümü, elektronca fakir ftalimid biriminin polihedral oligomerik silseskuokzan (POSS) ve propil sübstitüentleri ile fonksiyonlandırılmasına ve modifiye edilmiş alıcı birimlerin tiyofen ve 3,4-etilendioksitiyofen (EDOT) verici birimleri ile birleştirilmesi sonucu verici-alıcı-verici tipinde monomer ve polimerlerin elde edilmesine ayrılmıştır. Sonrasında sübstitüent ve verici grupların bu konjuge malzemelerin optik ve elektronik özellikleri üzerinde etkisinin daha iyi anlaşılması için elde edilen verici-alıcı-verici düzenindeki monomer ve polimerler incelenmiştir.

Tezin ikinci kısmı, TPD biriminin etilhekzil, POSS, azobenzen ve floren içeren dört farklı sübstitüentle modifikasyonuna odaklanmıştır. Bu sübstitüentlerden üçü ilk kez TPD alıcı birimine eklenmiştir. Bu işlevselleştirilmiş TPD alıcı birimleri, verici-alıcı-verici düzeninde konjuge organik monomerler oluşturmak için tiyofen, EDOT ve çözünür didesil zincirlerine sahip 3,4-propilendioksitiyofen (ProDOT) verici birimleri ile birleştirilmiştir. Verici-alıcı-verici konfigürasyonunda bu konjuge sistemlerin incelenmesi, farklı yapıdaki fonksiyonel sübstitüentlerin alıcı birim üzerindeki rolünün anlaşılması için büyük önem taşımaktadır. Ayrıca, bu sistemlerin optoelektronik özellikleri, yukarıda belirtilen fonksiyonel sübstitüentlerin yanı sıra verici birimlerin etkisini de aydınlatmak için araştırılmıştır. Son olarak, bu TPD bazlı verici-alıcı-verici düzenindeki yapılar, alıcı grubun optoelektronik özellikler üzerindeki etkisini görmek için PI bazlı benzerleri ile karşılaştırılmıştır.

Tezin üçüncü ve son bölümünde ise verici-alıcı-verici düzenindeki PI alıcı birim modifiye edilerek yeni bir çekirdek birimin oluşturulması sağlanmıştır. Bu modifikasyon, alıcı kısmın imid fonksiyonel grubunun diimide dönüştürülmesiyle sağlanmıştır. Elde edilen yeni sistem, hem diimid fonksiyonel grup hem de benzen halka yapısının, alıcı birim üzerindeki yapısal etkisine ışık tutmak için ayrıca

araştırılmıştır. Sentezlenen yeni sistemin optoelektronik özelliklerinin yanı sıra sahip olduğu kemilüminesans karakter de araştırılmıştır. Modifiye edilmiş çekirdek birimi içeren bu sistem için elde edilen optoelektronik özellikler, modifiye edilmemiş sistem için olanlarla birlikte karşılaştırmalı olarak rapor edilmiş ve tüm sonuçlar teorik hesaplamalarla da desteklenmiştir.

Bu tezde, verici ve alıcı birimlerin bant aralığı, nötr durum rengi ve elektrokromik performans gibi elektrokimyasal ve optik davranışlar üzerinde anahtar rol oynadığı, sübstitüentlerin ise polimerlerin optoelektronik özelliklerini önemli ölçüde değiştirmediği bulunmuştur. Ayrıca, verici birimlerin polimerlerin elektrokimyasal ve optik bant aralığı değerlerine etkisi araştırılmış, verici birimin gücüne bağlı olarak her serinin aynı eğilimi izlediği bulunmuştur ($E_{g,Thiophene} > E_{g,ProDOT} > E_{g,EDOT}$). Monomerlerin yükseltgenme potansiyelleri için de benzer bir eğilim tespit edilmiştir. Alıcı birimlerin optoelektronik özellikler üzerindeki etkisi araştırıldığında, TPD esaslı polimerler için PI esaslı polimere kıyasla daha iyi sonuçlar gözlemlenmiştir. Bu çalışma ayrıca, PI ve TPD gibi alıcılara, optoelektronik özelliklerini değiştirmeden yeni fonksiyonel gruplar takılarak yeni işlevsellikler kazandırılabileceği gösterilmiştir.

Anahtar Kelimeler: Alıcı-Verici-Alıcı Tipi Monomerler, Ftalimid ve Tiyeno[3,4-c]pirol-4,6-dion Verici Gruplar, Verici Grupta Yeni Sübstitüentler (POSS, Azobenzen, Floren), Kemilüminesans

To my parents

ACKNOWLEDGMENTS

I want to express my deepest gratitude to my supervisor Prof. Dr. Ahmet M. Önal who gave me a chance to be a member of his research group. He always supported me with a continuous patient and prentended me as if a member of his family. He was always gentle and understanding. I am so grateful to him for his guidance, advice, criticism throughout the research even after his retirement.

I would also like to express my heartfelt thanks to my co-supervisor Prof. Dr. Atilla Cihaner for his guidance, advice, and insight throughout the research He always encouraged me on my work when I felt disappointed. I could not succeed without his inspiring ideas. I am so lucky for being a member of his research group.

My special thanks are to Dr. Salih Ertan for spending time for me to solve my problems, acting with good intention and providing me a great friendship. His scientific support and motivation has a prominent role in my progress.

I would like to thank the members of Thesis Monitoring Committee Assoc. Prof. Dr. Görkem Günbaş and Prof. Dr. Seha Tirkeş for their valuable suggestions and comments throughout my research.

Also, I would like to thank my committee members Prof. Dr. Ali Çırpan and Assoc. Prof. Dr. Merve İçli Özkut for sparing their valuable time in my defense.

I would like to thank Dr. Güzide Aykent for her great friendship and good intention. She always motivated me during my PhD.

I would like to thank Burcu Balcı and Büşra Kesimal for their help in chemiluminecence measurements.

I wish to express my gratitude to my dear lab mates for their friendship and support.

I would like to thank the members of 602 and 102 for being sister to me. We are connected to each other with the special bonds.

I want to express my deepest gratitude to my parents for their sacrifice through my life and my education.

The technical assistance of METU Chemistry Department and Atılım University Chemical Engineering is gratefully acknowledged.

This work is partially funded by Scientific and Technological Research Council of Turkey (TÜBİTAK) under grant number 118Z067.

.

TABLE OF CONTENTS

ABSTRACT v

ÖZ..... viii

ACKNOWLEDGMENTS xii

TABLE OF CONTENTS xiv

LIST OF TABLES xviii

LIST OF FIGURES xix

LIST OF SCHEMES xxx

LIST OF ABBREVIATIONS xxxii

LIST OF SYMBOLS xxxv

1 INTRODUCTION 1

1.1 Introduction to Conductive Polymers 1

1.2 Conductivity Concept in Conjugated Polymers 3

1.2.1 Structure and Conjugation 3

1.2.2 Band Gap and Structural Factors 4

1.2.3 Conductivity Mechanism and Doping Process 9

1.2.4 Hopping Process 13

1.3 Synthesis of Conductive Polymers 13

1.3.1 Oxidative Chemical Polymerization 14

1.3.2 Transition Metal-Catalyzed Coupling Polymerizations 15

1.3.3 Electrochemical Polymerization 18

1.4 Characterization Techniques for Monomers and Conductive Polymers.. 20
1.4.1 Structural Characterization 20
1.4.2 Electrochemical Characterization 24
1.4.3 Optical Characterization 28
1.4.4 Spectroelectrochemical Characterization..... 31
1.5 Electrochromism 32
1.5.1 Band Gap 35
1.5.2 Optical Contrast 39
1.5.3 Switching Time..... 40
1.5.4 Coloration Efficiency..... 41
1.5.5 Stability..... 41
1.6 Chemiluminescence 42
1.6.1 Common Organic Chemiluminescent Compounds 45
1.7 Phthalimide Type Acceptor..... 47
1.7.1 Chemical Structure..... 47
1.7.2 Synthesis 49
1.8 Thieno[3,4-*c*]pyrrole-4,6-dione Type Acceptor..... 50
1.8.1 Chemical Structure..... 50
1.8.2 Synthesis 51
1.9 Phthalhyrazide Type Acceptor..... 52
1.9.1 Chemical Structure..... 52
1.9.2 Synthesis 53
1.10 Substituents 54
1.10.1 Polyhedral Oligomeric Silsesquioxanes 54

1.10.2 Azobenzene 55
1.10.3 Fluorene 57
1.11 The Aim of Study 58
2 EXPERIMENTAL 67
2.1 Materials 67
2.2 Instrumentation 68
2.3 Synthesis of Acceptor Units 69
2.3.1 Synthesis of Phthalimide Type Acceptors (PI) 69
2.3.2 Synthesis of Thieno[3,4-*c*]pyrrole-4,6-dione Type Acceptors (TPD) 70
2.4 Synthesis of Donor Units 72
2.4.1 Synthesis of 2-(Tributylstannyl)-3,4-ethylenedioxythiophene 72
2.4.2 Synthesis of Tributyl(3,3-didecyl-3,4-dihydro-2H-thieno [3,4-*b*] [1,4]dioxepin-6-yl)stannane 72
2.5 Synthesis of D- A- D Monomers 73
2.5.1 Synthesis of D- A- D Monomers Based on PI Type Acceptor Unit . 73
2.5.2 Synthesis of D- A- D Monomers Based on TPD Type Acceptor Units 75
2.5.3 Synthesis of D-A-D Monomers Based on Phthalhydrazide (PH) Type Acceptor Unit 79
3 RESULTS AND DISCUSSION 81
3.1 D-A-D Monomers Based on PI Type Acceptor Unit 81
3.1.1 Optical Properties of the Monomers 83
3.1.2 Electrochemical Properties of the Monomers 84

3.1.3 Electropolymerization and Spectroelectrochemical Properties of the PE(PI-POSS)E Film 87
3.2 D-A-D Monomers Based on TPD Acceptor Unit 93
3.2.1 D-A-D Monomers Based on TPD-EtHex Acceptor Unit 93
3.2.2 D-A-D Monomers Based on TPD-POSS Acceptor Unit 114
3.2.3 D-A-D Monomers Based on TPD-Azo Acceptor Unit 145
3.2.4 D-A-D Monomers Based on TPD-Fluo Acceptor Unit 172
3.3 D-A-D Monomers Based on PH Type Acceptor Unit 191
3.3.1 Optical Properties of the Monomer 191
3.3.2 Electrochemical Properties of the Monomer 192
3.3.3 Chemiluminescence Properties of the Monomer 195
4 CONCLUSION 203
REFERENCES 209
A. NMR Spectra of Monomers and Polymers 221
B. HRMS Data of Monomers 269
C. GPC Data of Polymers 281
D. TGA Data of Polymers 283
E. FTIR Spectra of Monomer and Polymer 285
CURRICULUM VITAE 287

LIST OF TABLES

TABLES

Table 3.1 Optical and electrochemical properties of the monomers 86
Table 3.2 Optoelectronic properties of PE(PI-POSS)E polymer film 92
Table 3.3 Optical and electrochemical properties of T(TPD-EtHex)T, E(TPD-EtHex)E and P(TPD-EtHex)P monomers 97
Table 3.4 Electrochemical properties of the polymers 101
Table 3.5 Optoelectronic properties of the polymer films on ITO in 0.1 M $TBAPF_6$/MeCN 107
Table 3.6 Optical and electrochemical properties of T(TPD-POSS)T, E(TPD-POSS)E and P(TPD-POSS)P monomers 120
Table 3.7 Electrochemical properties of the polymer films 125
Table 3.8 Optoelectronic properties of the polymer films on ITO in 0.1 M $TBAPF_6$/MeCN 132
Table 3.9 Optoelectronic properties of the polymer films on ITO in 0.1 M $TBAPF_6$/MeCN 139
Table 3.10 Optical and electrochemical properties of T(TPD-Azo)T, E(TPD-Azo)E and P(TPD-Azo)P monomers 152
Table 3.11 Electrochemical properties of the polymer films 158
Table 3.12 Optoelectronic properties of the polymer films on ITO in 0.1 M $TBAPF_6$/MeCN 168
Table 3.13 Optical and electrochemical properties of the monomers 177
Table 3.14 Electrochemical properties of the polymer films 181
Table 3.15 Optoelectronic properties of the polymer films on ITO in 0.1 M $TBAPF_6$/MeCN 189
Table 3.16 Optical and electrochemical properties of the monomers 195

LIST OF FIGURES

FIGURES

Figure 1.1. Some common conjugated polymers. 2
Figure 1.2. Schematic representation of both the structure and orbitals in (a) polyethylene and (b) PA. 4
Figure 1.3. Valence band (VB) and conduction band (CB) in conductor, semiconductor and insulator. 5
Figure 1.4. The schematic representation of donor-acceptor approach[32]. 8
Figure 1.5. A schematic representation of the formation of (a) polyene, (b) polaron, and (c) bipolaron, (d) soliton pair on a trans-polyacetylene chain by doping. 11
Figure 1.6. Schematic representation of hopping process. 13
Figure 1.7. (a) Schematic representation of electrochemcial cell used for electrochemical studies of monomers and polymers (b) a typical cyclic voltammogram. 27
Figure 1.8. (a) Anodically or (b) cathodically colored (c) two different colored and (d) multicolored polymers[80]. 33
Figure 1.9. Color wheel showing the appropriate relationship between polymer color and the color or wavelength of light absorbed [81,82] 34
Figure 1.10. Calculation of the electronic band gap from CV measurement..... 36
Figure 1.11. Calculation of the electronic band gap from DPV measurement. 37
Figure 1.12. Calculation of the optical band gap from spectroelectrochemical measurement. 38
Figure 1.13. A typical chronoabsorptometry and chronocoulometry experiments for the polymer film at 505 nm in 0.1 M $TBAPF_6$ /MeCN. 40
Figure 1.14. The common organic chemiluminescent compounds[90]. 44
Figure 1.15. Some luminol derivatives. 47
Figure 1.16. Chemical structure of TPD core unit. 51
Figure 1.17. Chemical structure of PH. 52
Figure 1.18. Three possible tautomeric structures for PH. 53

Figure 1.19. The chemical structure of POSS. 55
Figure 1.20. Chemical structure and atomic numbering of fluorene. 57
Figure 1.21. D-A-D monomers based on PI-POSS and PI-Propyl acceptor units. . 59
Figure 1.22. D-A-D monomers based on TPD-EtHex acceptor unit. 61
Figure 1.23. D-A-D monomers based on TPD-POSS acceptor unit. 62
Figure 1.24. D-A-D monomers based on TPD-Azo acceptor unit. 63
Figure 1.25. D-A-D monomers based on TPD-Fluo acceptor unit. 64
Figure 1.26. D-A-D monomer based on PH acceptor unit. 65
Figure 3.1. The structures of core units as acceptor. 81
Figure 3.2. Normalized (a) absorption and (b) emission spectra of monomers in DCM. Inset: The colors of the monomers (a) in daylight and (b) under UV lamp at 365 nm. 84
Figure 3.3. Cyclic voltammograms for (a) oxidation and (b) reduction of T(PI-POSS)T, T(PI-Propyl)T, E(PI-POSS)E and E(PI-Propyl)E on Pt electrode in 0.1 M $TBAPF_6$ dissolved in DCM at a scan rate of 100 mV/s vs. Ag/AgCl. 85
Figure 3.4. (a) Repetitive cyclic voltammograms of E(PI-POSS)E monomer on Pt disc electrode (b) cyclic voltammogram of PE(PI-POSS)E film coated on Pt disc electrode recorded in 0.1 M $TBAPF_6$ dissolved in DCM at a scan rate of 100 mv/s vs. Ag/AgCl. 88
Figure 3.5. (a) Scan rate dependence of PE(PI-POSS)E polymer film on Pt disc electrode recorded in 0.1 M $TBAPF_6$ solution in DCM at different scan rates from 20 mVs^{-1} to 200 mVs^{-1} with 20 mVs^{-1} increments and (b) relationship of anodic and cathodic current peaks as a function of scan rate for PE(PI-POSS)E polymer film. 89
Figure 3.6. Neutral state electronic absorption spectra of E(PI-POSS)E monomer in DCM and PE(PI-POSS)E polymer film coated on ITO. 90
Figure 3.7. The changes in the electronic absorption spectra of electrochemically coated PE(PI-POSS)E film on ITO recorded in 0.1 M $TBAPF_6$ dissolved in DCM as a function of applied potentials between -1.0 V to +1.3 V. Inset: The colors of the polymer film on ITO in neutral and oxidized states. 91

Figure 3.8. Chronoabsoptometry experiments for PE(PI-POSS)E film on ITO in 0.1 M $TBAPF_6$ dissolved in DCM when the polymer is switched for 10 s intervals between its redox states from -1.0 V to +1.3 V at 550 nm. 92
Figure 3.9. (a) Absorption and (b) emission spectra of monomers in DCM. Inset: the color of the monomers (a) in daylight and (b) under UV lamp at 365 nm. 96
Figure 3.10. Full scan cyclic voltammograms of the monomers on Pt disc electrode vs. Ag/AgCl in 0.1 M $TBAPF_6$ dissolved in MeCN/DCM ((10/1: v/v) for T(TPD-EtHex)T, (15/1: v/v) for E(TPD-EtHex)E and (5/3: v/v) for P(TPD-EtHex)P) at a scan rate of 100 mV/s. 97
Figure 3.11. The structure of polymers. 99
Figure 3.12. Repetitive cyclic voltammograms of (a) T(TPD-EtHex)T, (c) E(TPD-EtHex)E and (e) P(TPD-EtHex)P monomer recorded in 0.1 M $TBAPF_6$ dissolved in MeCN/DCM ((10/1: v/v) for T(TPD-EtHex)T, (15/1: v/v) for E(TPD-EtHex)E and (5/3: v/v) for P(TPD-EtHex)P) and cycling voltammograms of their corresponding polymer films (b) PT(TPD-EtHex)T, (d) PE(TPD-EtHex)E and (f) PP(TPD-EtHex)P polymer films recorded in 0.1 M $TBAPF_6$/MeCN on Pt disc electrode vs. Ag/AgCl at a scan rate of 100 mVs^{-1}. 100
Figure 3.13. Scan rate dependence of polymer films on Pt disc electrode recorded in 0.1 M $TBAPF_6$ solution (a) PT(TPD-EtHex)T, (c) PE(TPD-EtHex)E and (e) PP(TPD-EtHex)P in MeCN at different scan rates from 25 mVs^{-1} to 200 mVs^{-1} with 25 mVs^{-1} increments. The relationship of anodic and cathodic peak currents as a function of scan rate for (b) PT(TPD-EtHex)T, (d) PE(TPD-EtHex)E and (f) PP(TPD-EtHex)P polymer films. 102
Figure 3.14. Neutral state electronic absorption spectra of PT(TPD-EtHex)T, PE(TPD-EtHex)E and PP(TPD-EtHex)P films coated on ITO electrode in 0.1 M $TBAPF_6$/MeCN. 104
Figure 3.15. The changes in electronic absorption spectra of electrochemically deposited (a) PT(TPD-EtHex)T, (b) PE(TPD-EtHex)E and (c) PP(TPD-EtHex)P films on ITO recorded at various applied potentials in 0.1 M $TBAPF_6$/MeCN.

Insets: CVs of the films recorded with a scan rate of 20 mVs^{-1}. Inset: The colors of the films at neutral and oxidized states.....106
Figure 3.16. Chronoabsoptometry experiments for the polymer films on ITO in 0.1 M $TBAPF_6$/MeCN when the films were switched between redox states with an interval time of 10 s for (a) PT(TPD-EtHex)T (between -0.2 V and +1.3 V at 500 nm), (b) PE(TPD-EtHex)E (between -0.5 V and +1.5 V at 625 nm) and (c) PP(TPD-EtHex)P (between 0.0 V and +1.4 V at 600 nm and 660 nm). 109
Figure 3.17. Optical stability tests for polymer films on ITO when the films switched between redox states (-0.5 V and +1.2 V) with an interval of 3 s at 625 nm for PE(TPD-EtHex)E and at 600 nm for PP(TPD-EtHex)P.....109
Figure 3.18. (a) Electronic absorption spectra of PP(TPD-EtHex)P film on ITO and both chemically and electrochemically obtained PP(TPD-EtHex)P polymers in DCM (b) Electronic absorption and emission spectra of chemically obtained PP(TPD-EtHex)P-C polymer in DCM. 111
Figure 3.19. Changes in the absorption spectra of PP(TPD-EtHex)P-C dissolved in toluene during chemical oxidation by using 0.05 M $SbCl_5$ oxidant with 10 µL stepwise additions. Inset: absorption spectrum after chemical reduction by using hydrazine. Inset: Colors of polymer solution at neutral and oxidized states.....112
Figure 3.20. (a) The changes in electronic absorption spectra of spray coated PP(TPD-EtHex)P-C film on ITO recorded at various applied potentials between 0.0 V and +1.4 V in 0.1 M $TBAPF_6$/MeCN. Inset: The colors of the films at neutral and oxidized states. (b) Chronoabsoptometry experiments for PP(TPD-EtHex)P-C film when switched for 10 s intervals between 0.0 and +1.6 V at 600 and 655 nm). 113
Figure 3.21. (a) Absorption and (b) emission spectra of monomers in DCM. Inset: the color of the monomers (a) in daylight and (b) under UV lamp at 365 nm.....117
Figure 3.22. (a) Cyclic and (b) differential pulse voltammograms for full scan of T(TPD-POSS)T, E(TPD-POSS)E and P(TPD-POSS)P monomers on Pt electrode in 0.1 M $TBAPF_6$ dissolved in DCM at a scan rate of 100 mVs^{-1} vs. Ag/AgCl. ..119
Figure 3.23. The chemical structure of polymer films. 121

Figure 3.24. Repetitive cyclic voltammograms of (a) T(TPD-POSS)T, (c) E(TPD-POSS)E and (e) P(TPD-POSS)P monomer recorded in 0.1 M $TBAPF_6$ dissolved in MeCN/DCM ((1/1: v/v) and cycling voltammograms of their corresponding polymer films (b) PT(TPD-POSS)T, (d) PE(TPD-POSS)E and (f) PP(TPD-POSS)P polymer films recorded in 0.1 M $TBAPF_6$ dissolved in MeCN/DCM ((1:1, v:v) for PT(TPD-POSS)T), (2:1, v:v) for PE(TPD-POSS)E and PP(TPD-POSS)P) on Pt disc electrode vs. Ag/AgCl at a scan rate of 100 mVs^{-1}. 122
Figure 3.25. Scan rate dependence of polymer films on Pt disc electrode recorded in 0.1 M $TBAPF_6$ solution (a) PT(TPD-POSS)T in MeCN:DCM (1:1, v:v), (c) PE(TPD-POSS)E and (e) PP(TPD-POSS)P in MeCN:DCM (2:1, v:v) at different scan rates from 25 mVs^{-1} to 200 mVs^{-1} with 25 mVs^{-1} increments. The relationship of anodic and cathodic peak currents as a function of scan rate for (b) PT(TPD-POSS)T, (d) PE(TPD-POSS)E and (f) PP(TPD-POSS)P polymer films. 124
Figure 3.26. DPVs of polymer films recorded in 0.1 M $TBAPF_6$ dissolved in MeCN/DCM ((1:1, v:v) for PT(TPD-POSS)T), (2:1, v:v) for PE(TPD-POSS)E and PP(TPD-POSS)P) on Pt disc electrode vs. Ag/AgCl. 126
Figure 3.27. Neutral state absorption spectra of PT(TPD-POSS)T, PE(TPD-POSS)E and PP(TPD-POSS)P films coated on ITO electrode in 0.1 M $TBAPF_6$/MeCN. 127
Figure 3.28. The changes in electronic absorption spectra of electrochemically deposited (a) PT(TPD-POSS)T, (b) PE(TPD-POSS)E and (c) PP(TPD-POSS)P films on ITO recorded at various applied potentials in 0.1 M $TBAPF_6$/MeCN. Insets: CVs of the films recorded with a scan rate of 20 mVs^{-1}. Inset: The colors of the films at neutral and oxidized states. 130
Figure 3.29. Chronoabsoptometry experiments for the polymer films on ITO in 0.1 M $TBAPF_6$/MeCN when the films were switched between redox states with an interval time of 10 s for (a) PT(TPD-POSS)T (between 0.0 V and +1.3 V at 525 nm), (b) PE(TPD-POSS)E (between 0.0 V and +1.0 V at 545 nm and 600 nm) and (c) PP(TPD-POSS)P (between 0.0 V and +1.2 V at 585 nm and 640 nm)..... 132

Figure 3.30. Neutral state absorption spectra of chemically obtained PE(TPD-POSS)E-C and PP(TPD-POSS)P-C polymers dissolved in DCM. 134
Figure 3.31. Electronic absorption and emission spectra of chemically obtained PP(TPD-POSS)P-C polymer in DCM. 135
Figure 3.32. Changes in the absorption spectra of (a) PE(TPD-POSS)E-C and (b) PP(TPD-POSS)P-C dissolved in toluene during chemical oxidation by using 0.05 M $SbCl_5$ oxidant with 10 µL stepwise additions. Inset: absorption spectrum after chemical reduction by using hydrazine. Inset: Colors of polymer solution at neutral and oxidized states. 136
Figure 3.33. Neutral state electronic absorption spectra of spray coated PE(TPD-POSS)E-C and PP(TPD-POSS)P-C films on ITO electrode in 0.1 M $TBAPF_6$/MeCN. 137
Figure 3.34. The changes in electronic absorption spectra of spray coated (a) PE(TPD-POSS)E-C and (c) PP(TPD-POSS)P-C film on ITO recorded at various applied potentials in 0.1 M $TBAPF_6$/MeCN. Insets: CVs of the films recorded with a scan rate of 20 mVs^{-1}. Insets: The colors of the films at neutral and oxidized states. (b) Chronoabsoptometry experiments for polymer films when switched with an inteerval of 10 s for (b) PE(TPD-POSS)E-C (between -0.2 V and +1.2 V at 632 nm) and (d) PP(TPD-POSS)P-C (between 0.0 V and +1.3 V at 585 nm and 640 nm). 138
Figure 3.35. TGA thermograms of chemically obtained polymers. 140
Figure 3.36. (a) The Stern-Volmer plots of P(TPD-POSS)P ($1x10^{-4}$ M) in the presence of various metal ions (0.02 mM - 0.14 mM). Metal ions $FeCl_2.4H_2O$, $Fe(NO_3)_3.9H_2O$, $Cu(NO_3)_2.3H_2O$, $LiClO_4$, $Ni(NO_3)_2.9H_2O$, $Zn(NO_3)_2.4H_2O$, $Hg(NO_3)_2$, $Pb(NO_3)_2$, $Cd(NO_3)_2.4H_2O$ in DMF. Insets: The fluorescence emission spectra of P(TPD-POSS)P in DMF with successive addition of 0.02 mM - 0.14 Mm (a) Fe^{2+} and (b) Fe^{3+} when excited at 340 nm. (b) K_{sv} values of P(TPD-POSS)P in the presence of Fe^{2+}, Fe^{3+}, Cu^{2+}, Li^{+}, Ni^{2+}, Zn^{2+}, Hg^{2+}, Pb^{2+} and Cd^{2+}. 142
Figure 3.37. (a) The Stern-Volmer plots of PP(TPD-POSS)P-C (1 mg in 10 mL THF) in the presence of Fe^{2+} and Fe^{3+} metal ions (0.02 mM - 0.14 mM). Insets: The

fluorescence emission spectra of PP(TPD-POSS)P-C in THF with successive addition of 0.02 mM - 0.14 Mm (a) Fe^{2+} and (b) Fe^{3+} when excited at 510 nm. (b) K_{sv} values of P(TPD-POSS)P in DMF and PP(TPD-POSS)P-C in THF in the presence of Fe^{2+} and Fe^{3+}. 144
Figure 3.38. (a) Absorption and (b) emission spectra of the monomers in DCM. Inset: the color of the monomers (a) in daylight and (b) under UV lamp at 365 nm. 148
Figure 3.39. Normalized UV-Vis absorption spectra of P(TPD-Azo)P in different solvents. 149
Figure 3.40. (a) Full scan cyclic voltammograms of the monomers on Pt electrode vs. Ag/AgCl in 0.1 M $TBAPF_6$ dissolved in DCM at a scan rate of 100 mVs^{-1} and (b) differential pulse voltammograms of the monomers on Pt electrode vs. Ag/AgCl in 0.1 M $TBAPF_6$ dissolved in DCM. 151
Figure 3.41. The structures of polymers. 154
Figure 3.42. Repetitive cyclic voltammograms of the monomers recorded in 0.1 M $TBAPF_6$ solution (a) T(TPD-Azo)T, (c) E(TPD-Azo)E in DCM and (e) P(TPD-Azo)P in MeCN/DCM ((1/1: v/v) and the corresponding cycling voltammograms of polymer films recorded in 0.1 M $TBAPF_6$ solution (b) PT(TPD-Azo)T, (d) PE(TPD-Azo)E in DCM and (f) PP(TPD-Azo)P in MeCN on Pt disc electrode vs. Ag/AgCl at a scan rate of 100 mVs^{-1}. 155
Figure 3.43. DPVs of the polymer films on Pt disc electrode vs. Ag/AgCl recorded in 0.1 M $TBAPF_6$ dissolved in DCM for PT(TPD-Azo)T and PE(TPD-Azo)E, in MeCN for PP(TPD-Azo)P. 156
Figure 3.44. Scan rate dependence of the polymer films on Pt disc electrode recorded in 0.1 M $TBAPF_6$ solution (a) PT(TPD-Azo)T and (c) PE(TPD-Azo)E in DCM and (e) PP(TPD-Azo)P in MeCN at different scan rates from 25 mVs^{-1} to 200 mVs^{-1} with 25 mVs^{-1} increments. The relationship of anodic and cathodic peak currents as a function of scan rate for (b) PT(TPD-Azo)T, (d) PE(TPD-Azo)E and (f) PP(TPD-Azo)P polymer films. 157

Figure 3.45. Neutral state absorption spectra of PT(TPD-Azo)T, PE(TPD-Azo)E and PP(TPD-Azo)P films coated on ITO electrode in 0.1 M $TBAPF_6$/MeCN. 159
Figure 3.46. The changes in electronic absorption spectra of electrochemically deposited (a) PT(TPD-Azo)T, (b) PE(TPD-Azo)E and (c) PP(TPD-Azo)P films on ITO recorded at various applied potentials in 0.1 M $TBAPF_6$/MeCN. Insets: CVs of the films recorded with a scan rate of 20 mVs^{-1}. Inset: The colors of the films at neutral and oxidized states.....162
Figure 3.47. The changes in electronic absorption spectra of electrochemically deposited (a) PT(TPD-Azo)T, (b) PE(TPD-Azo)E and (c) PP(TPD-Azo)P films on ITO recorded at various applied potentials during n-doping in 0.1 M $TBAPF_6$/MeCN. Insets: CVs of the films recorded with a scan rate of 20 mVs^{-1}. Inset: The colors of the films at neutral and reduced states. 163
Figure 3.48. The changes in the absorption spectra of PP(TPD-Azo)P polymer dissolved in toluene during chemical oxidation by using 0.05 M $SbCl_5$ oxidant with 3 μL stepwise additions. Inset: Colors of the polymer solution at neutral and oxidized states. 164
Figure 3.49. Electronic absorption and emission spectra of electrochemically obtained PP(TPD-Azo)P polymer in toluene. 165
Figure 3.50. Chronoabsoptometry experiments for the polymer films on ITO in 0.1 M $TBAPF_6$/MeCN when the films were switched between redox states with an interval time of 10 s for (a) PT(TPD-Azo)T (between 0.0 V and +1.6 V at 525 nm), (b) PE(TPD-Azo)E (between -0.5 V and +1.3 V at 545 nm and 600 nm) and (c) PP(TPD-Azo)P (between 0.0 V and +1.3 V at 585 nm and 640 nm).....168
Figure 3.51. Electrochemical and optical stability tests for the polymer films on ITO in 0.1 M $TBAPF_6$/MeCN when the films switched between redox states (-0.5 V and +1.1 V) at 630 nm for (a) PE(TPD-Azo)E and (0.0 V and +1.1 V) at 610 nm for (b) PP(TPD-Azo)P with an interval of 1 s.....170
Figure 3.52. UV-Vis absorption spectra of (a) T(TPD-Azo)T, (b) E(TPD-Azo)E, (c) P(TPD-Azo)P and (d) PP(TPD-Azo)P before and after irradiation with Mercury UV light in toluene. 172

Figure 3.53. (a) Absorption and (b) emission spectra of the monomers in DCM. Inset: the colors of the monomers (a) in daylight and (b) under UV lamp at 365 nm. 174
Figure 3.54. (a) Full scan cyclic voltammograms of the monomers on Pt electrode vs. Ag/AgCl in 0.1 M $TBAPF_6$ dissolved in DCM at a scan rate of 100 mVs^{-1} and (b) differential pulse voltammograms of the monomers on Pt electrode vs. Ag/AgCl in 0.1 M $TBAPF_6$ dissolved in DCM. 176
Figure 3.55. The structures of the polymer films..... 178
Figure 3.56. Repetitive cyclic voltammograms of (a) E(TPD-Fluo)E and (c) P(TPD-Fluo)P monomer recorded in 0.1 M $TBAPF_6$ in DCM for E(TPD-Fluo)E, in MeCN/DCM ((1/3: v/v) for P(TPD-Fluo)P and the cycling voltammograms of their corresponding polymer films (b) PE(TPD-Fluo)E and (d) PP(TPD-Fluo)P polymer films recorded in 0.1 M $TBAPF_6$ in DCM for PE(TPD-Fluo)E, in MeCN for PP(TPD-Fluo)P) on Pt disc electrode vs. Ag/AgCl at a scan rate of 100 mVs^{-1}. . 179
Figure 3.57. DPVs of polymer films recorded in 0.1 M $TBAPF_6$ in DCM for PE(TPD-Fluo)E, in MeCN for PP(TPD-Fluo)P on Pt disc electrode vs. Ag/AgCl. 180
Figure 3.58. Scan rate dependence of the polymer films on Pt disc electrode recorded in 0.1 M $TBAPF_6$ solution (a) PE(TPD-Fluo)E in DCM and (c) PP(TPD-Fluo)P in MeCN at different scan rates from 25 mVs^{-1} to 200 mVs^{-1} with 25 mVs^{-1} increments. The relationship of anodic and cathodic current peaks as a function of scan rate for (b) PE(TPD-Fluo)E and (d) PP(TPD-Fluo)P polymer films..... 182
Figure 3.59. Neutral state absorption spectra of PE(TPD-Fluo)E and PP(TPD-Fluo)P films coated on ITO electrode in 0.1 M $TBAPF_6$/MeCN. 183
Figure 3.60. The changes in electronic absorption spectra of electrochemically deposited (a) PE(TPD-Fluo)E and (c) PP(TPD-Fluo)P films on ITO recorded at various applied potentials in 0.1 M $TBAPF_6$/MeCN. Insets: CVs of the films recorded with a scan rate of 20 mVs^{-1}. Inset: The colors of the films at neutral and oxidized states. 185

Figure 3.61. The changes in electronic absorption spectra of electrochemically deposited (a) PE(TPD-Fluo)E and (c) PP(TPD-Fluo)P films on ITO recorded at various applied potentials during n-doping in 0.1 M $TBAPF_6$/MeCN. Insets: CVs of the films recorded with a scan rate of 20 mVs^{-1}. Inset: The colors of the films at neutral and reduced states. 187
Figure 3.62. Chronoabsoptometry experiments for the polymer films on ITO in 0.1 M $TBAPF_6$/MeCN when the films were switched between redox states with an interval time of 10 s for (a) PE(TPD-Fluo)E (between -0.5 V and +1.2 V at 644 nm) and (b) PP(TPD-Fluo)P (between 0.0 V and +1.2 V at 609 nm and 668 nm). 188
Figure 3.63. Electrochemical and optical stability tests for the polymer films on ITO in 0.1 M $TBAPF_6$/MeCN when the films switched between redox states (-0.5 V and +1.1 V) at 630 nm for (a) PE(TPD-Fluo)E and (0.0 V and +1.1 V) at 605 nm for (b) PP(TPD-Fluo)P with an interval of 1 s. 190
Figure 3.64. (a) Absorption and (b) emission spectra of the monomer in DCM. Inset: The color of the monomer (a) in daylight and (b) under UV lamp at 365 nm. 192
Figure 3.65. Cyclic voltammogram of E(PH)E on Pt electrode vs. Ag/AgCl in 0.1 M $TBAPF_6$ dissolved in MeCN containing 5% BF_3-Et_2O by volume at a scan rate of 100 mVs^{-1} and (b) square wave voltammogram of E(PH)E on Pt electrode vs. Ag/AgCl in 0.1 M $TBAPF_6$ dissolved in MeCN containing 5% BF_3-Et_2O by volume. 194
Figure 3.66. Chemiluminescence intensities of $1.0x10^{-6}$ M (a) E(PH)E and (b) luminol in 0.1 M $NaOH_{(aq)}$ with $1x10^{-3}$ M of various oxidants. 196
Figure 3.67. Chemiluminescence intensities of $1.0x10^{-6}$ M luminol in 0.1 M $NaOH_{(aq)}$ with different H_2O_2 concentrations. 198
Figure 3.68. Chemiluminescence intensity of $1.0x10^{-6}$ M (a) E(PH)E and (b) luminol in 0.1 M $NaOH_{(aq)}$ with $1.0x10^{-3}$ M H_2O_2 (i) in the absence and (ii) in the presence of $1.0x10^{-3}$ M Fe^{3+} ion. 198

Figure 3.69. Chemiluminescence intensity of $1.0x10^{-6}$ M of (a) E(PH)E and (b) luminol in 0.1 M $NaOH_{(aq)}$ with $1.0x10^{-3}$ M H_2O_2 in the presence of $1.0x10^{-3}$ M of different metal ions. 199
Figure 3.70. Chemiluminescence intensity of $1.0x10^{-6}$ M of E(PH)E in 0.1 M $NaOH_{(aq)}$ with $1.0x10^{-3}$ M H_2O_2 in the presence of different concentrations of (a) Fe^{3+} and (b).Cu^{2+} ions. 200
Figure 3.71. Chemiluminescence intensity of $1.0x10^{-6}$ M of (a) E(PH)E and (b) luminol in 0.1 M $NaOH_{(aq)}$ with $1.0x10^{-3}$ M H_2O_2 in the presence of different hemin concentrations. 201
Figure 3.72. Chemiluminescence intensity of $1.0x10^{-6}$ M of (a) E(PH)E and (b) luminol in 0.1 M $NaOH_{(aq)}$ with $1.0x10^{-3}$ M H_2O_2 in the presence of blood samples diluted with water in different proportions. 201

LIST OF SCHEMES

SCHEMES

Scheme 1.1. The oxidative chemical polymerization of a five membered heterocyclic compound via $FeCl_3$. 14
Scheme 1.2. The general mechanism for transition metal catalyzed polycondensation reactions. 16
Scheme 1.3. The general mechanism for Stille cross coupling reaction. 17
Scheme 1.4. The general mechanism for Suzuki cross coupling reaction. 18
Scheme 1.5. The mechanism for the electrochemical polymerization of EDOT. 19
Scheme 1.6. CL reaction mechanism of luminol to produce light[99]. 46
Scheme 1.7. The PI and its resonance forms after loss of a proton[110] 48
Scheme 1.8. Reaction mechanism for the imide formation reaction. 49
Scheme 1.9. Synthesis of TPD unit from 3,4-thiophenedicarboxylic acid in three steps. 51
Scheme 1.10. Synthesis of TPD unit from 3,4-dibromothiophene in three steps. 52
Scheme 1.11. Synthesis of phthalhydrazide from PI derivative. 54
Scheme 1.12. Synthesis of phthalhydrazide from phthalic acid derivative. 54
Scheme 1.13. Trans-cis isomerization of azobenzene. 56
Scheme 3.1. Synthetic route for the synthesis of monomers, T(PI-POSS)T, T(PI-Propyl)T, E(PI-POSS)E and E(PI-Propyl)E. 82
Scheme 3.2. Electropolymerization of E(PI-POSS)E to afford PE(PI-POSS)E. 88
Scheme 3.3. Synthetic route for synthesis of T(TPD-EtHex)T, E(TPD-EtHex)E and P(TPD-EtHex)P monomers. 94
Scheme 3.4. Synthetic route for the synthesis of T(TPD-POSS)T, E(TPD-POSS)E and P(TPD-POSS)P. 115
Scheme 3.5. Synthetic route for the synthesis of T(TPD-Azo)T, E(TPD-Azo)E and P(TPD-Azo)P. 146
Scheme 3.6. Synthesis route for the monomers. 173
Scheme 3.7. Synthetic route for the synthesis of E(PH)E. 191

Scheme 3.8. The suggested mechanism for E(PH)E. 197

LIST OF ABBREVIATIONS

ABBREVIATIONS

A	Absorbance
A-D-A	Acceptor-Donor-Acceptor
BLA	Bond Length Alternation
$BF_3.Et_2O$	Borontrifluoride diethyletherate
$CDCl_3$	Deuterated chloroform
CE	Coloration Efficiency
CIE	Commission Internationale de l'Eclairage
CV	Cyclic Voltammetry
CVs	Cyclic Voltammograms
D-A	Donor-Acceptor
D-A-D	Donor-Acceptor-Donor
D-A-A	Donor-Acceptor-Acceptor
DCM	Dichloromethane
DMF	Dimethylformamide
DMSO	Dimethyl Sulfoxide
DPV	Differential Pulse Voltammetry
DPVs	Differential Pulse Voltammograms
EDOT	3,4-Ethylenedioxythiophene
EtOAc	Ethyl acetate

$FeCl_3$	Ferric chloride
FTIR	Fourier Transform Infrared
GPC	Gel Permeation Chromatography
HOMO	Highest Occupied Molecular Orbital
HRMS	High Resolution Mass Spectrometry
ICT	Intramolecular Charge Transfer
ITO	Indium Tin Oxide
LUMO	Lowest Unoccupied Molecular Orbital
MeCN	Acetonitrile
NMR	Nuclear Magnetic Resonance
PA	Polyacetylene
PANI	Polyaniline
PEDOT	Poly(3,4-ethylenedioxythiophene)
PF	Polyfuran
PFL	Polyfluorene
PH	Phthalhydrazide
PI	Phthalimide
POSS	Polyhedral oligomeric silsesquioxane
PP	Polypyrrole
PPP	Poly(p-phenylene)
PPV	Poly(*p*-phenylenevinylene)
ProDOT	3,4-Propylenedioxythiophene

PT	Polythiophene
Pt	Platinum
SWV	Square wave voltammetry
QY	Quantum Yield
T	Transmittance
$TBAPF_6$	Tetrabutylammonium hexafluorophosphate
TGA	Thermogravimetric Analysis
THF	Tetrahydrofuran
TMS	Tetramethylsilane
TLC	Thin layer chromatography
TPD	Thieno[3,4-*c*]pyrrole-4,6-dione
UV-Vis	Ultraviolet-visible

LIST OF SYMBOLS

SYMBOLS

℃	Celcius
Å	Angstrom
δ	Chemical shift
J	Coupling constant
E_g	Band gap
$E_g^{electro}$	Electrochemical band gap
E_g^{opt}	Optical band gap
Δ%T	Percent transmittance change
%T	Percent transmittance
ΔOD	Optical density change
ε	Dielectric constant
$E_{ox,m}$	Oxidation potential of monomer
$E_{ox,p}$	Oxidation potential of polymer
$E_{ox,onset,m}$	Oxidation onset potential of monomer
$E_{ox,onset,p}$	Oxidation onset potential of polymer
$E_{red,m}$	Reduction potential of monomer
$E_{red,p}$	Reduction potential of polymer
$E_{red,onset,m}$	Reduction onset potential for monomer
$E_{red,onset,p}$	Reduction onset potential for polymer

K_{sv}	Stern-Volmer constant
Q_d	Charge density
pH	Power of hydrogen
$t_{s,ox}$	Switching time for oxidation
$t_{s,red}$	Switching time for reduction
λ_{max}	Maximum wavelength
$\lambda_{max,abs}$	Absorption maximum
$\lambda_{max,em}$	Emission maximum

CHAPTER 1

INTRODUCTION

1.1 Introduction to Conductive Polymers

Polymers are synthetic or natural materials that are composed of the same kind of repeating subunits and this concept was first introduced by Staudinger in the year 1920. After his breakthrough finding, a new field has emerged as polymer science. This vital branch of science deals with the synthesis of new materials in a wide range from toys to aircrafts and their analysis in every aspect[1]. In the beginning, however, it was considered that all kind of polymer materials are non-conducting plastics since they are generally used as insulators especially in electronic industry. But this common thought has changed with the accidental discovery of conductivity in polyacetylene films by three scientists when these films were exposed to iodine vapour. This accidental discovery brought the Nobel Prize to Alan MacDiarmid, Hideki Shirakawa and Alan Heeger in Chemistry in 2000 and started a new era in polymer science known as " conductive polymers"[2, 3].

Conductive polymers as new generation materials offer many outstanding advantages over metals and inorganic semiconductors such as good solution processability, flexibility, light-weight, low cost and corrosion-resistant[4,5,6]. These advantegous properties enable them to be used in a wide range of applications such as optical displays, electrochromic devices, photovoltaic devices, batteries, transistors, smart windows, biosensors and bioelectronic devices[7,8].

Polyacetylene films as the first conjugated conductive polymer possess certain restrictions such as insolubility and the lack of air stability in their doped state[9,10]. After that, the research interest was directed to the synthesis of more stable and processable types of conjugated polymers. In this respect, heteroaromatic

conjugated structures gain attraction as the most appropriate class of materials to solve the problems possessed by polyacetylene film. Polyacetylene (PA), polythiophene (PT), polypyrrole (PP), polyfuran (PF), poly(p-phenylene) (PPP) poly(*p*-phenylenevinylene) (PPV), polyaniline (PANI), poly(3,4-ethylenedioxythiophene) (PEDOT) and polyfluorene (PFL) can be given as examples to the most common conjugated systems[2] as shown in Figure 1.1.

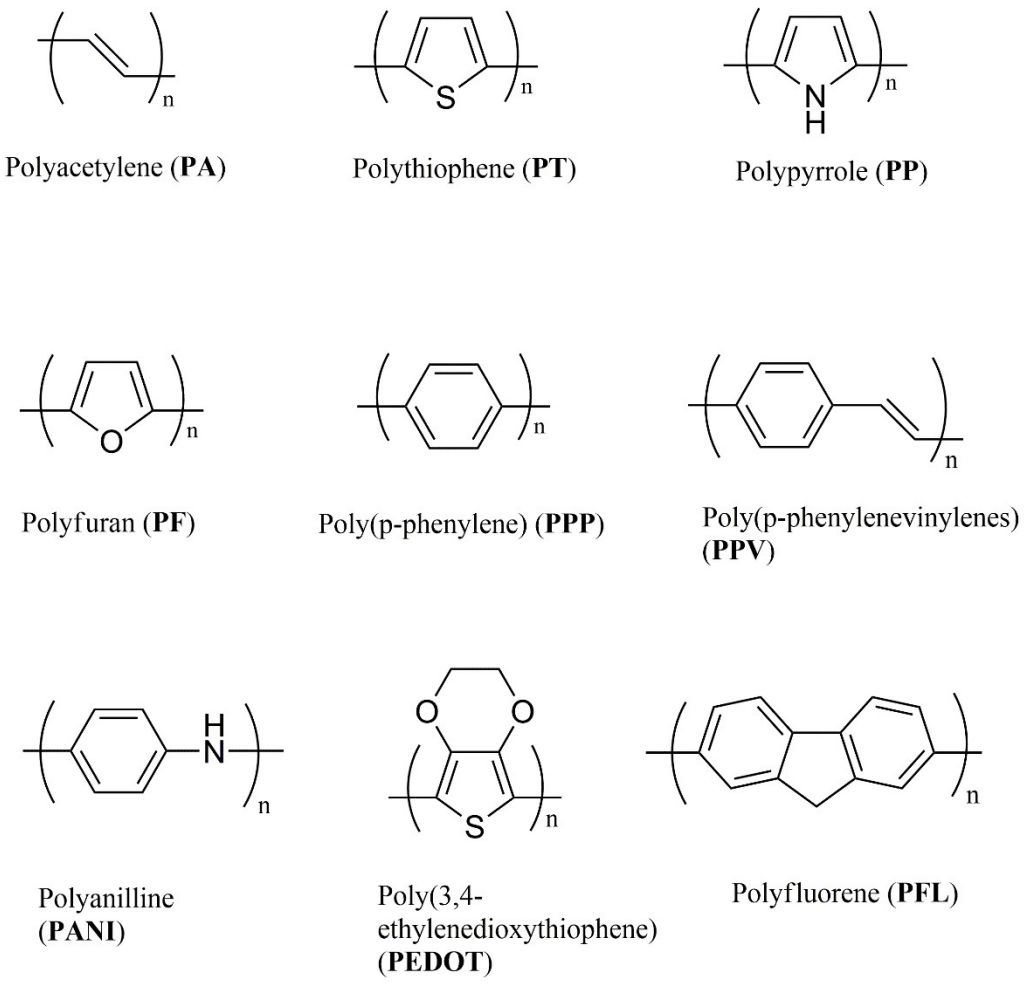

Figure 1.1. Some common conjugated polymers.

1.2 Conductivity Concept in Conjugated Polymers

1.2.1 Structure and Conjugation

The origin of conductivity in a polymer is based on the presence of a conjugated system with alternating single and double bonds providing continuous orbital overlapping due to the connected π-orbitals. The polymer becomes electronically conductive when the charge carriers move throughout the extended- π-orbital system along the polymer chain[8,11]. In an intrinsically conducting polymer, the highest occupied molecular orbital (HOMO) corresponds to the valence band while the lowest unoccupied molecular orbital (LUMO) refers to the conduction band[10]. The forbidden energy range between the filled valence band and empty conduction band is defined as a band gap which plays a key role in the determination of electrical properties of the polymer materials[12]. As depicted in Figure 1.2, PA chain consists of carbon atoms surrounded by three σ bonds and one π bond that results in alternating single and double bonds in the main backbone, whereas polyethylene involves single bonds in the main backbone with carbon atoms surrounded by four σ bonds. As it is seen from Figure 1.2, the HOMO-LUMO energy difference determines the band gap of the neutral polymer[13,14].

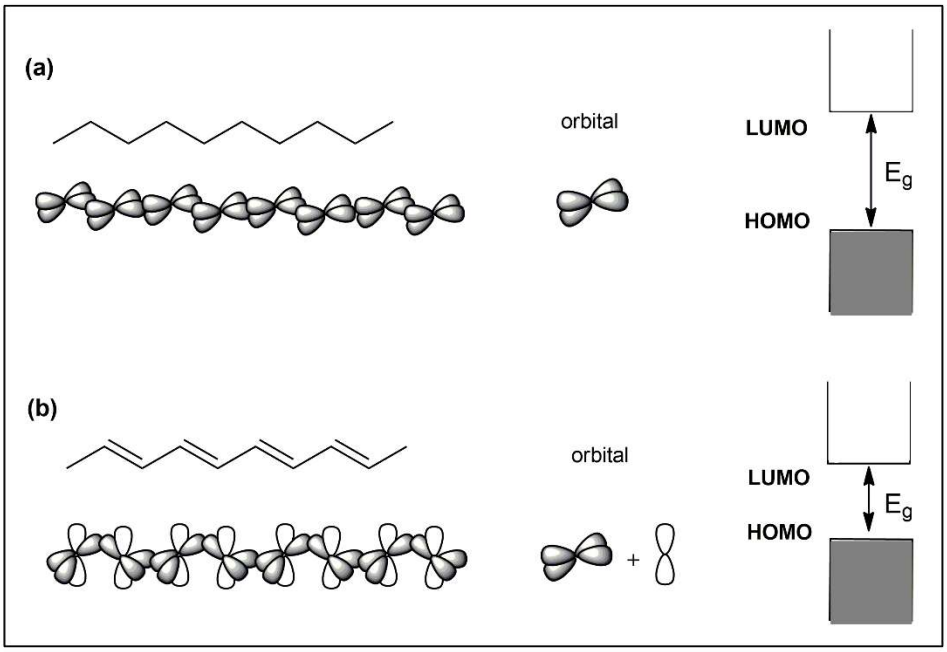

Figure 1.2. Schematic representation of both the structure and orbitals in (a) polyethylene and (b) PA.

1.2.2 Band Gap and Structural Factors

The band gap is defined as the energy separation between the valance band and conduction band and denoted as E_g[15]. The materials are generally classified into three main categories as metals, semiconductors and insulators according to their band gap width[11] as shown in Figure 1.3. When the valence band and conduction band merge with each other, the valence electrons are able to move and propagate freely in the conduction band. This kind of materials exhibits metallic behaviour[12,10]. In the case of semiconductors, a small energy gap exists between the valence band and conduction band which can be crossed by electrons upon excitation by creating a hole. The transport of hole and electron charge in this small energy gap provides the conduction of current. The energy gap between the valence band and conduction band in an insulator is too large to be passed by electrons and therefore they can not conduct electricity. There are several structural factors affecting the band gap energy level of intrinsic conductive polymers[11,15,16,17,18].

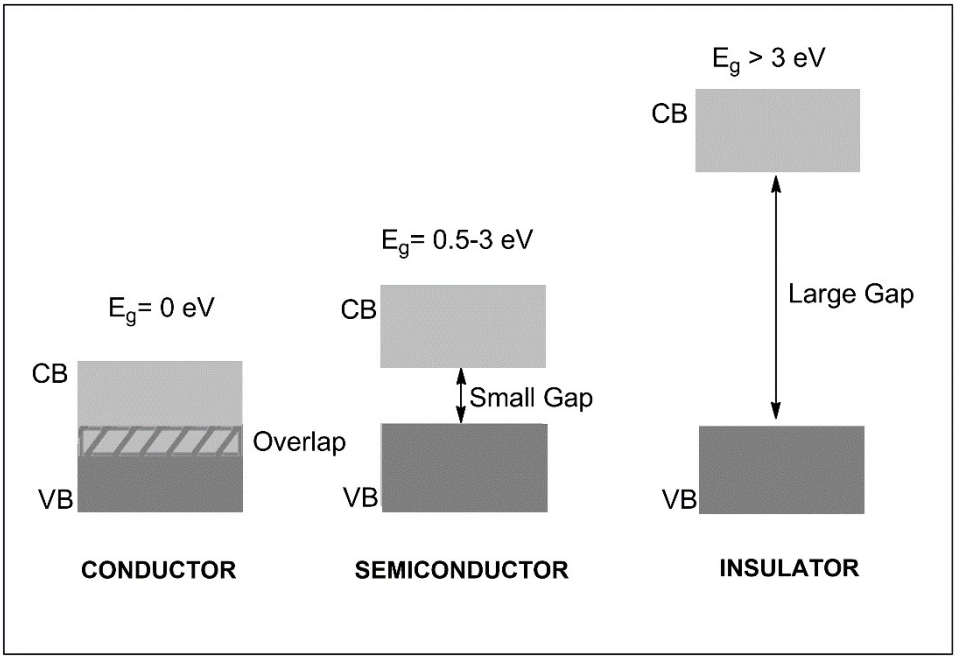

Figure 1.3. Valence band (VB) and conduction band (CB) in conductor, semiconductor and insulator.

1.2.2.1 Bond-Length Alternation

Bond-length alternation (BLA) is described as the difference between the average length of a single bond and the neighboring double or triple bond in a π-delocalized system. BLA is a physicochemical parameter to assess the geometric structure at the molecular level. It is well known that there is a close relation between BLA and band gap. As the change in bond length decreases, the band gap energy decreases as well. In a hypothetical case, the bond length between the C-C bonds should have an equal distance along the π-conjugated backbone to provide a complete electron delocalization. The elimination of BLA would render the progressive closure of the energy gap and results in the zero band gap material in one dimensional conjugated systems[19,20,21]. However, in real case, these systems are not stable and their π-electrons can be localized due to synergetic effect of electron-electron and electron-phonon interactions. As a result, π-conjugated polyene systems have an energy gap

around ~1.50 eV due to the major contribution of BLA to the band gap energy value[16].

1.2.2.2 Aromatic Resonance Energy

The resonance energy is defined as the difference between the total π-electron energy of a real conjugated molecule and a hypothetical reference structure with localized bonds. Since most of the conjugated organic polymers involve aromatic ring systems, it is crucial to clarify the connection among aromaticity, resonance and band gap[22]. In aromatic systems, two mesomeric forms with non-degenerate energy levels can occur by flip-flop between single and double bonds. The aromatic form shows considerably more stability than the quinoid form. The energy required to change from the aromatic form to quinoid form is directly related to the aromatic stabilization resonance energy of the aromatic moiety. The π-electrons are constrained within the aromatic ring due to this resonance effect and their delocalization is hindered along the polymer backbone. Therefore, this resonance effect leads to a contribution of the magnitude of band gap. It is apparent that the less aromatic polymer results in a lower band gap[16,22,23].

1.2.2.3 Rigidity of the Conjugated System

Rigidification is an effective strategy to form highly conjugated planar π-systems. Rigidification also provides the reduction of BLA and the enhancement of photoluminescence efficiency in conjugated systems[24]. When a polyaromatic system is lack of chemical rigidity, the backbone is easily distorted due to the rotational disorder around inter-annular single bonds. A mean dihedral angle thus occurs between two adjacent units, which restricts the delocalization of π-electron along the whole conjugated chain. Consequently, this inter-annular rotation increases the magnitude of band gap. The rigidification of π-conjugated polymers afford a substantial reduction in the band gap; however, the quantity of this

reduction can be restricted by potential inter-ring rotations in the conjugated chain[16,24,25,26,27].

1.2.2.4 Substituents

The introduction of substituents such as electron-donating or electron-withdrawing groups is the most straightforward strategy to tune the HOMO and LUMO energy levels and thereby the magnitude of band gap in a conjugated system. When the electron-donating groups are substituted to the system, they can induce an increase of HOMO level, which is followed by the reduction of the band gap. Moreover, electron donating alky chains tend to contribute band gap reduction by improving the long range order in the conjugated system. However, the substituted groups should not be too bulky to avoid deviation from planarity, non-bonding interactions and poor orbital overlap. In the case of the electron-withdrawing substituents, the reduction of band gap is attributed to increasing quinoid character of conjugated backbone as well as decreasing HOMO-LUMO energy levels[15,16,28,29,30] due to lowering in the LUMO energy level.

1.2.2.5 Intramolecular Attractions and Donor-Acceptor Approach

Recently, a new strategy to design and synthesize small band gap polymers was suggested by Havinga et al. in 1992. In this strategy, electron rich units are combined with electron deficient units in an alternating arrangement along a polymer backbone to bring about the eventual merging of valence and conduction band, thus providing intrinsic conduction in polymer material. Intramolecular charge transfer (ICT) created by the alternation of donor-acceptor units in polymer backbone can facilitate manipulation of the electronic structure leading to an absorption band at a lower energy. The strength of ICT can be adjusted through a painstaking selection of donor and acceptor units. The logic behind the donor-acceptor approach is to provide the hybridization of high lying HOMO of donor

moiety and low lying LUMO of acceptor moiety and hence to increase double bond character between donor and acceptor units, which leads to broadening of valence and conduction bands and hence a band gap reduction. Thus, the new donor-acceptor material can have an unusual small HOMO-LUMO separation relative to those of pristine donor and acceptor groups as shown in Figure 1.4. The band gap value is expected to be the lowest for an alternating donor-acceptor system when the electronegativity difference between donor and acceptor units is the highest[16,18,31].

In this sense, it is possible to synthesize different small molecules based on Donor-Acceptor (D-A) frameworks such as Donor-Acceptor-Donor (D-A-D), Donor-Acceptor- Acceptor (D-A-A) or Acceptor-Donor-Acceptor (A-D-A).

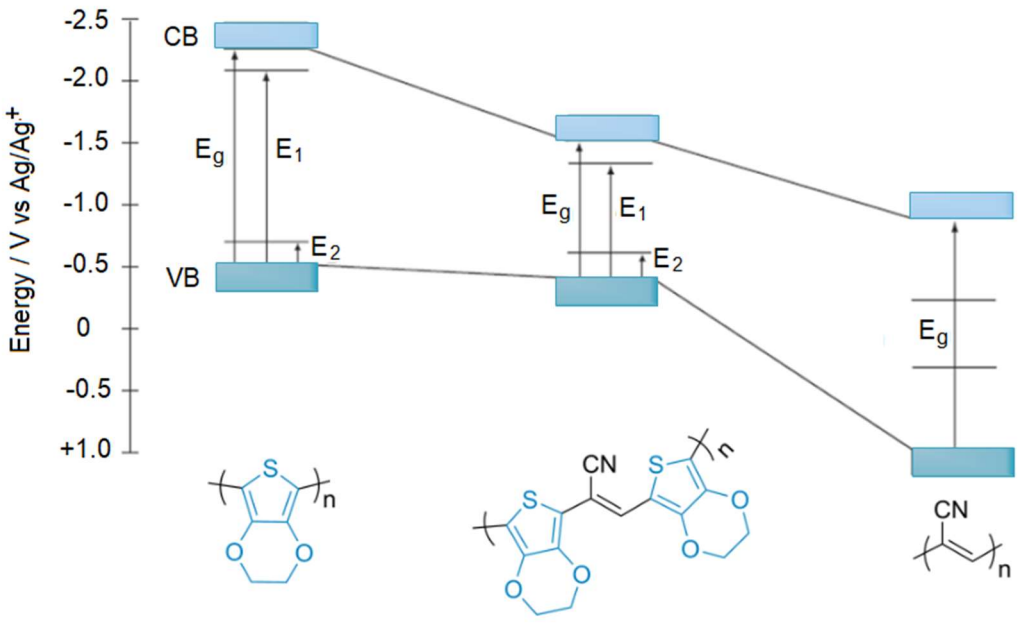

Figure 1.4. The schematic representation of donor-acceptor approach[32].

1.2.2.6 Intermolecular Attractions

Despite the lowering effect of numerous structural factors on the energy gap, there is one main problem faced by the conjugated system due to these structural factors, which is the lack of solubility. The insolubility in these systems is based on the compact structure of polymers due to the interchain interactions such as weak hydrogen bonding, Van der waals interactions or π-π stacking. The alkyl substituents can be introduced to the polymer chain to enhance solubility by disentangling the tightly π-stacked chains. However, two major drawbacks come along with the enhanced solubility. One of them is the loss of stability due to the disruption of the compact structure of polymers. The second one, on the other hand, is the dramatic increase in the energy gap due to the alkyl chains in the polymer backbone. These experimental observations reveal the contribution of the intermolecular interactions to the magnitude of band gap[16,30].

1.2.3 Conductivity Mechanism and Doping Process

The band gap concept is not enough to explain the conductivity process in the conjugated polymers. Indeed, the electrically conductive polymers are reported as insulators in their neutral state and their conductivity can switch from insulating to metallic only when they are doped. In order to reach high conductivities, doping is required. Due to the lack of an intrinsic charge carrier in a conjugated polymer, doping process needs a dopant which can either remove an electron from the polymer chain (oxidation) or add an electron to the mainchain (reduction). These oxidation and reduction processes provided by dopant are named as p-type and n-type doping, respecively. In p-type doping, the electron transfer occurs directly from HOMO of the valence band to the dopant species and generate a hole in the main backbone. On the contrary, in n-type doping, the electron moves directly from dopant species to the LUMO of conduction and leads to an increase in electron density. As a result of the doping process, the charge carriers appear in the polymer

backbone in the form of polarons (radical cation or anion), bipolarons (dication or dianion) or solitons. When one electron is removed from the valence band, the polaron is generated in the conjugated structure. If another electron is further ejected from the valence band, the bipolaron is formed. When the bipolarons are separated, they can form solitons. The movement of these charge carriers along the polymer backbone provides conductivity. Since the negatively charged carriers produced in n-type doping are not stable as positively charged carriers, p-type doping is generally more common for research and practical applications[17,33]. The doping process for the formation of charge carriers for both types are schematically represented in Figure 1.5.

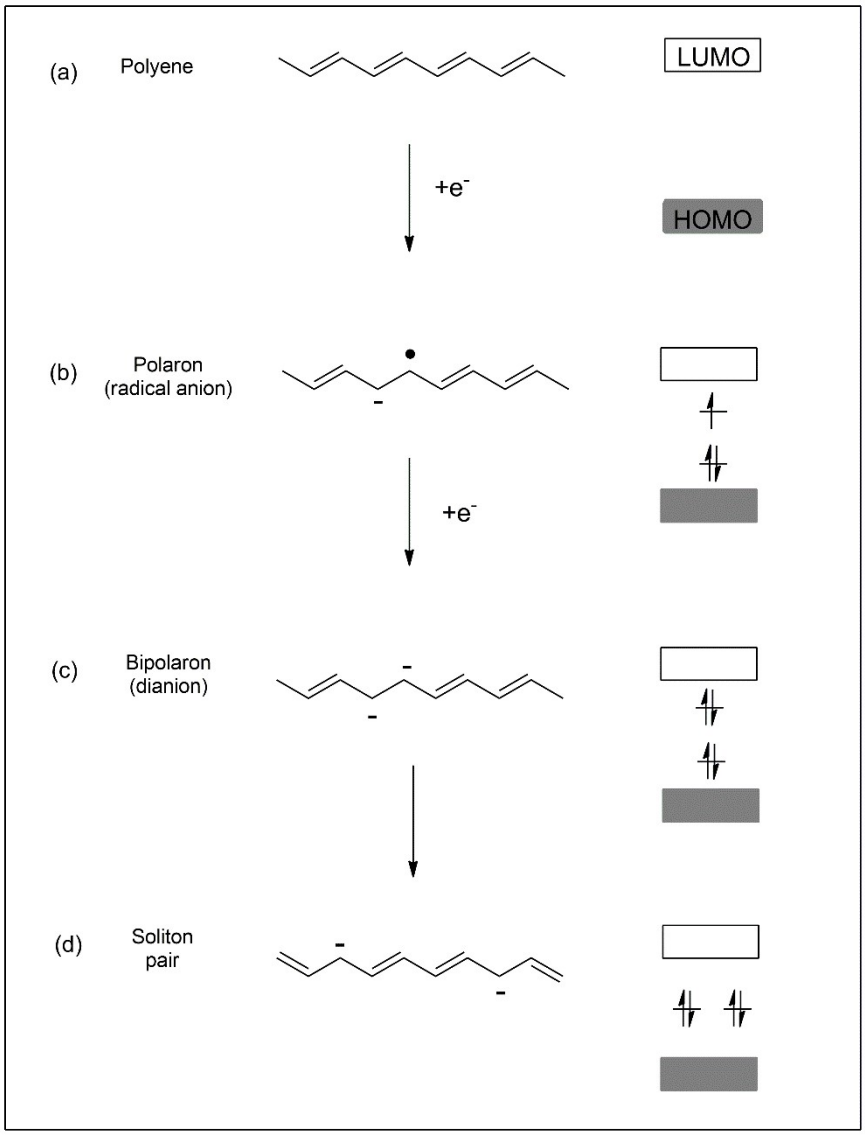

Figure 1.5. A schematic representation of the formation of (a) polyene, (b) polaron, and (c) bipolaron, (d) soliton pair on a trans-polyacetylene chain by doping.

In doping process, two different ways can be followed: chemical and elecrochemical doping. In chemical doping, the polymer is exposed to an oxidizing agents such as iodine or bromine or reducing agent such alkaline metals for p-type or n-type doping, respectively[34]. In chemical doping, charge-transfer redox reactions take place as follow:

(1) Oxidation (p-type doping)

$(\pi\text{-polymer})_n + \text{oxidant} \longrightarrow (\pi\text{-polymer})_n^{+}(\text{dopant anion})^{-}$

(2) Reduction (n-type doping)

$(\pi\text{-polymer})_n + \text{reductant} \longrightarrow (\pi\text{-polymer})_n^{-}(\text{dopant cation})^{+}$

Even though the chemical doping is considered as a simple and efficient process, the control of doping process can lead to incomplete doping because of the inhomogeneities observed in the intermediate structures. Therefore, the electrochemical doping is generally more preferred than chemical doping to figure out this problem[35].

In electrochemical doping, the potential difference between electrodes leads to charge transfer into and out of polymer in the form of addition or ejection of electron for n-doping and p-doping, respectively[35,36].

(1) Oxidation (p-type doping)

$(\pi\text{-polymer})_n + a(E^{-}) \longrightarrow [(\pi\text{-polymer})_n^{+a}(E^{-})_a] + ne^{-}$

(2) Reduction (n-type doping)

$(\pi\text{-polymer})_n + b(E^{+}) + ne^{-} \longrightarrow [(\pi\text{-polymer})_n^{-b}(E^{+})_b]$

where E, E^{-} and E^{+}represent electrolyte, anion, and cation, respectively. On the other hand, a and b refer to doping degree. In order to provide overall charge neutrality in a doped polymer chain, the counter ions from the electrolyte solution incorporate into the polymer film. As a result of doping, the charge carriers (polarons, bipolarons and solitons) are generated as previously stated[37].

1.2.4 Hopping Process

The transport of charge carriers in a conjugated system takes place in two different mechanisms which are intrachain and interchain mobility. In intrachain mobility, the movement of charge carriers occurs through a conjugated backbone. Conversely, in interchain mobility, the carriers move from one chain to a neighboring one or from a crystalline region to an amorphous one or vice versa through hopping or tunneling process[38] as shown in Figure 1.6.

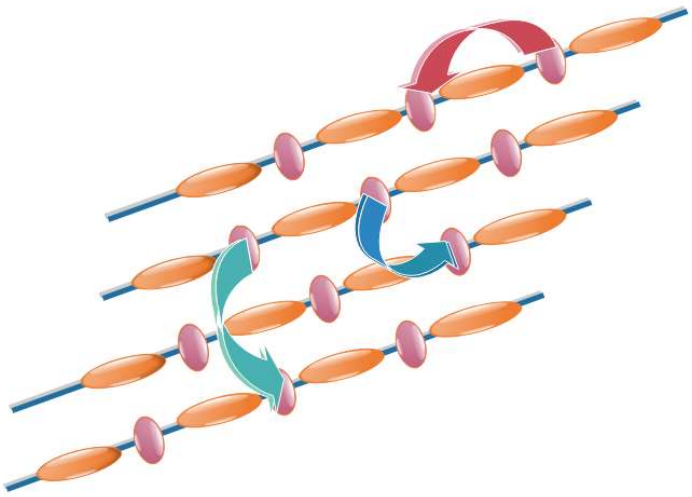

Figure 1.6. Schematic representation of hopping process.

1.3 Synthesis of Conductive Polymers

It is possible to synthesize the conductive polymers by using a variety of distinct methods such as chemical, electrochemical, concentrated emulsion, photochemical, methathesis solid-state, plasma, inclusion and pyrolysis. Among them, chemical and electrochemical polymerization are the most commonly used two techniques[2,39]. The chemical polymerization can be categorized into two classes: oxidative chemical polymerization and transtion metal-catalyzed coupling polymerization.

1.3.1 Oxidative Chemical Polymerization

Chemical polymerization is the common technique for large-scale production of conjugated polymers at a resonable price. The polymerization is carried out by exposing the conjugated monomers to an excess amount of chemical oxidant in a proper solvent with a continuous stirring to obtain the conductive polymer in the doped form. The polymerization occurs spontaneously and follow chain-growth mechanism (addition polymerization)[39]. The fundamental structural requirements for successful chemical polymerization are the stability and solubility as well as conjugation. In order to obtain high molecular weight polymers, the resulting oligomeric species or low molecular weight polymers produced in the polymerization process should be soluble and reactive enough for further polymerization. In an unsuccessful polymerization, termination process arises before the desired molecular weight is obtained [1,11,39]. In this type of polymerization, a large variety of species such as ferric chloride ($FeCl_3$), ferric sulfate, ferric perchlorate, cupper(II) perchlorate, cupper(II) chloride, antimony pentafluoride, hydrogen peroxide and ammonium persulfate and halogens can be used as chemical oxidizing agents [40,41,42]. The oxidative polymerization of a typical heterocyclic monomer with $FeCl_3$ is shown in Scheme 1.1.

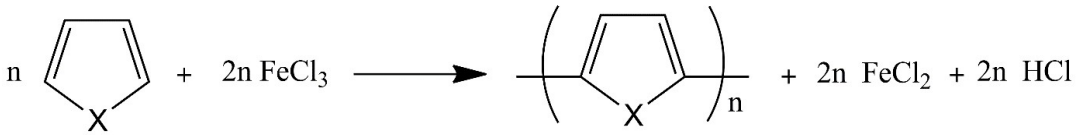

Scheme 1.1. The oxidative chemical polymerization of a five membered heterocyclic compound via $FeCl_3$.

Despite its numerous advantages, chemical polymerization has some limitations such as the low quality and conductivity of the polymer obtained together with a limited degree of polymerization[43,44].

1.3.2 Transition Metal-Catalyzed Coupling Polymerizations

The synthesis of the monomeric units or heteroaromatic conjugated polymers of a wide range of outstanding structural variety and regio-regularity can be carried out by polycondensation reaction with the use of organometallic catalyst or reagent. Transition metal catalyzed polycondensation reaction provides the C-C bond formation such as C_{sp2}-C_{sp2} and C_{sp}-C_{sp2}. In general, the metal catayzed oxidative addition reaction occurs across the C-X bond of electrophilic group followed by transmetallation with organometallic nucleophile. As a result, reductive elimination allows the C-C bond formation with the regeneration of active catalyst (Scheme 1.2). The most extensively utilized transition metal catalysts are nickel or palladium-containing complexes. The other metal complexes are used as well. Grignard reagents, boron reagents, stannanes, lithium, zinc or copper compounds can serve as an organometallic nucleophile. Depending on the type of organometallic nucleophile, polycondensation reactions can be categorized as Kumada-Corriu, Stille, Suzuki-Miyaura, Yamamoto, Sonogashira and so on. Stille and Suzuki-Miyaura couplings are the most significant types of transition metal catalyzed cross-coupling reaction[45].

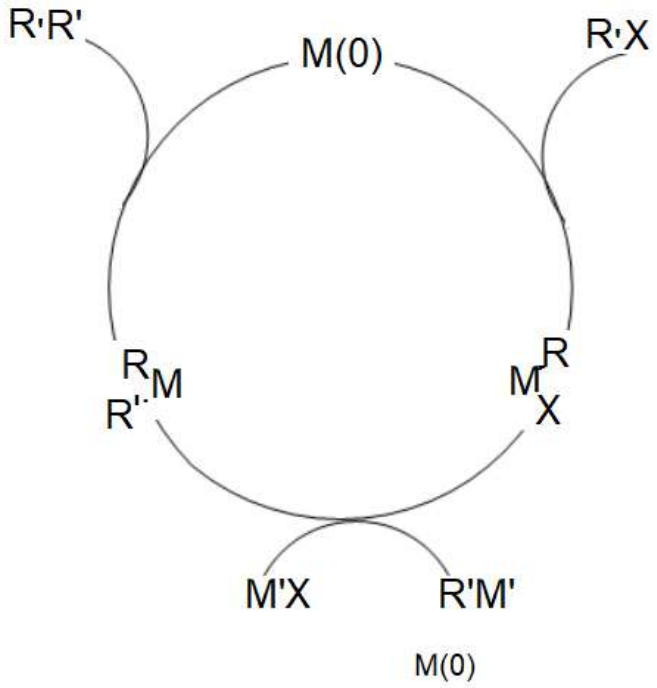

Scheme 1.2. The general mechanism for transition metal catalyzed polycondensation reactions.

1.3.2.1 Stille Coupling

Stille cross coupling is one of the efficient polycondensation reactions, which takes place between electron rich stannanes and electron deficient halides to form C-C bonds. Palladium-catalyzed cross coupling reaction can be catalyzed by either palladium (II) or palladium (0) complexes. When palladium (II) is utilized, it is firstly reduced to palladium(0) with the organotin compound. Then, palladium(0) reacts with organohalide species to generate organopalladium halide intermediate via oxidative addition. Transmetallation of the intermediate is followed by reductive elimination to form the final product and palladium (0) to complete the catalytic cycle[45,46].

The reaction conditions for the synthesis of small molecules via Stille cross coupling reaction can dramatically change for those of polymerization reaction. It is known that the synthesis of polymers with desired molecular weight has a great importance for the applicability of the resulting polymer. In order to get high molecular weight polymers, some parameters such as stoichiometry and reactivity of the monomers, nature of the solvents and the composition of catalyst systems should be arranged properly. Stille cross coupling reaction presents some benefits such as lessened oxygen sensitivity and milder reaction condition despite its drawbacks such as toxic stannylated monomers and the side products[45,46,47].

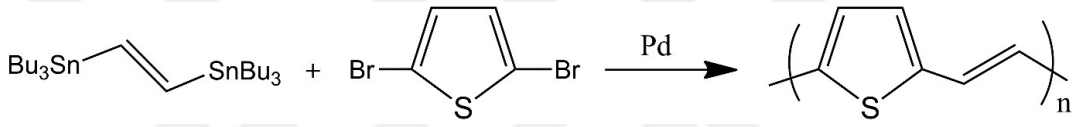

Scheme 1.3. The general mechanism for Stille cross coupling reaction.

1.3.2.2 Suzuki Coupling

Suzuki-Miyaura reaction is also efficient transition metal catalyzed cross coupling reaction for the formation of C_{sp2}-$C_{sp2.}$ This palladium-catalyzed polycondensation reaction takes place between the corresponding diboronic acid or ester and dihalide compounds[45].

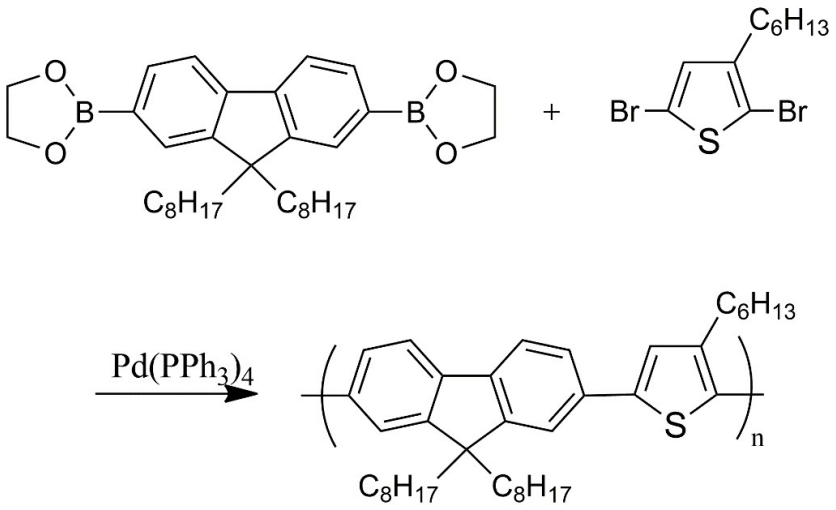

Scheme 1. 4. The general mechanism for Suzuki cross coupling reaction.

1.3.3 Electrochemical Polymerization

Electrochemical polymerization is a simple and straightforward technique which allows the rapid synthesis of the doped form of conducting polymer on the electrode surface by applying potential in the presence of an appropriate electrolyte medium. The electrochemical polymerization provides the fabrication of high quality polymer film with an adjustable film thickness[48]. This polymerization takes place in a three-electrode system involving working, reference and counter electrodes in an electrolyte medium which consists of monomer, supporting electrolyte, proper solvent and some other required additives. The electropolymerization can be achieved by applying either a constant current, constant potential or potentiodynamic methods[39]. For example, during electrochemical polymerization of thiophene via potentiodynamic technique, the monomer is oxidized through an applied potential to generate radical ion intermediate. At the next stage, the reactive radical cation/ion can react with either a neutral monomer or another intermediate to produce a dimer of radical cation[2]. The mechanism for the electropolymerization of 3,4-ethylenedioxythiophene (EDOT) is shown in Scheme 1.5 as a representative example for the electrochemical polymerization.

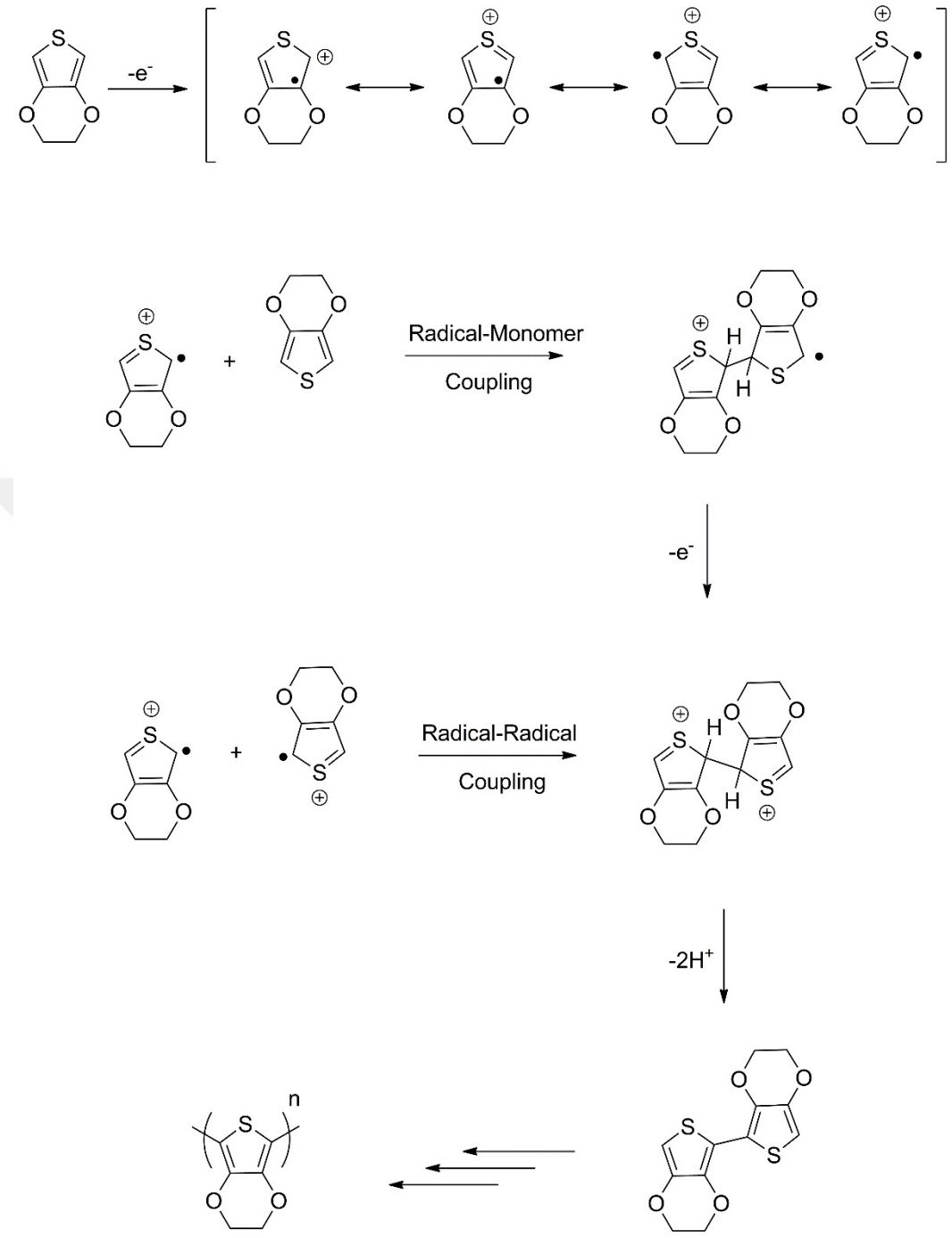

Scheme 1.5. The mechanism for the electrochemical polymerization of EDOT.

Electrochemical polymerization offers several advantages compared to chemical polymerization by providing flexibility in terms of distinct dopant use, fabrication of layered structures by sequential deposition and copolymer synthesis. The major disadvantages of this technique can be the need for high-cost equipment, small scale production, the inability of some monomers to polymerize via electrochemical method[39,48].

1.4 Characterization Techniques for Monomers and Conductive Polymers

A large variety of analytical techniques are available to investigate the properties of conductive polymers from all perspectives[11]. To provide a deeper understanding of these properties, characterization techniques can be used together in some circumstances. These techniques can be categorized under four main groups as structural, electrochemical, optical and spectroelectrochemical characterization depending on physical, chemical and electrochemical properties of conductive polymers [49,50].

1.4.1 Structural Characterization

Structural characterization techniques carry vital importance for confirmation of the identity of both monomers and polymers. Among them, Nuclear Magnetic Resonance (NMR), High Resolution Mass Spectrometry (HRMS), Gel Permeation Chromatography (GPC) and Fourier Transform Infrared (FTIR) are the most commonly used ones[11].

1.4.1.1 NMR

NMR spectroscopy is the most powerful tool used for the determination of structure in both solution and solid states. It allows the identification of certain atoms and groups in a molecule and their positions with respect to each other[51].

Structure conformation and chain orientation can be carried out by NMR[50]. NMR is an absorption type spectroscopy in which the energy transfer takes place between quantized energy states of nuclei depending on the applied magnetic field. This energy difference between the upper and lower energy states correspond to a wavelength in the radio frequency range. Each magnetic nuclei absorbs a certain radio frequency and flip from the lower energy state (parallel spin with the applied field) to the upper one (antiparallel spin with the applied field). The same frequency of energy is dissipated when the spin returns to its lower energy state. Consequently, the processed signal corresponding to this energy transition gives NMR spectrum. The nuclei with an odd number of protons or neutrons has a nonzero nuclear spin and thereby intrinsic nuclear magnetic while the nuclei with an even number of both have a zero spin quantum number and do not give NMR signal. In this respect, ^{1}H, ^{13}C, ^{15}N, and ^{31}P are the most widely used nuclei for NMR. The characteristic nature of NMR is resulted from the different electronic environment around nuclei due to different surrounding groups and the nature of bonding. As a result, different absorption frequency is obtained for each nuclei and expressed as a chemical shift with respect to a standard reference. Magnetically isotropic and chemically inert materials can be used as standard reference materials. Tetramethylsilane (TMS) is commonly employed as a chemical shift standard which is dissolved in the same solvent used for sample[52,53]. Organic deuterated solvents such as chloroform, dimethyl sulfoxide (DMSO), acetone, benzene, methanol, etc. are commonly used for NMR.

1.4.1.2 HRMS

HRMS is a powerful analytical technique allowing the exact mass determination with high accuracy. The measurement of the exact mass allows the classification, identification and confirmation of a chemical compound since it provides an additional dimension for the discrimation of molecules by measuring the mass of fragments making up the molecule at the 4^{th} and 5^{th} decimal place rather than an

integer number. In this technique, the molecules to be analyzed are vaporized and then ionized by electron ionization with or without fragmentation and then access the orbitrap mass spectrometer where these ions are separated according to their mass to charge ratios (m/z) in the electromagnetic field and detected in proportion to their abundance. The spectrum is given as the intensity of detected ions as a function of m/z ratio[54,55,56]. In the characterization of conductive polymers, HRMS is used for the determination of the exact mass of a conjugated monomer or trimeric unit rather than a polymer.

1.4.1.3 GPC

The molecular weight and molecular weight distribution are the characteristic features of a polymer. Unlike natural polymers, all synthetic polymers exhibit a dispersity in molecular weight which can be associated with their physical or performance properties. These characteristic features of a polymer sample can be identified by GPC which is a type of size exclusion chromatography used for the separation and purification of polymers. In this technique, polymer chains are separated according to their size and hydrodynamic volume due to their penetration into the pores of the stationary phase. As the polymer passes through the column with the help of the mobile phase, the smaller fragments can enter the pores of the stationary phase more easily and spent a longer time in that phase while the larger ones are entirely excluded from the pores and eluted from the column quickly. This process allows the separation of polymer chains of different sizes. GPC technique can be applied to a large variety of polymers depending upon the type of packing material utilized in the stationary phase. In order to afford efficient fractionation, the pore size of the packing gel should be comparable to the size of polymer chains. In addition, the eluting solvent in the mobile phase should dissolve the polymer sample completely and get wet on all the packing gel surface. The widely used eluents for GPC are tetrahydrofuran (THF), o-dichlorobenzene, trichlorobenzene and dimethylformamide (DMF). In the selection of an appropriate

column system, the parameters such as column type, column pore size and eluting solvent should be considered and the possible interaction of polymer-packing should be avoided [51].

1.4.1.4 FTIR

FTIR spectroscopy is a rapid and non-destructive technique for the characterization of polymers. It is a form of absorption spectroscopy using the region between visible and microwave in the electromagnetic spectrum. In a molecule, all atoms have continuous vibrational motions with respect to each other above absolute zero temperature. In these molecules, infrared absorption occurs depending on two conditions. The first one is the match of the radiant energy absorbed by the molecule with the energy difference between ground and excited states. The second condition is the presence of dipole moment change in the vibration mode. If not, radiant energy is not absorbed by vibrational mode and the molecule is referred to be infrared inactive. Two different types of molecular vibrations exist in a molecule which are stretching and bending. The frequency of absorption bands which is expressed as wavenumber unit are primarily determined by the geometry and relative masses of atoms and the force constant of the bonds in the molecule. The intensity of the bands expressed as either transmittance (T) or absorbance (A) are determined by the magnitude of dipole moment change as well[51].

FTIR is an useful technique for identification of an unknown polymer and analysis of functional groups in the polymer. It also provides information about the structural features of the chain, physical state, orientation and crystallinity of polymers. It is possible to carry out the simultaneous analysis of polymer structure during a course of polymerization reaction[51].

1.4.2 Electrochemical Characterization

The voltammetry is the most common tool for the investigation of the electrochemical properties of conductive polymers. A deep knowledge related to the physical properties of conductive polymers such as oxidation and reduction potentials of monomers and polymers, electrochemical band gap and electrochemical stability can be provided by voltammetry. Among voltammetry techniques, cyclic voltammetry and differential pulse voltammetry are the most common ones since these techniques are straightforward and versatile.

There are a vast number of parameters that affect the voltammetric study during the course of electrochemical polymerization. These parameters are the supporting electrolyte, the choice of solvent, the type of electrode, the applied potential and the temperature.

The supporting electrolyte

A supporting electrolyte is defined as any kind of ionic salt or ionizable compound that can be dissolved in a solvent. These materials should stay electroinactive within the range of potential employed. While choosing a supporting electrolyte, the solubility characteristics should be considered depending on the type of solvent used. The cation parts of the supporting electrolytes usually consist of alkali metal ions (Li^+, Na^+) or tetraalkyl ammonium ions (R_4N^+) while the anion parts are compromised either of halide ions (Br^-, Cl^-) or BF_4^-, PF_6^- or ClO_4^-. $LiClO_4$ is fairly soluble in some aprotic solvents, whereas $NaClO_4$ is barely soluble. Tetraalkyl ammonium electrolytes are very soluble in aprotic solvents and the oxidation potential range of their ClO_4^- salts is up to +1.6 V while their BF_4^- and PF_6^- salts provide an oxidation range up to +3.0 V[57,58].

A high concentration of supporting electrolytes is required for most electroanalytical processes to hold the migration effect on concentration polarization in a minimum level. Another function of the supporting electrolyte is to minimize the cell resistance and hence to diminish the IR drop[59].

Choice of Solvent

All electrochemical processes take place in a medium containing a solvent with dissolved supporting electrolyte. The choice of solvent is very important to satisfy the essential criteria for an electrochemical process. First of all, the solvent should have a good solvating power to dissolve all reactants and products and should have low viscosity to provide the rapid transport of the reactants and products. Moreover, the solvents should have a high dielectric constant (ε) to afford the electrical conductivity in electrolyte media and good electrochemical stability not to decompose at the potential where the reactant is oxidized. Lastly, the solvents should have a wide potential window for the electrochemical study not to limit redox process of reactant[60].

MeCN is one of the commonly employed solvents with a ε=37.5 in electrochemical studies since it has inert electrochemical properties in a wide range of potential window changing from -3.0 V to +3.0 V vs saturated calomel electrode.

Dichloromethane (DCM) (ε=8.93) is another common solvent used especially for oxidation of organic-based reactants. Its potential window limit is suitable up to +2.0 V.

The aprotic solvents such as dimethylformamide (ε=38.3) and dimethyl sulfoxide (ε=46.7) have excellent solubility characteristics for ionic species. These solvents are favourable candidates for cathodic processes since they have a reduction potential limit up to -3.0 V. However, they are also suitable for oxidation processes which occur not above +1.0 V due to their low stability in anodic region.

Water (ε=80.1) is free and non-toxic solvent which provides a high conductivity in electrolytic media. However, it is not suitable for organic molecules due to solubility problem. Morover, it is not proper for radical ion studies since it easily reacts with the radicals.

The other solvents such as propylene carbonate, THF, methanol, ethanol and nitromethane are also frequently employed for the electrochemical studies[60,61].

Types of electrodes: working, reference and counter electrodes

The voltammetric studies are performed in an electrochemical cell consisting of three electrodes which are submerged in an electrolyte solution involving the analyte to be studied. One of the electrodes is the working electrode at which the electrochemical event of interest is carried out. It is made up of redox-inert materials such as platinum, gold, glassy carbon, nickel or palladium. For the spectroelectrochemical studies, Indium Tin Oxide (ITO) glass is usually utilized as the working electrode. The type of working electrode is selected with respect to the conditions of electrochemical process. Furthermore, the electrode dimensions are held small enough to make the working electrode more polarized.

The other electrode is the reference electrode with a stable and well-established potential against which an external potential is applied to the working electrode. The applied potential is hence expressed as "vs" a specific reference. The common reference electrodes are the saturated calomel electrode, the Ag/AgCl electrode and the standard hydrogen electrode. The electrode is usually separated from the reaction medium by a porous frid. The junction potential created at the interface is minimized by matching the solvent and electrolyte inside the electrode with those of the external medium. The potential of the reference can vary for different experiments. The potential values obtained from different experiments are correlated with each other by using an internal reference compound. Ferrocene is frequently used in all measurements as an internal standard which can be reversibly oxidized to ferrocenium ion in MeCN at a potential of +0.48 V vs. Ag/Ag^{+} electrode.

The last electrode involved in the three-electrode system is the counter or auxiliary electrode which carries electricity from the signal source to the other electrodes through the solution to complete the electrical circuit. The surface area of the counter electrode should be larger than that of the working electrode not to inhibit the reaction taking place at the working electrode due to the slow reaction kinetics of the counter electrode limited by surface area. As counter electrodes,

electrochemically non-reactive materials such as platinum (Pt) in the form of wire, disks or graphite can be used[61].

1.4.2.1 Cyclic Voltammetry

Cyclic voltammetry (CV) is a powerful and straightforward tool for the investigation of redox processes of molecular species. When an external potential is applied to the working electrode with respect to the reference electrode, oxidation or reduction takes place on the surface of the working electrode when the potential matches the HOMO or LUMO energies. As the surface of the working electrode becomes adequately positive or negative, electron transfer occurs between the electrode surface and the reaction medium. This electron transfer is recorded as a measurable current flow between the working and counter electrodes. The direction of potential sweep determines whether the anodic or cathodic process takes place at the working electrode. When the potential is varied positively in the forward direction, an anodic trace is observed in the voltammogram. As the potential scan is reversed, the direction of current flow is also reversed and the inverse peak current is produced[61,62].

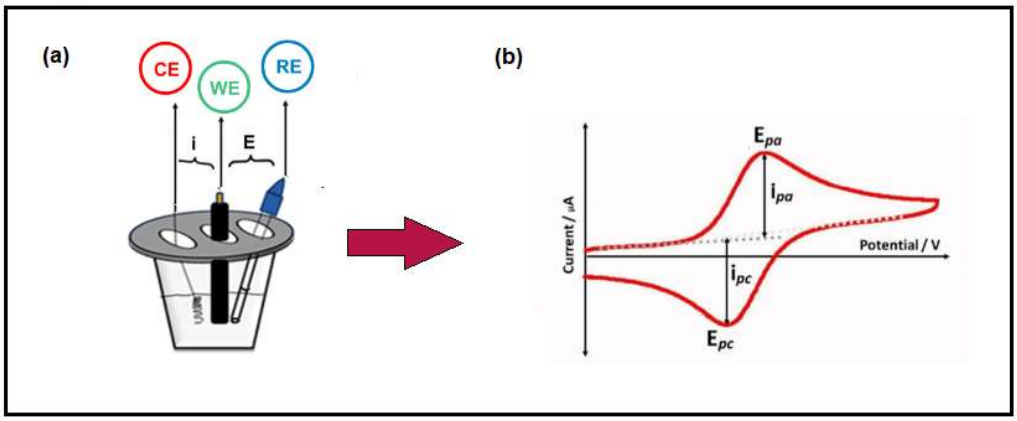

Figure 1.7. (a) Schematic representation of electrochemcial cell used for electrochemical studies of monomers and polymers (b) a typical cyclic voltammogram.

1.4.2.2 Differential Pulse Voltammetry

Differential pulse voltammetry (DPV) is a useful electrochemical method providing the minimization of capacitive background current. This is achieved by double current sampling by recording the current before the pulse and at the end of the pulse. The output signal is reported as the difference between these two currents. This current difference is plotted as a function of the potential applied in the form of a pulse superimposed on a staircase. As a result of dual current sampling, DPV allows the detection of analytes at a concentration as low as 10^{-8} M[63,64].

1.4.2.3 Controlled Potential Coulometry

Controlled potential coulometry is another electrochemical technique in which the potential of the working electrode is kept constant or varied in a controlled manner. As a response, two different variables can be monitored: the current as a function of time, or the charge as a function of time. In this technique, quantitative oxidation or reduction of electroactive species occurs until the completion of the process. Furthermore, the number of Faraday per mole of electroactive species consumed during the electrolysis can be determined[65,66].

1.4.3 Optical Characterization

Optical characterization techniques are valuable tools to examine the different aspects of conductive polymers. The spectroscopic quantities (absorbance, emission or transmittance) obtained with the interaction of optical radiation with matter are remarkably helpful for the determination of the electronic band structure involving the band gap, impurities and defects. Among these, Ultraviolet-Visible (UV-Vis) and fluorescence spectroscopies are commonly used for the

characterization of optical properties of semiconductors, surfaces and thin films as well as monomers[67].

1.4.3.1 UV-Vis Spectroscopy

UV-Vis spectroscopy is a very simple, fast and cost-effective technique in which absorption and transmission processes take place when the electromagnetic light interacts with the sample. The visible region of the electromagnetic spectrum and its vicinity (ultraviolet and near infrared) is used for this purpose. The change in the absorbance is monitored as a function of wavelength to obtain qualitative and quantitative information. In the region of interest, atom and molecules undergo electronic transitions. When the light passes through the sample, molecules involving bonding and non-bonding electrons can absorb the energy which promotes the electrons from bonding and non-bonding orbitals to empty anti-bonding orbitals. Consequently, the following electronic transitions can occur: σ to σ*, n to σ*, n to π* and π to π*. The transitions from σ or n orbitals to σ* orbital need a large amount of energy and hence take place in the far ultraviolet region or are weakly seen in the range of 180 – 240 nm. As a consequence, strong absorptions are not observed in the ordinary ultraviolet region for saturated groups. Both n to π* and π to π* type transitions are mostly seen in the molecules involving unsaturated centers and need less energy and thereby occur at longer wavelengths than σ to σ* and n to σ* transitions.

UV-Vis spectroscopy is extensively used for the quantitative analysis of the highly conjugated organic compounds like conjugated polymers or biological macromolecules. Their quantitative analyses are carried out in solution by using the Beer-Lambert law:

$$A = \log(I_o/I) = \varepsilon bc$$

where A is the absorbance, I_o is the intensity of incident light, I is the intensity of transmitted light, ε is the extinction coefficient or molar absorptivity, b is the cell

path length and c is the concentration of absorbing analyte in the solution. The law is valid only for monochromatic light and for an absorbance range involving a linear relationship with the analyte concentration[68,69].

1.4.3.2 Fluorescence Spectroscopy

Fluorescence is an optical phenomenon which deals with the fluorescent capable molecules known as fluorophore. These kinds of molecules can be intrinsically fluorescent or they can earn fluorescence property when a fluorophore is attached to these molecules. In the ground state, a fluorophore has the lowest energy level and thereby does not show fluorescence. When a fluorophore is illuminated with the light of a certain wavelength coming from an external source, the energy is absorbed. If the quantity of energy is appropriate, the molecule is excited to the higher energy level. Since the fluorophore is not stable in the higher energy state, the excited state lifetime lasts very short, such as 10^{-9} to 10^{-8} sec and some of its energy is lost in a non-radiative way during that time. When the fluorophore eventually returns to its ground state, the remaining energy is released in the form of emitted light with a longer wavelength. This process is known as fluorescence. The change in the energy of the emitted light with respect to excited light (less energy and longer wavelength) is named as Stokes' shift[70].

Fluorescence is typically observed in the aromatic systems. Most of the monomers and conjugated polymers containing extended aromatic systems exhibit the fluorescence property and can be used in many different applications such as sensors, solar cells and light emitting diodes[70].

Quantum Yield

Quantum yield (QY) is defined as the efficiency of a fluorescence emission which is calculated from the ratio of the number of emitted photons relative to the number of absorbed photons. To evaluate QY, a relative standard material carrying

fluorescence property is used. The calculation is done utilizing the equation given below:

$$QY_{(u)} = (A_s / A_u)(F_u / F_s)(n_u / n_s)^2 \, QY_{(s)}$$

where $QY_{(u)}$ is the fluorescence QY of unknown material, A is the quantity of absorbance, F is the area under the fluorescence emission curve, n is the refractive index of the solvents, **s** and **u** letters correspond to standard and unknown materials, respectively. Two important factors should be considered during the QY measurements: the choice of a standard material and the absorbance range of measurement. While choosing a standard material, the absorption and emission bands of standard should be as close as possible to those of the unknown material. Moreover, both of them should be excited at the same wavelength. While adjusting the absorbance range, it is important to choose the range where the emission intensity increases linearly with the analyte concentration. In fluorescence measurements, the optimum absorbance range lies between 0.05 and 0.04. Furthermore, the absorbance should not be too low to prevent the suppression of analyte signals with the impurities[70,71].

The QY is a relative quantity since it changes from one experiment to another for the same sample. Therefore, it is not considered as a reliable quantitative technique[71].

1.4.4 Spectroelectrochemical Characterization

Electrochemical analysis methods such as voltammetry, amperometry and impedance are quite useful to provide a wealth of information such as the concentration of species involved in the redox process, redox potentials of species and kinetics of charge transfer processes. However, information acquired from electrochemical analysis methods alone is not enough to provide structural information about the investigated system. Therefore, the integration of electrochemical methods with spectroscopic techniques allows the investigation of

structural changes in the molecule present at the electrode surface or in the solution and thereby renders the tracking of mechanism in an electrochemical reaction. The employment of electrochemistry along with spectroscopy brings about a new interdisciplinary field known as spectroelectrochemistry. A wide range of spectroscopic techniques such as electron spin resonance, Fourier transform infrared, UV-Vis spectroscopy, X-ray absorption spectroscopy, Raman spectroscopy, fluorescence and even NMR can be coupled with electrochemical methods. Among these, UV-Vis is the most standard technique used for the analysis of the conjugated polymers. It allows the tracking of optical changes of conjugated polymers during the electrosynthesis or doping/dedoping processes in real time. The use of time-resolved UV-Vis spectroelectrochemistry during the electropolymerization provides repeatable formation of polymer layers with a certain thickness. The polymer layers with a distinct doping level have the ability to absorb electromagnetic radiation which is proportional to layer thickness. Moreover, the use of this technique enables the simultaneous color determination and switching time between the colored states of electrochromic materials. It also enables the determination of band gap values of conductive polymer films[72,73,74].

1.5 Electrochromism

Electrochromism can be defined as reversible color change depending on the applied external voltage. This color change not only occurs in the visible region of electromagnetic spectrum but also occurs in the near-infrared region depending on the properties of the material.

The electrochromic materials can mainly be categorized into four major classes. The first one is the transition metal oxides such as TiO_2, WO_3 and V_2O_5. The second class involves the metal coordination complexes such as Prussion blue. Third class is comprised of organic monomeric compounds such as viologen. The last class is the organic conductive polymers such as PANI, PEDOT and poly(3,4-propylenedioxythiophene) (PProDOT)[75]. However, among them, organic based

electrochromic materials, especially the conductive polymers exhibit additional advantages such as fast switching time, high optical contrast and coloration efficiency, better ultraviolet stability, easy processing, low cost and tunable intrinsic properties[76,77,78].

Conductive polymers can be categorized into three main groups depending on their color transitions. The first group electrochromic polymers present at least one colored and one bleached state. These group polymers are known as anodically or cathodically colored polymers. The second group of polymers exhibits two different colored states. The last group electrochromic polymers has multicolored redox states with or without a bleached state[79]. Some examples for these type electrochromic polymers are illustrared in Figure 1.8.

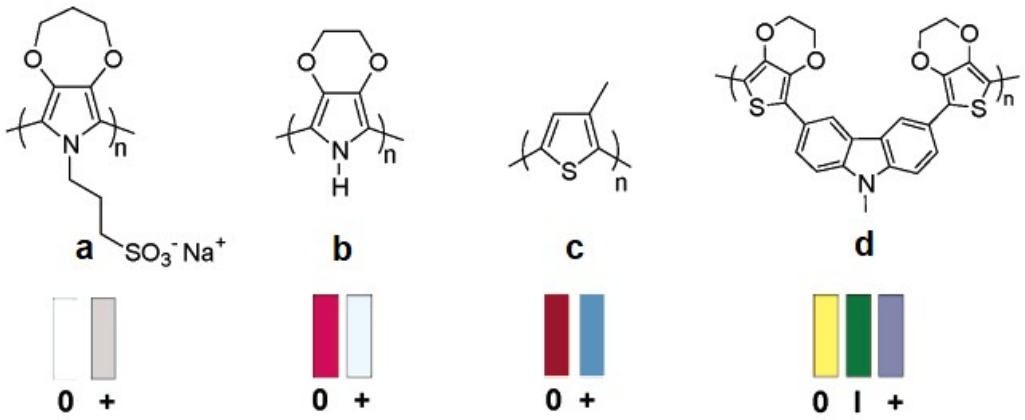

Figure 1.8. (a) Anodically or (b) cathodically colored (c) two different colored and (d) multicolored polymers[80].

The color of electrochromic polymers in their neutral state is determined by the magnitude of energy gap between HOMO and LUMO levels. The color of the polymer in its oxidized state depends on the formation of the new charge carriers: polarons and bipolarons. The color transitions in an electrochromic polymer are

also based on the migration of counter ions into and out of the matrix. As the new charged species form, they penetrate to this matrix and move through the film.

The perception of the polymer color and its interpretation are quite noteworthy. For this purpose, UV-Vis spectrometry is commonly utilized for the color analysis of electrochromic polymers since the observed color is directly related to the absorption spectrum of the polymer. The wavelength maxima of the material correspond to a specific range in the color wheel and the material is seen in its complementary color[81] as shown in Figure 1.9.

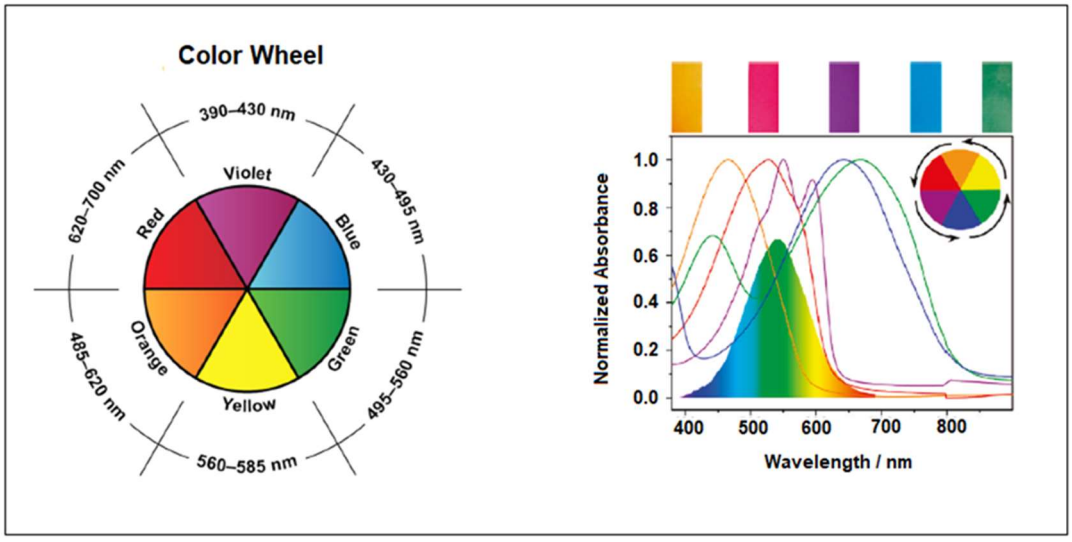

Figure 1.9. Color wheel showing the appropriate relationship between polymer color and the color or wavelength of light absorbed [81,82].

Colorimetry is a useful technique developed for the physical description of human color perception. In this technique, a standard and uniform color scale is required to compare the color of materials with each other correctly. In colorimetry, the color space of a material is expressed by three components which are hue (chromatic color, dominant wavelenght), saturation (chromaticity, tone, vividness/dullness) and brightness (lightness/darkness). There are two leading color spaces developed by the Internation Commision on Illumination (Commission Internationale de

l'Eclairage, CIE) used for defining the color of the objects. These are the xy chromaticity diagram and the L*a*b* color space. L*a*b* is commonly employed by electrochemists to describe the color space with quantitative metrics and light transmission changes for electrochromic polymers upon the applied potential. L* expresses the linear measurement of lightness (0= black, 100= diffuse white), a* and b* indicate the chromaticity coordinates. Here the a* refers to red-green balance (+a* is the red direction, -a* is the green direction) while b* represents yellow-blue balance (+b* is the yellow direction, -b* is the blue direction).

For a complete characterization of electrochromic polymers, some important parameters affecting the electrochromic properties of conjugated polymers such as band gap, optical contrast, switching time, coloration efficiency and stability should be elucidated[83,84].

1.5.1 Band Gap

Conjugated polymers are semiconductors with attractive properties that can be used for various applications such as solar cells, light emitting diodes and electrochromic devices. Most of the properties of semiconducting polymers are based on the band gap energy value since its magnitude plays a prominent role in the color of the absorbed or emitted photon. When the band gap value is ranged between 1.8 eV and 3.1 eV, the absorption or emission of light takes place in the visible region of the spectrum. Some experimental methods such as voltammetry or spectroelectrochemistry can be used for the evaluation of band gap.

In voltammetry, the oxidation (E_{ox}) and reduction (E_{red}) peak potentials of both monomer and polymer are measured using CV or DPV. For example, when the polymer is oxidized, an electron is removed from the valence band, on the other hand, an electron enters to conduction band during the reduction. Thus, measured E_{ox} and E_{red} are directly related to HOMO and LUMO energy levels and can be used to estimate the electronic band gap of the polymer. Ultimately, the electronic

band gap of the polymer is calculated in electron volt (eV) unit from the difference of onset potentials ($E_{ox,onset} - E_{red,onset}$) by multiplying the charge on the electron (e= −1.0 eV/V).

$$E_g(eV) = e(E_{ox,onset} - E_{red,onset}) \quad \text{(Equation 1.3)}$$

Despite the reliability of CV, the onset potentials of oxidation and reduction peaks can change as a function of scan rate. Therefore, DPV can be the choice of method for the detection of the same parameters due to its some advantages over CV such as enhanced discrimination of Faradaic currents and lower capacitive currents. Moreover, the onset potentials for a monomer or a polymer can certainly be determined from DPV. The calculation of the electronic band gap from the onset of oxidation and reduction peaks by using CV and DPV techniques is shown in Figure 1.10 and Figure 1.11, respectively.

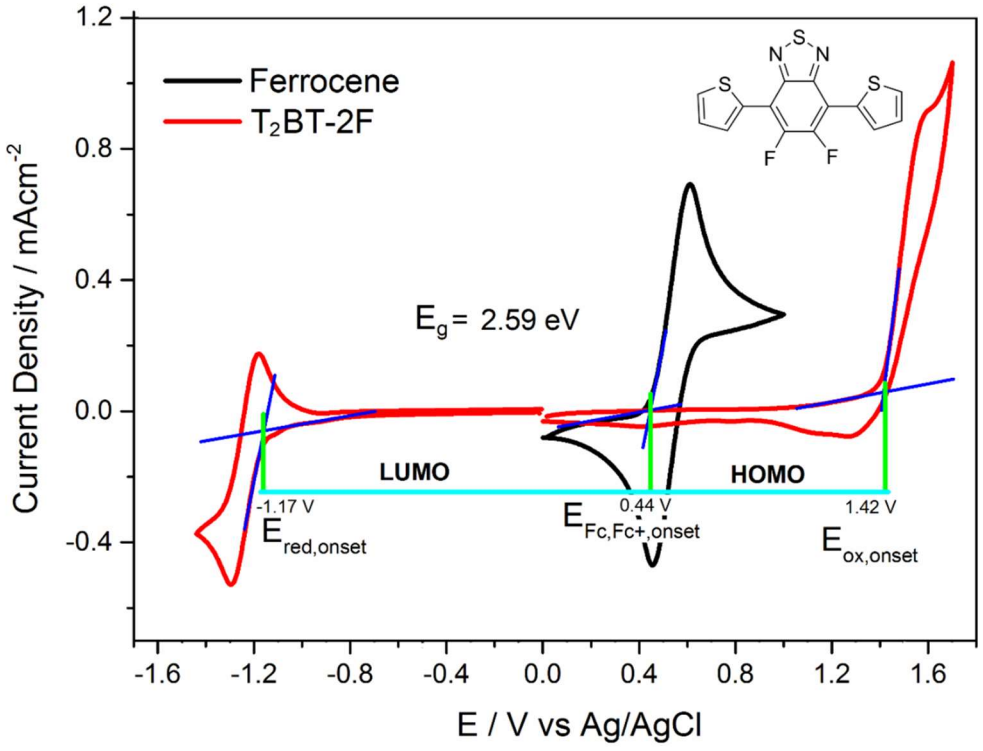

Figure 1.10. Calculation of the electronic band gap from CV measurement.

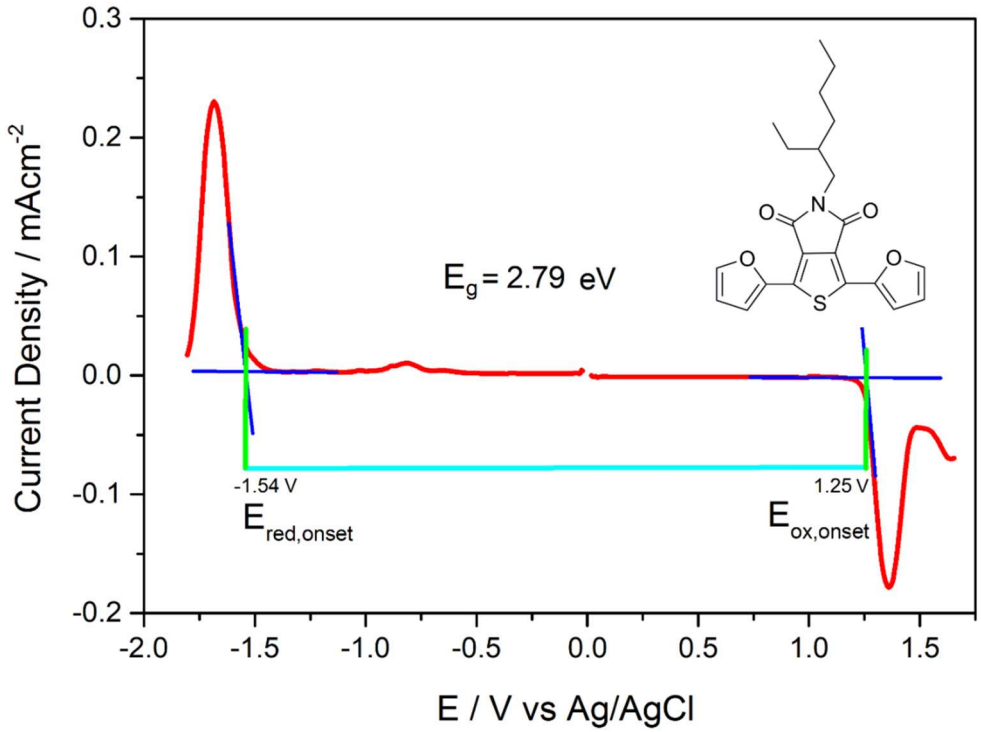

Figure 1.11. Calculation of the electronic band gap from DPV measurement.

In the spectroelectrochemical method, UV-Vis spectrum of the conjugated polymer in its neutral form is used to evaluate the band gap energy. In this spectrum, π to π* transitions belong to polymer film are observed in the higher-energy visible region or lower-energy near-infrared region. Through this method, the band gap energy is described as the onset of π to π* transitions and its determination can change depending on the narrow or broad onset of absorption peak. In the case of the absorption peak with narrow onset, the energy gap is usually selected as the wavelength at which it deviates from the absorbance baseline. In the case of a broad one, the optical band gap is determined by extrapolating the onset of π to π* absorbance to the background absorbance[85]. The calculation of band gap from the commencement of low energy end of π to π* transition band by using spectroelectrochemical method is shown in Figure 1.12.

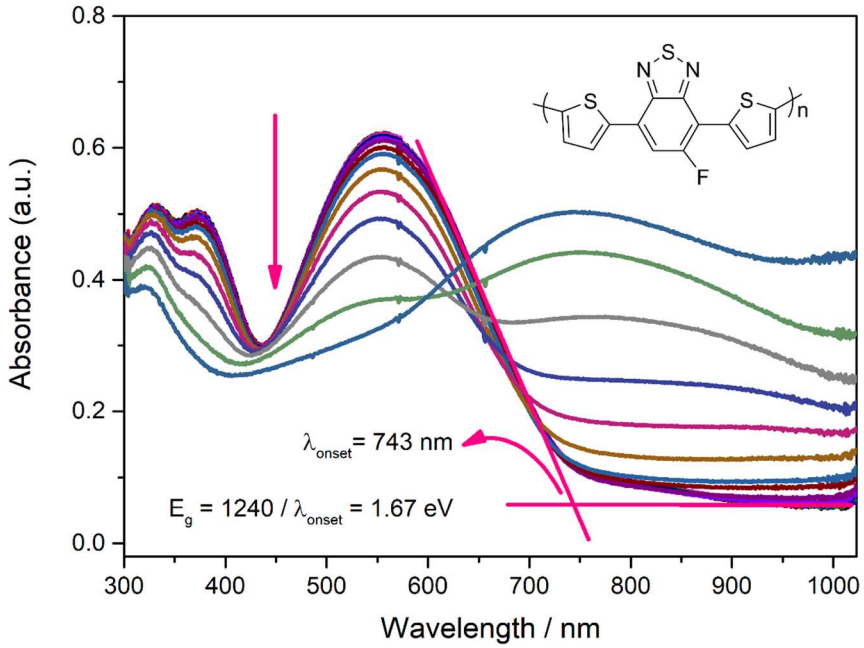

Figure 1.12. Calculation of the optical band gap from spectroelectrochemical measurement.

The discrepancies between the band gap values obtained by electrochemical and spectroelectrochemical methods are frequently encountered in the literature. The optical band gap values are generally found to be lower. It may be attributed to the red shift effect induced by ITO electrode on absorption maxima during spectroelectrochemical measurement[86]. Furthermore, in order to add an electron to a molecule, it needs more energy than the HOMO-LUMO separation of the neutral molecule: the electron also has to overcome the electrostatic repulsion, the Coulomb energy. This can also lead to the observation of higher value for electronically measured HOMO-LUMO gap (also called transport gap) as compared to an optical measurement.

1.5.2 Optical Contrast

Optical contrast which is also referred to as electrochromic contrast is defined as percent transmittance change (Δ%T) at a specified wavelength at which electrochromic material has its maximum optical contrast value. Optical contrast can be considered as the most prominent tool for the evaluation of an electrochrome. Optical contrast values are usually tracked and recorded by applying square wave potential steps to the electrochromic polymer film between two limits corresponding to fully oxidized and neutral states in front of a beam coming from a spectrophotometer. Furthermore, spectroelectrochemical measurements monitoring the charge carrier formation such as polaron and bipolaron can be used to evaluate overall electrochromic contrast over the entire visible spectrum. As the formation of charge carrier takes place in the long-wavelength optical region, the transmittance change can be obtained in the near-infrared region as well[79,80].

A typical chronoabsorptometry result associated with the chronocoulometry experiment switched between two limit states at a specified wavelength is depicted in Figure 1.13. According to these data, optical contrast is calculated by using Equation 1.4.

$$\Delta\%T = (\%T_{bleached} - \%T_{colored}) \qquad \text{Equation 1.4}$$

where $\%T_{bleached}$ and $\%T_{colored}$ are the bleached and colored percent transmittance values, respectively.

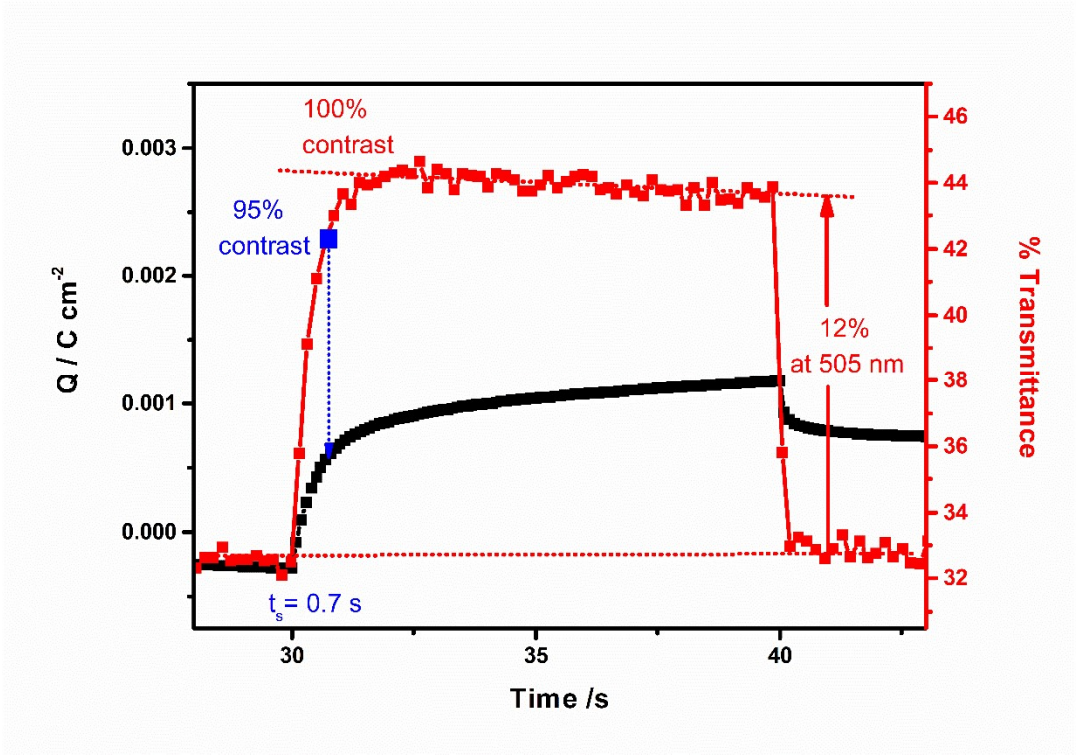

Figure 1.13. A typical chronoabsorptometry and chronocoulometry experiments for the polymer film at 505 nm in 0.1 M $TBAPF_6$ /MeCN.

1.5.3 Switching Time

Switching speed or response time is another important factor used to evaluate an electrochromic polymer. It is described as the time required for an electrochrome to switch between two redox states; fully neutralized and fully oxidized. The switching speed is based on several parameters such as ionic conductivity of the electrolyte, the accessibility of charge balancing counterions to the electroactive site, the extent of applied voltage, polymer film thickness and morphology. The switching time is determined from the 95% of the full optical contrast since the human eye can even perceive less than the full (100%) optical switch[79,80].

1.5.4 Coloration Efficiency

Coloration efficiency (CE) is defined as the ratio of total optical density change (ΔOD) to the injected or ejected charge density (Q_d) required to induce a full switch. Its calculation is carried out by monitoring the charge density and film transmittance at the same time with simultaneous chronocoulometry/ chronoabsorptometry experiments shown in Figure 1.13. It is important to select the applied potentials between the voltage extremes to induce a full optical switch. A more representative CE value is calculated for 95% of overall optical change as previously done in measurements of switching time since most of the perceptible optical contrast is acquired within the first 90 – 95% of full optical switch. It is calculated using the following equation (Equation 1.5).

$$CE = \Delta OD / Q_d = \log (T_{bleached} / T_{colored}) / Q_d \qquad \text{(Equation 1.5)}$$

where $T_{bleached}$ and $T_{colored}$ are the bleached and colored transmittance values, respectively [81,80].

1.5.5 Stability

Stability or cycle life is the last crucial factor used to evaluate the performance of the electrochromic materials. Electrochromic stability is generally affiliated with electrochemical stability in which electrochrome retains its redox stability without a measurable degradation upon repeated switching. When degradation occurs in an active redox couple, it leads to a rapid loss of electrochromic contrast hence affects the overall performance of the electrochromic material. The long-term switching stability experiments are performed in a three-electrode system with a button or ITO electrode in a sealed air-free cell via repeated potential cycling or by applying potential steps. Some parameters such as the potential range (partial or full switch), switch rate, the electrolyte used, exposure to light, oxygen or water are important when reporting a cycle life[79,81,80].

1.6 Chemiluminescence

Luminescence, in a more general sense, is defined as the light emitted by an atom or a molecule when these species return to the ground state from their excited state[87]. Luminescence phenomena can be classified into different categories depending on the source of energy necessary for excitation. These are photoluminescence initiated by absorption of light, thermoluminescence caused by heating, electroluminescence produced by electric discharge, triboluminescence initiated by friction, cristalloluminescence produced by crystallization and chemiluminescence initiated by a chemical reaction. Among them, chemiluminescence is a remarkable example for the generation of electromagnetic radiation in the ultraviolet, visible or infrared region as a result of chemical reaction in a direct or indirect way. In the direct chemiluminescence, the chemical reaction yields a primary excited state intermediate or product, which luminesces. In the indirect way, the excited state molecule donates its energy to another molecule, which then emits light. If the chemical reaction is triggered by enzymatic process or takes place within a living organism, the phenomenon is referred to as bioluminescence[88].

Chemiluminescence is not a common process for every molecule. For a molecule to undergo a chemiluminescence emission, there are some essential requirements.

(1) The chemical reaction has to be sufficiently exothermic to generate electronically excited state molecules for chemiluminescence.

(2) The reaction pathway should be favourable to supply energy for generation of electronically excited state. If the chemical energy is wasted as heat, the chemiluminescent reaction does not take place.

(3) Photon emission should have a favourable deactivation pathway. The proportion of other competitive non-radiative processes should be low enough compared to radiative chemiluminescence process [87,88].

In all the luminescence process, the intensity of emission is associated with the efficiency of the process. This efficiency is defined as quantum yield. The overall quantum yield of the chemiluminescent reaction is described as the number of photons emitted per number of molecules involved in a chemical reaction.

Up to now, many different chemiluminescent compounds have been synthesized. Lophine is the first synthetic chemiluminescent compound synthesized by Radziszewski. Lophine generates green light as a result of its reaction with oxygen in the presence of a strong base. The other organic chemiluminescent compounds are shown in Figure 1.14.[89,90].

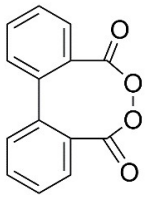

Diphenoyl Peroxide

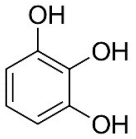

Benzene-1,2,3-triol

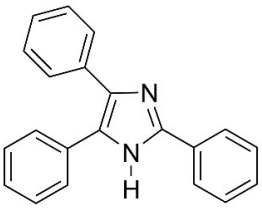

2,4,5-Triphenylimidazole
(Lophine)

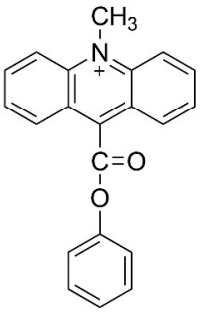

Acridinium Ester

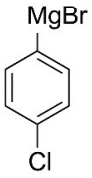

p-Chlorophenyl
Magnesiumbromide

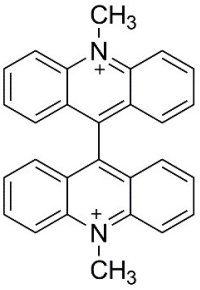

Dimethylbisacridinium
Nitrate (Lucigenin)

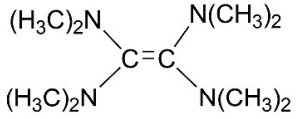

Tetrakis(dimethylamino) Ethylene

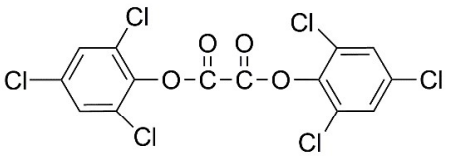

Bis(2,4,6-trichlorophenyl) Oxalate

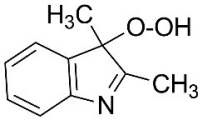

3-Hydroperoxy-2,3-
dimethyl-3H-indole

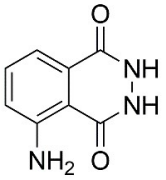

5-Amino-2,3-dihydrophthalazine-1,4-dione
(Luminol)

Figure 1.14. The common organic chemiluminescent compounds[90].

1.6.1 Common Organic Chemiluminescent Compounds

1.6.1.1 Phthalhydrazides (Luminol)

Chemiluminescence as an extensively used photon emission technique, has been the topic of many research papers due to its high quantum efficiency, high sensitivity, basic instrumentation without an external light source and low cost[91,92,93,94]. In this sense, luminol (3-aminophthalhyrazide) is the most widely utilized chemiluminescent material synthesized in 1853. However, its chemiluminescent property was discovered and reported by Albrecht in 1928 for the first time[95,96,97].

Luminol reaction follows a direct pathway in which the excited 3-aminophthalate dianion returns to the ground state by emitting green-blue light between 375 – 500 nm in a basic medium (pH= 8 - 11) involving protic solvents (i.e. water, ethanol) in the presence of an oxidizing agent together with a proper catalyst, especially metal ions. A wide range of catalysts such as transition metals or metal complexes can be used to trigger the chemiluminescent reaction of luminol, but the optimum conditions can change depending on the type of catalyst. The chemiluminescent process of luminol is also strongly affected by temperature, pH, ionic strength, solution composition, types of metal ions and oxidizing agents. The reaction mechanism of luminol is depicted in Scheme 1.6 [91,98,99,100].

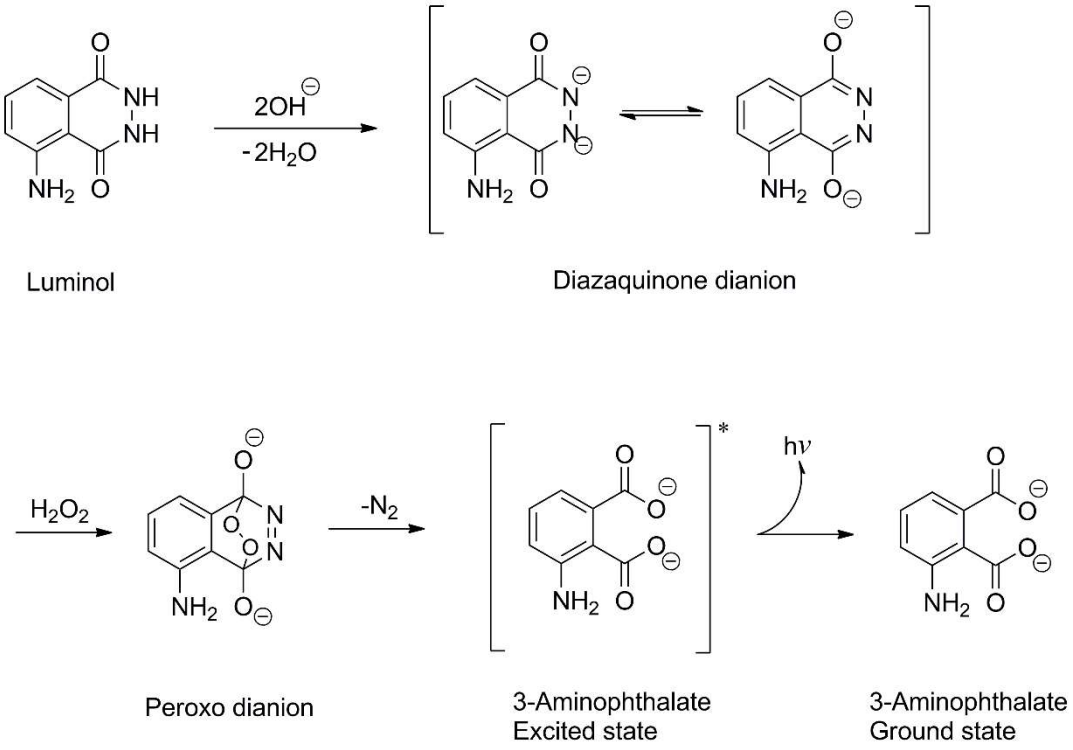

Scheme 1.6. CL reaction mechanism of luminol to produce light[99].

For luminol, quantum efficiency is found to be around 1%. However, its efficiency can be increased through structural modifications on it. Some luminol derivatives are illustrated in Figure 1.15 [98,101,102].

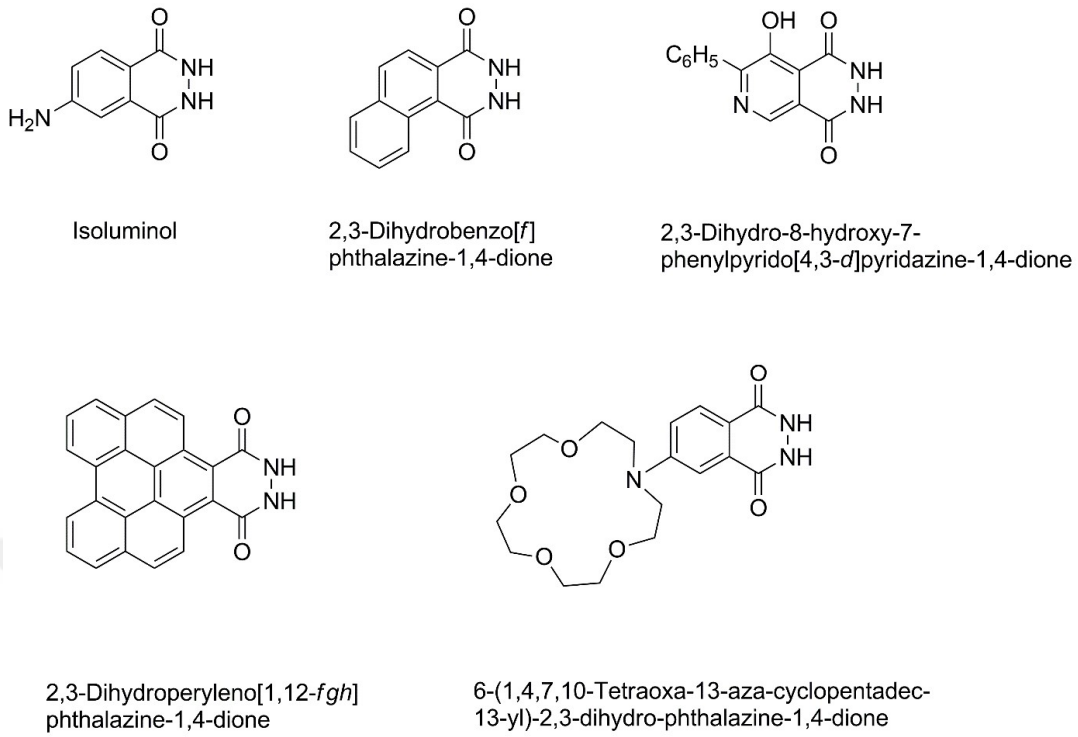

Figure 1.15. Some luminol derivatives.

Luminol can be used for many different applications especially as a sensor for the determination of biologically active compounds such as glucose, lactic acid, dopamine, folic acid and so on [103,104,105]. It can also be utilized in the analysis of food, pesticide as well as air pollution. Most importantly, it is commonly used for blood detection in forensic science [99,106,107].

1.7 Phthalimide Type Acceptor

1.7.1 Chemical Structure

Phthalimide (PI) is an imido derivative formed from phthalic acid. In organic chemistry, imide as a functional group involves two carbonyl groups connected to a nitrogen atom. Their structures resemble acid anhydrides. Imides are generally cyclic compounds which are derived from dicarboxylic acids, therefore they

receive their names from the parent acid. Since the imide groups are highly polar due to N-H center, they are soluble in polar solvents and can form hydrogen bonds as well. Furthermore, imides are acidic in nature and their acidity is more than amides because the adjacent C=O groups weaken the N-H bond due to electron withdrawing inductive effect and more resonance stabilization is afforded due to more delocalization of the negative charge. The chemical structure of PI and its resonance forms after removal of a proton is shown in Scheme 1.7 [108,109].

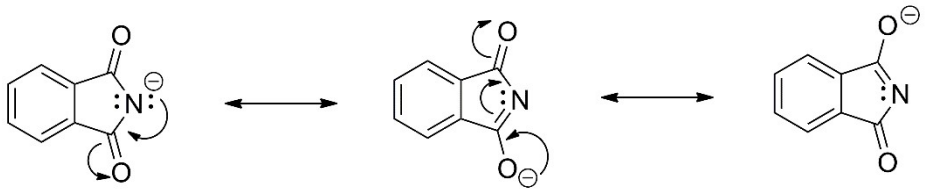

Scheme 1.7. The PI and its resonance forms after loss of a proton[110].

Phthalimides possess many outstanding properties such as oxidative stability, solvent resistance, good mechanical properties as well as symmetric, rigid and coplanar structure with an electron-withdrawing nature. Therefore, PI and N-substituted phthalimides represent a significant class of materials for a wide range of applications from the pharmaceutical industry to photovoltaics, from dye industry to plant growth regulation[108,109,110,111].

More importantly, phthalimides and N-substituted phthalimides are generally used for constructing organic π-conjugated materials, especially for high performance device applications. Since the phthalimides possess a small aromatic core with a good electron-withdrawing ability, they play a prominent role in D-A type conjugated polymers to tune their chemical structure and physical properties. Furthermore, it is easy and cheap to prepare PI from its starting material, phthalic anhydride, which renders the large scale synthesis. Lastly, stronger intermolecular and intramolecular interactions due to the incorporation of PI units between linking

bridges improve the π-π stacking properties and thereby facilitate the charge transport [112].

1.7.2 Synthesis

The synthesis of aliphatic or aromatic cyclic imides are achieved by the reaction of the corresponding anhydride or dicarboxylic acid derivatives with the reagent involving a reactive amino (-NH_2) group. The reaction takes place through the nucleophilic attack of the amino group to the anhydride unit. The mechanism for the synthesis of PI is depicted in Scheme 1.8 [108].

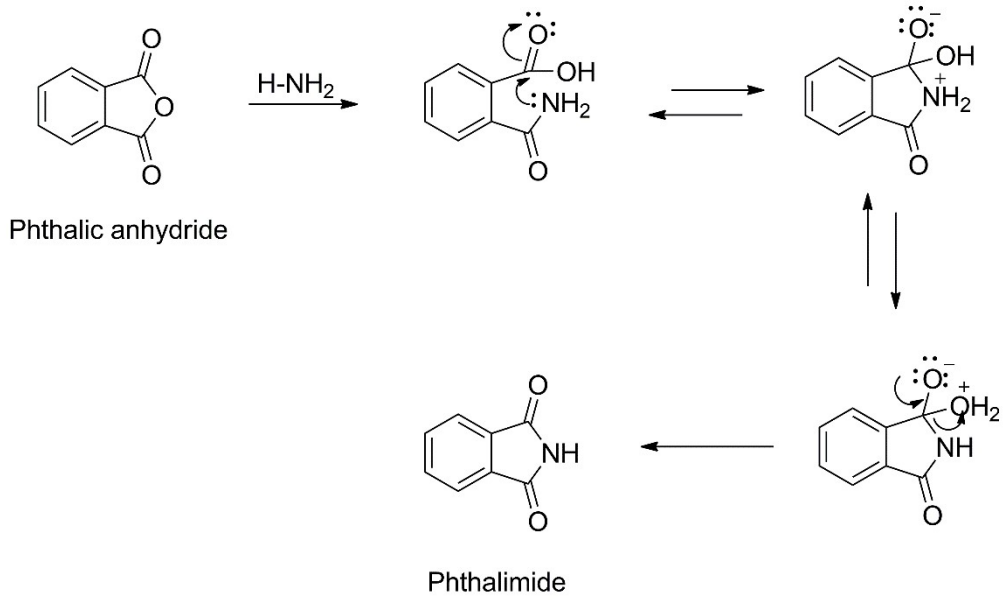

Scheme 1.8. Reaction mechanism for the imide formation reaction.

An alternative pathway for the synthesis of imides is the direct condensation of cyclic anhydrides or dicarboxylic acids with the formamide. In this synthetic route, the formamide can also act as the solvent, especially for aliphatic imides. For aromatic cyclic imides which are barely soluble in formamide, another suitable solvent is required to provide a homogenous reaction medium and high yield in the desired product[108].

1.8 Thieno[3,4-c]pyrrole-4,6-dione Type Acceptor

1.8.1 Chemical Structure

Thieno[3,4-*c*]pyrrole-4,6-dione (TPD) is the analog of PI obtained by substituting thiophene ring instead of benzene ring[113]. TPD unit (See Fig. 1.16) exhibits more quinoidal character due to the smaller aromatic energy of its thiophene ring as compared to that of the phenyl ring. Its enhanced quinoidal character not only imparts more delocalization to π-electrons but also imparts better skeleton coplanarity to the TPD core as compared to benzene-substituted analogs. Furthermore, two electron-withdrawing C=O groups at the 3,4-positions of thiophene ring in the TPD unit enhance the electron affinity and hence prevent the uplift of HOMO energy level for better matching with those of the donor units. In addition, intramolecular noncovalent S···O interactions exist between oxygen atoms of imide carbonyl groups and thienyl sulfur atoms, which unavoidably enhances the π-system coplanarity and further improves the ICT effect, affords lower band gap. More significantly, this S···O interaction can serve as a conformational lock to afford a large π-conjugated chain by appending TPD moiety into small aromatic systems. Lastly, due to the electron rich character of thiophene, the electrophilic attack to the α-position of the TPD unit can readily take place even than that of the PI counterpart, which enables the easy functionalization of imide group on the TPD core unit. Due to this facile substitution at the imide nitrogen with various functional groups, it is possible to impart solubility into the conjugated system and to control solid-state packing of the conjugated backbone without disrupting close π-π stacking for efficient charge carrier transport [114,115].

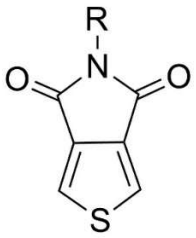

Figure 1.16. Chemical structure of TPD core unit.

1.8.2 Synthesis

The most common synthesis pathway of TPD involves three steps. In the first step, the hydrolysis of 3,4-thiophenedicarboxylic acid takes place when heated with acetic anyhdride (Ac_2O) to give the corresponding thiophene anhydride. The next step is followed by the condensation of thiophene anhydride with an amine compound. In the final step, ring closure occurs by using thionyl chloride ($SOCl_2$) in the presence of heat. However, the overall yield in this pathway is lower than expected due to the harsh reaction conditions such as high temperature or presence of $SOCl_2$, which results in the decomposition of the main product[116]. The reaction pathway is given in Scheme 1.9.

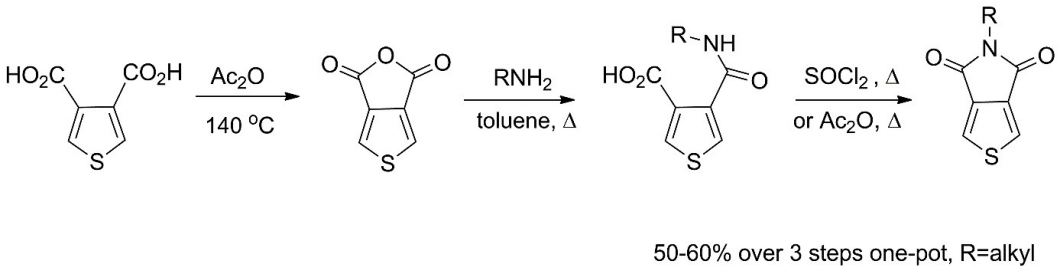

Scheme 1.9. Synthesis of TPD unit from 3,4-thiophenedicarboxylic acid in three steps.

The synthesis of TPD core unit can also be carried out from 3,4-dibromothiophene in three steps as shown in Scheme 1.10.

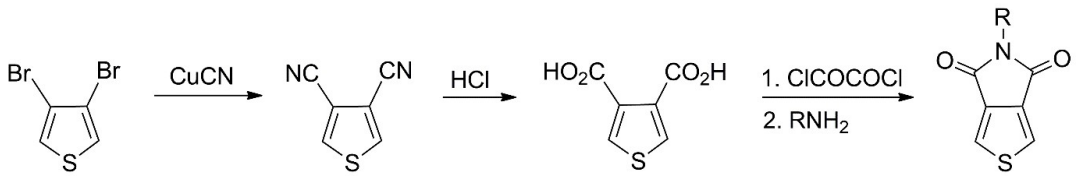

Scheme 1.10. Synthesis of TPD unit from 3,4-dibromothiophene in three steps.

1.9 Phthalhyrazide Type Acceptor

1.9.1 Chemical Structure

Cyclic azo compounds have received great attention of organic chemists with the development of new efficient synthesis methods. Among a wide variety of nitrogen containing heterocycles, polycyclic pyridazines are the most attractive ones since they are extensively used for many different applications from clinical applications to pharmacological activities. They have also unique optical and electrical properties[117,118]. In this structure, phthalhydrazide (PH) (1,4-phthalazinedione) is a bicyclic hydrazide derivative with a six-membered bridgehead phthalazine ring involving two C=O groups in 1,4 positions and a fused benzene ring at the 2,3 position as shown in Figure 1.17.

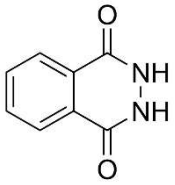

Figure 1.17. Chemical structure of PH.

There exist three possible tautomeric structures for PH but only one of the amide groups can tautomerize, not both of them at the same time (tautomerism only between 1 and 1b) as shown in Figure 1.18. This is due to the pyramidal orientation of nitrogen bonds in nontautomerized form, which allows only one C=N-N group to fit into a nonplanar structure without distortion of bond angle.

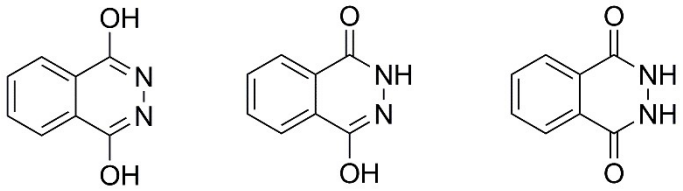

1a 1 1b

Figure 1.18. Three possible tautomeric structures for PH.

The physical properties of phthalazine derivatives are associated with the corresponding naphthalene derivatives as the properties of pyridazines are similar to benzene counterparts. The most commonly studied compounds in this group are the luminol and its derivatives due to their chemiluminescence properties as mentioned previously [117,119,120,121]. However, the use of phthalhydrazines as an acceptor for conductive polymer applications is very limited especially due to their solubility problem, destruction of the chemiluminescent unit and so on. Only a few publications report their use as organic polymer materials[122,123].

1.9.2 Synthesis

The cyclic hydrazide derivatives can be synthesized from the corresponding phthalic acid, ester, anhydride or imide derivatives when treated with a properly substituted hydrazine reagent. In the case of PH, the heating of PI derivative in the appropriate solvent containing hydrazine results in the formation of the main product, PH, together with the free amine [120]. The single step synthesis pathway is shown in Scheme 1.11.

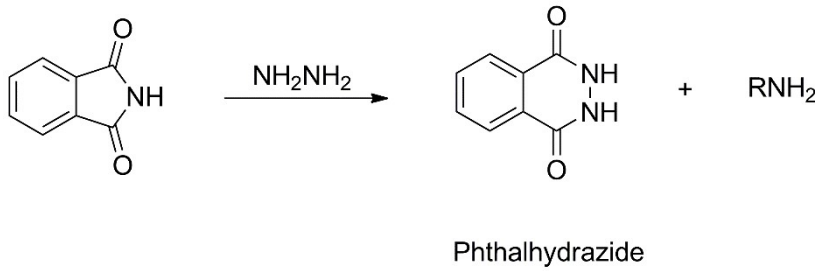

Scheme 1.11. Synthesis of phthalhydrazide from PI derivative.

Alternatively, phthalhydrazides can be synthesized in a single step from the phthalic acid derivative. When the phthalic acid is heated in a high-boiling solvent in the presence of hydrazine, acyl substitution reaction takes place with the removal of water to give the main product, PH similar to luminol synthesis [120], as shown in Scheme 1.12.

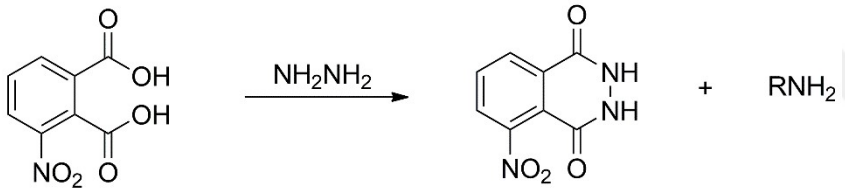

Scheme 1.12. Synthesis of phthalhydrazide from phthalic acid derivative.

1.10 Substituents

1.10.1 Polyhedral Oligomeric Silsesquioxanes

Silsesquioxanes are rigid and crystalline silica-like core structures with the general formula of $RSiO_{1.5}$ where R refers to a hydrogen atom or organic group. They can be formed as random, ladder or cage structures. Nowadays, the interest has been focused on the specific cage structures, which are commonly named as polyhedral oligomeric silsesquioxanes (POSS). These are 3-dimensional nano-sized cage structures ranging from 1 nm to 3 nm with alternated Si - O bonds. The cage

structure in Figure 1.19 involves eight corners which is abbreviated as T8 POSS and each vertex of this polyhedra is occupied by Si atoms. The vertex positions can be functionalized with many different reactive or unreactive organic groups such as alkyl, alkylene, acrylate, ester, chloro, hydroxyl, norborenyl or epoxide, which enables the incorporation of POSS into polymer backbone or network. The vertex substituents can be the same or different. According to this, two main types of T8 POSS molecules exist. In the first type, T8 POSS involves eight reactive or unreactive corner groups of the same kind. In the second type, T8 POSS bears only one reactive group and seven unreactive groups which are known as monofunctional POSS molecules. Unlike organic compounds, POSS derivatives are non-volatile, odorless and environmentally friendly. They are also good candidates to develop novel hybrid materials with improved mechanical, thermal and electrochemical properties[124,125,126,127]. The amine functionalized-POSS cages can be easily incorporated into phthalic anhydride unit to obtain POSS bearing PI derivative.

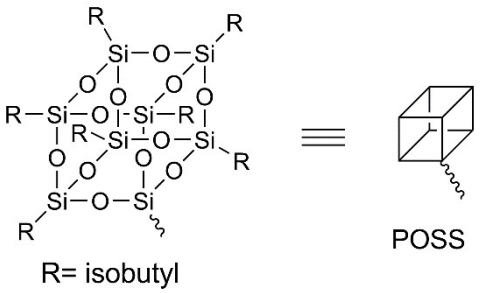

Figure 1.19. The chemical structure of POSS.

1.10.2 Azobenzene

Azo compounds represent an important class of organic molecules in the dye industry. Azo compounds are synthetic coloring agents which are widely used for the coloration of food, drugs, cosmetics and so on. Azobenzene as a small aromatic

member of azo molecules contains two phenyl rings connected by an azo group (N=N), as shown in Scheme 1.13. This class of compounds has some common properties such as strong electronic absorption and unique photochemistry. In particular, the conjugated azo chromophores exhibit strong absorption in the UV-Vis range of spectrum and their exact spectrum can be tuned by the ring-substitution pattern. The most interesting behavior of azo compounds is their reversible photo-switching character depending on the irradiation with light within the absorption range. Azobenzenes undergo trans-cis isomerization between two conformational states. The trans form is thermally stable whereas the cis configuration is metastable. Upon irradiation with UV light, trans azobenzenes are converted to cis form, which eventually returns to a more stable trans form on a timescale determined the substitution pattern of molecule. The trans-cis isomerization of azobenzene can also be achieved by mechanical stress or electrostatic stimulation. The presence of the substituents on aryl rings can change the rate and efficiency of trans-cis isomerization. Owing to its photochromic properties, azobenzene and its derivatives are extensively used to generate functional and photo-responsive materials for the applications of molecular devices and functional materials. Due to their robust and amenable character, they can easily incorporate into a broad variety of materials. The amine-functionalized azobenzene can be combined with thieno[3,4-c]furan-1,3-dione unit to synthesize the TPD derivative with the desired photochromic property [128,129,130,131].

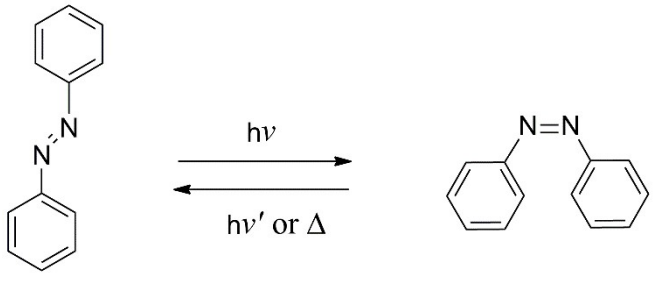

Scheme 1.13. Trans-cis isomerization of azobenzene.

1.10.3 Fluorene

Fluorene or 9*H*-fluorene is an isocyclic aromatic compound containing rigid planar biphenyl rings that are linked by a direct C-C bond and an adjacent methylene bridge in the 9 position with a high electronic symmetry, Figure 1.20. The methylene bridge provides the planarity of two phenyl rings, which improves their orbital overlap, rigidity and hence afford a high degree of conjugation in the aromatic system. Owing to the highly conjugated planar π-electron system, fluorene exhibits strong violet fluorescence and hence receives its name. Some fluorene derivatives have such a high fluorescence efficiency that their quantum yield can approach "unity". The acidity of protons in methylene bridge offers an active site for condensation reactions. Therefore, this position has the privilege of introducing side groups to provide functionality and processability in the resulting moiety. For example, alkylation of C-9 position of fluorenes enhances the solubility in organic solvents. The substitution at the methylene group can also tailor the electronic properties. Moreover, the aromatic hydrogens are also reactive towards electrophilic substitution reactions, especially at 2,7 and 4,5 positions. The functionalization of fluorenes on the aromatic ring or 9-fluorenyl position paves the way for the synthesis of unique fluorene derivatives with outstanding properties to be used for many different applications such as optoelectronics in material science or fluorescent markers in biomedical research [132,133,134].

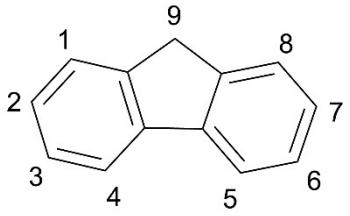

Figure 1.20. Chemical structure and atomic numbering of fluorene.

1.11 The Aim of Study

This study involves the synthesis and characterization of conjugated polymers based on D-A-D type monomers. The main aim of this study is to synthesize novel acceptor units that can be coupled with common donor moieties and to investigate their optical and electronic properties as well as their potential applications. The content of the thesis can be divided into three different parts depending on the type of acceptor unit.

First Part:

It is known that phthalimides have some promising properties such as low lying HOMO level, facile synthesis and easy functionalization at the imide nitrogen, which allow their use, especially for optoelectronic applications. A wide variety of different reagents with the amine functional group can be appended to the phthalic anhydride moiety through imidization reaction to obtain desired PI derivative. For this purpose, an inorganic-based amine compound, aminopropyl isobutyl POSS was chosen as a substituent to create a hybrid system bearing the advantages of both organic and inorganic components in a single structure. To enlight the effect of POSS cage on the PI acceptor unit, propylamine analogs were also synthesized for comparison sake. The substituted acceptor units were used together with thiophene and EDOT donor units to synthesize new D-A-D type monomers via Stille cross coupling reactions. The electrochemical and optical properties of these monomers and their corresponding polymers were investigated in terms of acceptor and ICT strength to elucidate the effect of the substituent on the acceptor unit as well as monomer and polymer film[135]. The synthesized D-A-D type monomers, T(PI-POSS)T, T(PI-Propyl)T, E(PI-POSS)E and E(PI-Propyl)E are depicted in Figure 1.21.

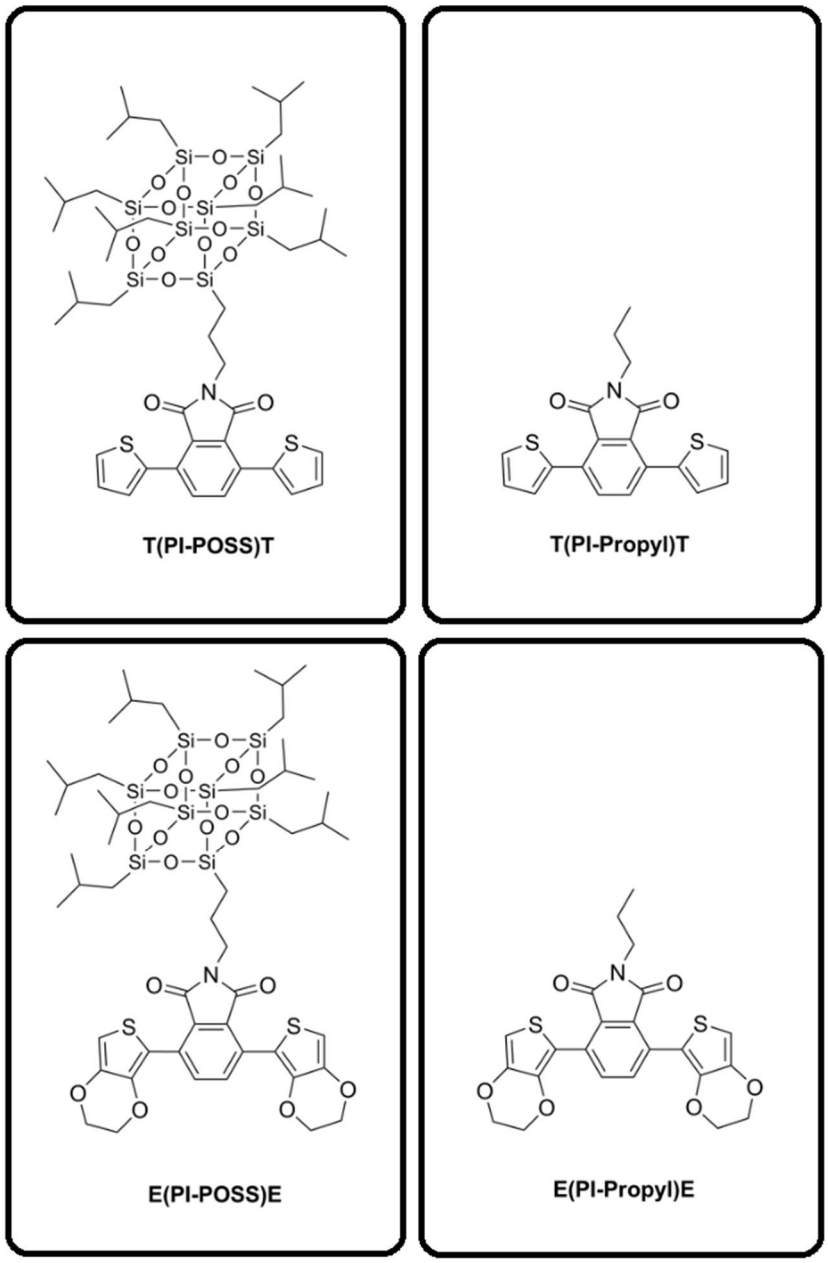

Figure 1.21. D-A-D monomers based on PI-POSS and PI-Propyl acceptor units.

Second Part:

It is known that TPD is an extensively used acceptor unit for the synthesis of new conjugated polymers. TPD unit presents a number of fascinating properties due to its symmetric, compact, coplanar structure, strong electron-deficient character and easily functionalized bridging nitrogen center. Therefore, this particular unit is utilized for several diverse applications such as high performance organic photovoltaics, field-effect transistors and light emitting diodes and so on. However, up to now, there are a limited number of studies for electrochromic applications of this acceptor unit. Furthermore, in the literature, only alkyl derivatives of the TPD units have been utilized for these applications[6]. In this respect, in our study, a series of novel TPD derivatives were synthesized with three different substituents and these new acceptor units, as well as their alkyl-substituted analog were employed for constructing new D-A-D type monomer and polymers, via Stille cross coupling reactions. For this purpose, thiophene, EDOT and dialkyl-substituted ProDOT were selected as the donor units. Didecyl-substituted ProDOT unit was preferred to prepare soluble conjugated polymer derivatives. Electrochemical and optical properties of the resulting monomers and polymers were investigated in terms of the donor group strength. In order to deduce the effect of substituent on the TPD core unit, these monomers were also compared with the other TPD counterparts consisting of different kind of pendant group for the same donor unit. The synthesized monomers can be divided into four categories depending on the type of acceptor unit.

In the first series, ethylhexyl-substituted TPD unit, 1,3-dibromo-5-(2-ethylhexyl)-4*H*-thieno[3,4-*c*]pyrrole-4,6(5*H*)-dione and three donor units, thiophene, EDOT and didecyl-substituted ProDOT were used to synthesize three new D-A-D monomers, T(TPD-EtHex)T (5-(2-ethylhexyl)-1,3-di(thienyl-2-yl)-4*H*-thieno[3,4-*c*]pyrrole-4,6(5*H*)-dione), E(TPD-EtHex)E (1,3-bis(2,3-dihydrothieno[3,4-*b*][1,4]dioxin-5-yl)-5-(2-ethylhexyl)-4*H*-thieno[3,4-*c*]pyrrole-4,6(5*H*)-dione) and P(TPD-EtHex)P (1,3-bis(3,3-didecyl-3,4-dihydro-2*H*-thieno[3,4-*b*][1,4]dioxepin-6-yl)-5-(2-ethylhexyl)-4*H*-thieno[3,4-*c*]pyrrole-4,6(5*H*)-dione). Their corresponding

polymers, PT(TPD-EtHex)T, PE(TPD-EtHex)E and PP(TPD-EtHex)P were synthesized via electrochemical polymerization. The soluble polymer derivative, PP(TPD-EtHex)P was also obtained via chemical polymerization method using chemical oxidative agent, $FeCl_3$. The synthesized monomer units were given in Figure 1.22.

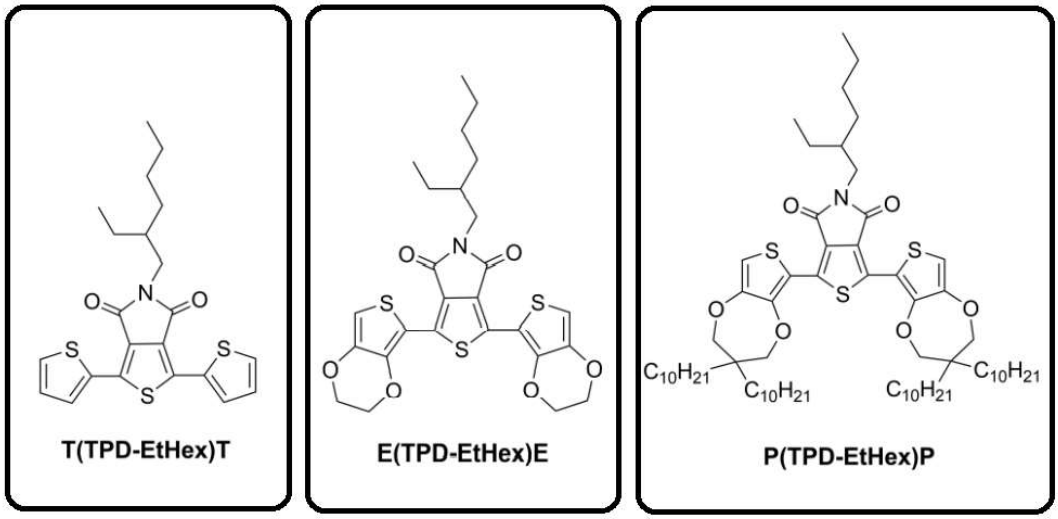

Figure 1.22. D-A-D monomers based on TPD-EtHex acceptor unit.

In the second series, propyl isobutyl POSS attached TPD derivative, 1,3-dibromo-5-(3-POSSpropyl)-thieno[3,4-*c*]pyrrole-4,6-dione, was utilized together with thiophene, EDOT and didecyl-substituted ProDOT donor groups to synthesize new TPD monomers, T(TPD-POSS)T (5-(3-POSSpropyl)-1,3-di(thienyl-2-yl)-4*H*-thieno[3,4-*c*]pyrrole-4,6(5*H*)-dione), E(TPD-POSS)E (1,3-bis(2,3-dihydrothieno[3,4-*b*][1,4]dioxin-5-yl)-5-(3-POSSpropyl)-4*H*-thieno[3,4-*c*]pyrrole-4,6(5*H*)-dione), and P(TPD-POSS)P (1,3-bis(3,3-didecyl-3,4-dihydro-2*H*-thieno[3,4-*b*][1,4]dioxepin-6-yl)-5-(3-POSSpropyl)-4*H*-thieno[3,4-*c*]pyrrole-4,6(5*H*)-dione). The optoelectronic properties of these monomers and their electrochemically obtained polymers (PT(TPD-POSS)T, PE(TPD-POSS)E and PP(TPD-POSS)P) were investigated from the perspective of donor unit and

substituent effect. The chemical polymerizations with $FeCl_3$ were also carried out to obtain soluble polymer derivatives. The synthesized monomers are shown in Figure 1.23.

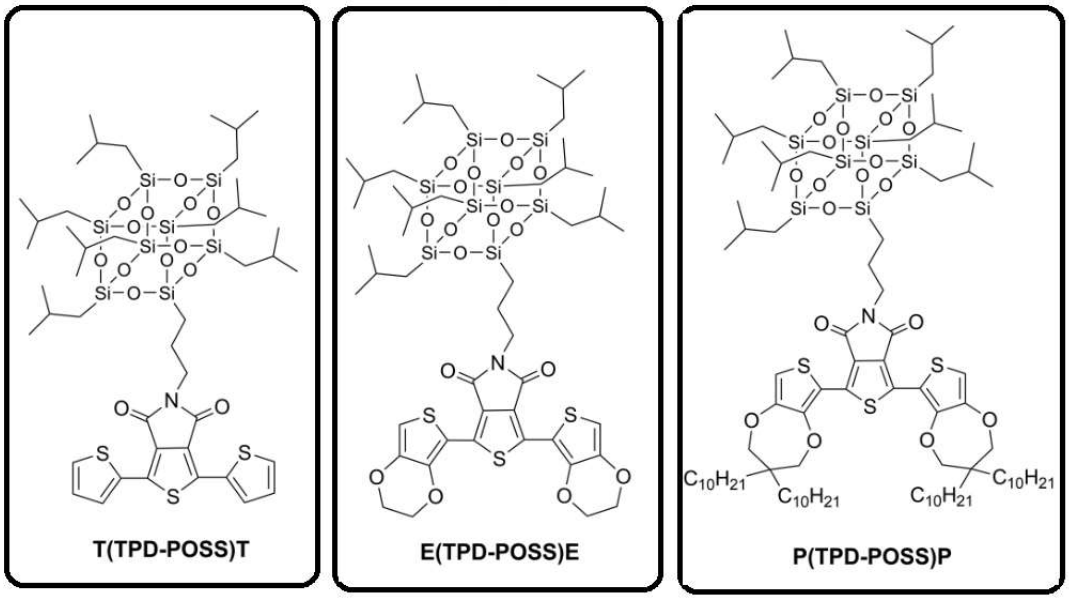

Figure 1.23. D-A-D monomers based on TPD-POSS acceptor unit.

In the third series, azobenzene-appended TPD core unit, 1,3-dibromo-5-(4-azobenzene)-thieno[3,4-*c*]pyrrole-4,6-dione was combined with thiophene, EDOT and didecyl-substituted ProDOT donor groups to obtain new D-A-D monomers, T(TPD-Azo)T (5-(4-azobenzene)-1,3-di(thienyl-2-yl)-4*H*-thieno[3,4-*c*]pyrrole-4,6(5*H*)-dione), E(TPD-Azo)E (1,3-bis(2,3-dihydrothieno[3,4-*b*][1,4]dioxin-5-yl)-5-(4-azobenzene)-4*H*-thieno[3,4-*c*]pyrrole-4,6(5*H*)-dione), and P(TPD-Azo)P (1,3-bis(3,3-didecyl-3,4-dihydro-2*H*-thieno[3,4-*b*][1,4]dioxepin-6-yl)-5-(4-azobenzene)-4*H*-thieno[3,4-*c*]pyrrole-4,6(5*H*)-dione) (Figure 1.24). The monomers were polymerized by electrochemical method to acquire the corresponding polymers, PT(TPD-Azo)T, PE(TPD-Azo)E and PP(TPD-Azo)P. Only PP(TPD-Azo)P derivative was soluble. The substituent and donor group effect were studied by comparing the monomers and polymers with their related analogs.

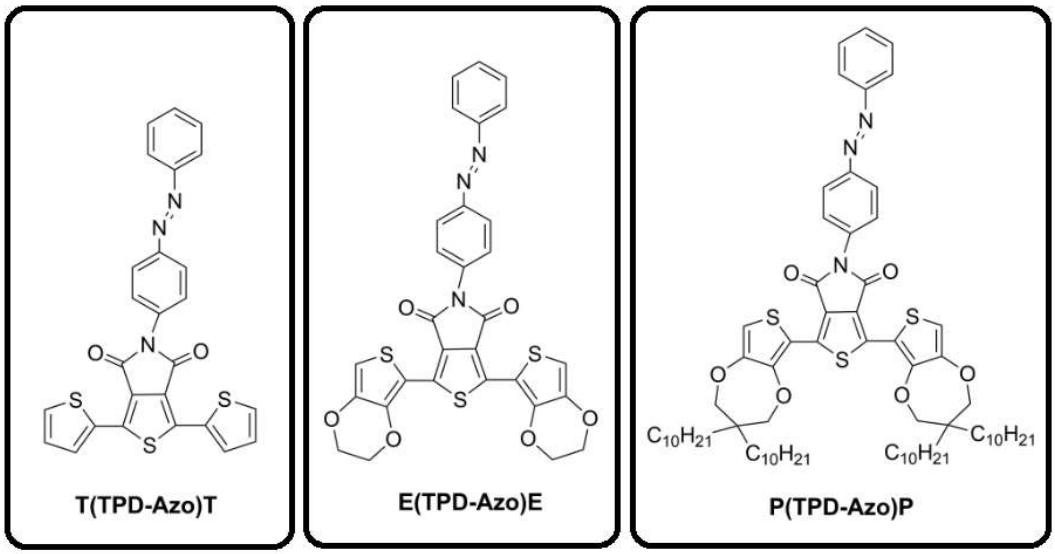

Figure 1.24. D-A-D monomers based on TPD-Azo acceptor unit.

In the last series, fluorene-substituted TPD unit, 1,3-dibromo-5-(2-fluorene)-thieno[3,4-*c*]pyrrole-4,6-dione was utilized to synthesize two new monomers with EDOT and didecyl-substituted ProDOT donor units, namely E(TPD-Fluo)E (1,3-bis(2,3-dihydrothieno[3,4-*b*][1,4]dioxin-5-yl)-5-(2-fluorene)-4*H*-thieno[3,4-*c*]pyrrole-4,6(5*H*)-dione), and P(TPD-Fluo)P (1,3-bis(3,3-didecyl-3,4-dihydro-2*H*-thieno[3,4-*b*][1,4]dioxepin-6-yl)-5-(2-fluorene)-4*H*-thieno[3,4-*c*]pyrrole-4,6(5*H*)-dione). The monomers were electrochemically polymerized to obtain the corresponding polymers, PE(TPD-Fluo)E and PP(TPD-Fluo)P. The monomers and polymers are depicted in Figure 1.25.

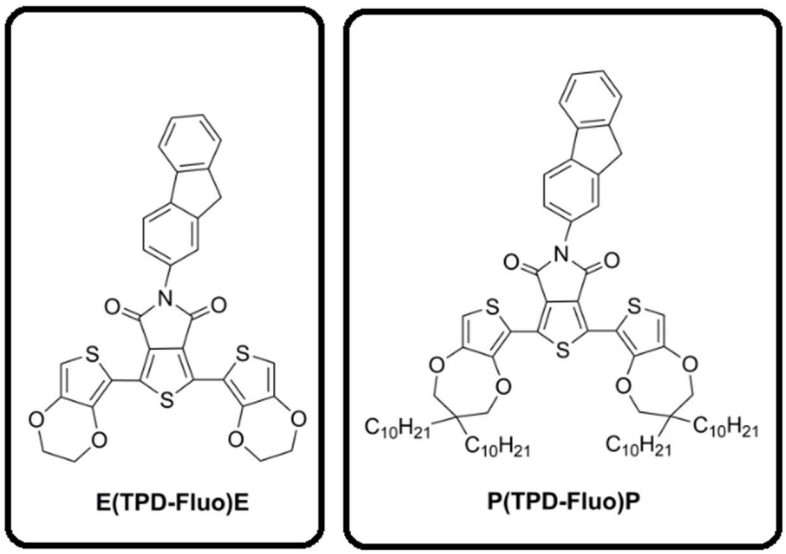

Figure 1.25. D-A-D monomers based on TPD-Fluo acceptor unit.

Third Part:

PH-type compounds possess a great potential for applications in forensic science and analytical sensors due to their chemiluminescent character. They can also have the potential of being used for the applications of light emitting diodes and electrochromic devices after integrated into trimeric monomers systems as well as the conjugated polymer chains[123]. In this part, a new D-A-D type PH derivative, E(PH)E (5,8-bis(2,3-dihydrothieno[3,4-*b*][1,4]dioxin-5-yl)-2,3-dihydrophthalazine-1,4-dione) was synthesized by using EDOT donor unit. The chemiluminescence properties of the resulting monomer was investigated as well as their optical and electrochemical properties. The monomer is shown in Figure 1.26.

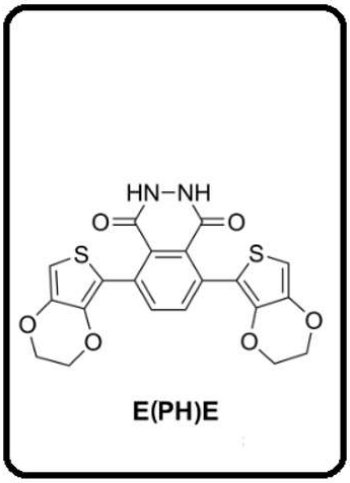

Figure 1.26. D-A-D monomer based on PH acceptor unit.

CHAPTER 2

EXPERIMENTAL

2.1 Materials

All chemicals and reagents were purchased from Merck, Sigma-Aldrich, TCI, Fluka, Acros, Riedel de Haen unless otherwise stated. THF, toluene, MeCN, DCM, ethanol, hexane, and ethyl acetate (EtOAc) were distilled prior their use. THF was refluxed with sodium and benzophenone until the appearance of blue color and distilled after 2 h. Toluene, MeCN and DCM were stirred with CaH_2 overnight and then distilled over it. Ethanol was refluxed with magnesium/iodine until the disappearance of brick color and distilled over it after 2 h. Simple distillation method was used for the distillation of hexane and ethylacetate.

Origin of all chemicals used in this work are given below:

Sodium metal, calcium hydride (CaH_2) (Sigma Aldrich, 95%), benzophenone (Sigma Aldrich, 99%) glacial acetic acid (Merck, 100%), acetic anhydride (Merck, ≥98.5 %), 1,4-dioxane (Acros Chemical, 99%), hydrazinum hydroxide (Merck, 80 %), chloroform (Sigma-Aldrich, 99 - 99.4%), DCM (Merck, ≥99%), ethyl acetate (Sigma Aldrich, ≥99.5%), thionyl chloride (Sigma Aldrich, ≥99%), sulfuric acid (Sigma Aldrich), 1-bromodecane (Sigma Aldrich, 98%), diethylmalonate (Aldrich, 99%), $LiAlH_4$ (Merck), 3,4-dimethoxythiophene (Sigma Aldrich, 97%), toluene-4-sulfonic acid monohydrate (Merck, ≥99%), 3,4-ethylenedioxythiophene (EDOT) (Sigma Aldrich, 97%), n-buthyllithium (n-BuLi) (Sigma Aldrich, 2.5 M in hexane), tributyltin chloride (Sigma Aldrich, 96%), 2-(tributylstannyl)thiophene (Sigma Aldrich, 97%), 3,6-dibromophthalic anhydride (TCI, >98%), 2,5-dibromo-3,4-dicarboxylic acid (Henan Tianfu Chemical Co., 98%), 1,3-dibromo-5-(2-ethylhexyl)-4*H*-thieno[3,4-*c*]pyrrole-4,6(5*H*)-dione (Sigma Aldrich, 97%), 4,7-

dibromo-2-(2-ethylhexyl)isoindoline-1,3-dione (Lumtec, >97%) propylamine (Sigma Aldrich, ≥99%), aminopropyl isobutyl POSS (Hybrid Plastics), 4-aminoazobenzene (TCI, >98%), 2-aminofluorene (Avocado Research Chemicals, 98%), bis(triphenylphospine)palladium(II) dichloride (Sigma Aldrich, 98%), magnesium sulfate (Sigma Aldrich, ≥98%), chloroform-D1 (Merck, deuteration degree min. 99.8%), dimethly sulfoxide-D6 (Merck, deuteration degree min. 99.8%), TLC aluminum sheets (Merck, 20 x 20, Silica gel 60 F254), aluminum oxide (Al_2O_3) (Fluka, Brokmann activity II; basic), silica gel (SiO_2) (Fluka, 0.060 – 0.200 mm, 60 Å), molecular sieves (Aldrich, 4 Å), tetrabutylammonium hexafluorophosphate ($TBAPF_6$) (Sigma Aldrich, 98%).

2.2 Instrumentation

NMR spectra were recorded using a Bruker Spectrospin Avance DPX-400 Spectrometer with tetramethylsilane (TMS) as the internal standard and chemical shifts were recorded in ppm units. High resolution mass spectra (HRMS) were obtained on a Waters SYNAPT G1 mass spectrometer under the electron impact (EI) mode. Gel Permeation Chromatography analysis was performed on Malvern Omnisec GPC system. TGA measurements were performed using Perkin Elmer Pyris 1 TGA instrument. UV-Vis absorption spectra were obtained by a Specord S600 spectrometer or Cary 60 model UV-Vis spectrometer. Colorimetric measurements were recorded on a Specord S600 spectrometer (standard illuminator D65, field of width 10° observer) and color space was defined by the International Commission of Illumination with luminance (L*), hue (a*) and intensity (b*) with the references of platinum cobalt DIN ISO 621, iodine DIN EN 1557 and Gardner DIN ISO 6430. Fluorescence emission spectra were acquired on Varian Cary Eclipse Fluorescence Spectrometer. FTIR spectra was obtained by Thermo Scientific Nicolet iS10 FTIR Spectrometer. Electrochemistry measurements were taken on Gamry PCl4/300 potentiostat-galvanostat system. Spectroelectrochemistry measurements were performed on a Specord S600 spectrometer combined with a

Gamry Reference 600 potentiostat-galvanostat. The cis-trans isomerization was carried out in a quartz cell and Sylvania Mercury lamp (100 watts) was used for irradiating the samples. Chemiluminescence measurements were carried out by Pro-K.2000 Rapid Kinetic System and the intensity of the emitted light was measured by using a photomultiplier tube in dark environment.

2.3 Synthesis of Acceptor Units

2.3.1 Synthesis of Phthalimide Type Acceptors (PI)

2.3.1.1 Synthesis of N-(3-POSSpropyl)-3,6-dibromophthalimide (PI-POSS)

A mixture of 3,6-dibromophthalic anhydride (101 mg, 0.33 mmol) and propylamine-POSS (317 mg, 0.36 mmol) in 15 mL of glacial acetic acid was heated to reflux for 4 h with stirring in a nitrogen flow[136,137]. After cooling the reaction mixture, the solvent was evaporated under vacuum and the crude mixture was washed with acetone to obtain the title compound as a white solid with 39% yield. ^{1}H-NMR (400 MHz, $CDCl_3$, δ/ppm): 7.58 (s, 2H), 3.61 (t, J = 7.1 Hz, 2H), 1.84 – 1.69 (m, 9H), 90 – 0.84 (m, 42H), 0.52 (dd, J = 6.9, 4.3 Hz, 16H) ; ^{13}C-NMR (100 MHz, $CDCl_3$, δ/ppm): 164.69, 139.45, 131.32, 117.47, 41.01, 25.69, 23.86, 22.49, 22.39, 21.92, 9.60.

2.3.1.2 Synthesis of N-propyl-3,6-dibromophthalimide (PI-Propyl)

In a two-necked round bottom flask, 3,6-dibromo phthalic anhydride (109 mg, 0.36 mmol) was dissolved in 15 mL of glacial acetic acid under nitrogen atmosphere. Propylamine (33 µL, 0.40 mmol) was added and the reaction mixture was refluxed for 4 h under inert atmosphere[136,137]. The reaction mixture was cooled down and glacial acetic acid was removed under reduced pressure and washed with excess ethanol to afford N-propyl-3,6-dibromophthalimide as a white solid with 61% yield

and used as obtained. ^{1}H-NMR (400 MHz, $CDCl_3$, δ/ppm): 7.66 (s, 2H), 3.71 – 3.63 (m, 2H), 1.77 – 1.66 (m, 2H), 0.96 (t, J = 7.4 Hz, 3H) ; ^{13}C-NMR (100 MHz, $CDCl_3$, δ/ppm): 164.89, 139.49, 131.29, 117.51, 40.19, 21.66, 11.33. HRMS calcd for $C_{11}H_9Br_2NO_2$, $[M+H]^+$: 347.9058, found: 347.9058.

2.3.2 Synthesis of Thieno[3,4-*c*]pyrrole-4,6-dione Type Acceptors (TPD)

2.3.2.1 Synthesis of 4,6-Dibromothieno[3,4-*c*]furan-1,3-dione

0.350 g of 2,5-dibromothiophene4-dicarboxylic acid (1.06 mmol) was added to 15 mL of Ac_2O in a 50 mL of two-neck flask. The mixture was refluxed at 75 ℃ for 3 h under inert atmosphere. After cooling to room temperature, Ac_2O was removed under reduced pressure to obtain the crude product. The crude product was washed with 1.0 mL of cold DCM and hexane and then recrytallized from toluene to obtain white crystals in a 80% yield[138,139].

2.3.2.2 Synthesis of 1,3-Dibromo-5-(3-POSSpropyl)-thieno[3,4-*c*]pyrrole-4,6-dione (TPD-POSS)

A mixture of 0.460 g of 4,6-dibromothieno[3,4-c]furan-1,3-dione (1.47 mmol) and 1.350 g of propylamine-POSS (1.54 mmol) in a 5 mL of freshly distilled and degassed THF was stirred at 50 ℃ for 4 h under inert atmosphere. Then, the cooled reaction mixture was concentrated under reduced pressure to remove all volatiles. Then, 3 mL of $SOCl_2$ was added to the crude product and heated to 55 ℃ for 3 h. The whole mixture content was cooled down and added dropwise to the mixture containing 50 mL of cold water and 25 mL of cold methanol. The resulting precipitate was recovered by filtration and washed with excess MeCN. The white product was obtained in 92% yield. ^{1}H-NMR (400 MHz, $CDCl_3$, δ/ppm): 3.59 (t, J = 6.5 Hz, 2H), 1.94 – 1.78 (m, 7H), 1.78 – 1.68 (m, 2H), 0.95 (d, J = 6.3 Hz, 42H),

0.65 – 0.53 (m, 16H) ; ^{13}C-NMR (100 MHz, $CDCl_3$, δ/ppm): 160.19, 134.84, 112.76, 41.31, 25.50, 23.86, 22.48, 22.38, 21.83, 9.53.

2.3.2.3 Synthesis of 1,3-Dibromo-5-(4-azobenzene)-thieno[3,4-*c*]pyrrole-4,6-dione (TPD-Azo)

0.280 g of 4,6-dibromothieno[3,4-*c*]furan-1,3-dione (0.90 mmol) and 0.195 g of 4-aminoazobenzene (0.99 mmol) were combined in a 3 mL of dry and oxygen free THF and heated to 50 ℃ for 4 h under good stirring. The reaction mixture was cooled down to room temperature and then THF was removed via rotary evaporator. After that, 2 mL of $SOCl_2$ was added to the reaction mixture and heated to 55 ℃ for 3 h and then cooled down. The reaction content was added dropwise to the cold mixture containing 50 mL of water and 25 mL of methanol. The precipitate was filtered off, washed with excess hot ethanol to remove residual 4-aminoazobenzene and dried in vacuum. The product was isolated as flaky orange precipitate in a yield of 84%. ^{1}H-NMR (400 MHz, $CDCl_3$, δ/ppm): 8.05 (d, J = 8.8 Hz, 2H), 7.94 (d, J = 6.68 Hz, 2H), 7.60 – 7.49 (m, 5H) ; ^{13}C-NMR (100 MHz, $CDCl_3$, δ/ppm): 159.03, 152.57, 151.77, 134.13, 133.57, 131.37, 129.15, 126.85, 123.49, 123.02, 114.53. HRMS calcd for $C_{18}H_9Br_2N_3O_2S$, $[M+H]^+$: 491.8840, found: 491.8828.

2.3.2.4 Synthesis of 1,3-Dibromo-5-(2-fluoerene)-thieno[3,4-*c*]pyrrole-4,6-dione (TPD-Fluo)

0.358 g of 4,6-dibromothieno[3,4-*c*]furan-1,3-dione (1.15 mmol) and 0.228 g of 2-aminofluorene (1.26 mmol) were added to a 5 mL of freshly distilled THF and then stirred at 50 ℃ for 4 h under an inert atmosphere. After cooling to the room temperature, THF was evaporated at a reduced pressure. The resulting mixture was stirred at 55 ℃ for 3 h after the addition of 3 mL of $SOCl_2$ and then allowed to reach room temperature. The final mixture was poured drop by drop into the cold

methanol: water mixture (25 mL:50 mL). The resulting precipitate was recovered by filtration, washed excessively with hot ethanol and dried under vacuum. The beige precipitate was isolated as the final product in 54% yield. ^{1}H-NMR (400 MHz, $CDCl_3$, δ/ppm): 7.88 (d, J = 8.1 Hz, 1H), 7.81 (d, J = 7.4 Hz, 1H), 7.56 (d, J = 7.4 Hz, 1H), 7.53 (s, 1H), 7.42 – 7.32 (m, 3H), 3.96 (s, 2H) ; ^{13}C-NMR (100 MHz, $CDCl_3$, δ/ppm): 159.56, 144.00, 143.60, 142.17, 140.73, 134.34, 129.80, 127.28, 126.95, 125.23, 125.11, 123.26, 120.26, 120.22, 114.11, 36.99. HRMS calcd for $C_{19}H_9Br_2NO_2S$, $[M+H]^+$: 475.8779, found: 475.8803.

2.4 Synthesis of Donor Units

2.4.1 Synthesis of 2-(Tributylstannyl)-3,4-ethylenedioxythiophene

EDOT (1.0 g, 7 mmol) was dissolved in freshly distilled THF (15 mL) under an argon atmosphere and cooled to -78 °C. To this solution, n-butyllithium (2.9 mL, 2.5 M in hexane) was added dropwise. The resulting mixture was stirred for 1.5 h at -78 °C. Then, tributyltin chloride (1.90 mL, 7 mmol) dissolved in 3 mL of dry THF was added dropwise. The mixture was allowed to reach room temperature slowly and stirred at this temperature overnight. After removing the THF, the residue was extracted with DCM and brine. The combined organic phases were dried over $MgSO_4$ and filtered. The solvent was evaporated to afford a product of light yellow oil and used without any further purification (97% yield). ^{1}H-NMR (400 MHz, $CDCl_3$, δ/ppm): 6.61 (s, 1H), 4.22 – 4.16 (m, 4H), 1.67 – 1.50 (m, 6H), 1.41 – 1.30 (m, 6H), 1.18 – 1.08 (m, 6H), 0.99 – 0.85 (m, 9H).

2.4.2 Synthesis of Tributyl(3,3-didecyl-3,4-dihydro-2H-thieno [3,4-*b*] [1,4]dioxepin-6-yl)stannane

Didecyl-ProDOT (1.25 g, 2.9 mmol) was dissolved in a 10 mL of dry THF under argon atmosphere. At -78 °C, n-butyllithium (1.2 mL, 2.5 M in hexane) was added

dropwise and the mixture was stirred for 1.5 h while maintaining the temperature at -78 °C. Tributyltin chloride (0.8 mL, 2.9 mmol) was dissolved in 2 mL THF and added to this solution dropwise. The mixture was warmed to room temperature slowly and stirred overnight. The solvent was removed under reduced pressure and the crude mixture was poured into DCM and washed with brine. The organic phase was separated and dried over $MgSO_4$. After filtration, the solvent was evaporated to obtain yellow oil product and used as obtained (93% yield). ^{1}H-NMR (400 MHz, $CDCl_3$, δ/ppm): 6.60 (s, 1H), 3.78 – 3.64 (m, 4H), 1.61 – 1.35 (m, 12H), 1.33 – 0.94 (m, 42H), 0.88 – 0.73 (m, 15H).

2.5 Synthesis of D- A- D Monomers

Stille cross-coupling reaction was used for the synthesis of D-A-D monomers. The acceptor (1 equiv) was dissolved in dry THF and purged with argon in a two-necked round flask. The mixture was heated until the reflux starts at around 72 °C. The donor (2.2 equiv) was added to the mixture dropwise after diluting with THF. After 1 h refluxing, 5% mol of $Pd(PPh_3)_2Cl_2$ was mixed with THF and added to the system dropwise. The reaction mixture was stirred at reflux temperature between 36 h and 48 h until the reaction has been completed. The progress of the reaction was followed by TLC. After the reaction mixture was cooled down to room temperature, the solvent was removed under vacuum. The crude product was washed with brine and DCM mixture three times and dried with anhydrous magnesium sulfate. For further purification, column chromatography and recrystallization techniques were used to obtain target compounds as described below[6].

2.5.1 Synthesis of D- A- D Monomers Based on PI Type Acceptor Unit

The monomer **T(PI-POSS)T**, **T(PI-Propyl)T**, **E(PI-POSS)E** and **E(PI-Propyl)E** were synthesized via Stille cross coupling reaction by using the brominated

acceptors; PI-POSS and PI-Propyl and the stannylated donors; thiophene and EDOT (2-(tributylstannyl)thiophene, 2-(tributylstannyl)-3,4-ethylenedioxythiophene) as described aforementioned procedure.

T(PI-POSS)T

The product was isolated as yellow solid from silica column by using hexane: EtOAc (10:1) as eluent (44% yield). ^{1}H-NMR (400 MHz, $CDCl_3$, δ/ppm): 7.70 (d, J= 3.63 Hz, 2H), 7.66 (s, 2H), 7.37 (d, J= 5.07 Hz, 2H), 7.07 (dd, J = 5.0, 3.8 Hz, 2H), 3.57 (t, J= 7.06 Hz, 2H), 1.79 – 1.71 (m, 7H), 1.60 – 1.51 (m, 2H), 0.85 (dd, J = 6.83, 8.24 Hz, 42H), 0.51 (dd, J = 6.9, 1.2 Hz, 16H) ; ^{13}C-NMR (100 MHz, $CDCl_3$, δ/ppm): 167.10, 137.26, 135.71, 132.23, 130.05, 127.98, 127.70, 127.51, 40.58, 25.74, 23.87, 22.52, 22.42, 22.04, 9.69. HRMS calcd for $C_{47}H_{77}NO_{14}Si_8S_2$, $[M+H]^+$: 1168.3018, found: 1168.3007.

T(PI-Propyl)T

It was obtained as yellow solid by purifiying with column chromatography with hexane: EtOAc (9:1) eluent system and further purification by recrystallization with hexane (46% yield). ^{1}H-NMR (400 MHz, $CDCl_3$, δ/ppm): 7.77 (d, J= 1.12 Hz, 2H), 7.46 (s, 2H), 7.18 – 7.15 (m, 2H), 3.64 (t, J= 7.3 Hz, 2H), 1.73 – 1.66 (m, 2H), 0.96 – 0.91 (m, 3H) ; ^{13}C-NMR (100 MHz, $CDCl_3$, δ/ppm): 167.28, 137.24, 135.78, 132.29, 130.00, 127.99, 127.70, 127.56, 39.74, 21.79, 11.41. HRMS calcd for $C_{19}H_{15}NO_2S_2$, $[M+H]^+$: 354.0622, found: 354.0626.

E(PI-POSS)E

The yellow solid was purified from silica column by using hexane: EtOAc (8:1) eluent sysyem with successive recrystallization from hexane (45% yield). ^{1}H-NMR (400 MHz, $CDCl_3$, δ/ppm): 7.70 (s, 2H), 6.50 (s, 2H), 4.25 (s, 8H), 3.63 (t, J= 7.0 Hz, 2H), 1.90 – 1.77 (m, 7H), 1.75 – 1.68 (m, 2H), 0.92 (dd, J = 11.9, 6.6 Hz, 42H), 0.57 (dd, J = 7.0, 3.8 Hz, 16H) ; ^{13}C-NMR (100 MHz, $CDCl_3$, δ/ppm): 166.58, 141.42, 140.22, 135.89, 129.16, 129.09, 111.29, 100.64, 64.49, 40.37,

25.69, 23.84, 22.50, 22.42, 22.10, 9.64. HRMS calcd for $C_{51}H_{81}NO_{18}Si_8S_2$, $[M+H]^+$: 1284.3128, found: 1284.3083.

E(PI-Propyl)E

The product was obtained as yellow solid by passing from silica column with hexane: EtOAc (10:1) eluent system (56% yield). ^{1}H-NMR (400 MHz, $CDCl_3$, δ/ppm): 7.71 (s, 2H), 6.50 (s, 2H), 4.26 (s, 8H), 3.6 (t, J= 7.20 Hz, 2H), 1.71 – 1.60 (m, 2H), 0.95 – 0.89 (t, J= 7.41 Hz, 3H) ; ^{13}C-NMR (100 MHz, $CDCl_3$, δ/ppm): 166.75, 141.44, 140.24, 135.96, 129.12, 111.24, 100.68, 64.53, 64.49, 39.52, 21.84, 11.34. HRMS calcd for $C_{23}H_{19}NO_6S_2$, $[M+H]^+$: 470.0732, found: 470.0721.

2.5.2 Synthesis of D- A- D Monomers Based on TPD Type Acceptor Units

The monomers were synthesized by Stille cross coupling reaction of TPD based brominated acceptor units (TPD-EtHex, TPD-POSS, TPD-Azo and TPD-Fluo) and stannylated thiophene, EDOT and didecyl-ProDOT donor units (2-(tributylstannyl)thiophene, 2-(tributylstannyl)-3,4-ethylenedioxythiophene and tributyl(3,3-didecyl-3,4-dihydro-2H-thieno [3,4-*b*] [1,4]dioxepin-6-yl)stannane) according to the procedure previously described[6].

T(TPD-EtHex)T

The green solid was afforded by using a hexane: EtOAc (25:1) eluent (82% yield). m.p.: 130 – 133 ˚C. ^{1}H-NMR (400 MHz, $CDCl_3$, δ/ppm): 7.94 (dd, J = 3.7, 1.0 Hz, 2H), 7.35 (dd, J = 5.1, 0.9 Hz, 2H), 7.04 (dd, J = 5.0, 3.8 Hz, 2H), 3.48 (d, J = 7.32 Hz, 2H), 1.81 – 1.70 (m, 1H), 1.32 – 1.19 (m, 8H), 0.72-0.92 (m, 6H) ; ^{13}C-NMR (100 MHz, $CDCl_3$, δ/ppm): 162.90, 136.45, 132.45, 129.91, 128.61, 128.44, 128.41, 42.50, 38.27, 30.61, 28.61, 23.91, 23.05, 14.11, 10.48. HRMS calcd for $C_{22}H_{23}NO_2S_3$, $[M+H]^+$: 430.0969, found: 430.0968.

E(TPD-EtHex)E

The product was obtained as orange solid by using silica column with hexane: EtOAc (24:1) eluent (60% yield). m.p. 195 – 198 ˚C. ^{1}H-NMR (400 MHz, $CDCl_3$, δ/ppm): 6.54 (s, 2H), 4.46 – 4.41 (m, 2H), 4.30 – 4.25 (m, 2H), 3.54 (d, J= 7.4 Hz, 2H), 1.81-1.91 (m, 1H), 1.54-1.60 (m, 2H), 1.24-1.36 (m, 6H), 0.84-0.93 (m, 6H) ; ^{13}C-NMR (100 MHz, $CDCl_3$, δ/ppm): 163.19, 141.05, 140.94, 134.38, 126.44, 109.56, 103.04, 65.48, 64.23, 42.31, 38.16, 30.60, 28.59, 23.90, 23.06, 14.09, 10.48. HRMS calcd for $C_{26}H_{27}NO_6S_3$, $[M+H]^+$: 546.1079, found: 546.1080.

P(TPD-EtHex)P

The oily green compound was obtained by purifiying with hexane: EtOAc (125:1) eluent system (76% yield). ^{1}H-NMR (400 MHz, $CDCl_3$, δ/ppm): 6.54 (s, 2H), 3.96 (s, 4H), 3.83 (s, 4H), 3.45 (d, J= 7.3 Hz, 2H), 1.83 – 1.70 (m, 1H), 1.65 – 1.50 (m, 2H), 1.32 – 1.12 (m, 80H), 0.88 – 0.75 (m, 18H) ; ^{13}C-NMR (100 MHz, $CDCl_3$, δ/ppm): 163.26, 149.03, 148.68, 135.00, 126.76, 113.73, 107.47, 77.71, 77.64, 43.86, 42.29, 38.17, 31.98, 31.92, 30.62, 30.53, 29.71, 29.66, 29.63, 29.37, 28.60, 26.84, 23.94, 23.06, 22.68, 14.09, 13.59, 10.49. HRMS calcd for $C_{68}H_{111}NO_6S_3$, $[M+H]^+$: 1134.7652, found: 1134.7652.

T(TPD-POSS)T

The purification was conducted via two successive silica gel column by using hexane: EtOAc (15:1) and hexane: DCM (5:1) and one alumina column with hexane: DCM (5:1) to obtain yellowish green solid compound (80% yield). ^{1}H-NMR (400 MHz, $CDCl_3$, δ/ppm): 8.01 (dd, J = 1.0, 3.71 Hz, 2H), 7.41 (dd, J = 1.03, 5.06 Hz, 2H), 7.10 (dd, J = 3.78, 5.02 Hz, 2H), 3.64 (t, J = 7.1 Hz, 2H), 1.90 – 1.74 (m, 9H), 0.94 (dd, J = 6.5, 5.3 Hz, 42H), 0.60 (dd, J = 6.9, 5.6 Hz, 16H) ; ^{13}C-NMR (100 MHz, $CDCl_3$, δ/ppm): 162.44, 136.39, 132.48, 129.87, 128.55, 128.51, 128.40, 40.94, 25.71, 23.87, 22.51, 22.41, 22.00, 9.63. HRMS calcd for $C_{45}H_{75}NO_{14}Si_8S_3$, $[M+H]^+$: 1174.2582, found: 1174.2827.

E(TPD-POSS)E

The purification was carried out by using two successive silica gel column chromatography with hexane: EtOAc (5:1) and hexane: DCM (5:1) eluent systems and one alumina column with hexane: DCM (5:2) to afford yellow crystalline solid (77% yield). ^{1}H-NMR (400 MHz, $CDCl_3$, δ/ppm): 6.53 (s, 2H), 4.45 – 4.40 (m, 4H), 4.33 – 4.24 (m, 4H), 3.62 (t, J = 7.1 Hz, 2H), 1.91 – 1.72 (m, 9H), 0.94 (dd, J = 6.6, 4.8 Hz, 42H), 0.59 (dd, J = 7.0, 5.0 Hz, 16H) ; ^{13}C-NMR (100 MHz, $CDCl_3$, δ/ppm): 162.77, 141.00, 140.89, 134.41, 126.42, 109.63, 103.03, 65.46, 64.21, 40.74, 25.68, 23.86, 22.50, 22.41, 22.07, 9.69. HRMS calcd for $C_{49}H_{79}NO_{18}Si_8S_3$, $[M+H]^+$: 1290.2692, found: 1290.3033.

P(TPD-POSS)P

The purification was achieved by silica gel with hexane: EtOAc (5:1) and hexane: DCM (5:1) as eluents and alumina column with hexane to obtain oily greenish orange compound (76% yield). ^{1}H-NMR (400 MHz, $CDCl_3$, δ/ppm): 6.62 (s, 2H), 4.03 (s, 4H), 3.91 (s, 4H), 3.61 (t, J = 6.7 Hz, 2H), 1.94 – 1.67 (m, 9H), 1.41 (s, 8H), 1.37 – 1.22 (m, 64H), 1.00 – 0.91 (m, 42H), 0.88 (t, J = 6.7 Hz, 12H), 0.60 (dd, J = 7.0, 4.1 Hz, 16H) ; ^{13}C-NMR (100 MHz, $CDCl_3$, δ/ppm): 161.08, 147.25, 146.90, 133.22, 125.04, 112.16, 105.78, 75.96, 75.88, 42.12, 38.98, 30.25, 30.19, 28.80, 27.98, 27.94, 27.90, 27.64, 23.97, 22.13, 21.19, 20.95, 20.79, 20.67, 20.30, 12.36, 7.91. HRMS calcd for $C_{91}H_{163}NO_{18}Si_8S_3$, $[M+H]^+$: 1878.9265, found: 1879.1223.

T(TPD-Azo)T

The yellowish orange solid compound was obtained by using silica gel column with hexane: DCM (1:4) and alumina column with DCM (72% yield). ^{1}H-NMR (400 MHz, $CDCl_3$, δ/ppm): 8.11 – 8.04 (m, 4H), 7.95 (d, J = 6.0 Hz, 2H), 7.66 (d, J = 8.6 Hz, 2H), 7.57 – 7.47 (m, 5H), 7.18 – 7.14 (m, 2H) ; ^{13}C-NMR (100 MHz, $CDCl_3$, δ/ppm): 161.28, 152.64, 151.56, 137.95, 134.34, 132.29, 131.23, 130.27,

129.15, 129.11, 128.56, 127.58, 127.13, 123.39, 123.00. HRMS calcd for $C_{26}H_{15}N_3O_2S_3$, $[M+H]^+$: 498.0405, found: 498.0410.

E(TPD-Azo)E

The compound was obtained as light orange solid by using silica gel column with hexane: DCM (1:4) and alumina column with DCM and further purification with recrystallization from MeCN (65% yield). ^{1}H-NMR (400 MHz, $CDCl_3$, δ/ppm): 8.06 (d, J = 8.7 Hz, 2H), 7.95 (d, J = 6.9 Hz, 2H), 7.70 (d, J = 8.7 Hz, 2H), 7.57 – 7.48 (m, 3H), 6.57 (s, 2H), 4.44 (dd, J = 5.1, 2.9 Hz, 4H), 4.29 (dd, J = 5.1, 2.9 Hz, 4H). HRMS calcd for $C_{30}H_{19}N_3O_6S_3$, $[M+H]^+$: 614.0514, found: 614.0526.

P(TPD-Azo)P

The product was purified by successive silica gel columns with hexane: EtOAc (5:1) and hexane: DCM (2:1) and final alumina column with hexane: DCM (3:1) to obtain tacky orange solid (68% yield). ^{1}H-NMR (400 MHz, $CDCl_3$, δ/ppm): 8.04 (d, J = 8.73, 2H), 7.94 (dd, J = 8.2, 1.2 Hz, 2H), 7.66 (m, J = 8.74, 2H), 7.56 – 7.45 (m, 3H), 6.65 (s, 2H), 4.05 (s, 4H), 3.92 (s, 4H), 1.44 (s, 8H), 1.37 – 1.20 (m, 64H), 0.88 (t, J = 6.8 Hz, 12H) ; ^{13}C-NMR (100 MHz, $CDCl_3$, δ/ppm): 161.51, 152.65, 151.21, 149.06, 149.02, 136.48, 134.74, 131.10, 129.08, 127.03, 125.68, 123.28, 122.98, 113.70, 108.13, 77.70, 43.86, 31.95, 30.56, 29.76, 29.70, 29.68, 29.41, 22.95, 22.72, 14.14. HRMS calcd for $C_{72}H_{103}N_3O_6S_3$, $[M+H]^+$: 1202.7087, found: 1202.7340.

E(TPD-Fluo)E

The pure yellow compound was isolated by using successive silica gel columns with hexane: DCM (1:4) and hexane: EtOAc (1:4) and final alumina column with DCM (71% yield). ^{1}H-NMR (400 MHz, $CDCl_3$, δ/ppm): 7.88 (d, J = 8.0 Hz, 1H), 7.82 (d, J = 7.3 Hz, 1H), 7.63 (s, 1H), 7.56 (d, J = 7.5 Hz, 1H), 7.46 (d, J = 7.9 Hz, 1H), 7.40 (t, J= 7.2 Hz, 1H), 7.35 – 7.31 (m, 1H), 6.58 (s, 2H), 4.46 (s, 4H), 4.30 (s, 4H), 3.96 (s, 2H). HRMS calcd for $C_{31}H_{19}NO_6S_3$, $[M+H]^+$: 598.0453, found: 598.0477.

P(TPD-Fluo)P

The compound was isolated as greenish yellow solid by two succesive silica gel columns with hexane: DCM (50:1) and hexane: EtOAc (25:1) and final alumina column with hexane: DCM (4:1) (59% yield). ^{1}H-NMR (400 MHz, CDCl3, δ/ppm): 7.86 (d, J = 8.1 Hz, 1H), 7.80 (d, J = 7.4 Hz, 1H), 7.61 (s, 1H), 7.54 (d, J = 7.4 Hz, 1H), 7.45 (dd, J = 8.1, 1.8 Hz, 1H), 7.38 (t, J = 7.5 Hz, 1H), 7.31 (td, J = 7.4, 1.1 Hz, 1H), 6.64 (s, 2H), 4.05 (s, 4H), 3.94 (s, 2H), 3.92 (s, 4H), 1.43 (s, 8H), 1.36 – 1.21 or 1.29 (d, J = 17.4 Hz, 64H), 0.88 (t, J = 6.8 Hz, 12H) ; ^{13}C-NMR (100 MHz, $CDCl_3$, δ/ppm): 162.10, 149.02, 148.95, 143.75, 143.64, 141.39, 141.09, 136.14, 130.81, 126.93, 126.82, 126.06, 125.58, 125.05, 123.57, 120.14, 119.97, 113.78, 107.98, 77.71, 43.88, 36.98, 32.01, 31.94, 30.55, 29.74, 29.68, 29.66, 29.39, 22.95, 22.70, 14.11. HRMS calcd for $C_{73}H_{103}NO_6S_3$, $[M+H]^+$: 1186.7026, found: 1186.7230.

2.5.3 Synthesis of D-A-D Monomers Based on Phthalhydrazide (PH) Type Acceptor Unit

For the synthesis of PH type monomer, D-A-D monomers based on PI acceptor units were synthesized first and then acceptor unit of these trimeric system was converted to PH type acceptor. For this purpose, a D-A-D monomer was synthesized via Stille cross-coupling reaction of the commercial acceptors (PI-EtHex) with EDOT donor unit.

2.5.3.1 Synthesis of D-A-D Monomer Based on PI Acceptor Unit

E(PI-EtHex)E

The isolation of pure compound was achieved via successive silica gel columns with hexane: DCM (5:3) and hexane: EtOAc (4:1) to obtain transparent green product (69% yield). ^{1}H-NMR (400 MHz, $CDCl_3$, δ/ppm): 7.72 (s, 2H), 6.52 (s,

2H), 4.27 (s, 8H), 3.56 (d, J = 7.2 Hz, 2H), 1.88 – 1.77 (m, 1H), 1.32 (ddd, J = 10.1, 8.4, 3.2 Hz, 8H), 0.91 (t, J = 6.8 Hz, 6H) ; ^{13}C-NMR (100 MHz, $CDCl_3$, δ/ppm): 166.86, 141.30, 140.08, 135.82, 128.95, 128.93, 111.13, 100.55, 64.37, 41.67, 38.17, 30.48, 28.53, 23.68, 22.94, 13.98, 10.37. HRMS calcd for $C_{28}H_{29}NO_6S_2$, $[M+H]^+$: 540.1515, found: 540.1513.

2.5.3.2 Synthesis of D- A- D Monomer Based on PH Type Acceptor Unit

The monomer (1 equiv, 0.16 mmol) was dissolved in a mixture of ethanol/1,4-dioxane (1/1: v/v, 4 mL) and then hydrazine hydrate (N_2H_5OH) (1 equiv, 0.3 mL, 0.16 mmol) was added to this solution. The mixture was allowed to reflux at 100 ℃ for 48 h. Then, the crude mixture was cooled down to room temperature and filtered to collect the precipitate. After that, the crude precipitate was washed with a mixture of ethanol/1,4-dioxane (50 mL) and finally hexane (50 mL) to afford the product[140].

E(PH)E

A white solid compound was obtained after purification (27% yield). ^{1}H-NMR (400 MHz, d-DMSO, δ/ppm): 9.02 (s, 2H), 7.58 (s, 2H), 6.62 (s, 2H), 4.21 (s, 8H) ; ^{13}C-NMR (100 MHz, d-DMSO, δ/ppm): 166.38, 141.47, 139.22, 134.97, 130.95, 129.30, 113.63, 100.13, 64.80, 64.42. HRMS calcd for $C_{20}H_{14}N_2O_6S_2$, $[M+H]^+$: 443.0372, found: 443.0367.

CHAPTER 3

RESULTS AND DISCUSSION

Three different core units were employed as acceptor moieties in this study, which are PI, TPD and PH. The chemical structures of brominated core units are given in Figure 3.1.

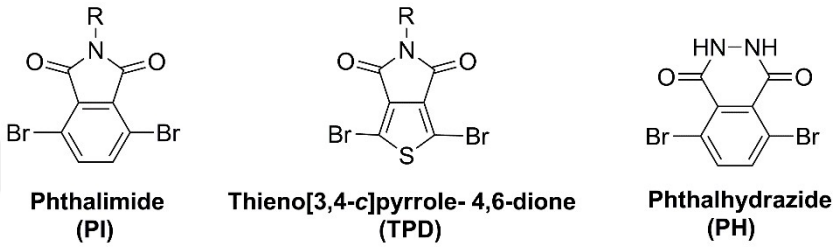

Figure 3.1. The structures of core units as acceptor.

The obtained monomers synthesized from these core acceptor units are classified under 6 different titles depending on the type of core acceptor unit and the substituent attached on the acceptor.

3.1 D-A-D Monomers Based on PI Type Acceptor Unit

In this part, two series of D-A-D monomers were synthesized by using thiophene and EDOT donor units and modified PI acceptor units. POSS-propylamine appended acceptor unit and its POSS free derivative were coupled with aforementioned donor groups (thiophene and EDOT) to obtain four different D-A-D monomers, namely T(PI-POSS)T, T(PI-Propyl)T, E(PI-POSS)E and E(PI-Propyl)E. The synthesis of the monomers were depicted in Scheme 3.1.

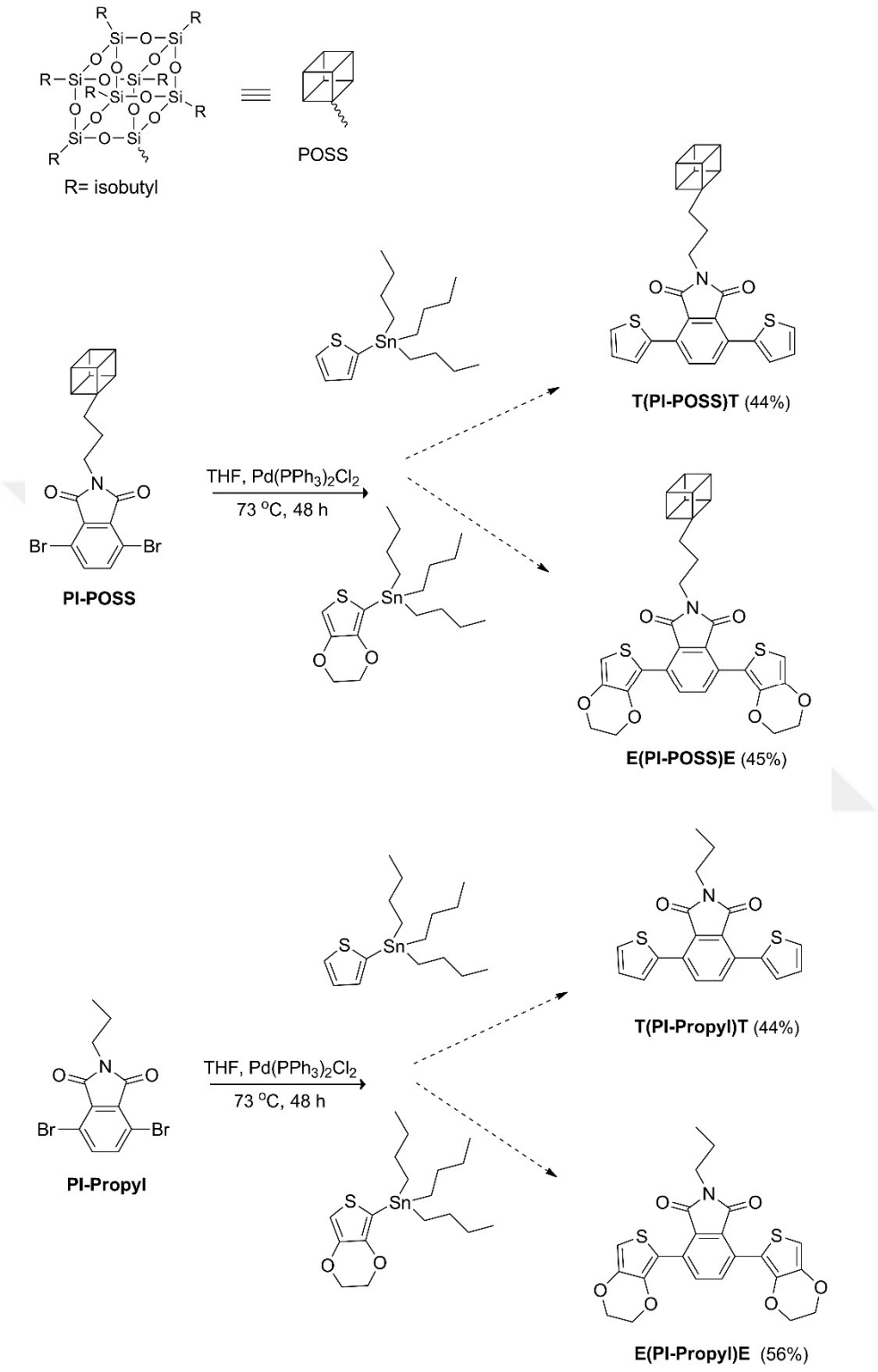

Scheme 3.1. Synthetic route for the synthesis of monomers, T(PI-POSS)T, T(PI-Propyl)T, E(PI-POSS)E and E(PI-Propyl)E.

3.1.1 Optical Properties of the Monomers

Firstly, the UV-Vis spectra of the monomers were recorded in DCM and the obtained results are depicted together for comparison sake. The absorption maxima were detected at 325 nm, 324 nm, 335 nm and 335 nm for T(PI-POSS)T, T(PI-Propyl)T, E(PI-POSS)E and E(PI-Propyl)E, respectively. As it can be seen from Figure 3.1 (a), EDOT bearing analogs have a 10 nm red shift due to better conjugation between the acceptor unit and EDOT as compared to their thiophene counterparts[6]. The dual band, the one at lower wavelength is due to π-π* transition and the higher wavelength one is due to ICT, is not observed in this case due to poor interaction between donor and acceptor units. Thus, the absence of dual band reveals that PI unit, independent of its substituent, is a poor acceptor unit[141]. The fluorescence emission spectra of the monomers, upon excitation at 300 nm, were also recorded in DCM and the maxima of emission bands for T(PI-POSS)T, T(PI-Propyl)T, E(PI-POSS)E and E(PI-Propyl)E were detected at 480 nm, 484 nm, 500 nm and 507 nm, respectively. As shown in Figure 3.1 (b), EDOT containing group undergoes a nearly 20 nm red shift as compared to thiophene analogs. The emission color changed from greenish blue for T(PI-POSS)T and T(PI-Propyl)T to green for E(PI-POSS)E and E(PI-Propyl)E. The large Stoke's shift was observed for all the monomers, which indicates the conformational change of molecules upon excitation[142,143].

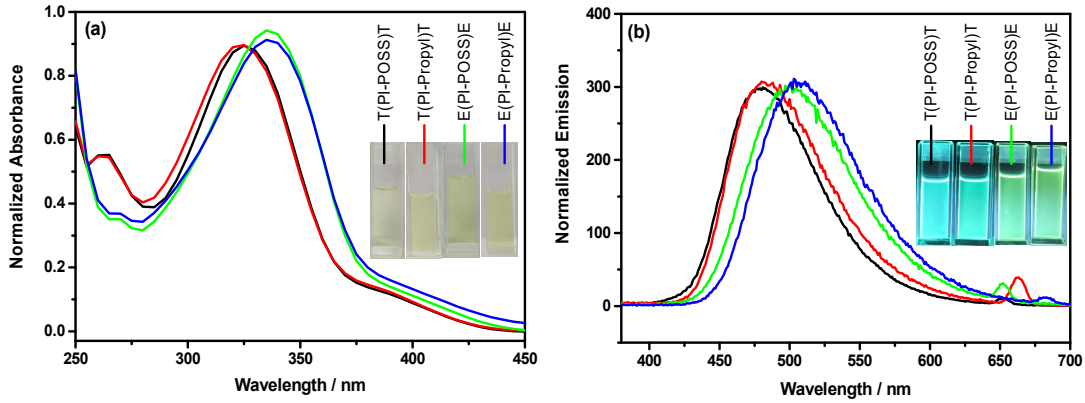

Figure 3.2. Normalized (a) absorption and (b) emission spectra of monomers in DCM. Inset: The colors of the monomers (a) in daylight and (b) under UV lamp at 365 nm.

3.1.2 Electrochemical Properties of the Monomers

The electrochemical behaviours of the monomers were investigated via cyclic voltammetry in 0.1 M $TBAPF_6$ dissolved in DCM and the obtained results are given in Figure 3.2 to understand the effect of POSS unit attached to the acceptor moiety. As seen from Figure 3.2 (a), all the monomers revealed one irreversible oxidation peak centered at 1.72 V for T(PI-POSS)T, 1.68 V for T(PI-Propyl)T, 1.36 V for E(PI-POSS)E and 1.35 V for E(PI-Propyl)E versus Ag/AgCl (see Table 3.1). The close inspection of the voltammogram shows that E(PI-POSS)E and E(PI-Propyl)E monomers with EDOT donor units have lower oxidation potentials as compared to their parent monomers bearing thiophene due to greater donating ability of EDOT unit[144]. However, the presence of POSS unit does not have a noticeable effect on the electrochemical behaviour; therefore, nearly the same oxidation potential values were observed for the monomers with the same donor group. On the other hand, the monomer T(PI-POSS)T, T(PI-Propyl)T, E(PI-POSS)E and E(PI-Propyl)E exhibited reversible reduction peaks during cathodic scan at -1.56 V, -1.48 V, -1.60 V and -1.55 V vs. Ag/AgCl, respectively. As seen in

Figure 3.2 (b), more negative reduction potentials were obtained for EDOT derivatives due to higher electron density of the trimeric systems bearing EDOT donor units as compared to thiophene ones. All aforementioned data obtained from electrochemical measurements are depicted in Table 3.1 together with the ones obtained from optical measurements.

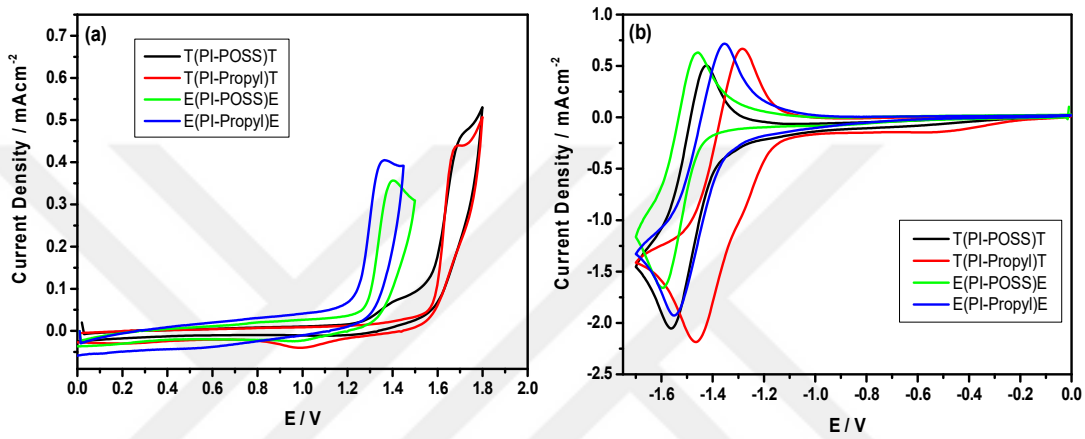

Figure 3.3. Cyclic voltammograms for (a) oxidation and (b) reduction of T(PI-POSS)T, T(PI-Propyl)T, E(PI-POSS)E and E(PI-Propyl)E on Pt electrode in 0.1 M $TBAPF_6$ dissolved in DCM at a scan rate of 100 mV/s vs. Ag/AgCl.

Table 3.1 Optical and electrochemical properties of the monomers

Monomer	T(PI-POSS)T	T(PI-Propyl)T	E(PI-POSS)E	E(PI-Propyl)E
$\lambda_{max,abs}$ (nm)	325	324	335	335
$\lambda_{max,em}$ (nm)	480	484	500	507
$E_{ox,m}$ (V)	1.72	1.68	1.36	1.35
$E_{red,m}$ (V)	-1.56	-1.48	-1.60	-1.55
$E_{ox,onset,m}$ (V)	1.57	1.57	1.29	1.25
$E_{red,onset,m}$ (V)	-1.39	-1.28	-1.45	-1.36
HOMO (eV)	-6.28	-6.28	-6.00	-5.96
LUMO (eV)	-3.32	-3.43	-3.26	-3.35

3.1.3 Electropolymerization and Spectroelectrochemical Properties of the PE(PI-POSS)E Film

Because the other monomers are incapable, the electrochemical polymerization is achieved only for E(PI-POSS)E monomer to obtain its corresponding polymer (Scheme 3.2). The electropolymerization of E(PI-POSS)E was performed potentiodynamically between 0.0 V and +1.5 V on Pt disc electrode in DCM containing 0.1 M $TBAPF_6$ and the resulting voltammogram is given in Figure 3.4. As shown in Figure 3.4 (a), after the first cycle, a new reversible redox couple started to appear and the current intensity of this redox couple increased after each successive scan, which indicates the formation of an electroactive polymer film on the working electrode surface, namely PE(PI-POSS)E. The redox behavior of PE(PI-POSS)E film was investigated via CV in a monomer-free electrolyte solution. As seen in Figure 3.4 (b), the polymer film revealed a reversible redox couple with a half wave of 0.53 V. The scan rate dependency study was performed by recording their CVs in the anodic region at different scan rates changing from 20 mVs^{-1} to 200 mVs^{-1} with 20 mV increments and the resulting voltammograms are depicted in Figure 3.5. As it is seen from the figure, the peak intensity of the reversible redox couple increased linearly as a function of scan rate, which indicates the non-diffusion controlled redox process of PE(PI-POSS)E film on the electrode surface.

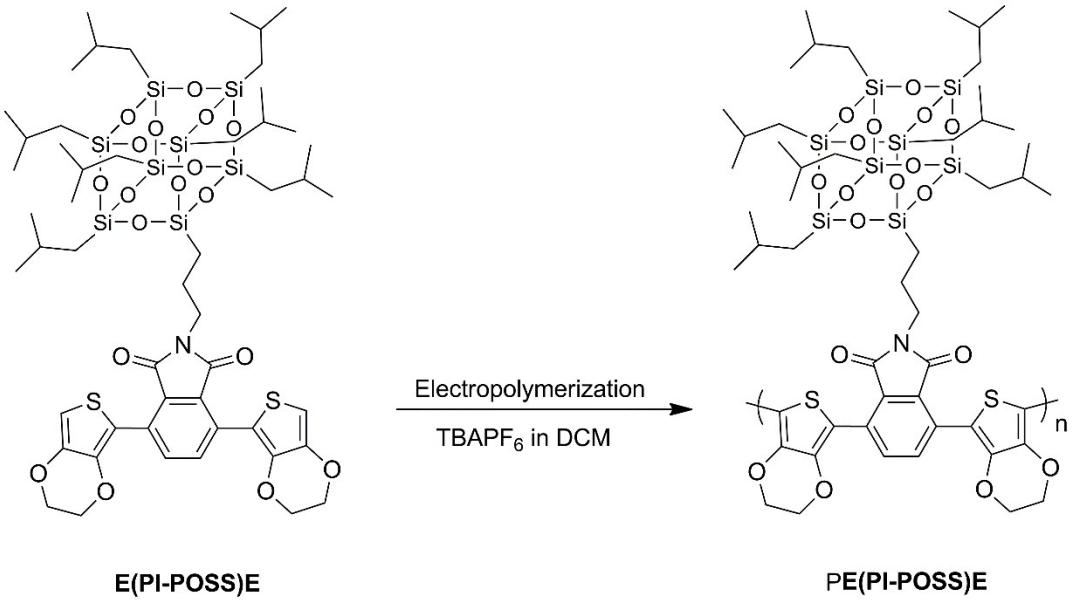

Scheme 3.2. Electropolymerization of E(PI-POSS)E to afford PE(PI-POSS)E.

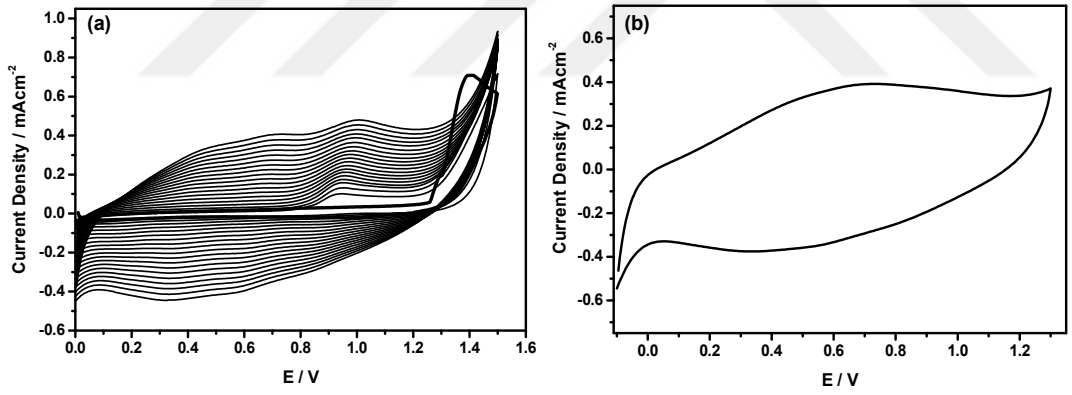

Figure 3.4. (a) Repetitive cyclic voltammograms of E(PI-POSS)E monomer on Pt disc electrode (b) cyclic voltammogram of PE(PI-POSS)E film coated on Pt disc electrode recorded in 0.1 M $TBAPF_6$ dissolved in DCM at a scan rate of 100 mv/s vs. Ag/AgCl.

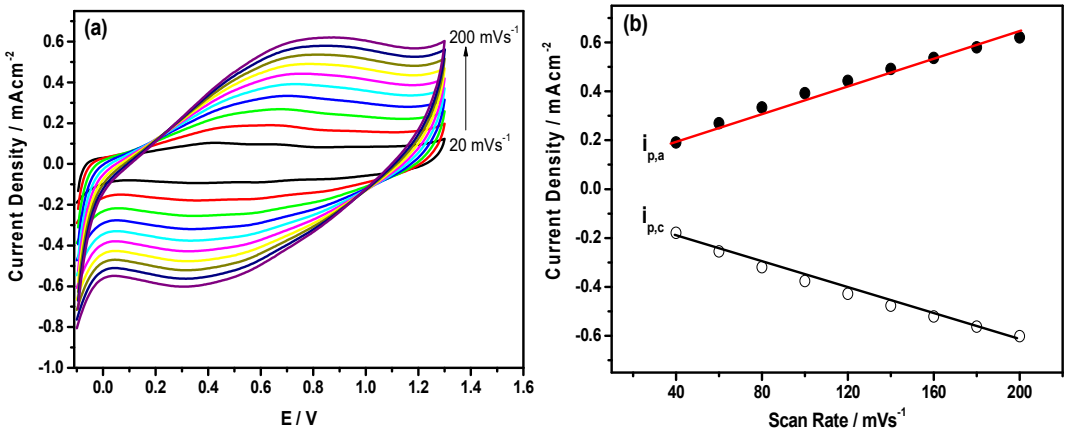

Figure 3.5. (a) Scan rate dependence of PE(PI-POSS)E polymer film on Pt disc electrode recorded in 0.1 M $TBAPF_6$ solution in DCM at different scan rates from 20 mVs^{-1} to 200 mVs^{-1} with 20 mVs^{-1} increments and (b) relationship of anodic and cathodic current peaks as a function of scan rate for PE(PI-POSS)E polymer film.

In order to investigate opto-electronic properties, PE(PI-POSS)E polymer film was deposited on the ITO electrode via potentiodynamic method in the potential range between 0.0 V to +1.5 V with 30 cycles. The polymer film was washed with monomer-free electrolyte solution before spectroelectrochemical studies. The neutral state absorption spectra of PE(PI-POSS)E film coated on ITO is depicted in Figure 3.6 together with that of the monomer. The careful inspection of the figure reveals that both monomer and its corresponding polymer have only one absorption band attributed to π-π* transition. The absorption band maxima for E(PI-POSS)E and PE(PI-POSS)E were found to be at 335 nm and 550 nm, respectively. The π-π* transition band of polymer exhibits a large red shift at around 215 nm as compared to that of monomer. This red shift detected in the π-π* transition band is observed due to the increase in conjugation length as the polymerization takes place.

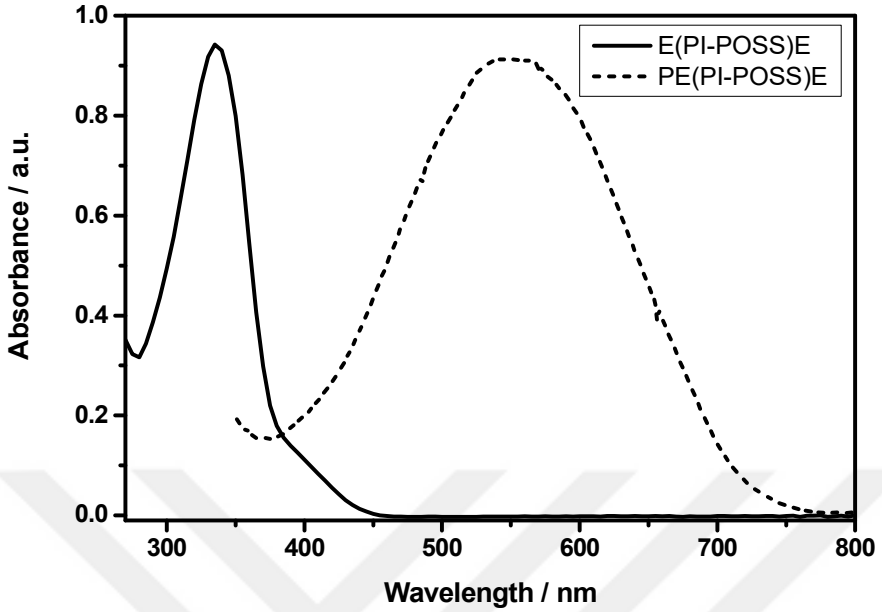

Figure 3.6. Neutral state electronic absorption spectra of E(PI-POSS)E monomer in DCM and PE(PI-POSS)E polymer film coated on ITO.

For the investigation of the optical and electrochemical properties of PE(PI-POSS)E polymer film on ITO, the spectroelectrochemical studies were carried out in a cell containing 0.1 M $TBAPF_6$/DCM electrolyte solution. In the monomer-free system, the absorption changes were recorded under various applied potential from –1.0 V to +1.3 V and the resulting spectra are given in Figure 3.7. As expected from an electrochromic polymer, upon oxidation the intensity of π-π* transition band at 550 nm started to diminish while a new absorption band appeared at around 830 nm, which indicates the formation of polaron charge carriers. Upon further oxidation, the intensity of polaron band started to decline when bipolaron band intensified at about 1000 nm. The optical band gap of PE(PI-POSS)E film was calculated as 1.72 eV from the absorption edge of π-π* transition band. The optical contrast was found to be 33% at 550 nm when the polymer film is switched in its redox states with a residence time of 10 s by using square wave potential technique as shown in Figure 3.8. The switching time for oxidation, the time required to

obtain 95% of full optical contrast for oxidation and CE were found to be 2.5 s and 306 cm^2/C, respectively. The switching time for neutralization, the time required to obtain 95% of full optical contrast for neutralization was found to be 8.2 s. This high switching time for neutralization shows the slow movement of counter ions outside of polymer backbone due to strong electrostatic attractions between polymer backbone and counter ions. As seen from the inset of Figure 3.7, PE(PI-POSS)E film exhibited color change from grey to eggplant purple when it changes from neutral to oxidized state, respectively. These colorimetric results belong to the polymer film were also defined by L*, a*, b* values and these values are listed in Table 3.2 together with all foregoing results.

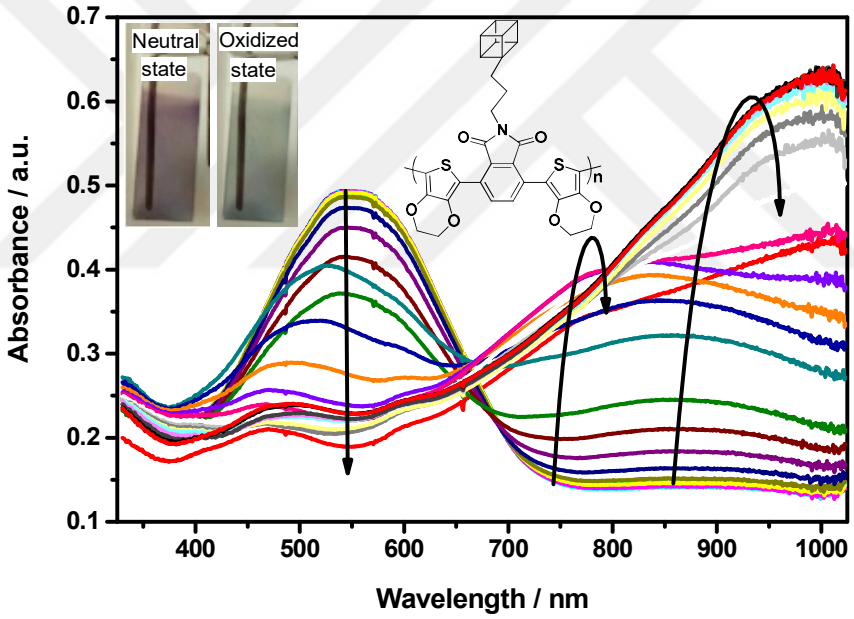

Figure 3.7. The changes in the electronic absorption spectra of electrochemically coated PE(PI-POSS)E film on ITO recorded in 0.1 M $TBAPF_6$ dissolved in DCM as a function of applied potentials between -1.0 V to +1.3 V. Inset: The colors of the polymer film on ITO in neutral and oxidized states.

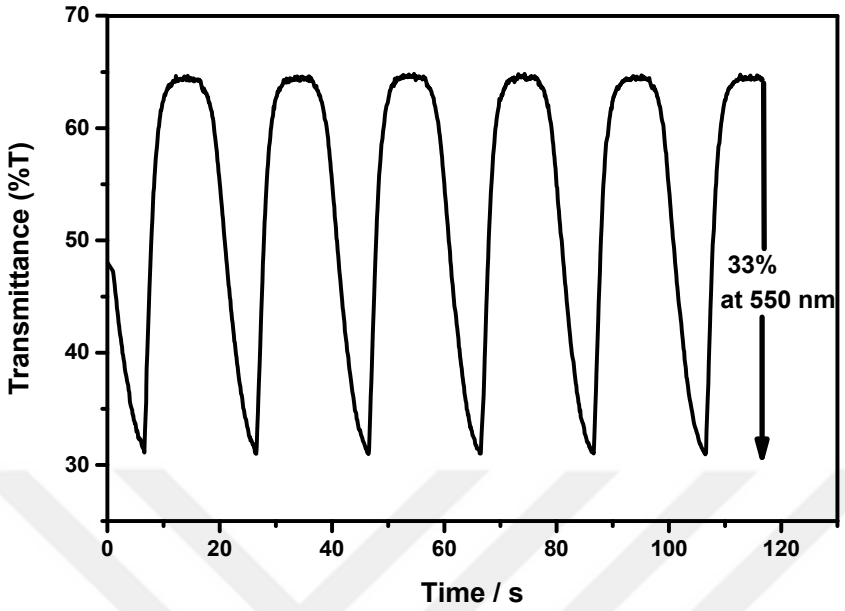

Figure 3.8. Chronoabsoptometry experiments for PE(PI-POSS)E film on ITO in 0.1 M $TBAPF_6$ dissolved in DCM when the polymer is switched for 10 s intervals between its redox states from -1.0 V to +1.3 V at 550 nm.

Table 3.2 Optoelectronic properties of PE(PI-POSS)E polymer film

Polymer	**PE(PI-POSS)E**
λ_{max} (nm)	550
E_g^{opt} (eV)	1.72
Δ%T	33
CE (cm^2/C)	306
$t_{s,ox}^a$ (s)	2.5

Table 3.2 (continued)

$t_{s,red}$[a] (s)	8.2
Color at neutral state L*, a*, b*	66.1, 11.4, -15.5
Color at oxidized state L*, a*, b*	82.2, -2.7, -0.1

[a] 95% of full switch from colored to bleached states.

3.2 D-A-D Monomers Based on TPD Acceptor Unit

3.2.1 D-A-D Monomers Based on TPD-EtHex Acceptor Unit

This part involves the synthesis of three D-A-D monomers based on ethyl hexyl-substituted TPD acceptor unit and thiophene, EDOT and didecyl-ProDOT donor units. These monomers were named as T(TPD-EtHex)T, E(TPD-EtHex)E and P(TPD-EtHex)P.

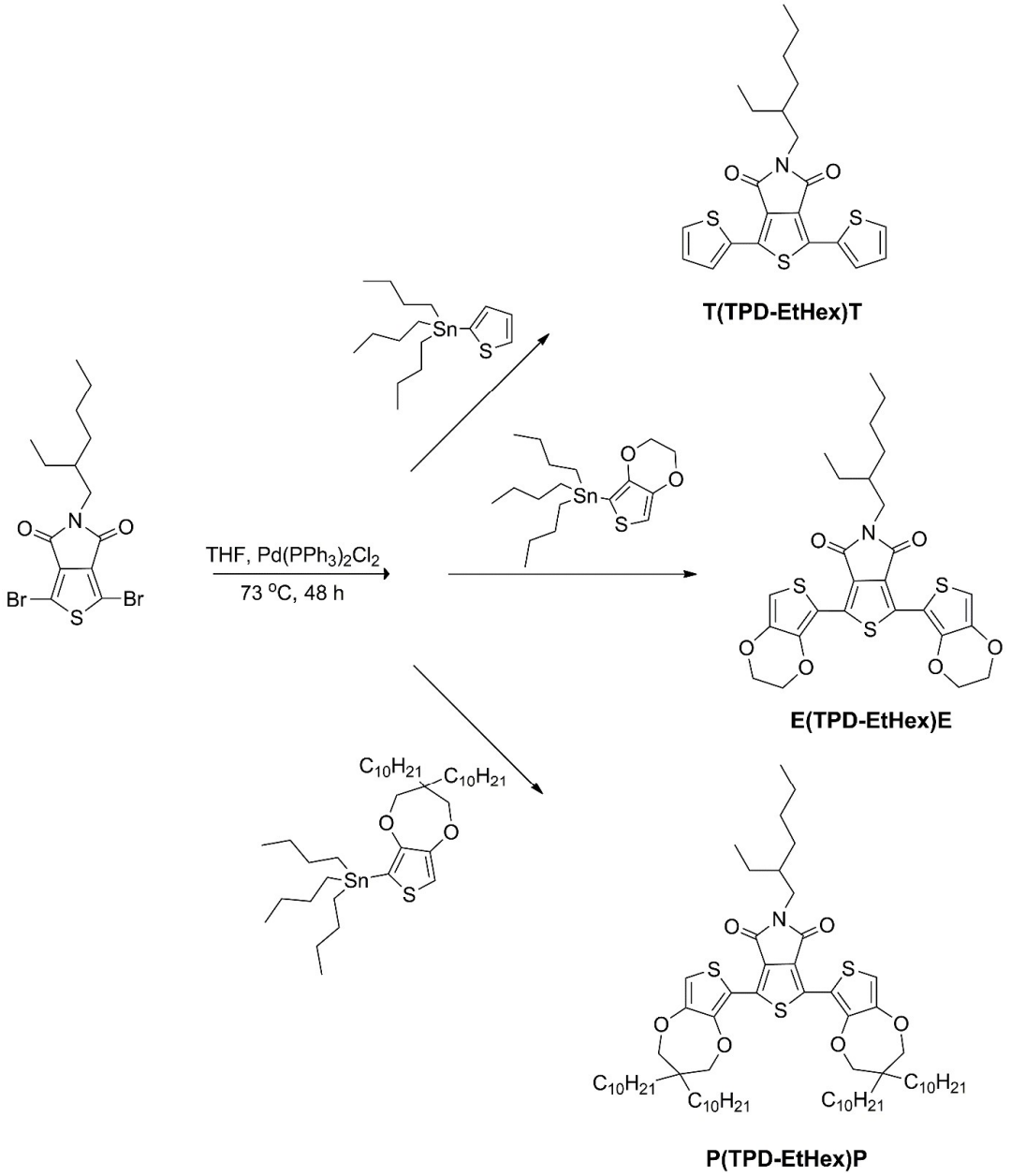

Scheme 3.3. Synthetic route for synthesis of T(TPD-EtHex)T, E(TPD-EtHex)E and P(TPD-EtHex)P monomers.

3.2.1.1 Optical Properties of the Monomers

In order to get a better insight on the optical properties of monomers, electronic absorption and fluorescence emission spectra were recorded in DCM and the resulting spectra are given in Figure 3.9. As seen from the Figure 3.9 (a), the monomers exhibit dual bands in their absorption spectra as a fingerprint of D-A-D type monomers. The bands that appear at higher energy wavelengths due to π-π* transition were observed at 270 nm, 277 nm and 277 nm for T(TPD-EtHex)T, E(TPD-EtHex)E and P(TPD-EtHex)P, respectively. The lower energy bands attributed to the ICT between donor and acceptor units were detected at 383 nm, 398 nm and 393 nm for T(TPD-EtHex)T, E(TPD-EtHex)E and P(TPD-EtHex)P, respectively [145,146,147]. The slight red shift in the absorption spectra of E(TPD-EtHex)E monomer proves the better conjugation between donor and acceptor as compared to other two. As seen in Figure 3.9 (b), the fluorescence spectra of the monomers exhibit emission bands at 463 nm, 480 nm and 473 nm upon excitation at 340 nm for T(TPD-EtHex)T, E(TPD-EtHex)E and P(TPD-EtHex)P, respectively. The large Stoke's shift observed at around 80 nm for all monomers reveals the conformational changes that take place in the molecules when excited[142,143].

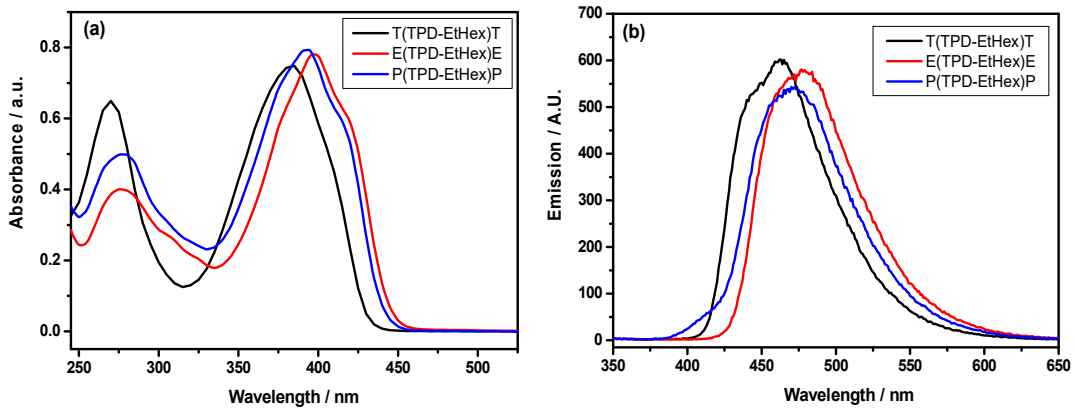

Figure 3.9. (a) Absorption and (b) emission spectra of monomers in DCM. Inset: the color of the monomers (a) in daylight and (b) under UV lamp at 365 nm.

3.2.1.2 Electrochemical Properties of the Monomers

For the investigation of electrochemical properties, cyclic voltammograms of monomers were recorded in 0.1 M $TBAPF_6$ dissolved in MeCN/DCM mixture and the obtained voltammograms are depicted in Figure 3.10. As seen from Figure 3.10, during anodic scan, all monomers reveal one irreversible oxidation peak centered at 1.42 V, 1.03 V and 1.14 V vs Ag/AgCl for T(TPD-EtHex)T, E(TPD-EtHex)E and P(TPD-EtHex)P monomers, respectively. Among them, E(TPD-EtHex)E exhibits the lowest oxidation potential due to higher donor strength of EDOT than thiophene and didecyl-ProDOT bearing counterparts. During the cathodic scan, as shown in Figure 3.9, quasi-reversible reduction peaks are observed for three monomers with the reduction potentials at -1.42 V, -1.58 V and -1.60 V vs Ag/AgCl for T(TPD-EtHex)T, E(TPD-EtHex)E and P(TPD-EtHex)P, respectively. More negative reduction potentials are observed for E(TPD-EtHex)E and P(TPD-EtHex)P monomers as a consequences of higher electron density of D-A-D systems with EDOT and ProDOT derivatives[144]. All the results obtained from the electrochemical measurements are tabulated in Table 3.3 together with the optical data.

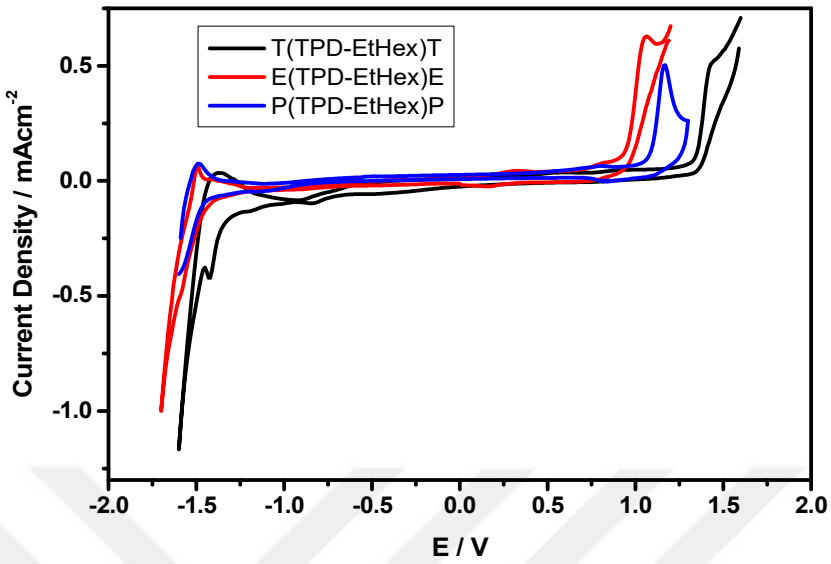

Figure 3.10. Full scan cyclic voltammograms of the monomers on Pt disc electrode vs. Ag/AgCl in 0.1 M $TBAPF_6$ dissolved in MeCN/DCM ((10/1: v/v) for T(TPD-EtHex)T, (15/1: v/v) for E(TPD-EtHex)E and (5/3: v/v) for P(TPD-EtHex)P) at a scan rate of 100 mV/s.

Table 3.3 Optical and electrochemical properties of T(TPD-EtHex)T, E(TPD-EtHex)E and P(TPD-EtHex)P monomers

Monomer	**T(TPD-EtHex)T**	**E(TPD-EtHex)E**	**P(TPD-EtHex)P**
$\lambda_{max,abs}$ **(nm)**	270, 383	277, 398	277, 393
$\lambda_{max,em}$ **(nm)**	463	480	475
$E_{ox,m}$ **(V)**	1.42	1.03	1.14
$E_{red,m}$ **(V)**	-1.42	-1.58	-1.60
$E_{ox,onset,m}$ **(V)**	1.34	0.95	1.08
$E_{red,onset,m}$ **(V)**	-1.35	-1.45	-1.46

Table 3.3 (continued)

HOMO (eV)	-6.05	-5.66	-5.79
LUMO (eV)	-3.36	-3.26	-3.25
$E_g^{electro}$ (eV)	2.69	2.40	2.54
E_g^{opt} (eV)	2.88	2.79	2.82
QY	0.110	0.065	0.045

3.2.1.3 Electropolymerization and Spectroelectrochemical Properties

All the monomers were electropolymerized on Pt disc electrode via potential cycling by applying potentials between 0.0 V and +1.5 V for T(TPD-EtHex)T, -0.3 V and +1.15 V for E(TPD-EtHex)E, 0.0 V and +1.22 V for P(TPD-EtHex)P vs Ag/AgCl in 0.1 M $TBAPF_6$ dissolved in a MeCN/DCM mixture to obtain their corresponding polymers (see Figure 3.11) and the resulting voltammograms are depicted in Figure 3.12 (a), (c) and (e). During repetitive scans, new redox couples appear and intensify at around +1.3 V, +0.4 V and +0.8 V vs Ag/AgCl for PT(TPD-EtHex)T, PE(TPD-EtHex)E and PP(TPD-EtHex)P, respectively. The peak current intensities of redox couples increases with the increasing scan number as the electroactive polymer film forms on the surface of working electrode. The electrochemical behavior of the polymer films on Pt disc electrode was investigated one by one by recording their CVs during both anodic and cathodic regions in a monomer free electrolyte solution. The cyclic voltammograms are depicted separately in Figure 3.12 (b), (d) and (f). To elucidate the effect of donor groups on the redox behavior in D-A-D systems, the voltammograms are closely inspected and it was found that, all monomers exhibit one reversible oxidation peak at +1.34 V for PT(TPD-EtHex)T, +0.41 V for PE(TPD-EtHex)E and +0.87 V for PP(TPD-EtHex)P. Moreover, a reversible reduction peak was also observed at -1.57 V for PT(TPD-EtHex)T, -1.66 V for PE(TPD-EtHex)E and -1.60 V for PP(TPD-EtHex)P vs Ag/AgCl, during the cathodic scan. The obtained electrochemical data are listed

in Table 3.4, together with oxidation and reduction onset values of the polymers. The electrochemical E_g values of the polymers were calculated from HOMO and LUMO levels by using these onset potentials. The lowest E_g value was observed for PE(TPD-EtHex)E (1.55 eV) as compared to PT(TPD-EtHex)T (2.37 eV) and PP(TPD-EtHex)P (2.16 eV), which is explained by the higher donor strength of EDOT group.

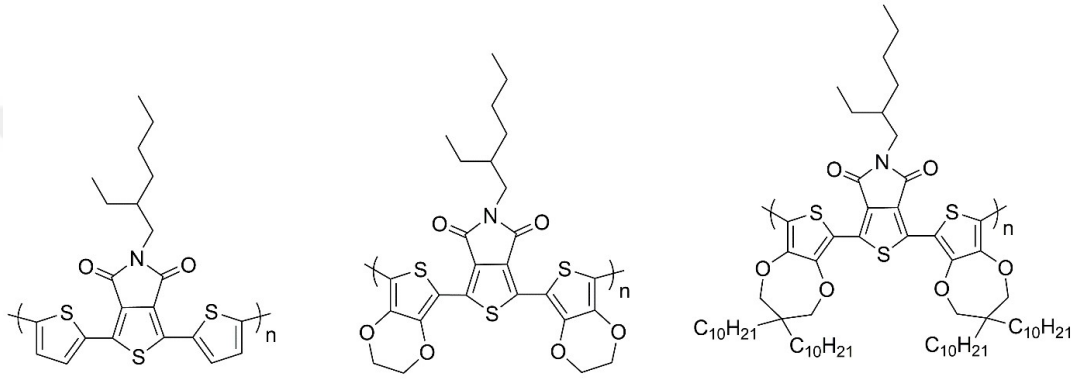

Figure 3.11. The structure of polymers.

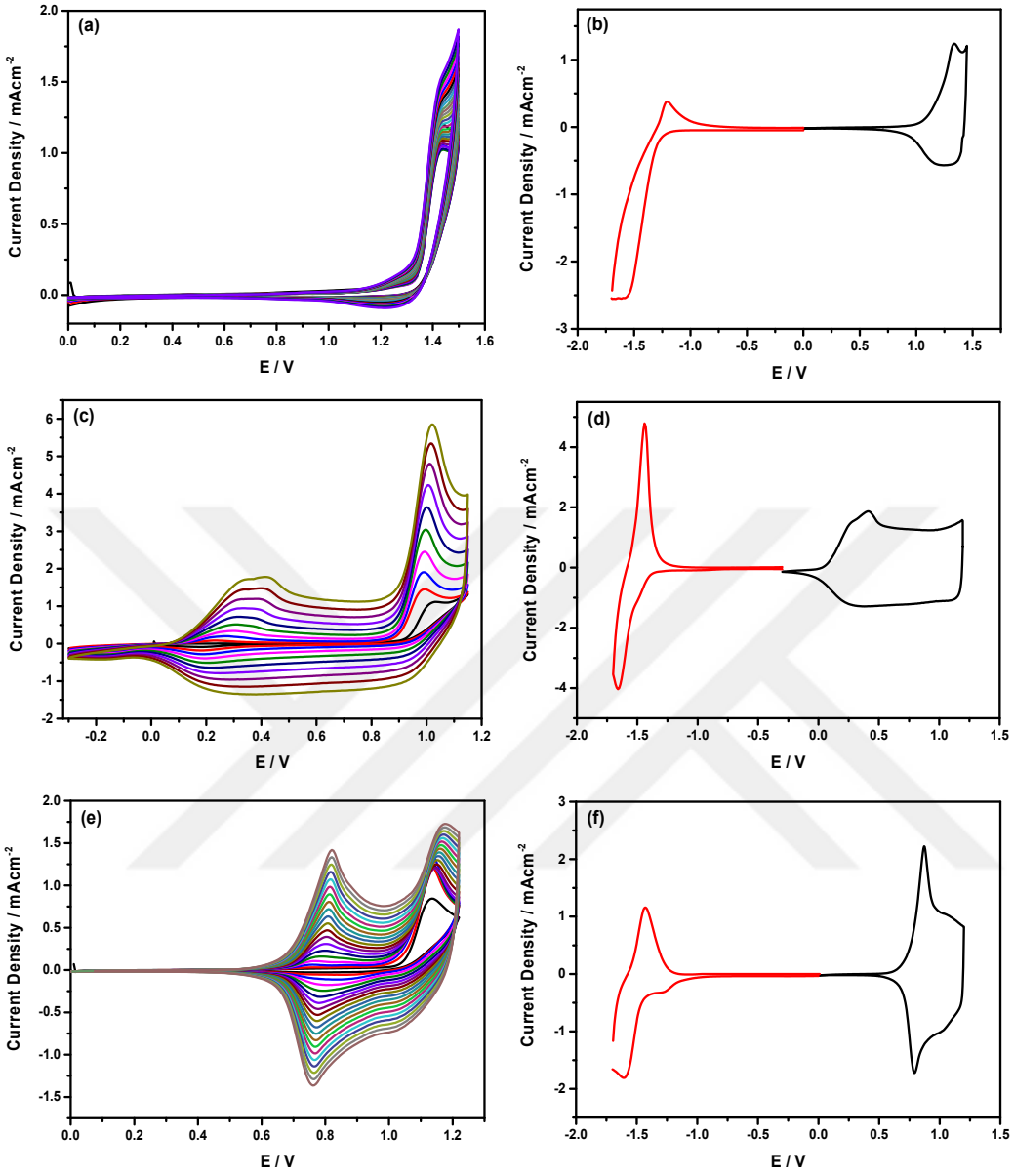

Figure 3.12. Repetitive cyclic voltammograms of (a) T(TPD-EtHex)T, (c) E(TPD-EtHex)E and (e) P(TPD-EtHex)P monomer recorded in 0.1 M $TBAPF_6$ dissolved in MeCN/DCM ((10/1: v/v) for T(TPD-EtHex)T, (15/1: v/v) for E(TPD-EtHex)E and (5/3: v/v) for P(TPD-EtHex)P) and cycling voltammograms of their corresponding polymer films (b) PT(TPD-EtHex)T, (d) PE(TPD-EtHex)E and (f) PP(TPD-EtHex)P polymer films recorded in 0.1 M $TBAPF_6$/MeCN on Pt disc electrode vs. Ag/AgCl at a scan rate of 100 mVs^{-1}.

Table 3.4 Electrochemical properties of the polymers

Polymer	PT(TPD-EtHex)T	PE(TPD-EtHex)E	PP(TPD-EtHex)P
$E_{ox,p}$ (V)	1.34	0.41	0.87
$E_{red,p}$ (V)	-1.57	-1.66	-1.60
$E_{ox,onset,p}$ (V)	1.08	0.05	0.73
$E_{red,onset,p}$ (V)	-1.29	-1.50	-1.43
$E_g^{electro}$ (eV)	2.37	1.55	2.16
E_g^{opt} (eV)	1.82	1.58	1.69
HOMO (eV)	-5.79	-4.76	-5.44
LUMO (eV)	-3.42	-3.21	-3.28

The peak current for a reversible redox couple can be directly proportional to analyte concentration and square root of the scan rate according to Randles-Sevcik equation[148]. On the contrary, electrochemical process for a polymer film which takes place in a monomer-free electrolyte solution is quasi-reversible and this redox process is not diffusion-controlled due to the formation of immobilized polymer film at the electrode surface and does not obey Randles-Sevcik equation. Instead, the peak current for this redox process is expressed by the theory of immobilized redox centers. According to this theory, the peak current linearly increases with the scan rate and the relationship of peak current intensity as a function of scan rate determines whether the redox process is diffusion-controlled or not[149,150]. Accordingly, the scan rate study conducted for the polymer films revealed that the current intensity of the redox couples increases linearly as a function of scan rate during p-doping, which indicates that the redox process is not diffusion-controlled for well-adhered polymer films on the Pt electrode surface. (Figure 3.13)

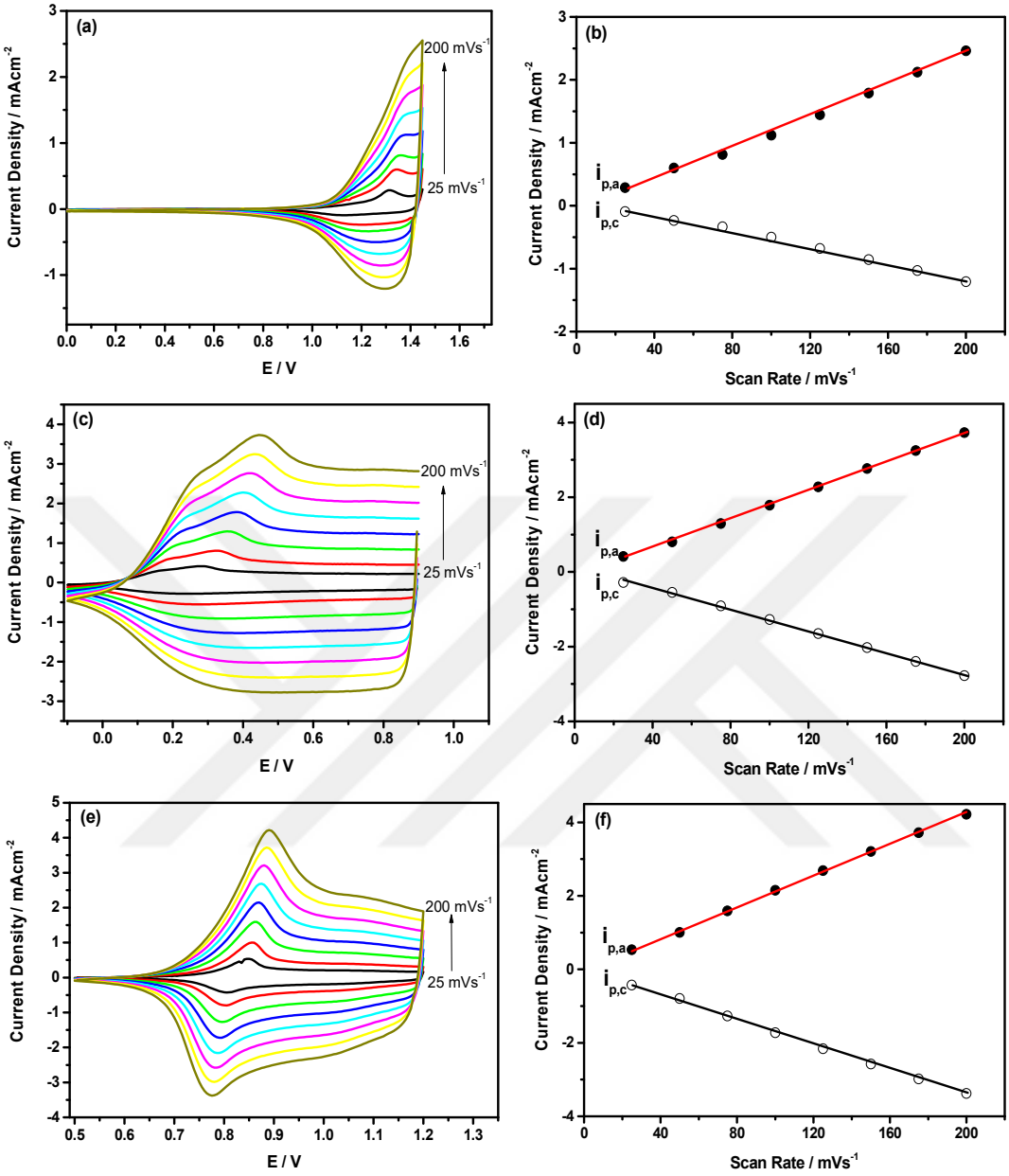

Figure 3.13. Scan rate dependence of polymer films on Pt disc electrode recorded in 0.1 M $TBAPF_6$ solution (a) PT(TPD-EtHex)T, (c) PE(TPD-EtHex)E and (e) PP(TPD-EtHex)P in MeCN at different scan rates from 25 mVs^{-1} to 200 mVs^{-1} with 25 mVs^{-1} increments. The relationship of anodic and cathodic peak currents as a function of scan rate for (b) PT(TPD-EtHex)T, (d) PE(TPD-EtHex)E and (f) PP(TPD-EtHex)P polymer films.

In order to elucidate the effect of different donor groups on the electrochromic properties in a D-A-D system, the polymer films were electrodeposited on ITO working electrode by using potentiodynamic method. During spectroelectrochemical studies, the polymer films on ITO were placed into cuvettes containing monomer-free electrolyte solution and firstly their neutral state absorption spectra are recorded for comparison sake. As seen in Figure 3.14, all the polymer films exhibit one absorption band at 500, 625 and 600 nm for PT(TPD-EtHex)T, PE(TPD-EtHex)E and PP(TPD-EtHex)P films due to the π-π* transition. It is worth to mention that, although PT(TPD-EtHex)T does not exhibit any vibronic coupling, there is a clear vibronic coupling especially in the case of PP(TPD-EtHex)P indicating solid-state order of polymer backbones[151,152]. From the onset of π-π* transition, optical band gap values of the polymers were calculated as 1.82 eV, 1.58 eV and 1.69 eV for PT(TPD-EtHex)T, PE(TPD-EtHex)E and PP(TPD-EtHex)P, respectively (see Table 3.4). As it is expected from EDOT bearing polymer, the lowest E_g value was observed for PE(TPD-EtHex)E.

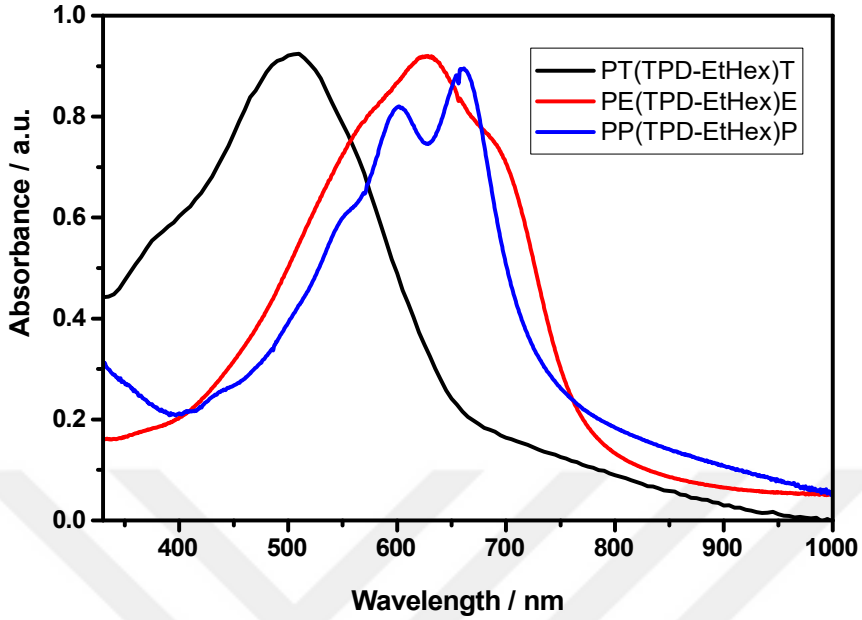

Figure 3.14. Neutral state electronic absorption spectra of PT(TPD-EtHex)T, PE(TPD-EtHex)E and PP(TPD-EtHex)P films coated on ITO electrode in 0.1 M $TBAPF_6$/MeCN.

For further investigation of optoelectronic properties, the changes in electronic absorption spectra of polymers were recorded as a function of externally applied potential and the results are depicted in Figure 3.15. As seen from the figure, during the anodic scan, the π-π* transition bands started to lose its intensity as a new absorption bands arise at about 900 nm for PT(TPD-EtHex)T, 685 nm for PE(TPD-EtHex)E and 850 nm for PP(TPD-EtHex)P due to the generation of polaron charge carriers. Finally, the changes in electronic absorption spectra of polymer films upon oxidation are reflected by a color change; from brick red to gray for PT(TPD-EtHex)T, blue/violet to sky blue for PE(TPD-EtHex)E and blue to highly light blue for PP(TPD-EtHex)P, respectively as shown in Figure 3.15 and L*, a*, b* values corresponding to these colors are listed in Table 3.5.

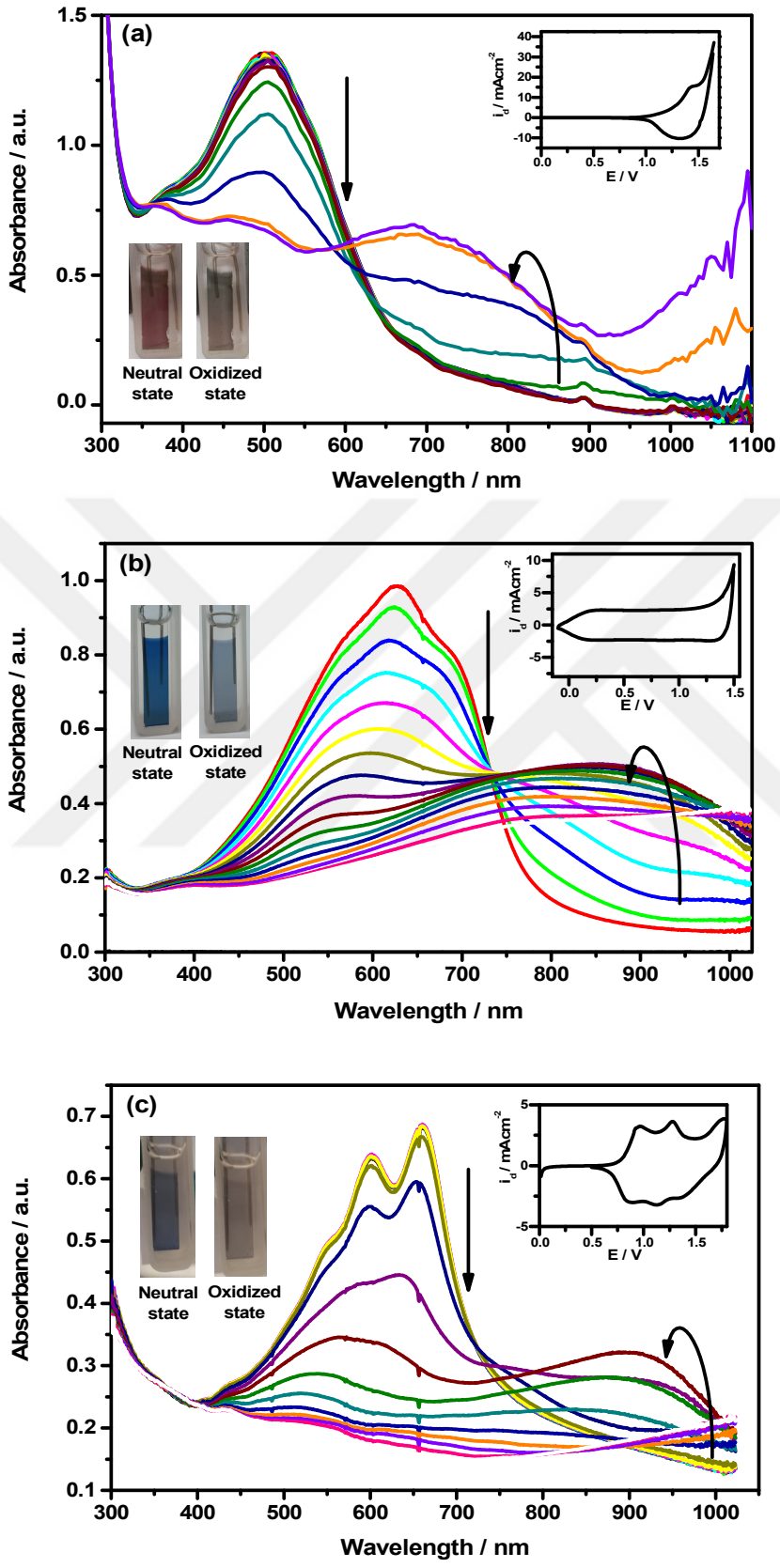
(a)
Absorbance / a.u.
Wavelength / nm
Neutral state
Oxidized state
i_d / mAcm^-2
E / V
(b)
Absorbance / a.u.
Wavelength / nm
Neutral state
Oxidized state
i_d / mAcm^-2
E / V
(c)
Absorbance / a.u.
Wavelength / nm
Neutral state
Oxidized state
i_d / mAcm^-2
E / V

Figure 3.15. The changes in electronic absorption spectra of electrochemically deposited (a) PT(TPD-EtHex)T, (b) PE(TPD-EtHex)E and (c) PP(TPD-EtHex)P films on ITO recorded at various applied potentials in 0.1 M $TBAPF_6$/MeCN. Insets: CVs of the films recorded with a scan rate of 20 mVs^{-1}. Inset: The colors of the films at neutral and oxidized states.

The transmittance spectra of polymer films were recorded between their neutral and oxidized states in 10 s time interval by using square wave potential technique and the results are given in Figure 3.16. As seen in the figure, the percent transmittance change for PT(TPD-EtHex)T, PE(TPD-EtHex)E and PP(TPD-EtHex)P between redox states were found to be 21%, 41% and 52%, respectively. The oxidation response time, neutralization response time and CE for 95% of full optical switch were found to be 3.3 s, 0.6 s and 183 cm^2/C at 500 nm for PT(TPD-EtHex)T, 0.6 s, 0.2 s and 424 cm^2/C at 625 nm for PE(TPD-EtHex)E and 0.5 s, 2.0 s and 281 cm^2/C at 660 nm for PP(TPD-EtHex)P, respectively. All values are listed in Table 3.5.

Table 3.5 Optoelectronic properties of the polymer films on ITO in 0.1 M $TBAPF_6$/MeCN

Polymer	**PT(TPD-EtHex)T**	**PE(TPD-EtHex)E**	**PP(TPD-EtHex)P**	**PP(TPD-EtHex)P-C**
λ_{max} (nm)	500	625, 685	600, 660	600, 655
E_g^{opt} (eV)	1.82	1.58	1.69	1.76
Δ%T	21	41	52	60
CE (cm^2/C)	183	424	281	329
$t_{s,ox}$[a] (s)	3.3	0.6	0.5	1.0
$t_{s,red}$[a] (s)	0.6	0.2	2.0	1.0
Color at neutral state L*, a*, b*	58.9, 23.9, 7.8	40.6, 6.5, -43.0	64.0, -4.5, -23.4	55.4,-1.7, -35.1
Color at oxidized state L*, a*, b*	78.6, -3.1, 12.9	76.5, -3.5, -7.8	86.1, 1.5, 5.2	86.0, 1.7, 0.9

[a] 95% of full switch from colored to bleached states.

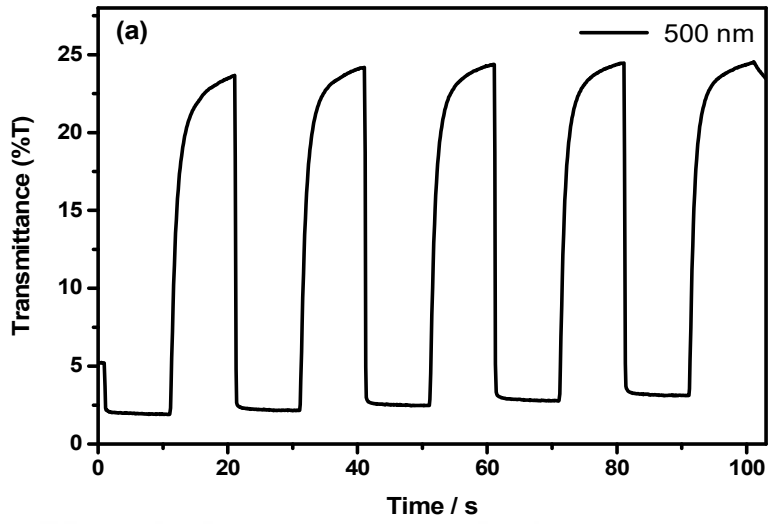
(a)
500 nm
Transmittance (%T)
Time / s
0
5
10
15
20
25
0
20
40
60
80
100

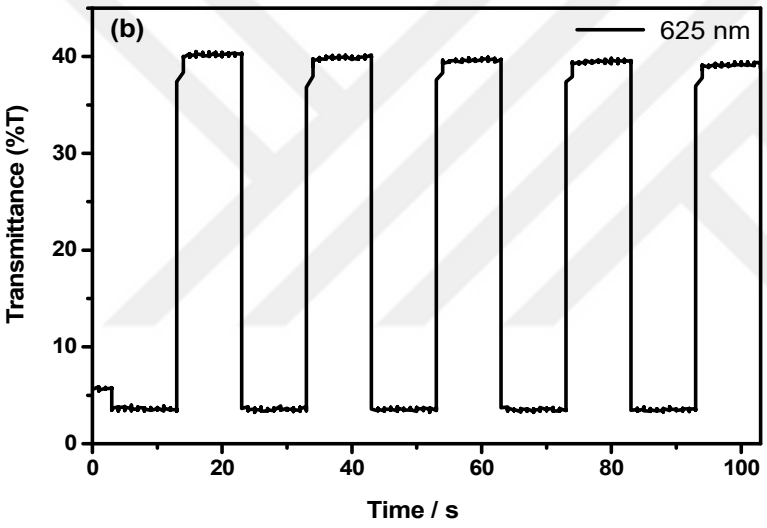
(b)
625 nm
Transmittance (%T)
Time / s
0
10
20
30
40
0
20
40
60
80
100

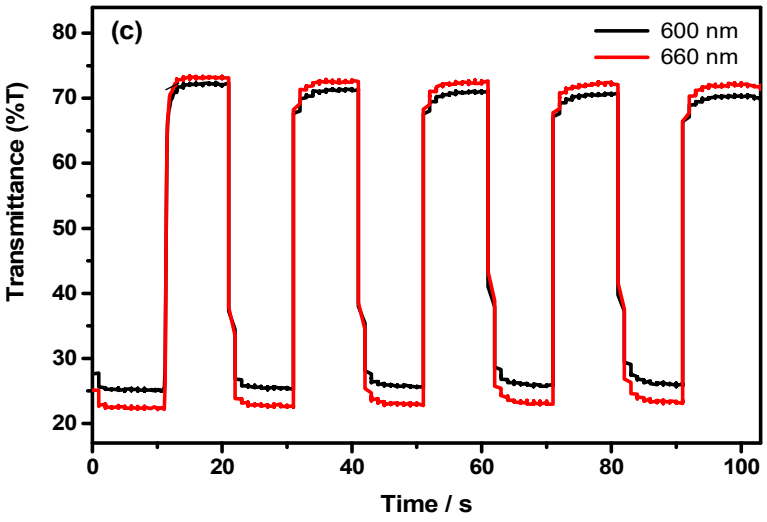
(c)
600 nm
660 nm
Transmittance (%T)
Time / s
20
30
40
50
60
70
80
0
20
40
60
80
100

Figure 3.16. Chronoabsoptometry experiments for the polymer films on ITO in 0.1 M $TBAPF_6$/MeCN when the films were switched between redox states with an interval time of 10 s for (a) PT(TPD-EtHex)T (between -0.2 V and +1.3 V at 500 nm), (b) PE(TPD-EtHex)E (between -0.5 V and +1.5 V at 625 nm) and (c) PP(TPD-EtHex)P (between 0.0 V and +1.4 V at 600 nm and 660 nm).

Stability is a key parameter for an electrochromic polymer. For that reason, the optical and electrochemical stability of electrochemically coated PE(TPD-EtHex)E and PP(TPD-EtHex)P films on ITO were examined under ambient conditions via potential cycling. Since PT(TPD-EtHex)T film is not stable on the ITO electrode for a long time, it was not tested. The stability tests were carried out by switching between neutral (-0.5 V) and oxidized (+1.2 V) states with a residence time of 3 s. The tests reveal that both films retain their opto-electrochemical stability even after 1200 cycles as shown in Figure 3.17.

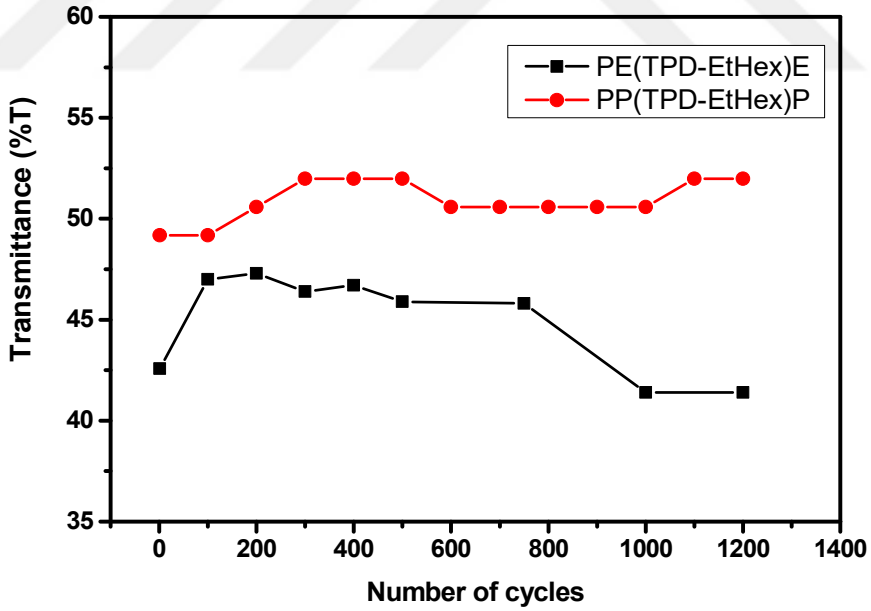

Figure 3.17. Optical stability tests for polymer films on ITO when the films switched between redox states (-0.5 V and +1.2 V) with an interval of 3 s at 625 nm for PE(TPD-EtHex)E and at 600 nm for PP(TPD-EtHex)P.

3.2.1.4 Chemical Polymerization and Spectroelectrochemical Properties

Since the electrochemically obtained PP(TPD-EtHex)P film is completely soluble in common organic solvents such as toluene, DCM, chloroform, THF, etc., PP(TPD-EtHex)P was also polymerized utilizing $FeCl_3$ as a chemical oxidant. The structure of chemically obtained polymer PP(TPD-EtHex)P-C was confirmed by ^1H NMR spectra in $CDCl_3$ (see Appendix Figure A.26). When ^1H NMR spectra of the monomer is compared with that of polymer, the broadening is observed in the peaks of monomer as it is polymerized. Also, the peak observed at 6.4 ppm due to C-H proton on the α-position of didecyl-ProDOT disappeared completely, which indicates the formation of a linear polymer backbone via coupling at the α-position. Comparision of the FTIR spectra of P(TPD-EtHex)P and its polymer PP(TPD-EtHex)P-C, on the other hand, revealed disappearance of the peaks at about 856 cm^{-1} and 3100 cm^{-1} due to C-5 aromatic C-H strechings[153]. These observations clearly indicate the polymer formation via C-5 position of the ProDOT heteroaromatic ring (see Appendix Figure E.1). For further characterization, the molecular weight of the polymer was determined by using GPC. The number average molecular weight of PP(TPD-EtHex)P-C was determined as 7,243 Da (see Appendix Figure C.1 for GPC chromatogram).

The electronic absorption spectra of both chemically and electrochemically obtained soluble PP(TPD-EtHex)P polymer were recorded in DCM and the resulting spectra are depicted in Figure 3.18 (a) together with that of electrochemically obtained one on ITO. When the absorption spectrum of chemically obtained PP(TPD-EtHex)P-C polymer in DCM is compared with that of electrochemically obtained one, a 10 nm red shift was noted as compared to that of electrochemically obtained one. This red shift can be explained by the enhanced conjugation length for chemically obtained PP(TPD-EtHex)P-C as compared to electrochemically obtained one. Furthermore, when the electronic absorption spectrum of electrochemically obtained polymer in DCM was compared with that of the electrochemically coated film on ITO, a 10 nm blue shift was noted in the

absorption maximum of the polymer in DCM as compared to the polymer on ITO. This can be explained by the disappearance of π-π* stacking between chains[154] in the solution. The fluorescence emission spectrum of the chemically obtained polymer was also recorded in DCM and given in Figure 3.18 (b) together with its absorption spectrum. As it is seen from the figure, PP(TPD-EtHex)P-C exhibits an emission band at around 690 nm with a red color emission when excited at 510 nm.

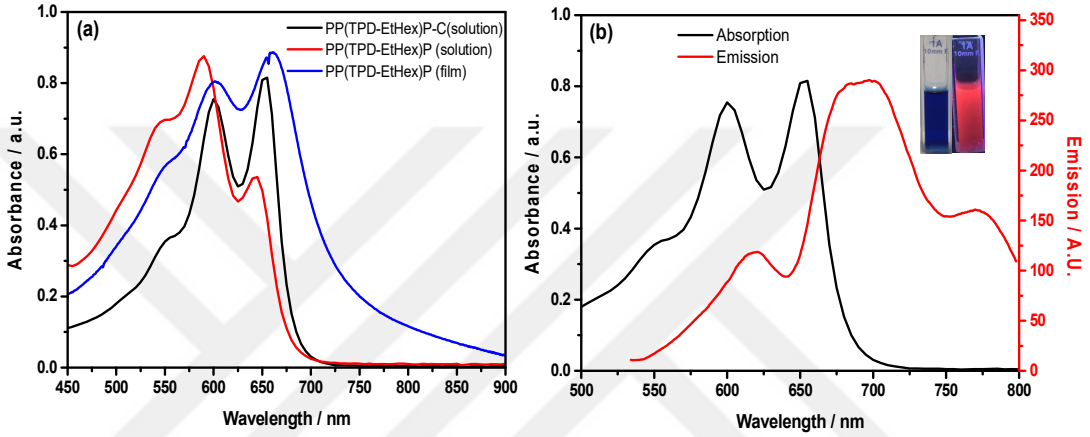

Figure 3.18. (a) Electronic absorption spectra of PP(TPD-EtHex)P film on ITO and both chemically and electrochemically obtained PP(TPD-EtHex)P polymers in DCM (b) Electronic absorption and emission spectra of chemically obtained PP(TPD-EtHex)P-C polymer in DCM.

The chromic properties of solution-processable PP(TPD-EtHex)P-C polymer can also be changed via chemical methods. The polymer solution can be chemically oxidized and reduced–reversibly via stepwise additions of $SbCl_5$ and N_2H_5OH, respectively. As shown in Figure 3.19, the changes observed in the absorption spectra during chemical p-doping of the solution-processable polymer in toluene were almost identical to the one recorded during electrochemical p-doping of PP(TPD-EtHex)P film on ITO. As it can be seen in the figure, the intensity of π-π* transition bands at 600 nm and 655 nm starts to decline with the formation of a new band at 900 nm as a consequence of the generation of polaron charge carriers with

the addition of $SbCl_5$. Then, upon the addition of N_2H_5OH, the doped polymer solution returns back to its neutral form.

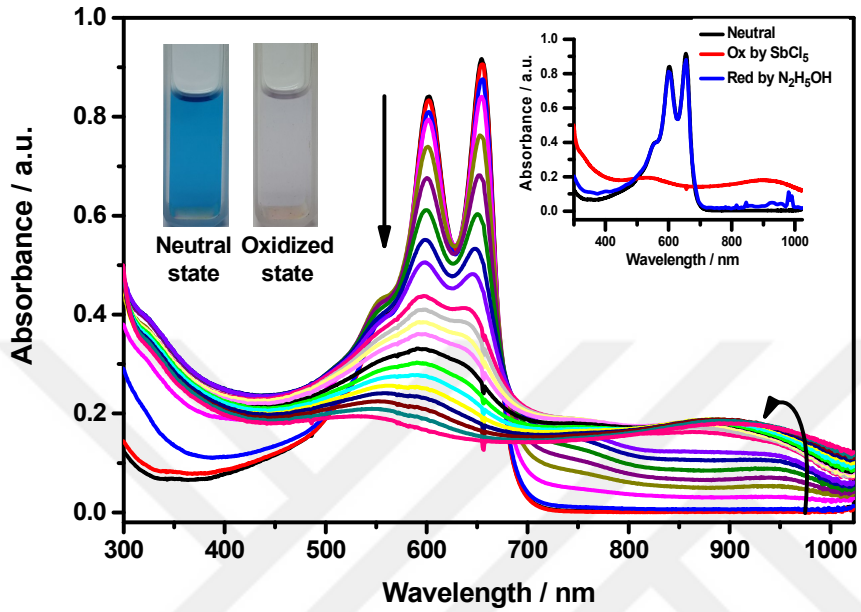

Figure 3.19. Changes in the absorption spectra of PP(TPD-EtHex)P-C dissolved in toluene during chemical oxidation by using 0.05 M $SbCl_5$ oxidant with 10 µL stepwise additions. Inset: absorption spectrum after chemical reduction by using hydrazine. Inset: Colors of polymer solution at neutral and oxidized states.

To investigate the spectroelectrochemical properties of the chemically synthesized PP(TPD-EtHex)P-C polymer, it was spray coated on an ITO surface and the changes in the electronic absorption spectra as a function of applied potential is given in Figure 3.20 (a). Comparison of this figure with Figure 3.15 (c), reveals that both chemically (PP(TPD-EtHex)P-C) and electrochemically (PP(TPD-EtHex)P) prepared films exhibit very similar spectroscopic changes during their electrochemical p-doping. The E_g value was calculated from the onset of the low energy end of π-π* transition band to be 1.76 eV. The optical contrast, switching time for oxidation/neutralization and CE for the spray coated PP(TPD-EtHex)P-C film were calculated as 60%, 1.0 s and 329 cm^2/C at 655 nm, respectively, from

Figure 3.20 (b) and the results are also tabulated in Table 3.5 together with the E_g and L*, a*, b* values of electrochemically obtained film for comparison sake. The highest optical contrast and shortest switching time were observed for PP(TPD-EtHex)P among the other polymer films due to alky substituents of the ProDOT unit, which facilitates the ion movement by increasing the distance between chains. The longer switching time observed for spray coated counterpart of PP(TPD-EtHex)P film can be explained by film quality, which is mainly based on the type of coating. On the other hand, among all polymer films, the lowest band gap and the highest CE were observed for PE(TPD-EtHex)E polymer film.

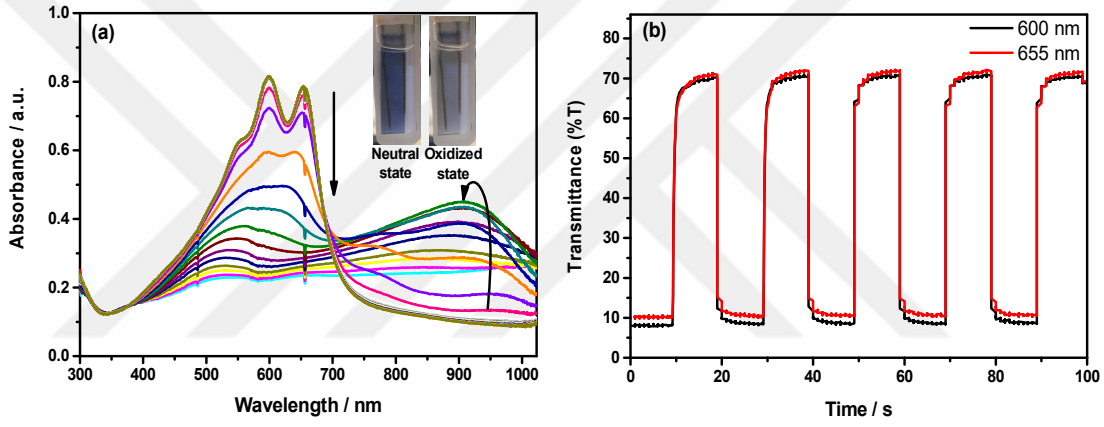

Figure 3.20. (a) The changes in electronic absorption spectra of spray coated PP(TPD-EtHex)P-C film on ITO recorded at various applied potentials between 0.0 V and +1.4 V in 0.1 M $TBAPF_6$/MeCN. Inset: The colors of the films at neutral and oxidized states. (b) Chronoabsoptometry experiments for PP(TPD-EtHex)P-C film when switched for 10 s intervals between 0.0 and +1.6 V at 600 and 655 nm).

The long-term stability of spray coated PP(TPD-EtHex)P-C film was also tested via potential cycling under the same conditions and it was found that the film preserves its optical activity only up to 300 cycles. This also reveals the advantage of electrochemical deposition technique over spray coating technique.

3.2.2 D-A-D Monomers Based on TPD-POSS Acceptor Unit

In this part, the focus of study is directed on the modification of TPD acceptor unit by appending a new kind of substituent, propyl isobutyl POSS through bridging nitrogen atom to obtain a new TPD derivative named as TPD-POSS. This new acceptor unit was coupled with thiophene, EDOT and didecyl-ProDOT donor units to obtain new D-A-D systems, namely T(TPD-POSS)T, E(TPD-POSS)E and P(TPD-POSS)P. The synthetic route for the synthesis is given in Scheme 3.4.

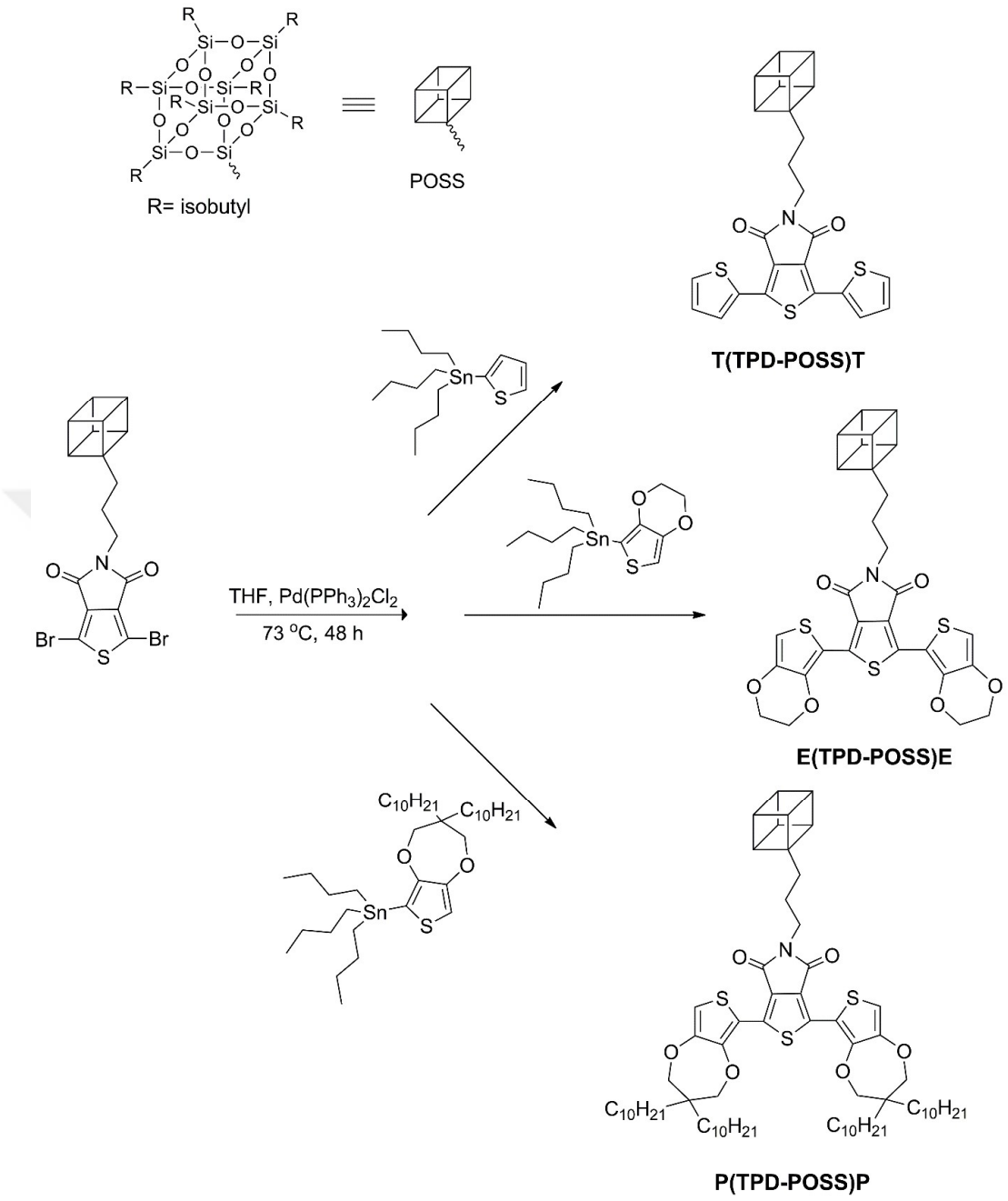

Scheme 3.4. Synthetic route for the synthesis of T(TPD-POSS)T, E(TPD-POSS)E and P(TPD-POSS)P.

3.2.2.1 Optical Properties of the Monomers

In order to enlighten the effect of both donor units and POSS substituent attached on the TPD acceptor unit on the optical characteristics of monomers, the electronic absorption spectra of three monomers were recorded in DCM and the resulting spectra are depicted in Figure 3.21 (a). All the monomers display similar absorption spectra with two characteristic peaks. The higher energy band attributed to the localized π-π* transitions were detected at 269 nm for T(TPD-POSS)T, 275 nm for E(TPD-POSS)E and 276 nm for P(TPD-POSS)P and the lower energy band assigned to strong ICT interactions, characteristics of D-A-D type monomers, were observed at 383 nm for T(TPD-POSS)T, 398 nm for E(TPD-POSS)E and 393 nm for P(TPD-POSS)P. The slight red shift noted in both higher- and lower-energy bands when going from thiophene to EDOT might be due to enhanced ICT interactions between the donor and acceptor units since EDOT has a higher donor strength as compared to thiophene. The fluorescence emission spectra of the monomers, recorded in DCM, displayed luminescence maxima at 460 nm for T(TPD-POSS)T, 480 nm for E(TPD-POSS)E and 477 nm for P(TPD-POSS)P upon excitation at 340 nm (see Figure 3.21 (b)). The observed absorption and emission maxima are also listed in Table 3.6. A comparison of tabulated absorption and emission maxima for POSS bearing monomers with that of ethylhexyl bearing monomers indicates that substituent on the acceptor unit has no appreciable effect on the photo physical properties of the monomers.

Furthermore, comparison of absorption and emission maxima of the spectra exhibited relatively large Stoke's shift around 80 nm (from 77 nm to 84 nm), implying the conformational changes occuring in the molecules upon excitation[142,143].

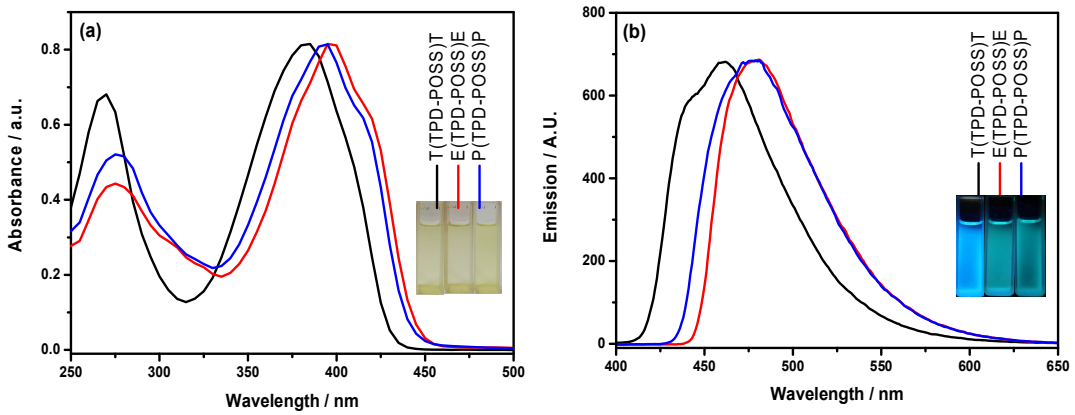

Figure 3.21. (a) Absorption and (b) emission spectra of monomers in DCM. Inset: the color of the monomers (a) in daylight and (b) under UV lamp at 365 nm.

Moreover, fluorescence quantum yields of the monomers in THF were determined by using the following equation:

The eqn: $QY_X = QY_{ST}\,(Grad_X/Grad_{ST})(n_X^2/n_{ST}^2)$

where

QY_X: Fluorescence quantum yield

Grad: gradient from the plot of integrated fluorescence intensity vs absorbance

n: refractive index

Quinine sulfate in 0.1 M H_2SO_4 solution (QY_Q= 0.546) was used as a standard and QY values of the monomers were calculated as 0.112 for T(TPD-POSS)T, 0.074 for E(TPD-POSS)E and 0.075 for P(TPD-POSS)P. Furthermore, the higher QY values were noted for the POSS-substituted monomers as compared to their ethyl hexyl bearing counterparts, which shows that the existence of the POSS unit has an enhancing effect on QY values. All the results obtained for the photophysical properties of the monomers are listed in Table 3.6.

3.2.2.2 Electrochemical Properties of the Monomers

In order to evaluate the electrochemical characteristics of the monomers, both CV and DPV measurements were conducted in DCM involving 0.1 M $TBAPF_6$ as a supporting electrolyte. The CVs recorded at room temperature are shown in Figure 3.22 (a). As it is seen, the CVs of three monomers consist of an irreversible oxidation peak during the anodic scans. On the other hand, during the cathodic scans, T(TPD-POSS)T monomer reveals quasi-reversible reduction peak while the other monomers show irreversible reduction peaks. The observed oxidation and reduction peak potentials are also tabulated in Table 3.6 together with their onset potentials estimated from DPV measurements (see Figure 3.22 (b)).

A more careful inspection of Table 3.6 shows that the oxidation peak and onset potentials of the monomer sharply decrease with a magnitude of at least 400 mV when thiophene donor unit is replaced with EDOT unit, which can be explained by the higher donating ability of EDOT unit as compared to thiophene. On the contrary, a much smaller decrease was observed in their reduction peaks and onset potentials as compared to their oxidation potentials. This is because the reduction potentials are associated with the LUMO energy levels of the acceptor unit. Therefore, the reduction potentials do not alter much since the same acceptor unit is involved in all three monomers. The HOMO and LUMO energy levels of the monomers estimated from the onset redox potentials are also listed in Table 3.6. A careful examination of the table apparently reveals that optoelectronic properties of the monomers show alterations depending on the type of donor unit rather than the substituent on the acceptor unit.

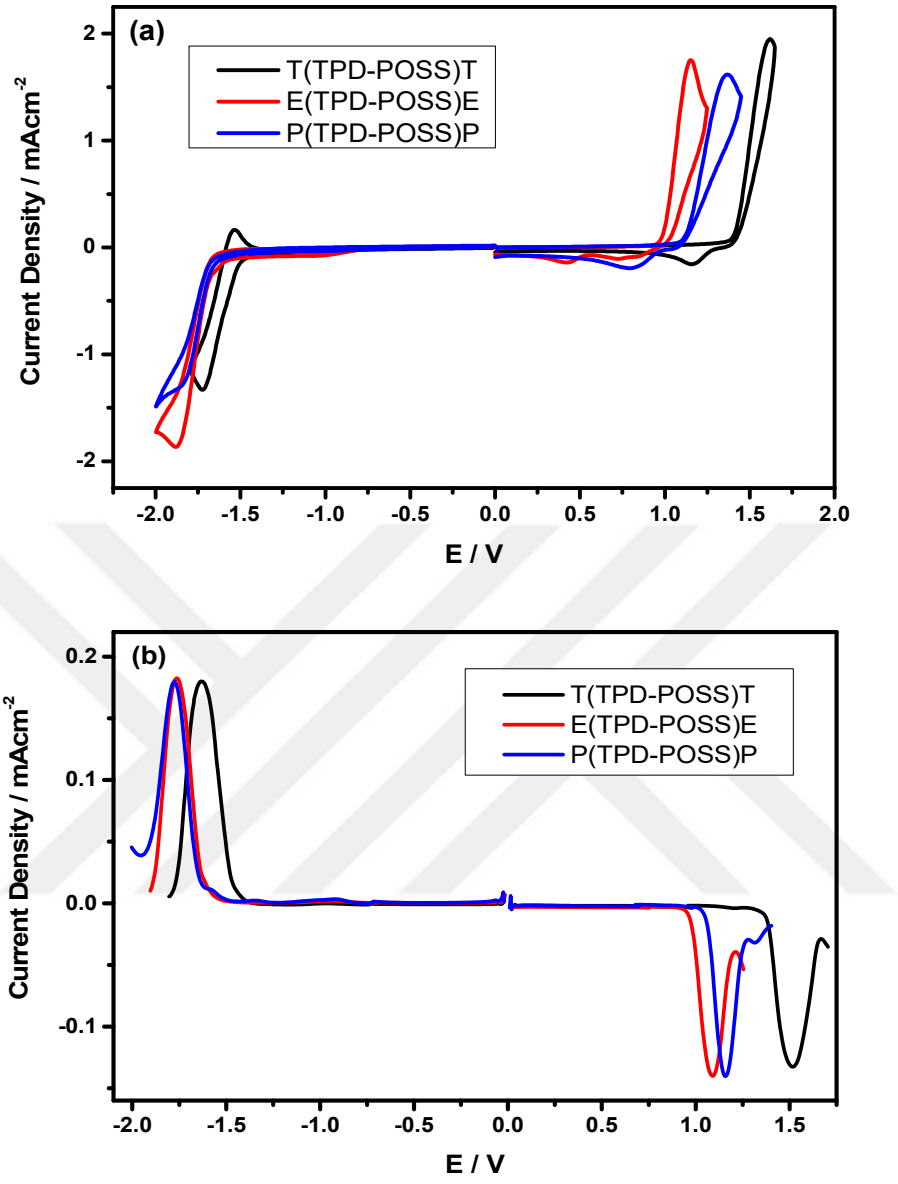

Figure 3.22. (a) Cyclic and (b) differential pulse voltammograms for full scan of T(TPD-POSS)T, E(TPD-POSS)E and P(TPD-POSS)P monomers on Pt electrode in 0.1 M $TBAPF_6$ dissolved in DCM at a scan rate of 100 mVs^{-1} vs. Ag/AgCl.

Table 3.6 Optical and electrochemical properties of T(TPD-POSS)T, E(TPD-POSS)E and P(TPD-POSS)P monomers

Monomer	T(TPD-POSS)T	E(TPD-POSS)E	P(TPD-POSS)P
$\lambda_{max,abs}$ (nm)	269, 383	275, 398	276, 393
$\lambda_{max,em}$ (nm)	460	480	477
$E_{ox,m}$ (V)	1.62	1.15	1.37
$E_{red,m}$ (V)	-1.72	-1.89	-1.85
$E_{ox,onset,m}$ (V)	1.38	0.98	1.06
$E_{red,onset,m}$ (V)	-1.47	-1.63	-1.65
HOMO (eV)	-6.09	-5.69	-5.77
LUMO (eV)	-3.24	-3.08	-3.06
$E_g^{electro}$ (eV)	2.85	2.61	2.71
E_g^{opt} (eV)	2.88	2.79	2.81
QY	0.112	0.074	0.075

3.2.2.3 Electrochemical Polymerization and Spectroelectrochemical Properties

Firstly, all the three monomers were electrochemically polymerized on Pt disc electrode via potentiodynamic method in 0.1 M $TBAPF_6$ dissolved in a DCM/MeCN mixture. The structure for the polymer films is depicted in Figure 3.23. The electropolymerization for each monomer was carried out in the potential range from 0.0 V to +1.55 V, +1.15 V and +1.20 V versus Ag/AgCl for T(TPD-POSS)T, E(TPD-POSS)E and P(TPD-POSS)P, respectively. The obtained voltammograms during repetitive potential cycling are given in Figure 3.24. After observing the first irreversible oxidation peak, which is responsible for the electropolymerization, new redox couples start to appear at about +1.2 V for

PT(TPD-POSS)T, from +0.3 V to +0.9 V for PE(TPD-POSS)E and at about +0.8 V for PP(TPD-POSS)P as shown in Figure 3.24 (a), (c) and (e). After each successive scan, the current intensifies steadily due to the formation of an electroactive polymer film on the surface of Pt disc working electrode. After completion of the polymer formation, the electrode surface was washed with MeCN to remove all other species on the polymer film for further investigation.

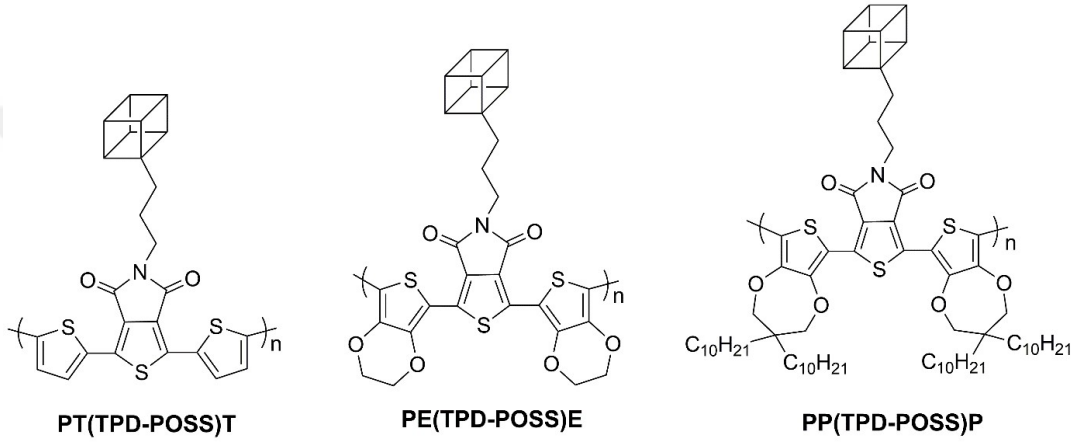

Figure 3.23. The chemical structure of polymer films.

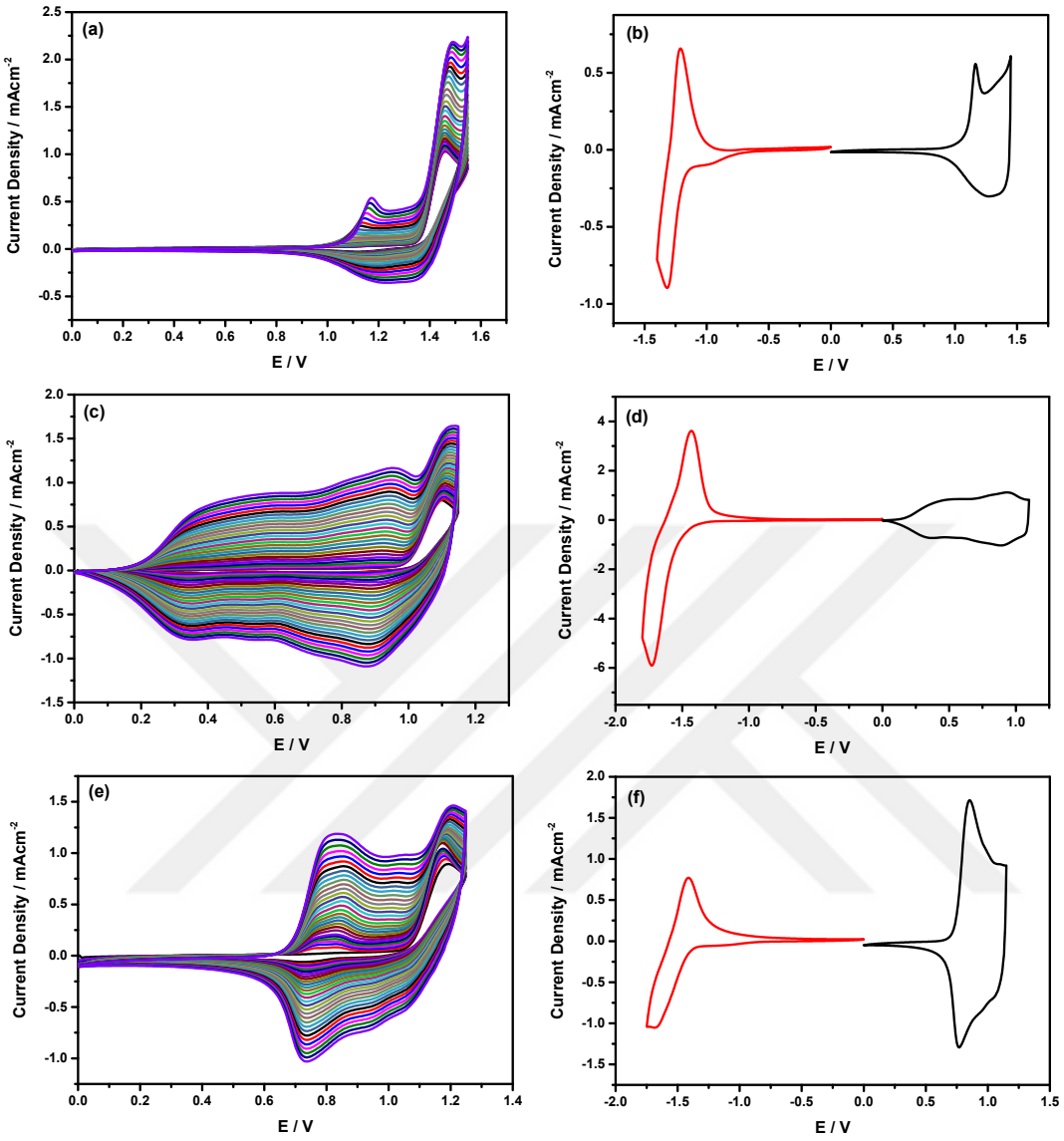

Figure 3.24. Repetitive cyclic voltammograms of (a) T(TPD-POSS)T, (c) E(TPD-POSS)E and (e) P(TPD-POSS)P monomer recorded in 0.1 M $TBAPF_6$ dissolved in MeCN/DCM ((1/1: v/v) and cycling voltammograms of their corresponding polymer films (b) PT(TPD-POSS)T, (d) PE(TPD-POSS)E and (f) PP(TPD-POSS)P polymer films recorded in 0.1 M $TBAPF_6$ dissolved in MeCN/DCM ((1:1, v:v) for PT(TPD-POSS)T), (2:1, v:v) for PE(TPD-POSS)E and PP(TPD-POSS)P) on Pt disc electrode vs. Ag/AgCl at a scan rate of 100 mVs^{-1}.

To gain more insight into the redox behaviors of the polymer films, their CVs and DPVs are recorded in a monomer free electrolyte solution during doping and de-doping of polymer films in both anodic and cathodic regions. The resulting voltammograms are given in Figure 3.24 (b), (d) and (f). As shown in the figure, all the films present reversible redox peaks during both anodic and cathodic scans. Furthermore, the scan rate dependency study was carried out at different scan rates from 25 mVs^{-1} to 200 mVs^{-1} with an increment of 25 mVs^{-1}. The linear dependency of the current density on the scan rate reveals a non-diffusion controlled redox process taking place on well-adhered polymer films on the electrode surface as depicted in Figure 3.25.

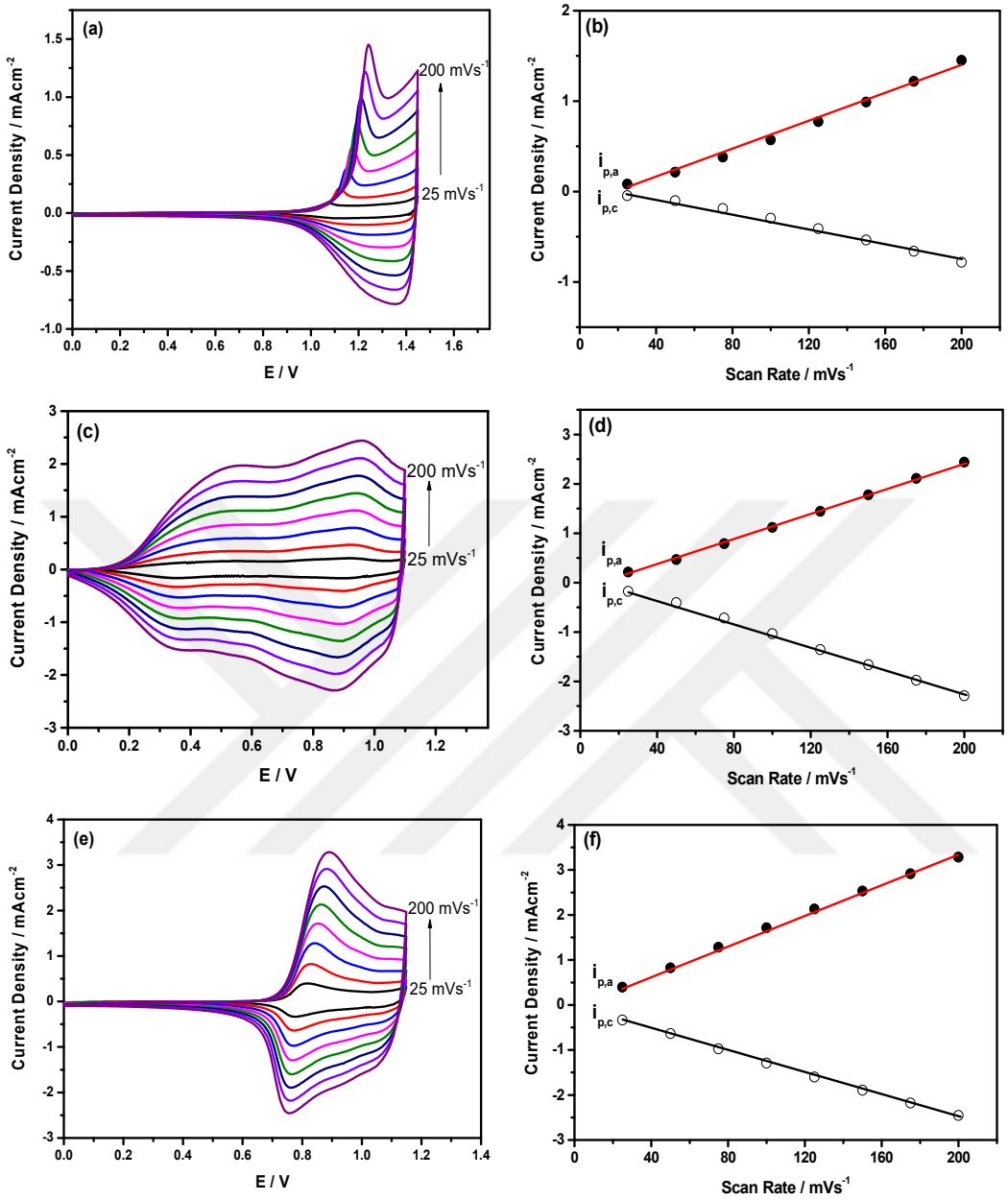

Figure 3.25. Scan rate dependence of polymer films on Pt disc electrode recorded in 0.1 M $TBAPF_6$ solution (a) PT(TPD-POSS)T in MeCN:DCM (1:1, v:v), (c) PE(TPD-POSS)E and (e) PP(TPD-POSS)P in MeCN:DCM (2:1, v:v) at different scan rates from 25 mVs^{-1} to 200 mVs^{-1} with 25 mVs^{-1} increments. The relationship of anodic and cathodic peak currents as a function of scan rate for (b) PT(TPD-POSS)T, (d) PE(TPD-POSS)E and (f) PP(TPD-POSS)P polymer films.

Table 3.7 Electrochemical properties of the polymer films

Polymer	**PT(TPD-POSS)T**	**PE(TPD-POSS)E**	**PP(TPD-POSS)P**
$E_{ox,p}$ (V)	1.16	0.51	0.85
$E_{red,p}$ (V)	-1.32/-1.21	-1.73/-1.43	-1.68/-1.41
$E_{ox,onset,p}$ (V)	1.12	0.16	0.72
$E_{red,onset,p}$ (V)	-1.17	-1.39	-1.34
$E_g^{electro}$ (eV)	2.29	1.55	2.06
E_g^{opt} (eV)	1.79	1.64	1.78
HOMO (eV)	-5.83	-4.87	-5.43
LUMO (eV)	-3.54	-3.32	-3.37

The electrochemical band gap values of the polymer films are estimated from the onset potentials obtained from DPV measurements depicted in Figure 3.26. These onset potentials of the films are also tabulated in Table 3.7 together with electrochemical E_g values. A detailed inspection of the table indicates that PE(TPD-POSS)E has the lowest onset potentials and lowest E_g value among the three polymers. These results are in accordance with the ones obtained from their corresponding monomers. It is also noteworthy that the trend observed in E_g values of the polymers ($E_{g,PE(TPD\text{-}POSS)E} < E_{g,PP(TPD\text{-}POSS)P} < E_{g,PT(TPD\text{-}POSS)T}$) is the same as the one observed for their ethylhexyl appended analogues[6]. When all of these results are taken into account, it can be safely concluded that the effect of the pendant group on the acceptor unit is quite negligible, most probably due to the lack of conjugation between the TPD acceptor unit and POSS substituent. In such cases, the optical and electrochemical properties of the monomers and their corresponding polymers are only related to the strength of donor units.

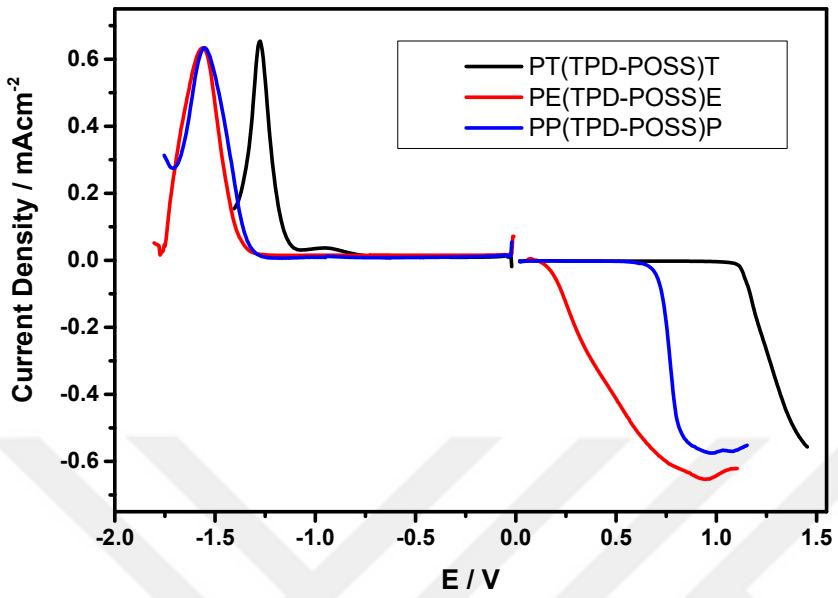

Figure 3.26. DPVs of polymer films recorded in 0.1 M $TBAPF_6$ dissolved in MeCN/DCM ((1:1, v:v) for PT(TPD-POSS)T), (2:1, v:v) for PE(TPD-POSS)E and PP(TPD-POSS)P) on Pt disc electrode vs. Ag/AgCl.

In order to investigate the electrochromic features, PT(TPD-POSS)T, PE(TPD-POSS)E and PP(TPD-POSS)P polymer films were deposited on ITO glass electrodes via potential cycling. The spectroelectrochemical measurements were carried out by monitoring the changes in the electronic absorption spectra under applied external potentials. In their neutral states, the absorption maxima due to π-π* transitions for PT(TPD-POSS)T, PE(TPD-POSS)E and PP(TPD-POSS)P were found to be 525 nm, 545 nm and 585 nm, respectively (see Figure 3.27). In the case of PE(TPD-POSS)E and PP(TPD-POSS)P, the splitting in the π-π* transition bands shows the existence of a concrete vibronic shoulder especially for PP(TPD-POSS)P, indicating the increased π-π stacking in the polymer backbone[151,155]. The optical E_g values of polymer films were calculated from the onsets of π-π* transition bands and the results are listed in Table 3.8. Taking the results into account, the identical trend is observed in the the variation of optical E_g values as

in the case of electrochemical E_g values albeit all the optical values are somehow lower than the electrochemical ones.

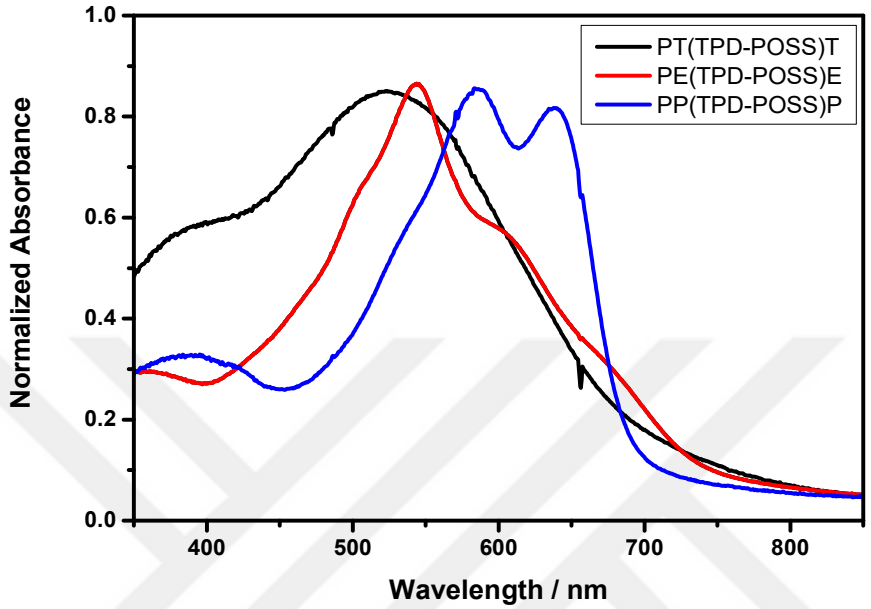

Figure 3.27. Neutral state absorption spectra of PT(TPD-POSS)T, PE(TPD-POSS)E and PP(TPD-POSS)P films coated on ITO electrode in 0.1 M $TBAPF_6$/MeCN.

For the three polymer films, the recorded spectra during their potential scanning from 0.0 V to +1.3 V for PT(TPD-POSS)T, from 0.0 V to +1.0 V for PE(TPD-POSS)E and from 0.0 V to +1.2 V for PP(TPD-POSS)P are given in Figure 3.28. A careful examination of the spectroelectrochemical measurements reveals that π-π* transition bands loose their intensities during p-doping, whereas new bands are formed at 740 nm, 846 nm and 872 nm for PT(TPD-POSS)T, PE(TPD-POSS)E and PP(TPD-POSS)P, respectively. The appearance of new bands shows the formation of polaron charge carriers during p-doping of the polymer films. Upon further oxidation, these bands undergo blue shift by the emergence of another new

band beyond 950 nm. These spectroelectrochemical changes are also followed by color changes: reddish pink, dark blue and blue in their colored states and grey, light blue and colorless in their bleached states for PT(TPD-POSS)T, PE(TPD-POSS)E and PP(TPD-POSS)P, respectively. The color cordinates of the films in their colored and bleached states are represented by L*, a*, b* values and tabulated in Table 3.8.

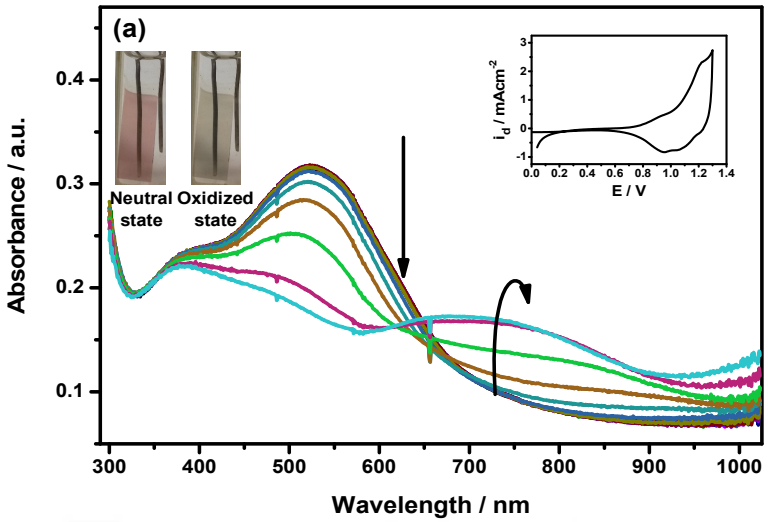
(a)
Neutral state
Oxidized state
Absorbance / a.u.
Wavelength / nm
E / V

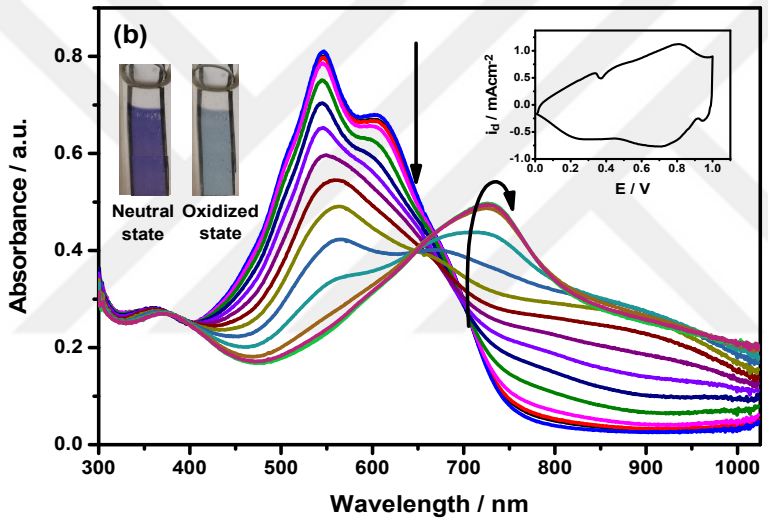
(b)
Neutral state
Oxidized state
Absorbance / a.u.
Wavelength / nm
E / V

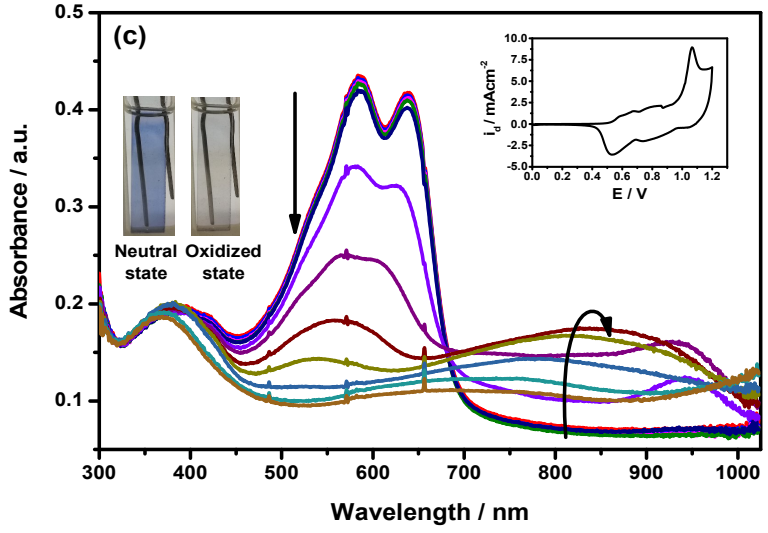
(c)
Neutral state
Oxidized state
Absorbance / a.u.
Wavelength / nm
E / V

Figure 3.28. The changes in electronic absorption spectra of electrochemically deposited (a) PT(TPD-POSS)T, (b) PE(TPD-POSS)E and (c) PP(TPD-POSS)P films on ITO recorded at various applied potentials in 0.1 M $TBAPF_6$/MeCN. Insets: CVs of the films recorded with a scan rate of 20 mVs^{-1}. Inset: The colors of the films at neutral and oxidized states.

In order to obtain the electrochromic data for the polymer films, they are switched repeatedly between two extreme (neutral and oxidized) states with a switching time of 10 s via square wave potential technique (see Figure 3.29) and the resulting data is presented in Table 3.8. The electrochromic contrasts are found to be 18% at 525 nm for PT(TPD-POSS)T, 46% at 545 and 33% at 600 nm for PE(TPD-POSS)E and 50% at 585 nm and 52% at 640 nm for PP(TPD-POSS)P. The oxidation response time, neutralization response time and CE to reach 95% full contrast were calculated as 0.6 s, 0.5 s and 204 cm^2/C at 525 nm for PT(TPD-POSS)T, 0.6 s, 0.6 s and 472 cm^2/C at 545 nm for PE(TPD-POSS)E, 0.4 s, 0.3 s and 522 cm^2/C at 585 nm for PP(TPD-POSS)P, respectively. A more careful comparison of the spectroelectrochemical data clearly indicates that both electrochromic contrast and CE values are enhanced when going from thiophene bearing polymer to ProDOT bearing polymer. Moreover, the shortest switching time is observed for ProDOT containing polymer film since long alky chains provide interchain separation and thereby facilitates ion movement during switching. Furthermore, the POSS appended PT(TPD-POSS)T film exhibits quite fast switching time as compared to its ethylhexyl appended counterpart. This result indicates that the bulky POSS cages can also contribute to interchain separation for the fast ion movement.

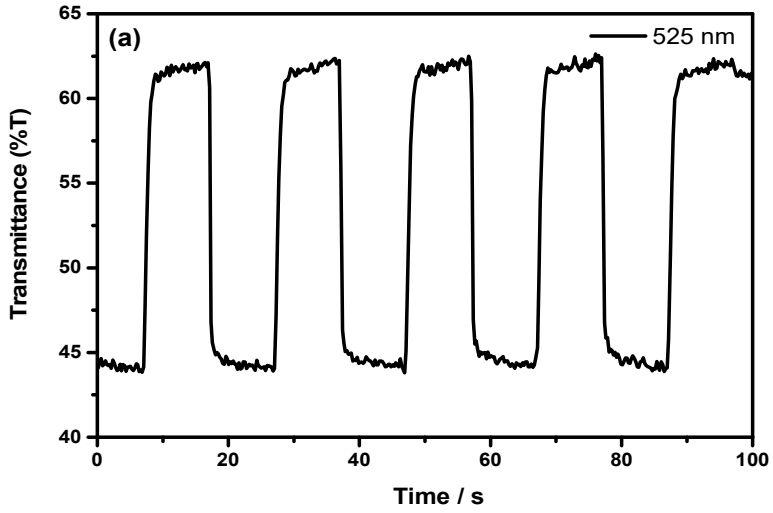
(a)
525 nm
Transmittance (%T)
Time / s

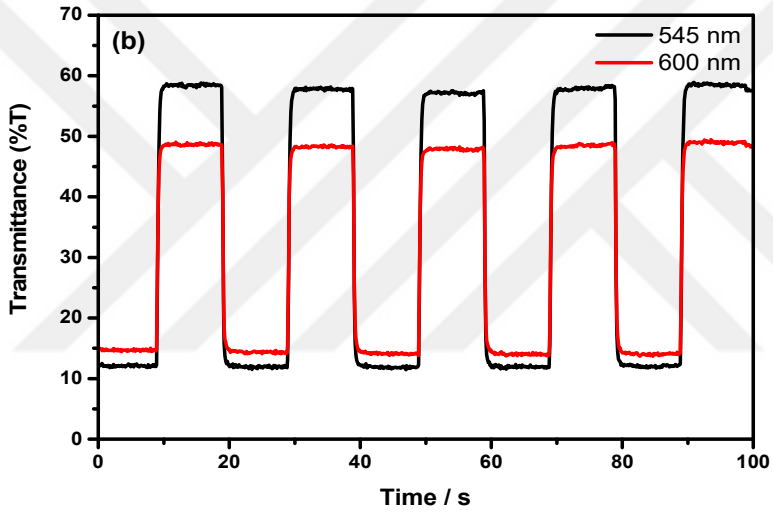
(b)
545 nm
600 nm
Transmittance (%T)
Time / s

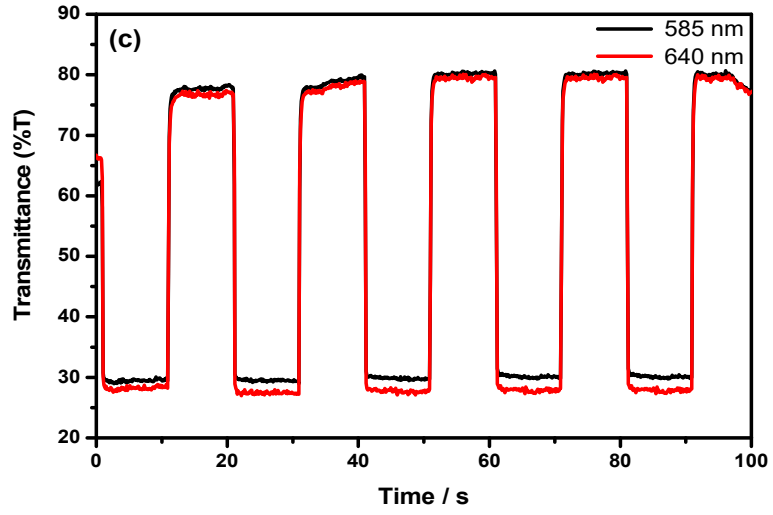
(c)
585 nm
640 nm
Transmittance (%T)
Time / s

Figure 3.29. Chronoabsoptometry experiments for the polymer films on ITO in 0.1 M $TBAPF_6$/MeCN when the films were switched between redox states with an interval time of 10 s for (a) PT(TPD-POSS)T (between 0.0 V and +1.3 V at 525 nm), (b) PE(TPD-POSS)E (between 0.0 V and +1.0 V at 545 nm and 600 nm) and (c) PP(TPD-POSS)P (between 0.0 V and +1.2 V at 585 nm and 640 nm).

Table 3.8 Optoelectronic properties of the polymer films on ITO in 0.1 M $TBAPF_6$/MeCN

Polymer	**PT(TPD-POSS)T**	**PE(TPD-POSS)E**	**PP(TPD-POSS)P**
λ_{max} (nm)	525	545, 600	585, 640
E_g^{opt} (eV)	1.79	1.64	1.78
Δ%T	18	46, 33	50, 52
CE (cm^2/C)	204	472, 387	522, 550
$t_{s,ox}$[a] (s)	0.6	0.6, 0.6	0.4, 0.4
$t_{s,red}$[a] (s)	0.5	0.6, 0.7	0.3, 0.3
Color at neutral state L*, a*, b*	75.18, 8.23, -2.09	53.60, 8.07, -35.27	71.71, -7.54, -24.3
Color at oxidized state L*, a*, b*	82.76, 5.36, 4.90	81.05, -7.54, -7.55	90.98, -0.18, 0.91

[a] 95% of full switch from colored to bleached states.

3.2.2.4 Chemical Polymerization and Spectroelectrochemical Properties

It is worth noting that when POSS appendages are used instead of ethylhexyl unit, all the electrochemically obtained POSS-substituted polymers exhibit solubility in common organic solvents unlike ethylhexyl-substituted ones. This result reveals that POSS unit can easily imparts solubility to the polymers. This property makes the POSS bearing conjugated polymers a good candidate for various applications. Therefore, in order to obtain the solution processable polymers in larger quantities, PE(TPD-POSS)E and PP(TPD-POSS)P polymers were also polymerized via oxidative chemical polymerization by using $FeCl_3$. Characterization of PE(TPD-POSS)E-C and PP(TPD-POSS)P-C were conducted by ^{1}H NMR and GPC. When ^{1}H NMR spectra of the polymers are compared with the corresponding monomer spectra, it is seen that the peaks in polymer spectra are broadened as compared to those of the monomers. Additionally, the disappearance of the peak attributed to H atom at α-position of both E(TPD-POSS)E and P(TPD-POSS)P monomers indicates that polymerization takes place at this position (see Appendix Figure A.31 and Figure A.34 for the ^{1}H NMR of PE(TPD-POSS)E-C and PP(TPD-POSS)P-C, respectively).

From GPC analysis, the number average molecular weights of PE(TPD-POSS)E-C and PP(TPD-POSS)P-C polymers were found to be 31,039 Da and 18,950 Da, respectively (see Appendix Figure C.2 and Figure C.3 for GPC chromatogram of PE(TPD-POSS)E-C and PP(TPD-POSS)P-C, respectively). After structural characterization, in order to investigate the optoelectronic features of the chemically obtained polymers, the spectroelectrochemical studies were conducted in both solution and film form. Firstly, the soluble polymers obtained via chemical method were dissolved in DCM and their absorption spectra were recorded for comparison sake. The resulting spectra are given in Figure 3.30. As seen in the figure, it was found that the optical bandgap of PE(TPD-POSS)E-C polymer, calculated from low energy onset of polymer solution, is lower than that of

PP(TPD-POSS)-C. The same trend was observed as in the case of polymer films obtained via electrochemical polymerization of the monomers.

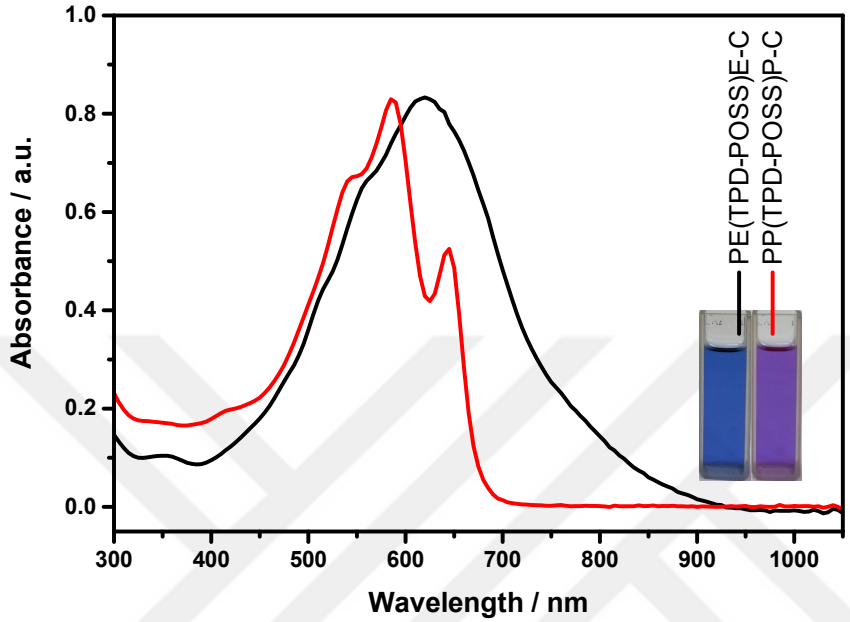

Figure 3.30. Neutral state absorption spectra of chemically obtained PE(TPD-POSS)E-C and PP(TPD-POSS)P-C polymers dissolved in DCM.

The emission characteristics of chemically obtained polymers were also investigated in DCM and it was found that only PP(TPD-POSS)P-C polymer displays appreciable fluorescence emission. The recorded emission spectrum in DCM is depicted in Figure 3.31 together with its absorption spectrum. As seen from the figure, the two emission peaks are observed for PP(TPD-POSS)P-C at 615 nm and 670 nm corresponding to red color emission (see inset photos of Figure 3.31)

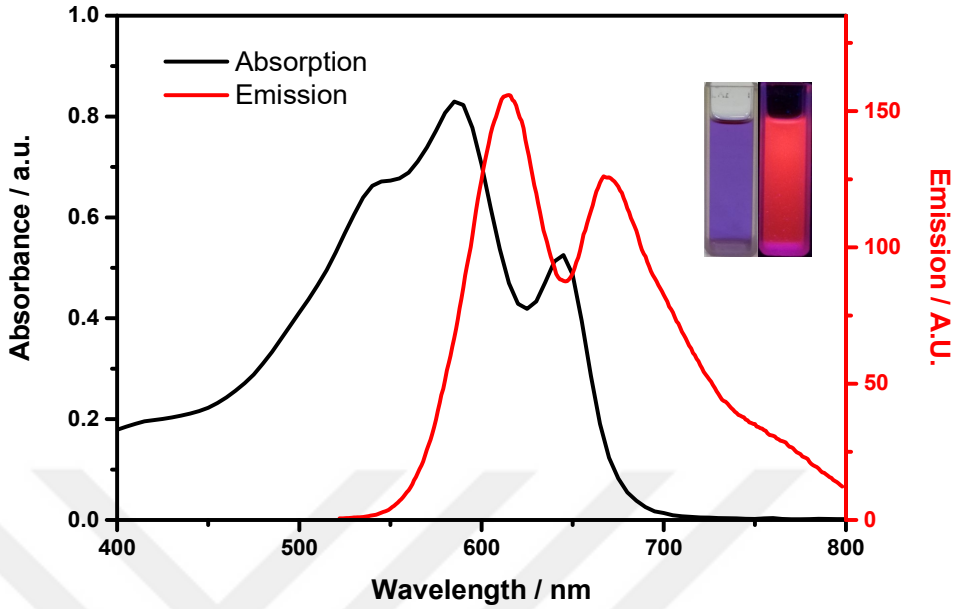

Figure 3.31. Electronic absorption and emission spectra of chemically obtained PP(TPD-POSS)P-C polymer in DCM.

It is worth mentioning that solutions of PE(TPD-POSS)E and PP(TPD-POSS)P in toluene can be reversibly oxidized and reduced via stepwise additions of $SbCl_5$ and N_2H_5OH, respectively. The changes recorded in the electronic absorption spectra, depicted in Figure 3.32, during the chemical oxidation of the polymer solutions were almost the same as the one recorded during in-situ electrochemical oxidation of polymer films on ITO (see Figure 3.28 (c) for comparison). In each case, upon addition of $SbCl_5$ or the potential applied, the π-π* transition bands start to decline simultaneously with the emergence of concomitant absorption bands beyond π-π* transition bands. In the case of chemical doping, the reduction of the polymer solutions is achived by stepwise addition of 0.2 M N_2H_5OH to obtain the absorption spectra in their neutral forms.

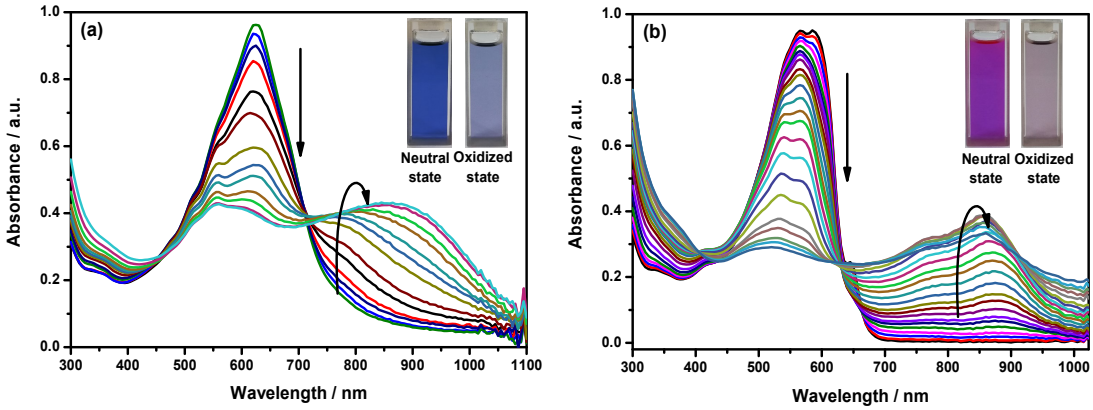

Figure 3.32. Changes in the absorption spectra of (a) PE(TPD-POSS)E-C and (b) PP(TPD-POSS)P-C dissolved in toluene during chemical oxidation by using 0.05 M $SbCl_5$ oxidant with 10 µL stepwise additions. Inset: absorption spectrum after chemical reduction by using hydrazine. Inset: Colors of polymer solution at neutral and oxidized states.

In order to investigate the spectroelectrochemical features of the chemically obtained PE(TPD-POSS)E-C and PP(TPD-POSS)P-C polymers, they were coated on the ITO working electrode surface by spray coating. The spectroelectrochemical studies of the resulting spray coated films were conducted in 0.1 M $TBAPF_6$ /MeCN and the related data is given in Table 3.9 for comparison purpose with those of electrochemically coated ones. Firstly, the neutral absorption spectra of the spray coated polymer films on ITO were recorded and given in Figure 3.33. The absorption maxima of the spray coated films were detected at about 632 nm and 585 nm with a vibronic shoulder at 640 nm for PE(TPD-POSS)E-C and PP(TPD-POSS)P-C, respectively. As it can also be seen from the figure, contrary to the electrochemically coated films on ITO, PE(TPD-POSS)E-C film exhibits a red shift as compared to that of PP(TPD-POSS)P-C. This result may be attributed to the extended conjugation length of chemically obtained PE(TPD-POSS)E-C film as compared to the electrochemically obtained one. The optical E_g values for chemically obtained PE(TPD-POSS)E-C and PP(TPD-POSS)P-C solid films were

calculated from the absorption band edge of the UV-Vis spectra as 1.52 eV and 1.80 eV, respectively. Among the solid films, the lowest E_g is detected in PE(TPD-POSS)E polymer film for both chemically and electrochemically obtained forms, which is most probably due to the higher donor ability of EDOT as compared to ProDOT.

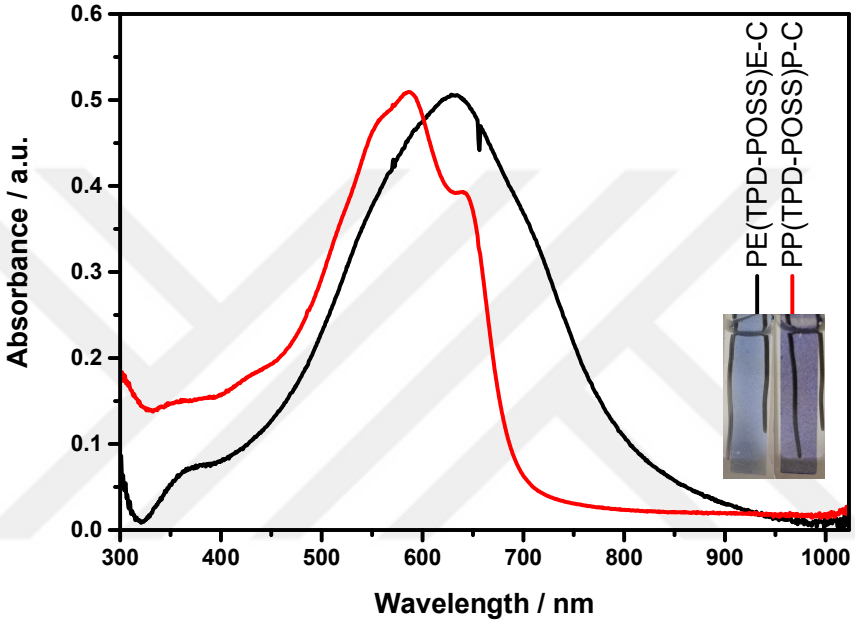

Figure 3.33. Neutral state electronic absorption spectra of spray coated PE(TPD-POSS)E-C and PP(TPD-POSS)P-C films on ITO electrode in 0.1 M $TBAPF_6$/MeCN.

The changes in the absorption spectra of spray coated films under various applied external potentials are depicted in Figure 3.34 together with its chronoabsoptometry study. The electrochromic properties such as transmittance change, CE, oxidation switching time and neutralization switching time of the spray coated films were found to be 30%, 954 cm^2/C, 0.7 s and 2.0 s for PE(TPD-POSS)E-C and 23%, 995 cm^2/C, 1.0 s and 6.4 s for PP(TPD-POSS)P-C, respectively and these results are also listed in Table 3.9. The close examination of these results reveals that while the CE is improved for spray coated film, optical

contrast and switching time values are not as high as the electrochemically obtained one which may be attributed to the quality of coating and film morphology. Also, the higher switching time was observed for neutralization of spray coated films as compared to oxidation of them due to the slow movement of counter ions outside of polymer backbone.

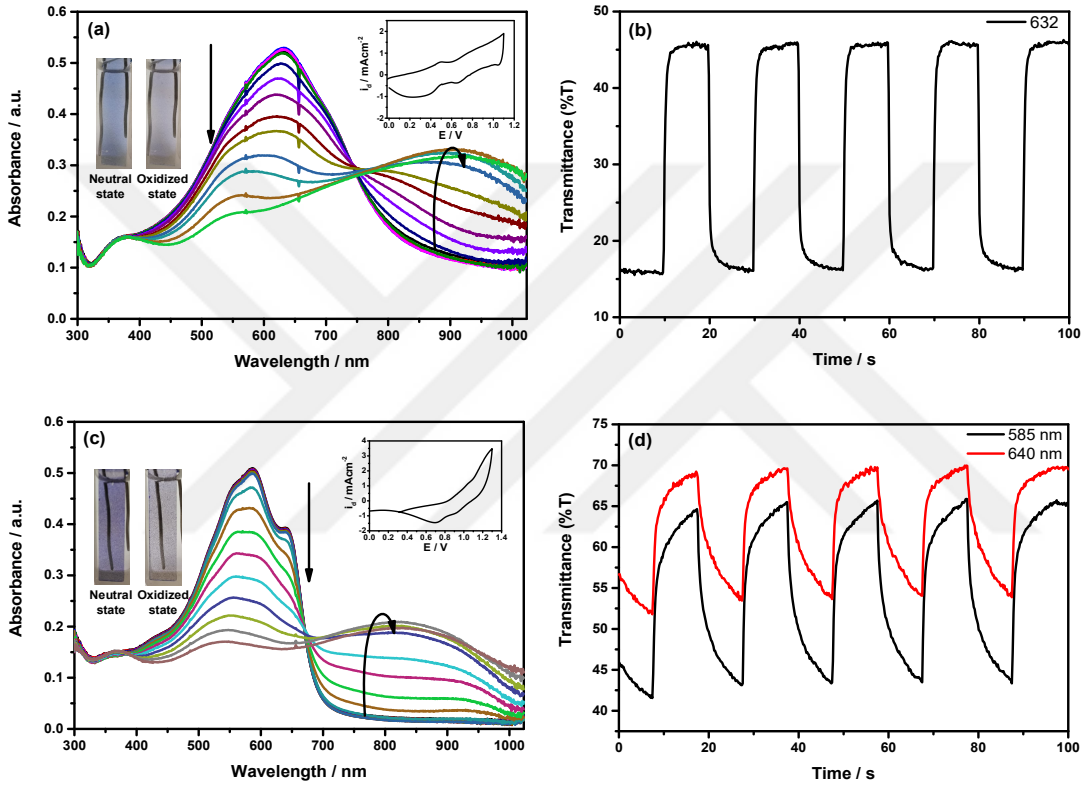

Figure 3.34. The changes in electronic absorption spectra of spray coated (a) PE(TPD-POSS)E-C and (c) PP(TPD-POSS)P-C film on ITO recorded at various applied potentials in 0.1 M $TBAPF_6$/MeCN. Insets: CVs of the films recorded with a scan rate of 20 mVs^{-1}. Insets: The colors of the films at neutral and oxidized states. (b) Chronoabsoptometry experiments for polymer films when switched with an inteerval of 10 s for (b) PE(TPD-POSS)E-C (between -0.2 V and +1.2 V at 632 nm) and (d) PP(TPD-POSS)P-C (between 0.0 V and +1.3 V at 585 nm and 640 nm).

Table 3.9 Optoelectronic properties of the polymer films on ITO in 0.1 M $TBAPF_6$/MeCN

Polymer	**PE(TPD-POSS)E-C**	**PP(TPD-POSS)P-C**
λ_{max} (nm)	632	585, 640
E_g^{opt} (eV)	1.52	1.80
Δ%T	30	23, 17
CE (cm^2/C)	954	995, 720
$t_{s,ox}$[a] (s)	0.7	1.3, 1.0
$t_{s,red}$[a] (s)	2.0	6.4, 6.0
Color at neutral state L*, a*, b*	77.33, -3.41, -18.46	70.78, 3.15, -23.42
Color at oxidized state L*, a*, b*	87.51, 1.10, -5.98	84.91, 2.95, -5.10

[a] 95% of full switch from colored to bleached states.

For the investigation of thermal features of the chemically obtained polymers, the thermogravimetric analysis (TGA) technique was used. For this aim, TGA measurements were recorded for POSS appended PE(TPD-POSS)E-C and PP(TPD-POSS)P-C polymers and their ethylhexyl appended analogues to elucidate the effect of POSS appendage on thermal stability (see Appendix Figure D.1, Figure D.2, Figure D.3 and Figure D.4 for TGA thermograms of PE(TPD-EtHex)E-C, PP(TPD-EtHex)P-C, PE(TPD-POSS)E-C and PP(TPD-POSS)P-C, respectively). All the measurements were carried out at the same conditions with a heating rate of 10 °C under nitrogen atmosphere and the resulting TGA thermograms are depicted together in Figure 3.35. As it can be seen from the

thermograms, the onset temperatures for 5% weight-loss were observed at 439 °C, 406 °C, 329 °C and 230 °C for PE(TPD-POSS)E-C, PP(TPD-POSS)P-C, PE(TPD-EtHex)E-C and PP(TPD-EtHex)P-C polymers, respectively. These results show that POSS appended polymers exhibit the higher onset temperatures as compared to their ethylhexyl appended analogues. It can be clearly stated that POSS substituents impart thermal stability to the polymer film, which is very crucial and desired function for photovoltaic and optoelectronic device applications.

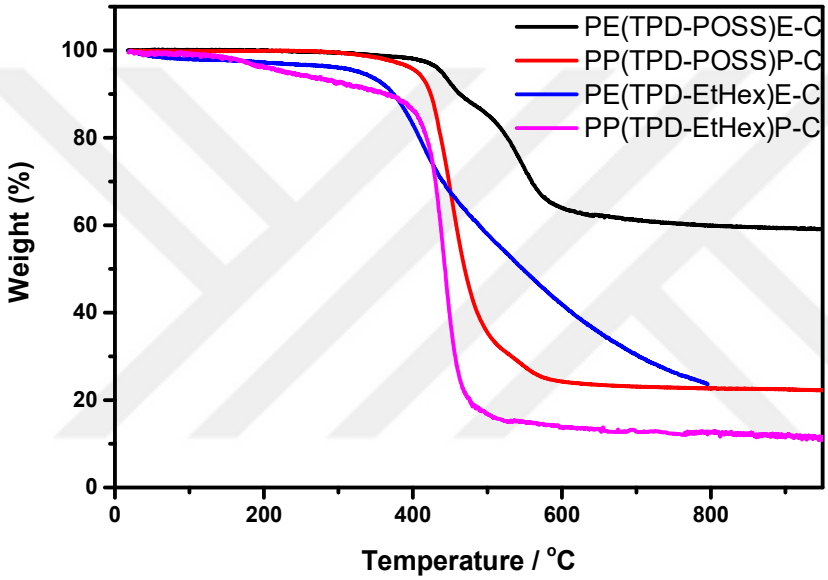

Figure 3.35. TGA thermograms of chemically obtained polymers.

Since PP(TPD-POSS)P was found to be a fluorescence emitter, the sensing ability of the chemically obtained PP(TPD-POSS)P polymer and its corresponding monomer, P(TPD-POSS)P was investigated by monitoring the changes in the emission spectra upon addition of different metal ions. First of all, the binding affinity of the monomer was investigated towards Fe^{2+}, Fe^{3+}, Cu^{2+}, Li^{+}, Ni^{2+}, Zn^{2+}, Hg^{2+}, Pb^{2+} and Cd^{2+} ions and the results are given in the from of Stern-Volmer plot in Figure 3.36 (a). As it can be seen from the plot, P(TPD-POSS)P exhibits binding

affinity only towards Fe^{2+}, Fe^{3+} and Cu^{2+} metal ions. The inset (a) and (b) of Figure 3.36 (a) indicates the steady decrease in fluorescence intensity with stepwise addition of Fe^{2+} and Fe^{3+} metal ions due to electron or energy transfer between metal ion and P(TPD-POSS)P fluorophore. Unlike stronger affinity of P(TPD-POSS)P towards Fe^{2+} and Fe^{3+} ions, quite smaller affinity was observed towards Cu^{2+} ion as it can be grasped from the K_{sv} values depicted in Figure 3.36 (b). The figure also shows that K_{sv} value for Fe^{3+} ion ($3.9x10^3$) is higher than that of Fe^{2+} ion ($2.3x10^3$). This might be assigned to higher charge density of Fe^{3+} ion.

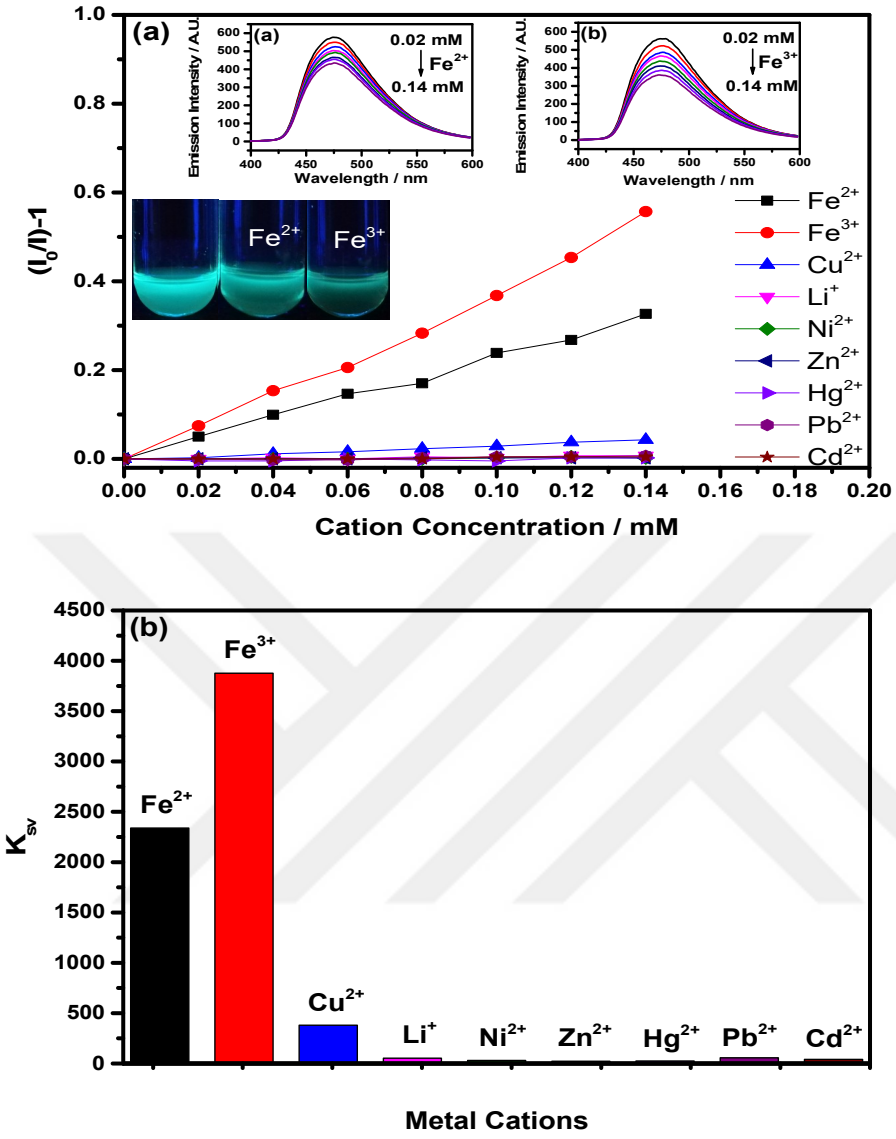

Figure 3.36. (a) The Stern-Volmer plots of P(TPD-POSS)P ($1x10^{-4}$ M) in the presence of various metal ions (0.02 mM - 0.14 mM). Metal ions $FeCl_2.4H_2O$, $Fe(NO_3)_3.9H_2O$, $Cu(NO_3)_2.3H_2O$, $LiClO_4$, $Ni(NO_3)_2.9H_2O$, $Zn(NO_3)_2.4H_2O$, $Hg(NO_3)_2$, $Pb(NO_3)_2$, $Cd(NO_3)_2.4H_2O$ in DMF. Insets: The fluorescence emission spectra of P(TPD-POSS)P in DMF with successive addition of 0.02 mM - 0.14 Mm (a) Fe^{2+} and (b) Fe^{3+} when excited at 340 nm. (b) K_{sv} values of P(TPD-POSS)P in the presence of Fe^{2+}, Fe^{3+}, Cu^{2+}, Li^{+}, Ni^{2+}, Zn^{2+}, Hg^{2+}, Pb^{2+} and Cd^{2+}.

Since the monomer shows strong binding affinity only towards Fe^{2+} and Fe^{3+} ions, the binding affinity of the polymer was also investigated only for these ions. The changes in the fluorescence intenstiy for PP(TPD-POSS)P-C polymer were recorded in THF upon stepwise addition of Fe^{2+} and Fe^{3+} ions and the obtained results are depicted in the form of Stern-Volmer plot in Figure 3.37 (a) together with inset figures corresponding to the recorded spectra during Fe^{2+} and Fe^{3+} additions. Moreover, K_{sv} values estimated from the slope of Stern-Volmer plots are given in Figure 3.37 (b) for both monomer and polymer solutions. As seen from the figure, K_{sv} values obtained for Fe^{2+} ($6.64x10^3$ M^{-1}) and Fe^{3+} ($9.31x10^3$ M^{-1}) ions in polymer solution increase more than two-fold as compared to that in monomer. This strong binding affinity of the polymer towards Fe^{2+} and Fe^{3+} ions can also be seen by naked eye under UV light (see Inset photo in Figure 3.37 (a)). The observed ion sensing behaviour of PP(TPD-POSS)P-C makes the polymer highly desired for sensor applications.

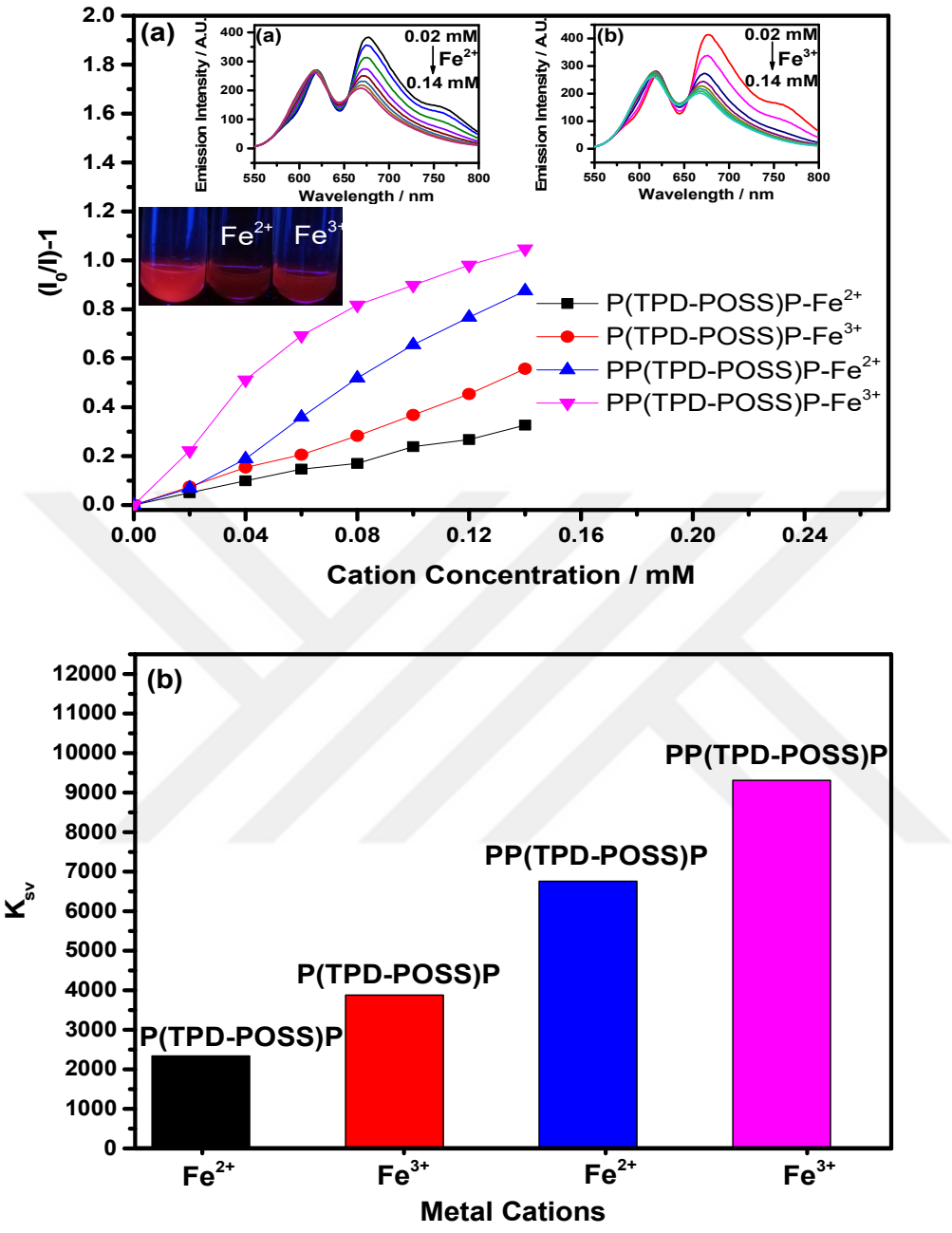

Figure 3.37. (a) The Stern-Volmer plots of PP(TPD-POSS)P-C (1 mg in 10 mL THF) in the presence of Fe^{2+} and Fe^{3+} metal ions (0.02 mM - 0.14 mM). Insets: The fluorescence emission spectra of PP(TPD-POSS)P-C in THF with successive addition of 0.02 mM - 0.14 Mm (a) Fe^{2+} and (b) Fe^{3+} when excited at 510 nm. (b) K_{sv} values of P(TPD-POSS)P in DMF and PP(TPD-POSS)P-C in THF in the presence of Fe^{2+} and Fe^{3+}.

3.2.3 D-A-D Monomers Based on TPD-Azo Acceptor Unit

In this part, azobenzene-substituted TPD moiety is synthesized as a new type of TPD-based acceptor units. This new type of acceptor is utilized for the synthesis of novel D-A-D systems, namely, T(TPD-Azo)T, E(TPD-Azo)E and P(TPD-Azo)P by coupling with thiophene, EDOT and didecyl-ProDOT donors. The photoswitching properties of the monomers were investigated as well as their electrochromic properties.

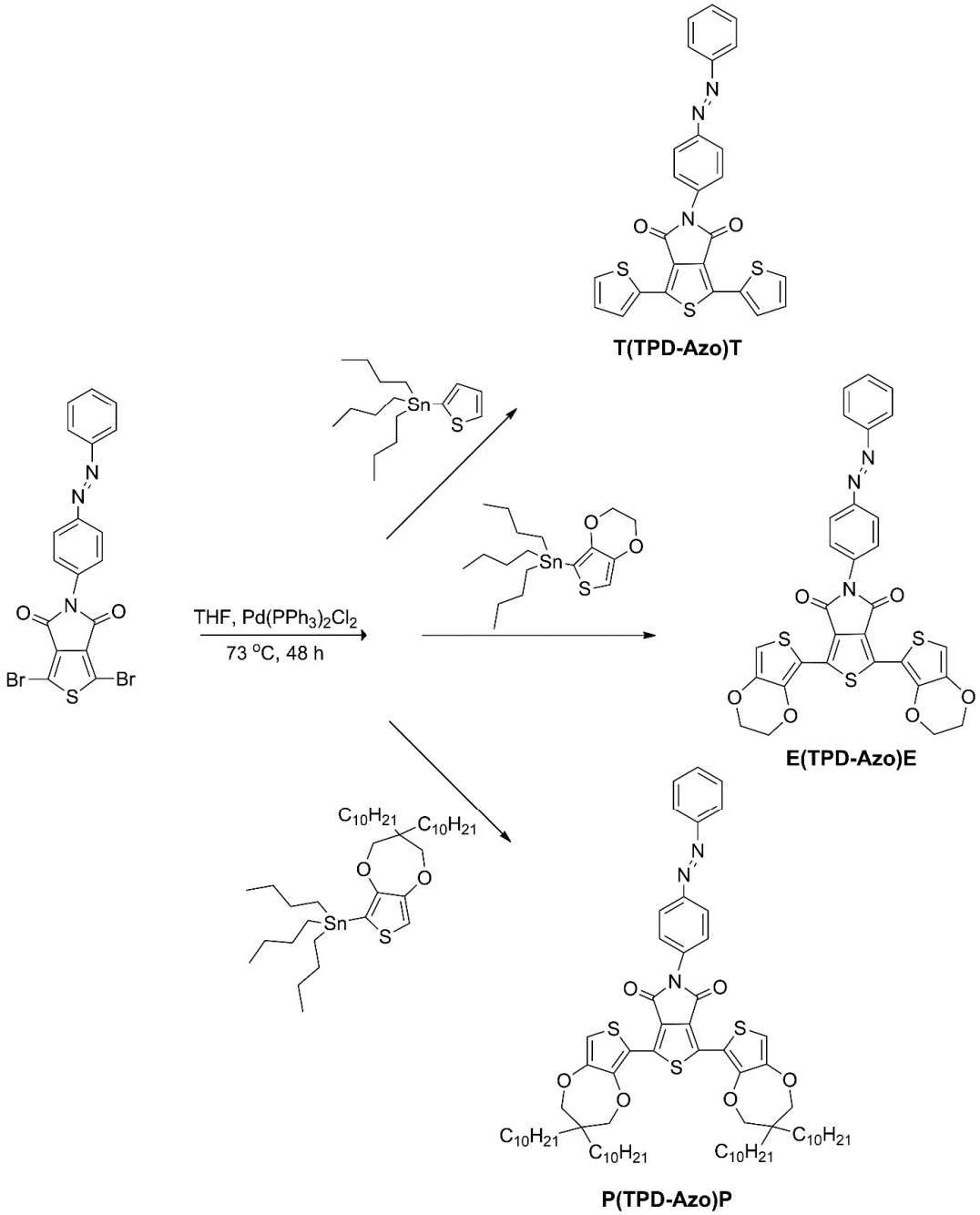

Scheme 3.5. Synthetic route for the synthesis of T(TPD-Azo)T, E(TPD-Azo)E and P(TPD-Azo)P.

3.2.3.1 Optical Properties of the Monomers

In order to understand the structure-property relationships in this new D-A-D type monomers, where a new substituent, azobenzene is attached to TPD core unit, the optical properties were investigated. For this aim, their electronic absorption and emission spectra are recorded in DCM and the resulting spectra are depicted in Figure 3.38 (a) and (b), respectively. As seen from the Figure 3.38 (a), the weak absorption band is observed at 265 nm in high energy region for all three monomers. The main absorption bands observed in the middle energy region at 343 nm for T(TPD-Azo)T, 335 nm for E(TPD-Azo)E and 333 nm for P(TPD-Azo)P refer to π-π* transition band of trans-azobenzene resulting from azobenzene appendage on the TPD acceptor unit[156]. Moreover, a third absorption bands in the low energy region is observed in the case of E(TPD-Azo)E and P(TPD-Azo)P at 405 nm and 400 nm, respectively, which is most probably due to ICT. However, this band is not obviously observed is the case of T(TPD-Azo)T monomer since it is not well-separated from π-π* transition band of azobenzene. Therefore, the low energy band onsets were compared instead of the low energy band maxima and it was noted that the low energy onset at 439 nm for T(TPD-Azo)T was shifted to longer wavelengths for E(TPD-Azo)E and P(TPD-Azo)P at 456 nm and 451 nm, respectively. In order to confirm the presence of ICT bands in these monomers, UV-Vis absorption spectrum of P(TPD-Azo)P monomer was recorded in solvents of different polarities as a representative example and depicted in Figure 3.39. A slight red shift from 440 nm to 452 nm in the onset of low energy band was noted with increasing solvent polarity. On the other hand, no such a red shift was noted for the π-π* transition band attributed to azobenzene. These observations indicate that ICT is responsible for the lower energy band. This can be explained by the poor donor nature of thiophene unit as compared to the other two units. The fluorescence emission spectra of the monomers were given in Figure 3.38 (b). As seen from the figure, all three monomers have a very low emission intensity, which is practically imperceptible to the human eye (see inset photo of Figure 3.38 (b)).

This confirms that azobenzene substituent has a quencing effect on the conjugated D-A-D system. Albeit that, these low emission bands are observable from the recorded spectra and their maxima are noted in Table 3.10. As seen from the table, the emission band maximum at 472 nm for T(TPD-Azo)T is slightly red shifted to 479 nm for E(TPD-Azo)E and to 475 nm for P(TPD-Azo)P. From the low energy shoulder maxima, a significant Stoke's shift is observed at around 70 nm, which indicates the conformational changes occuring in the molecules when excited[142,143].

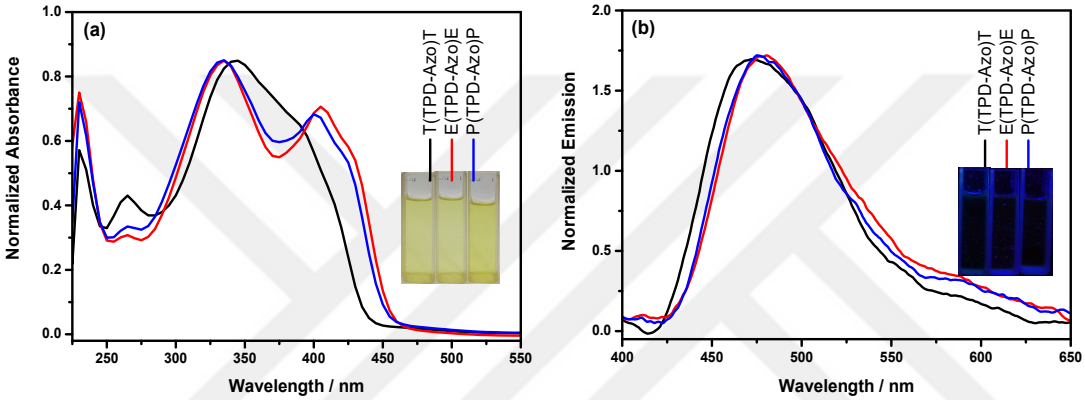

Figure 3.38. (a) Absorption and (b) emission spectra of the monomers in DCM. Inset: the color of the monomers (a) in daylight and (b) under UV lamp at 365 nm.

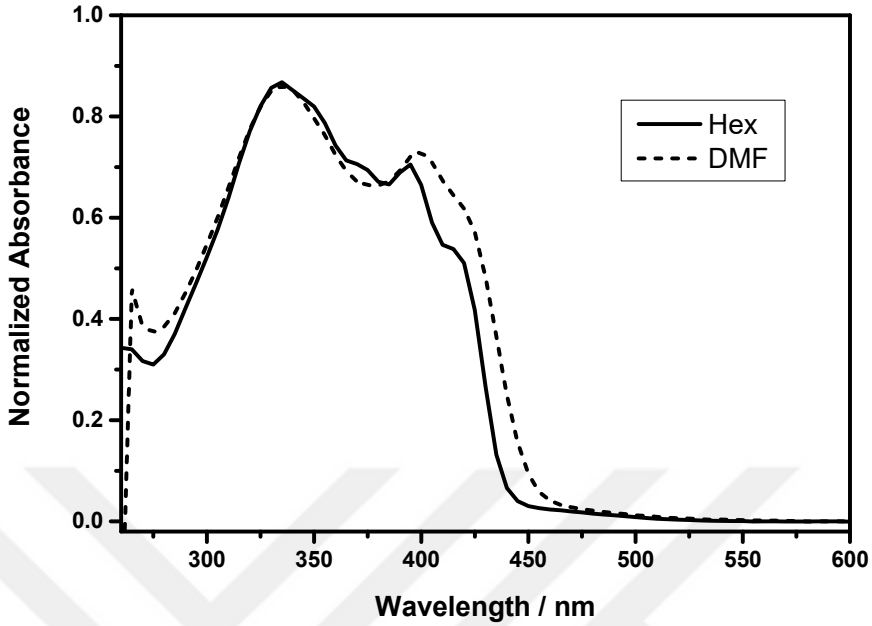

Figure 3.39. Normalized UV-Vis absorption spectra of P(TPD-Azo)P in different solvents.

3.2.3.2 Electrochemical Properties of the Monomers

In order to examine the effect of different electron donating groups on the redox behaviors of synthesized monomers, both CVs and DPVs of the monomers were recorded in an electrolyte solution containing 0.1 M $TBAPF_6$ dissolved in DCM vs Ag/AgCl and the resulting voltammograms are presented in Figure 3.40. As shown in Figure 3.40 (a), the monomers, T(TPD-Azo)T, E(TPD-Azo)E and P(TPD-Azo)P exhibit one irreversible oxidation peak at 1.53 V, 1.11 V and 1.20 V vs Ag/AgCl during the anodic scan and one quasi-reversible reduction peak at -1.29 V, -1.36 V and -1.38 V vs Ag/AgCl during the cathodic scan, respectively. The electrochemical data obtained from CV measurements are listed in Table 3.10 together with the corresponding electrochemical data obtained from the DPV measurements (Figure 3.40 (b)). The detailed examination of Table 3.10 reveals that among the three monomers, E(TPD-Azo)E exhibits the lowest oxidation and

onset potentials due to stronger electron donating nature of EDOT which increases the HOMO energy level and makes removal of electron easier. The reduction potentials of the monomers, on the other hand, were found to be nearly identical regardless of the donor unit. This is not surprising since the acceptor units that determine the LUMO energy levels are the same for all three monomers. Moreover, the trend observed in the oxidation potentials for the three monomers synthesized in this work ($E_{ox,T(TPD\text{-}Azo)T} > E_{ox,P(TPD\text{-}Azo)P} > E_{ox,E(TPD\text{-}Azo)E}$) are in good agreement with that of previously synthesized ethlyhexyl- and POSS-substituted analogs. By taking all these results into account, it can be concluded that the trend observed in the oxidation potentials is solely determined by donor groups of the monomers. On the other hand, detailed inspection and comparison of reduction potential of the TPD-based monomers revealed that the reduction potentials show variations depending on aryl or alky substituents on the acceptor unit. The reduction potentials of all azobenzene-substituted monomers are drastically shifted to more positive values with a magnitude of about 400 mV. This shift clearly originates from the substituent effect on the acceptor unit. Azobenzene as an electron withdrawing substituent increases the electron deficiency of the acceptor unit and as a result reduction potentials become more positive compared to ethylhexyl- and POSS-substituted analogs.

The HOMO and LUMO energy levels of the azobenzene-substituted monomers were calculated from the redox onset potentials obtained from DPV measurements and the results are listed in Table 3.10 together with electrochemical E_g values obtained from HOMO-LUMO energy levels. The E_g values were calculated as 2.53 eV for T(TPD-Azo)T, 2.18 eV for E(TPD-Azo)E and 2.28 eV for P(TPD-Azo)P. Among the three monomers, as expected, E(TPD-Azo)E monomer was found to have the lowest E_g due to higher donor strength of EDOT unit, which is most probably due to effective ICT between donor and acceptor units. This proves the effective HOMO-LUMO interaction of EDOT containing monomers which is in accordance with our previous results[6].

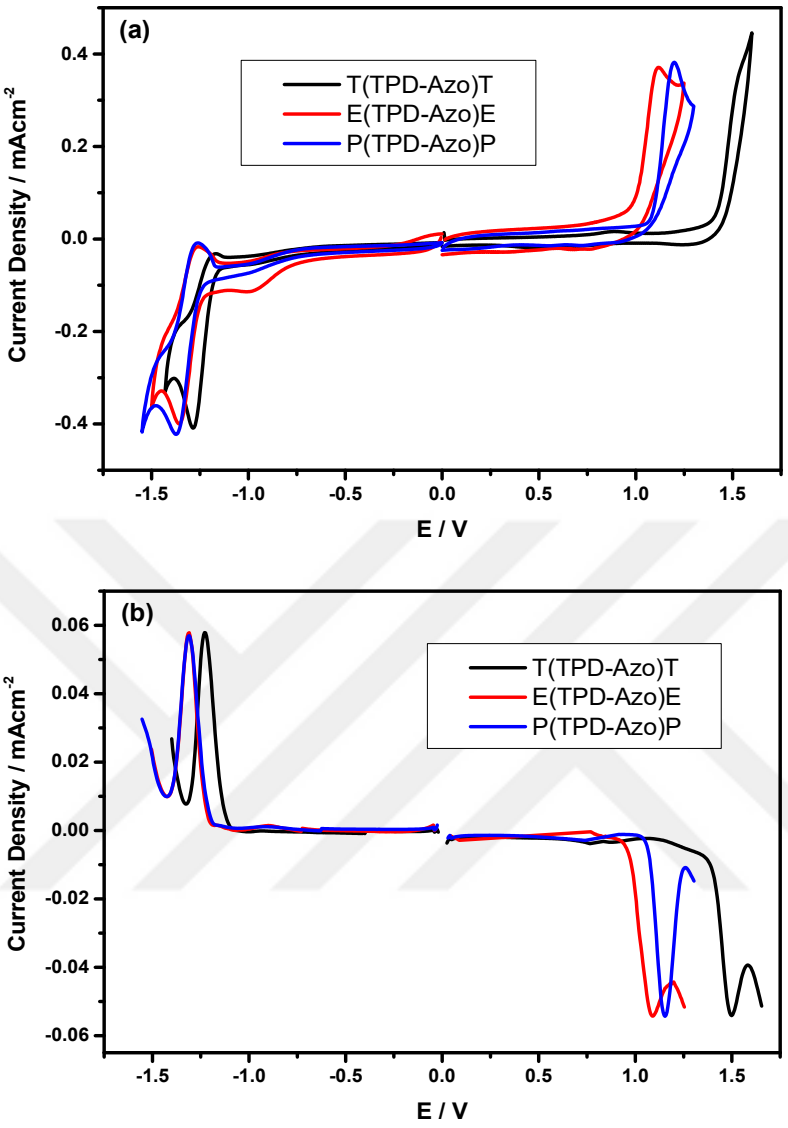

Figure 3.40. (a) Full scan cyclic voltammograms of the monomers on Pt electrode vs. Ag/AgCl in 0.1 M $TBAPF_6$ dissolved in DCM at a scan rate of 100 mVs^{-1} and (b) differential pulse voltammograms of the monomers on Pt electrode vs. Ag/AgCl in 0.1 M $TBAPF_6$ dissolved in DCM.

Table 3.10 Optical and electrochemical properties of T(TPD-Azo)T, E(TPD-Azo)E and P(TPD-Azo)P monomers

Monomer	**T(TPD-Azo)T**	**E(TPD-Azo)E**	**P(TPD-Azo)P**
$\lambda_{max,abs}$ (nm)	265, 343, -	265, 335, 405	265, 333, 400
$\lambda_{max,em}$ (nm)	472	475	479
CV			
$E_{ox,m}$ (V)	1.53	1.11	1.20
$E_{red,m}$ (V)	-1.29	-1.36	-1.38
$E_{ox,onset,m}$ (V)	1.42	0.99	1.09
$E_{red,onset,m}$ (V)	-1.16	-1.24	-1.25
HOMO (eV)	-6.13	-5.70	-5.80
LUMO (eV)	-3.55	-3.47	-3.46
$E_g^{electro}$ (eV)	2.58	2.23	2.34
DPV			
$E_{ox,m}$ (V)	1.50	1.09	1.15
$E_{red,m}$ (V)	-1.23	-1.31	-1.31
$E_{ox,onset,m}$ (V)	1.40	0.96	1.06
$E_{red,onset,m}$ (V)	-1.13	-1.22	-1.22
HOMO (eV)	-6.11	-5.67	-5.77
LUMO (eV)	-3.58	-3.49	-3.49
$E_g^{electro}$ (eV)	2.53	2.18	2.28
E_g^{opt} (eV)	2.83	2.72	2.75

3.2.3.3 Electrochemical Polymerization and Spectroelectrochemical Properties

The electrochemical characteristics of the polymers were examined to better understand the influence of different donor units azobenzene appendages on the TPD unit. As mentioned above all the monomers exhibit one irreversible oxidation peak during the anodic scan. The irreversible nature of the oxidation process arises from the fact that the radical cation formed after the one electron oxidation undergoes rapid coupling reactions (either radical-radical or radical-monomer couplings) which results in the deposition of an insoluble polymer film on the working electrode surface. Thus, the monomers synthesized in this work are electrochemically polymerized on Pt disc electrode via repetitive potential cycling from 0.0 V to +1.65 V for T(TPD-Azo)T, from 0.0 V to +1.25 V for E(TPD-Azo)E and from 0.0 V to +1.30 V for P(TPD-Azo)P. After the first anodic scan, the electroactive polymer films start to grow on the electrode surface with the formation of new reversible redox couples. The redox couples gradually intensify during successive scans, resulting in an increase in film thickness (see Figure 3.41 for the polymer repeat units). The recorded CVs during electropolymerization is given in Figure 3.42. After the deposition of the polymer films on the working electrode, the films were washed with MeCN to remove all other species such as residual monomers and electrolyte. Following that, CV and DPV measurements were performed in both the anodic and cathodic regions to elucidate the electrochemical features of the polymer films. Full scan cyclic voltammograms, which are measured in a monomer free electrolyte solution are depicted separately in Figure 3.42 (b), (d) and (f), while the corresponding stacked DPVs are shown in Figure 3.43. The examination of cyclic voltammograms reveals that a quasi-reversible oxidation peak is observed for each polymer film during p-doping, whereas a quasi-reversible reduction peak is observed only in the case of PE(TPD-Azo)E and PP(TPD-Azo)P unlike PT(TPD-Azo)T during n-doping. The irreversible reduction peak observed in the case of PT(TPD-Azo)T indicates that n-

doping process for this polymer film is irreversible. Furthermore, the more close inspection of the recorded cyclic voltammogram during p-doping demonstrates that PT(TPD-Azo)T and PP(TPD-Azo)P films exhibit one redox couple at around +1.30 V and +0.95 V, respectively, whereas PE(TPD-Azo)E film presents a very broad and multi-step redox couple between +0.1 V to +0.9 V. These features could be associated with slow doping process due to well-packed polymer backbone.

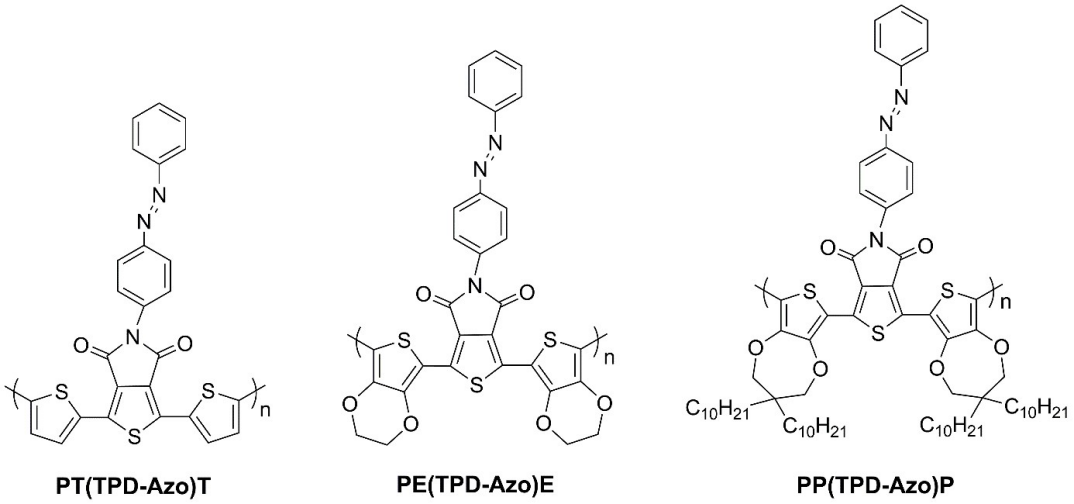

Figure 3.41. The structure of polymers.

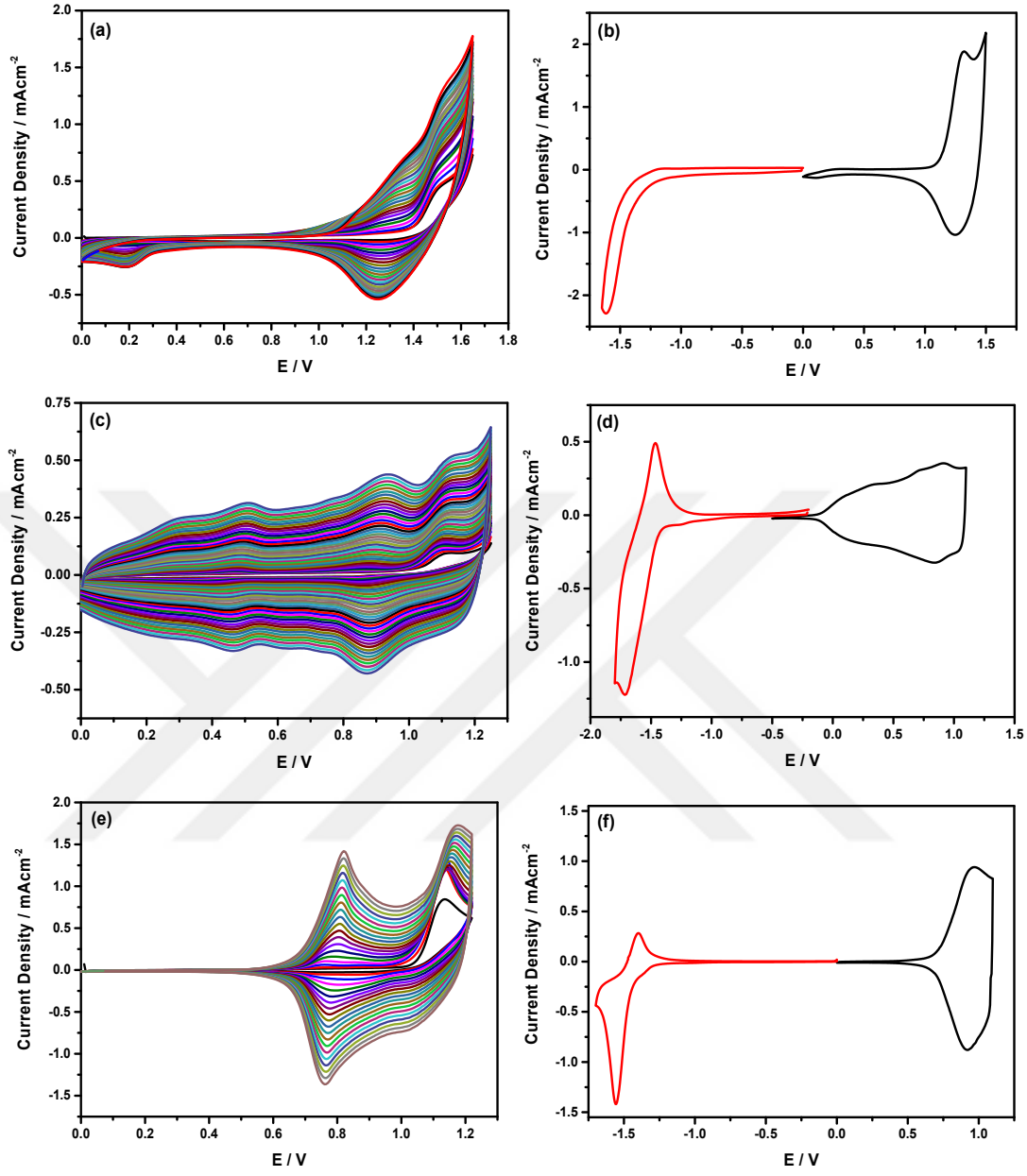

Figure 3.42. Repetitive cyclic voltammograms of the monomers recorded in 0.1 M $TBAPF_6$ solution (a) T(TPD-Azo)T, (c) E(TPD-Azo)E in DCM and (e) P(TPD-Azo)P in MeCN/DCM ((1/1: v/v) and the corresponding cycling voltammograms of polymer films recorded in 0.1 M $TBAPF_6$ solution (b) PT(TPD-Azo)T, (d) PE(TPD-Azo)E in DCM and (f) PP(TPD-Azo)P in MeCN on Pt disc electrode vs. Ag/AgCl at a scan rate of 100 mVs^{-1}.

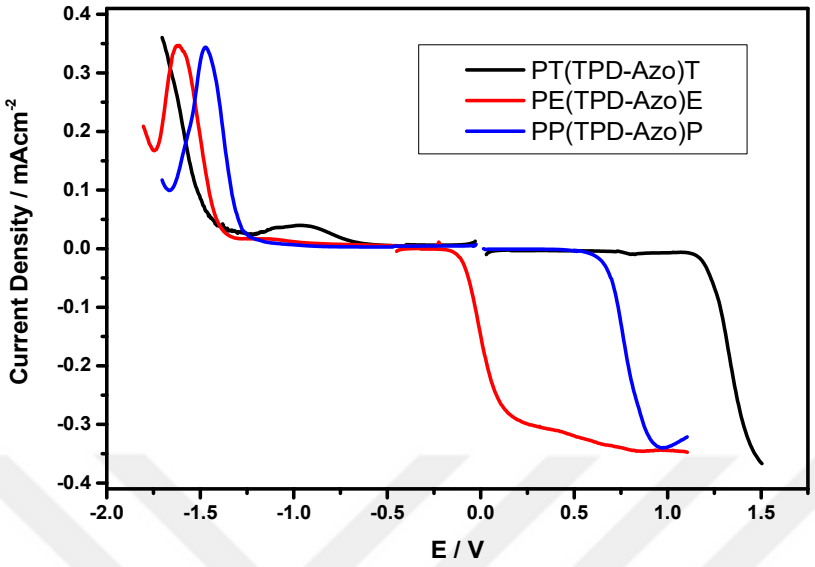

Figure 3.43. DPVs of the polymer films on Pt disc electrode vs. Ag/AgCl recorded in 0.1 M $TBAPF_6$ dissolved in DCM for PT(TPD-Azo)T and PE(TPD-Azo)E, in MeCN for PP(TPD-Azo)P.

In order to elucidate the electrochemical E_g values of the polymer films, the onset potential values are determined from the CV measurements and listed in Table 3.11 together with E_g values. Among three polymers, as expected, PE(TPD-Azo)E was found to have the lowest electrochemical E_g value with a magnitude of 1.51 eV. The trend in the E_g values of the polymer films is determined as $E_{g,PE(TPD\text{-}Azo)E} < E_{g,PP(TPD\text{-}Azo)P} < E_{g,PT(TPD\text{-}Azo)T}$. This trend is expected and it is in accordance with our previous results obtained from ethylhexyl and POSS appended analogs. Moreover, the scan rate dependency study was performed by recording their CVs in the anodic region at different scan rates changing from 25 mVs^{-1} to 200 mVs^{-1} with 25 mV increments and the resulting voltammograms are given in Figure 3.44 together with their linearity curves. As shown in Figure 3.44 (b), (d) and (f), the linear dependency of the peak current on the scan rate confirms that the reversible redox processes occurring on the well-adhered polymer film surfaces are not diffusion-controlled.

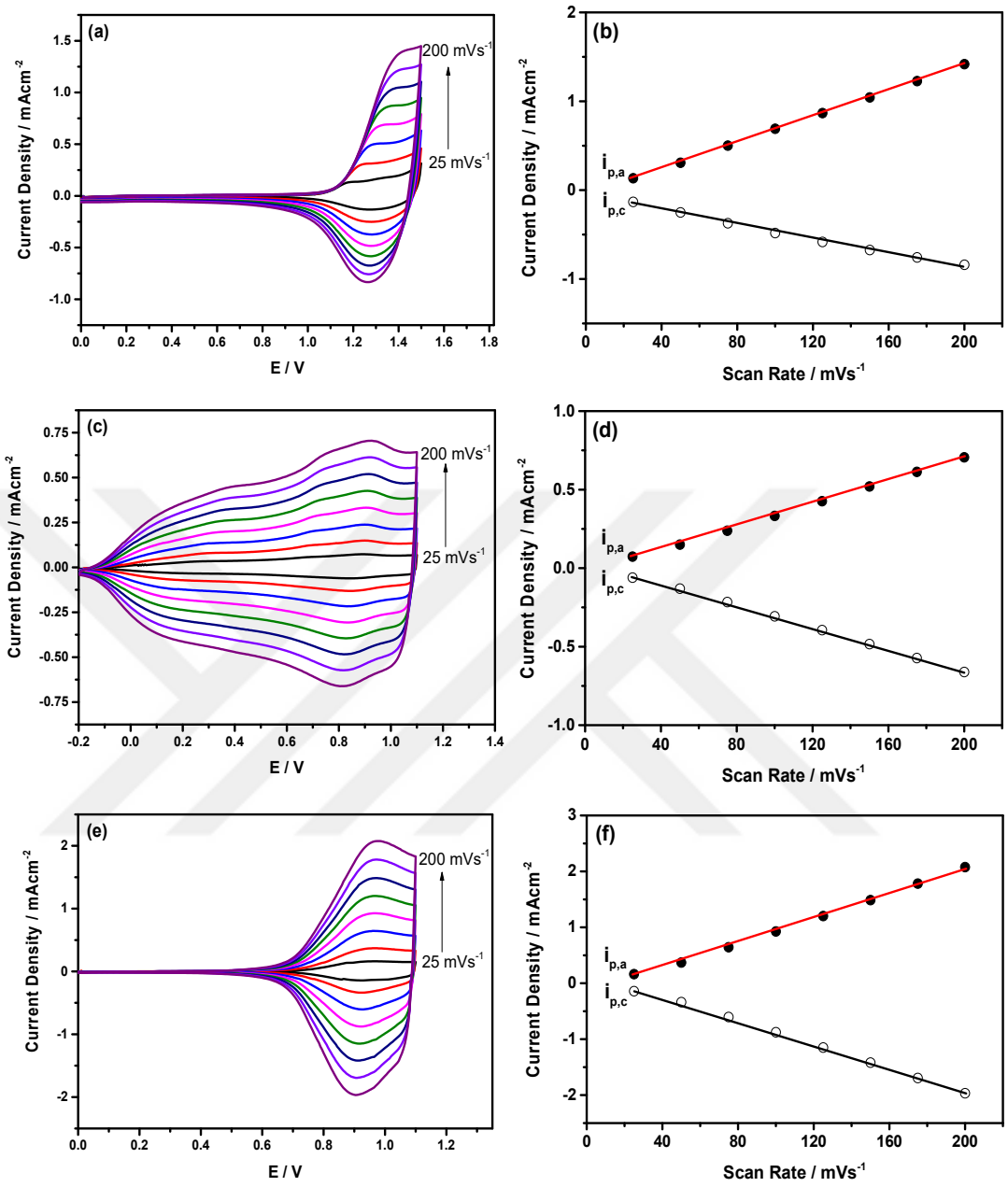

Figure 3.44. Scan rate dependence of the polymer films on Pt disc electrode recorded in 0.1 M $TBAPF_6$ solution (a) PT(TPD-Azo)T and (c) PE(TPD-Azo)E in DCM and (e) PP(TPD-Azo)P in MeCN at different scan rates from 25 mVs^{-1} to 200 mVs^{-1} with 25 mVs^{-1} increments. The relationship of anodic and cathodic peak currents as a function of scan rate for (b) PT(TPD-Azo)T, (d) PE(TPD-Azo)E and (f) PP(TPD-Azo)P polymer films.

Table 3.11 Electrochemical properties of the polymer films

Polymer	PT(TPD-Azo)T	PE(TPD-Azo)E	PP(TPD-Azo)P
$E_{ox,p}$ (V)	1.32	0.92	0.97
$E_{red,p}$ (V)	-1.61	-1.71	-1.55
$E_{ox,onset,p}$ (V)	1.13	-0.09	0.72
$E_{red,onset,p}$ (V)	-1.37	-1.42	-1.44
$E_g^{electro}$ (eV)	2.50	1.51	2.16
E_g^{opt} (eV)	1.71	1.54	1.68
HOMO (eV)	-5.84	-4.62	-5.43
LUMO (eV)	-3.34	-3.29	-3.27

The spectroelectrochemistry is the best way of elucidating the electrochromic properties of the obtained polymers by applying a voltage change. For this purpose, the polymers were deposited on ITO working electrode via potentiodynamic method and firstly their electronic absorption spectra were recorded in their neutral states. The obtained spectra are depicted in Figure 3.45 and the dual band characteristic is observed for each film. The higher energy bands appear at 337 nm, 333 nm and 344 nm and the lower energy bands at 505 nm, 630 nm and 612 nm for PT(TPD-Azo)T, PE(TPD-Azo)E and PP(TPD-Azo)P films, respectively. A vibronic shoulder at about 672 was observed in the case of PP(TPD-Azo)P, which demonstrates the high degree of molecular ordering in polymer backbone due to effective interchain π-π stacking. The observed higher energy bands at around 300 nm are most probably due to the azobenzene substituent present on the TPD unit while the low energy bands are assigned to π-π* transition bands of the polymer films. The optical E_g values of the polymer films are estimated to be 1.71 eV for PT(TPD-Azo)T, 1.54 eV for PE(TPD-Azo)E and 1.68 eV for PP(TPD-Azo)P by using the low energy onset of the π-π* transition. These results are listed in Table

3.12 together with electrochemical E_g values. The same trend can be seen in the table for the variation of optical and electrochemical E_g values.

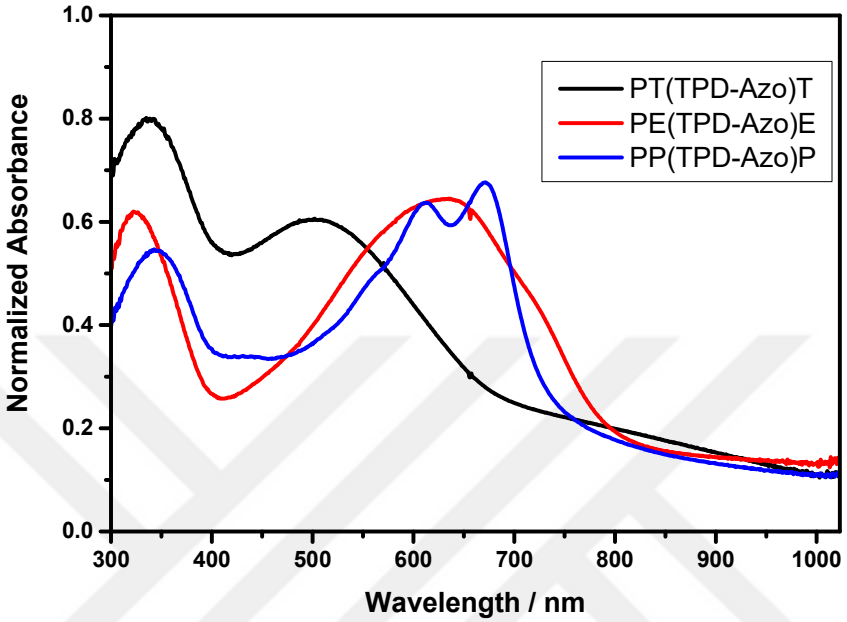

Figure 3.45. Neutral state absorption spectra of PT(TPD-Azo)T, PE(TPD-Azo)E and PP(TPD-Azo)P films coated on ITO electrode in 0.1 M $TBAPF_6$/MeCN.

The changes in optoelectronic properties of the polymer films were examined as a function of externally applied potential during p-type doping and the results are shown in Figure 3.46. As expected from an electrochromic polymer, during the anodic scan, the intensity of π-π* transition bands for each polymer film decreases simultaneously with the generation of new bands beyond 800 nm because of the formation of polaron charge carriers. Further electrochemical oxidation reduces π-π* transition bands to a minimum as polaron absorption bands shift to a shorter wavelength. This is accompanied by the emergence of another absorption band beyond 1000 nm. The formation of this higher wavelength absorption band is associated with the generation of bipolaron charge carriers. The voltammograms measured during the anodic scan are also shown in the inset of Figure 3.46. These spectral changes in the polymer films are reflected as a color change and their color

coordinates are expressed with L*, a*, b* values as reported in Table 3.12. Upon electrochemical oxidation, the colors of the PT(TPD-Azo)T, PE(TPD-Azo)E and PP(TPD-Azo)P polymer films are turned from brick red to gray, blue to gray, and blue to gray, respectively.

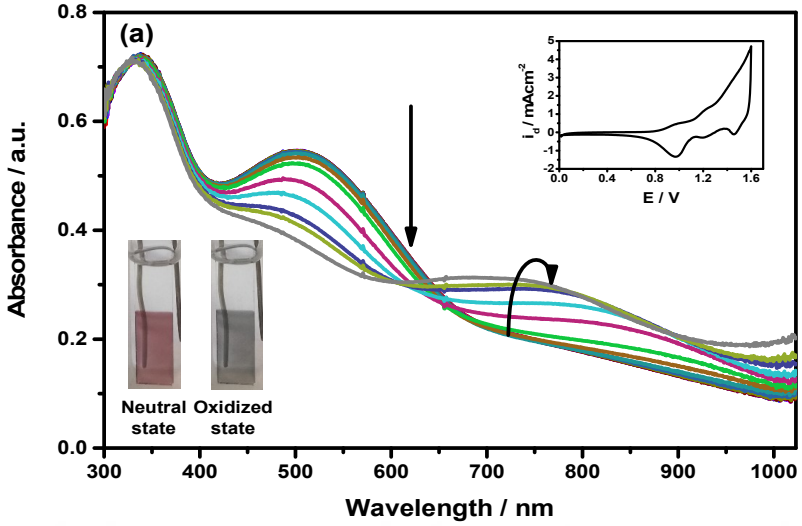
(a)
Absorbance / a.u.
Wavelength / nm
Neutral state
Oxidized state
i_d / mAcm^{-2}
E / V

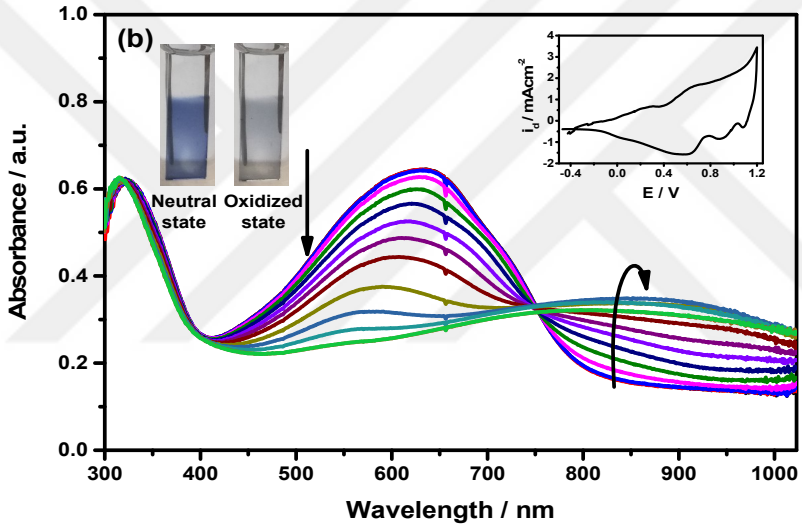
(b)
Absorbance / a.u.
Wavelength / nm
Neutral state
Oxidized state
i_d / mAcm^{-2}
E / V

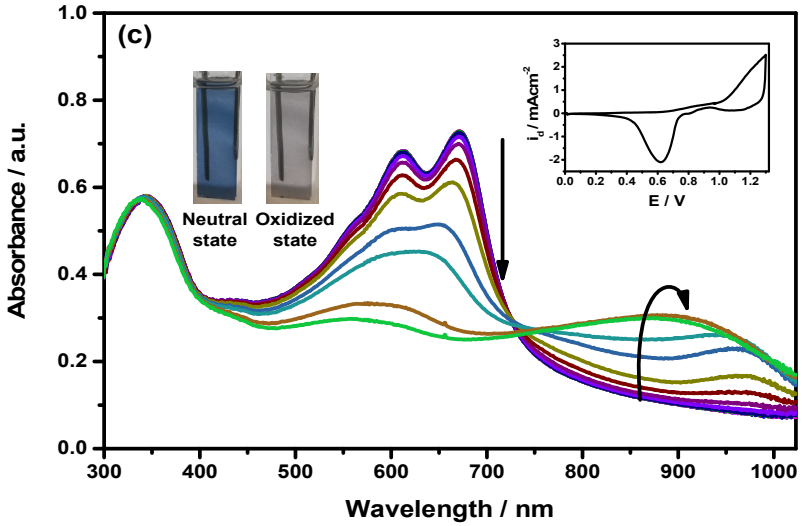
(c)
Absorbance / a.u.
Wavelength / nm
Neutral state
Oxidized state
i_d / mAcm^{-2}
E / V

Figure 3.46. The changes in electronic absorption spectra of electrochemically deposited (a) PT(TPD-Azo)T, (b) PE(TPD-Azo)E and (c) PP(TPD-Azo)P films on ITO recorded at various applied potentials in 0.1 M $TBAPF_6$/MeCN. Insets: CVs of the films recorded with a scan rate of 20 mVs^{-1}. Inset: The colors of the films at neutral and oxidized states.

The changes in optical spectra of the films, PE(TPD-Azo)E and PP(TPD-Azo)P were also recorded during the cathodic scan to prove that the films are also n-dopable (see Figure 3.47). Since PT(TPD-Azo)T was not stable during n-doping as compared to its EDOT and ProDOT analogs, it is not involved in spectroelectrochemistry studies. Similar changes were also noted during n-type doping of the polymer films. Upon electrochemical reduction, π-π* absorption bands are bleached out whereas a new lower energy band centered at 800 nm for PE(TPD-Azo)E and 850 nm for PP(TPD-Azo)P emerges. The formation of these new bands is associated with the generation of negative charge carriers. This clearly demonstrates that PE(TPD-Azo)E and PP(TPD-Azo)P polymers are n-type dopable, which is confirmed by reversible redox couple recorded at negative potential (see Inset of Figure 3.47 (a) and (b)). During n-doping, the changes in the absorption spectra are represented by a color change from blue to gray for PE(TPD-Azo)E and from blue to tranmissive light gray for PP(TPD-Azo)P in their neutral and reduced states, respectively. The L*, a*, b* values corresponding to these color changes were also noted in Table 3.12. In literature, the number of n-dopable conjugated polymers is quite limited, therefore the development of efficient n-dopable materials has a great priority for future studies[157,158].

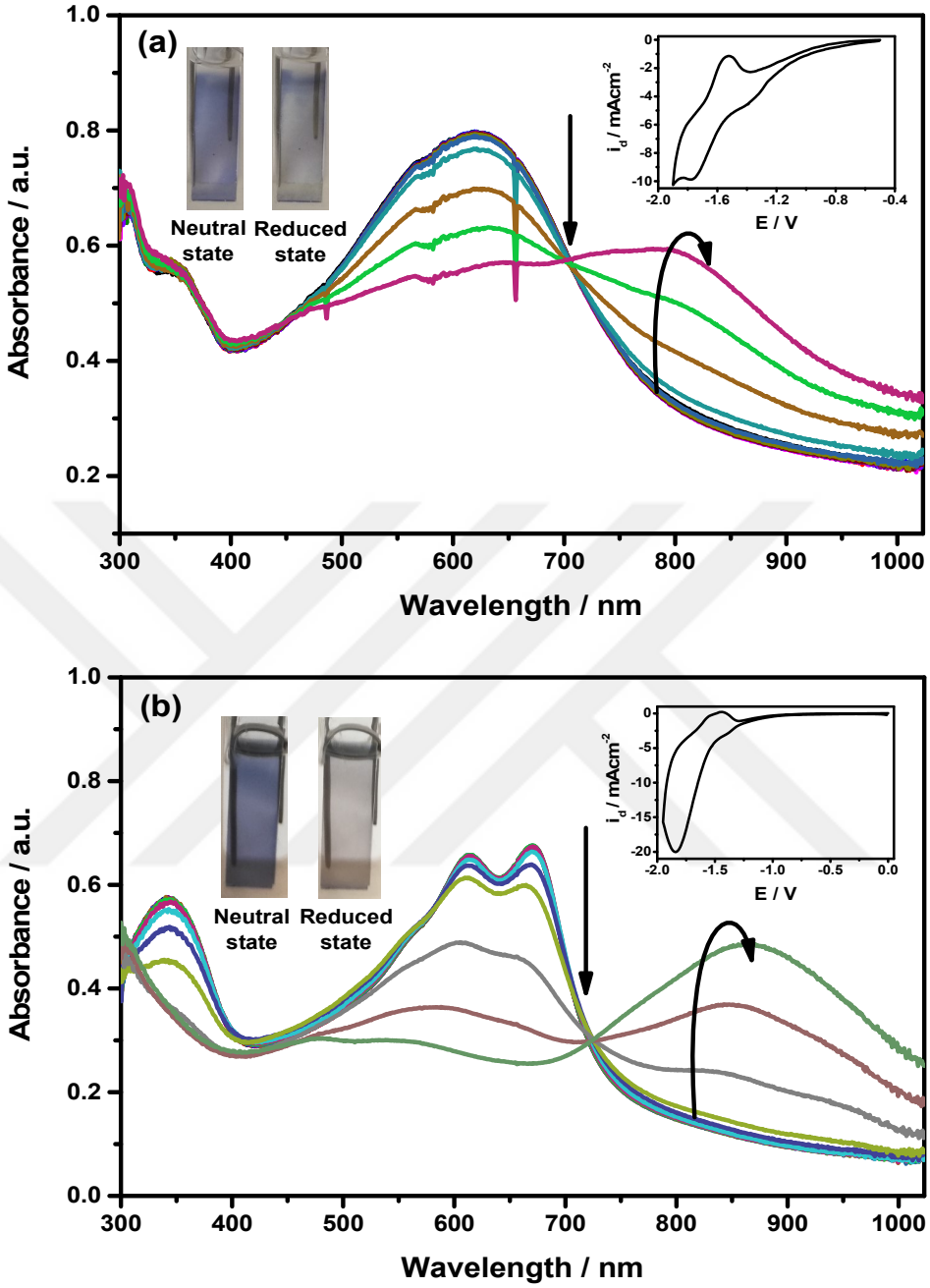

Figure 3.47. The changes in electronic absorption spectra of electrochemically deposited (a) PT(TPD-Azo)T, (b) PE(TPD-Azo)E and (c) PP(TPD-Azo)P films on ITO recorded at various applied potentials during n-doping in 0.1 M $TBAPF_6$/MeCN. Insets: CVs of the films recorded with a scan rate of 20 mVs^{-1}. Inset: The colors of the films at neutral and reduced states.

It is noteworthy that PP(TPD-Azo)P polymer is completely soluble in common organic solvents thanks to the long alkyl chains of ProDOT unit. By the help of this property, chromic behavior of the polymer was also investigated via chemical oxidation method by using 0.05 M $SbCl_5$ solution as an oxidizing agent. The chemical doping process of the polymer in solution was investigated by recording the changes in electronic absorption spectra upon stepwise additions of $SbCl_5$ solution, as illustrated in Figure 3.48 and very similar changes were observed as in the electrochemical p-doping. The π-π* transition band of the polymer centered at 602 nm started to diminish. This change is accompanied by the formation of a new absorption band centered at 850 nm, which is originated from polaronic charge carriers. Moreover, PP(TPD-Azo)P dissolved in DCM exhibits fluorescence emission at about 610 and 715 nm (see Figure 3.49) corresponding to red light.

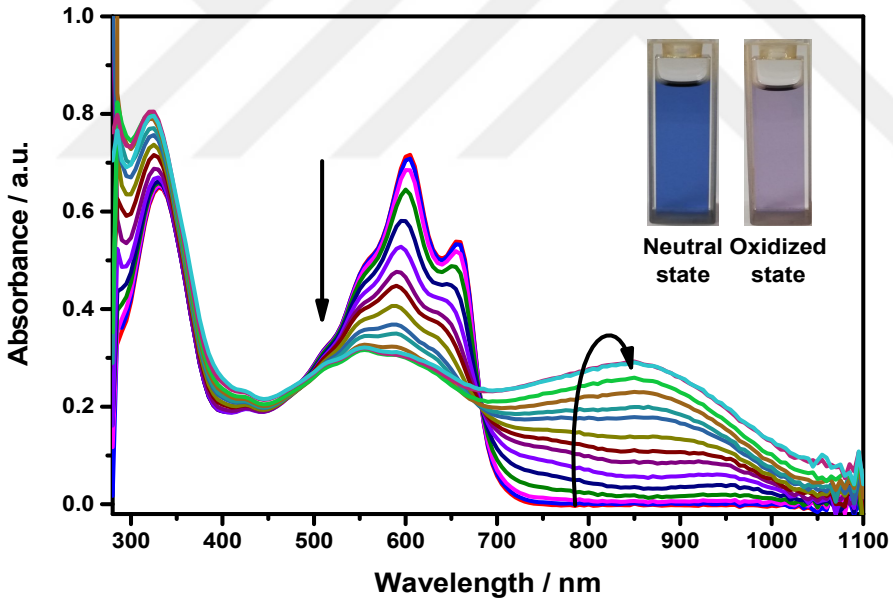

Figure 3.48. The changes in the absorption spectra of PP(TPD-Azo)P polymer dissolved in toluene during chemical oxidation by using 0.05 M $SbCl_5$ oxidant with 3 µL stepwise additions. Inset: Colors of the polymer solution at neutral and oxidized states.

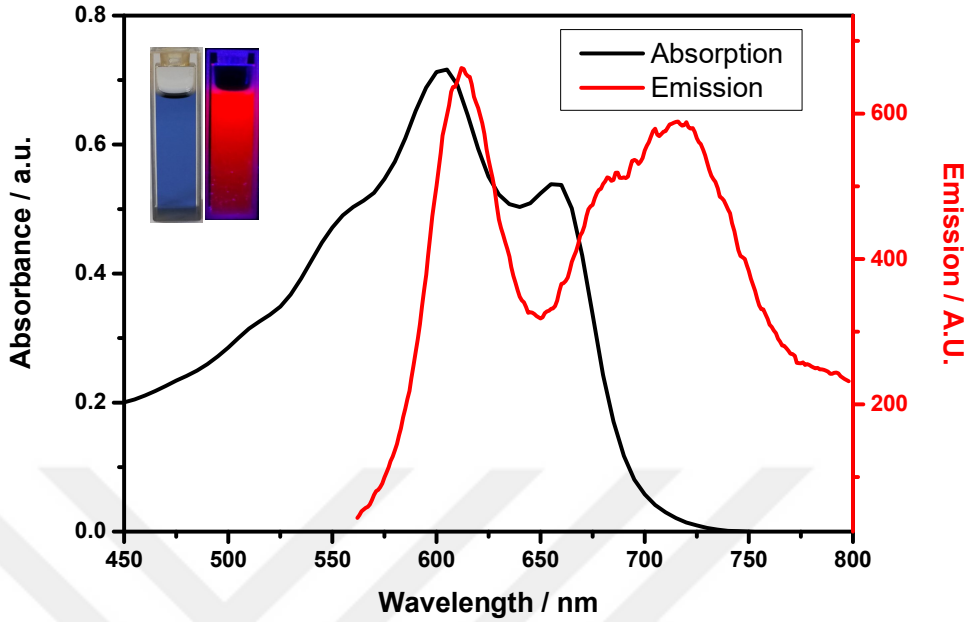

Figure 3.49. Electronic absorption and emission spectra of electrochemically obtained PP(TPD-Azo)P polymer in toluene.

The electrochromic properties (i.e. optical contrast, switching time and CE of the polymer films were determined by chronoabsorptometry study. For this aim, the electrochemically coated films repeatedly switched from their neutral states to fully oxidized states with a switching time of 10 s via square wave potential method (see Figure 3.50). The resulting data are listed in Table 3.12. As shown in the table, the optical contrast was calculated as 12% at 505 nm for PT(TPD-Azo)T, 32% at 630 nm for PE(TPD-Azo)E and 41% at 612 nm and 42% at 672 for PP(TPD-Azo)P. The oxidation switching time and CE to reach 95% of full contrast for the polymer films were found to be 0.7 s and 129 cm^2/C for PT(TPD-Azo)T, 0.4 s and 454 cm^2/C for PE(TPD-Azo)E and 0.4 s and 726 cm^2/C for PP(TPD-Azo)P, respectively. A careful examination of the Table 3.12 reveals that when switching from thiophene bearing polymer film to didecyl-ProDOT bearing polymer film, all electrochromic properties improve, indicating the interchain separation effect of the ProDOT unit due to long alkyl chains. Increased chain distance facilitates ion

transport through the polymer structure during the doping process, resulting in higher optical contrast and shorter response time, making them promising candidates for electrochromic applications.The neutralization switching time of the polymer films was not too different from oxidation switching time and found to be 0.3 s, 0.4 s and 0.4 s for PT(TPD-Azo)T, PE(TPD-Azo)E and PP(TPD-Azo)P, respectively.

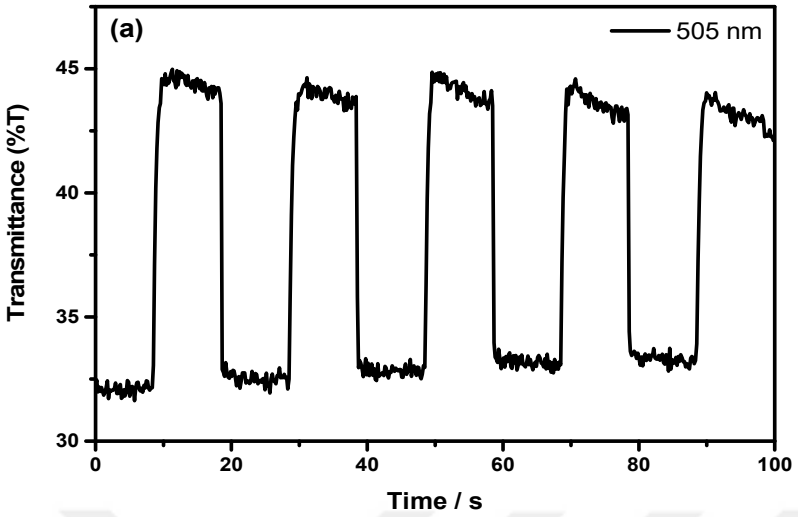
(a)
505 nm
Transmittance (%T)
45
40
35
30
0
20
40
60
80
100
Time / s

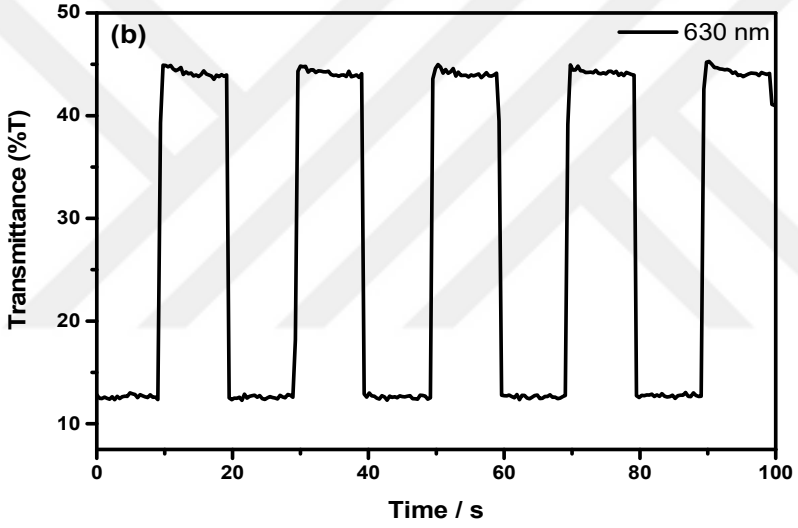
(b)
630 nm
Transmittance (%T)
50
40
30
20
10
0
20
40
60
80
100
Time / s

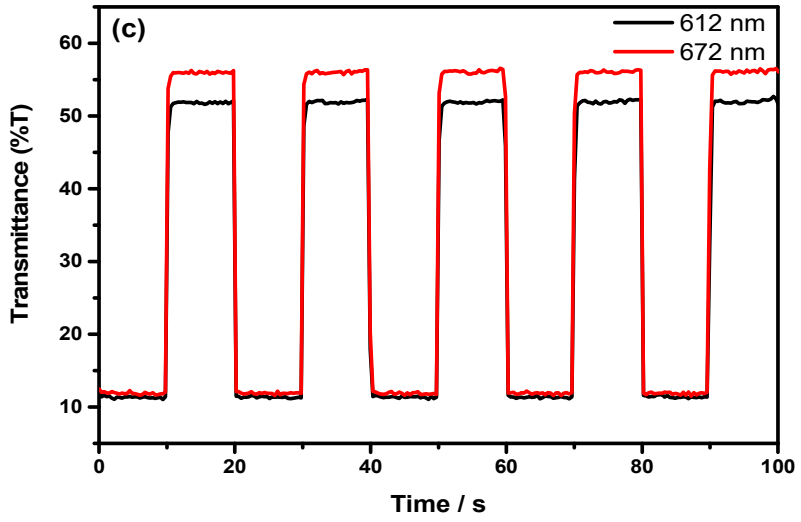
(c)
612 nm
672 nm
Transmittance (%T)
60
50
40
30
20
10
0
20
40
60
80
100
Time / s

Figure 3.50. Chronoabsoptometry experiments for the polymer films on ITO in 0.1 M $TBAPF_6$/MeCN when the films were switched between redox states with an interval time of 10 s for (a) PT(TPD-Azo)T (between 0.0 V and +1.6 V at 525 nm), (b) PE(TPD-Azo)E (between -0.5 V and +1.3 V at 545 nm and 600 nm) and (c) PP(TPD-Azo)P (between 0.0 V and +1.3 V at 585 nm and 640 nm).

Table 3.12 Optoelectronic properties of the polymer films on ITO in 0.1 M $TBAPF_6$/MeCN

Polymer	**PT(TPD-Azo)T**	**PE(TPD-Azo)E**	**PP(TPD-Azo)P**
λ_{max} (nm)	505	630	612, 672
E_g^{opt} (eV)	1.71	1.54	1.68
Δ%T	12	32	41, 44
CE (cm^2/C)	129	454	750, 762
$t_{s,ox}$[a] (s)	0.7	0.4	0.4, 0.4
$t_{s,red}$[a] (s)	0.3	0.4	0.4, 0.4
Color at neutral state L*, a*, b*	64.63, 12.49, 3.81	63.60, -3.12, -22.21	63.69,-10.77,-16.70
Color at oxidized state L*, a*, b*	70.99, 0.65, 8.54	79.94, -1.11, -2.33	76.68, 0.68, -2.27
Color at reduced state L*, a*, b*	-	55.98, -1.21, -13.46	73.72, 1.41, -4.10

[a] 95% of full switch from colored to bleached states.

The stability of the electrochromic materials is one of the key parameters. For that reason, both electrochemical and optical stability of polymer films were studied under ambient conditions by applying an external potential between redox states. For this purpose, PE(TPD-Azo)E and PP(TPD-Azo)P polymer films were tested via square wave potential method within a potential range from -0.5 V to +1.1 V and from 0.0 V to +1.1 V, respectively. The films were pre-conditioned during first 500 cycles for PE(TPD-Azo)E and 1500 cycles for PP(TPD-Azo)P to obtain regular cyclic voltammetric behavior and the switching was manintained along 10000 cycles and 16000 cycles for PE(TPD-Azo)E and PP(TPD-Azo)P, respectively. The recorded test results are depicted in Figure 3.51. As shown in the figure, the stability tests revealed that both films preserved their electrochemical activity even after thousands of switching. Furthermore, PP(TPD-Azo)P film revealed highly stable behavior by preserving 89 % of its optical activity even after 16000 cyles, which proves its long term stability. PE(TPD-Azo)P film also showed high optical stability by retaining 51% of its optical activity after 10000 cyles.

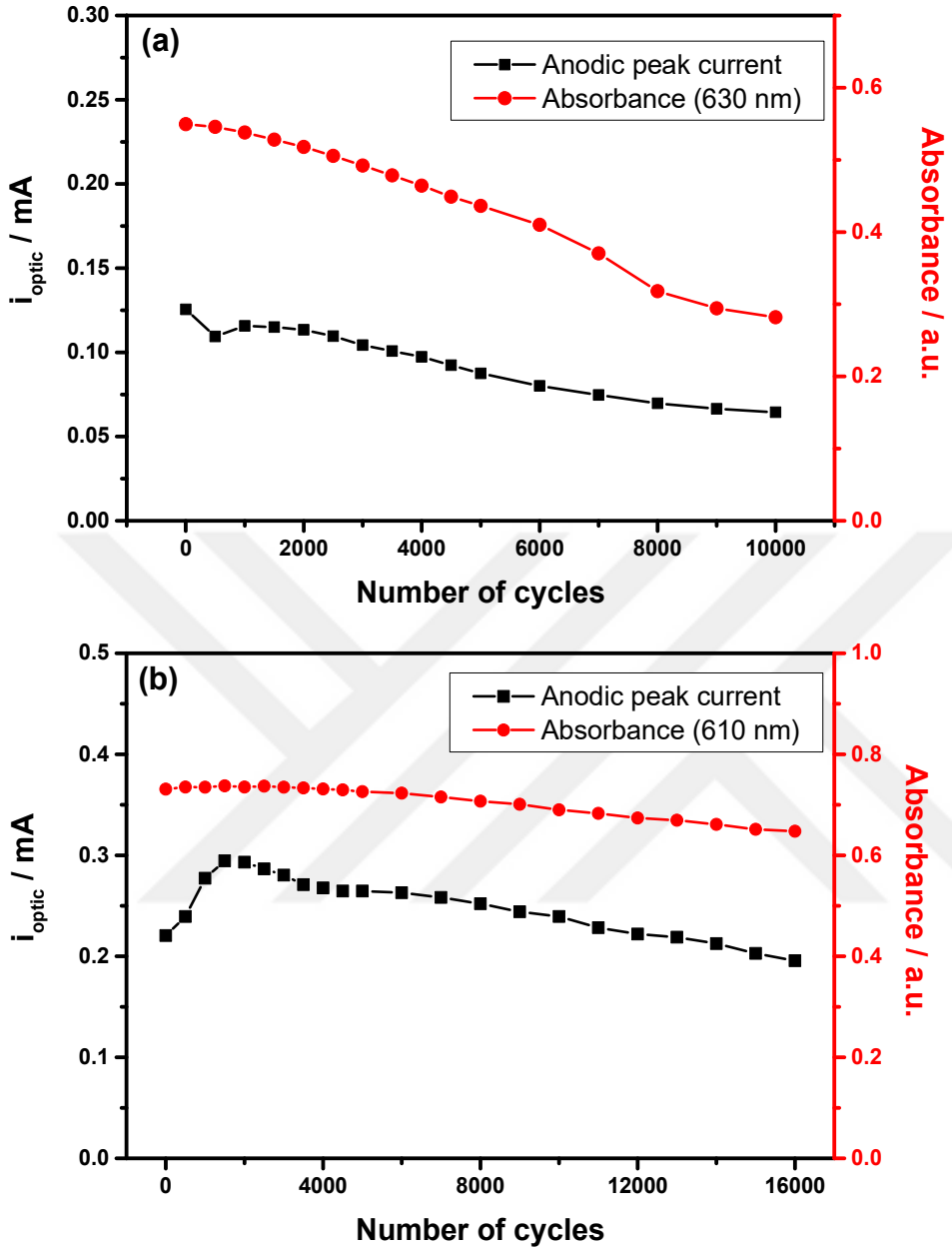

Figure 3.51. Electrochemical and optical stability tests for the polymer films on ITO in 0.1 M $TBAPF_6$/MeCN when the films switched between redox states (-0.5 V and +1.1 V) at 630 nm for (a) PE(TPD-Azo)E and (0.0 V and +1.1 V) at 610 nm for (b) PP(TPD-Azo)P with an interval of 1 s.

In order to elucidate the effect of an azobenzene moiety on photo-responsive behavior of azobenzene-substituted monomers and polymer, UV-Vis absorption spectra of T(TPD-Azo)T, E(TPD-Azo)E, P(TPD-Azo)P and PP(TPD-Azo)P were examined in toluene during irradiation. For comparison sake, all measurements were performed at the same conditions under irradiation with Mercury UV lamb at ambient temperature and changes in their UV-Vis absorption spectra depending on irradiation time are depicted in Figure 3.52. Upon irradiation, the intensity of main peak at around 335 nm assigned to π-π* transition of trans-azobenzene resulting from azobenzene appendage on side group started to decline gradually in all trimeric monomers and the polymer, indicating trans to cis photoisomerization of azobenzene. The absorption intensity of the monomers and the polymer increase back when exposed to day light, implying the cis to trans conversion. The tendencies for variations of peak intensities were consistent in all monomers except the polymer solution. The very small decrease and increase was observed in the absorption intensity of the π-π* transition band of azobenzene moiety for the polymer solution as compared to that of monomers contrary to prolonged irradiation times for the PP(TPD-Azo)P solution. Additionally, the cis to trans conversion did not go to completion in both monomers and the polymer in solution despite the sufficiently prolonged exposure to day light. This incomplete return can be attributed to steric and electronic configuration of rigid conjugated backbone, which is more enhanced for the polymer[159].

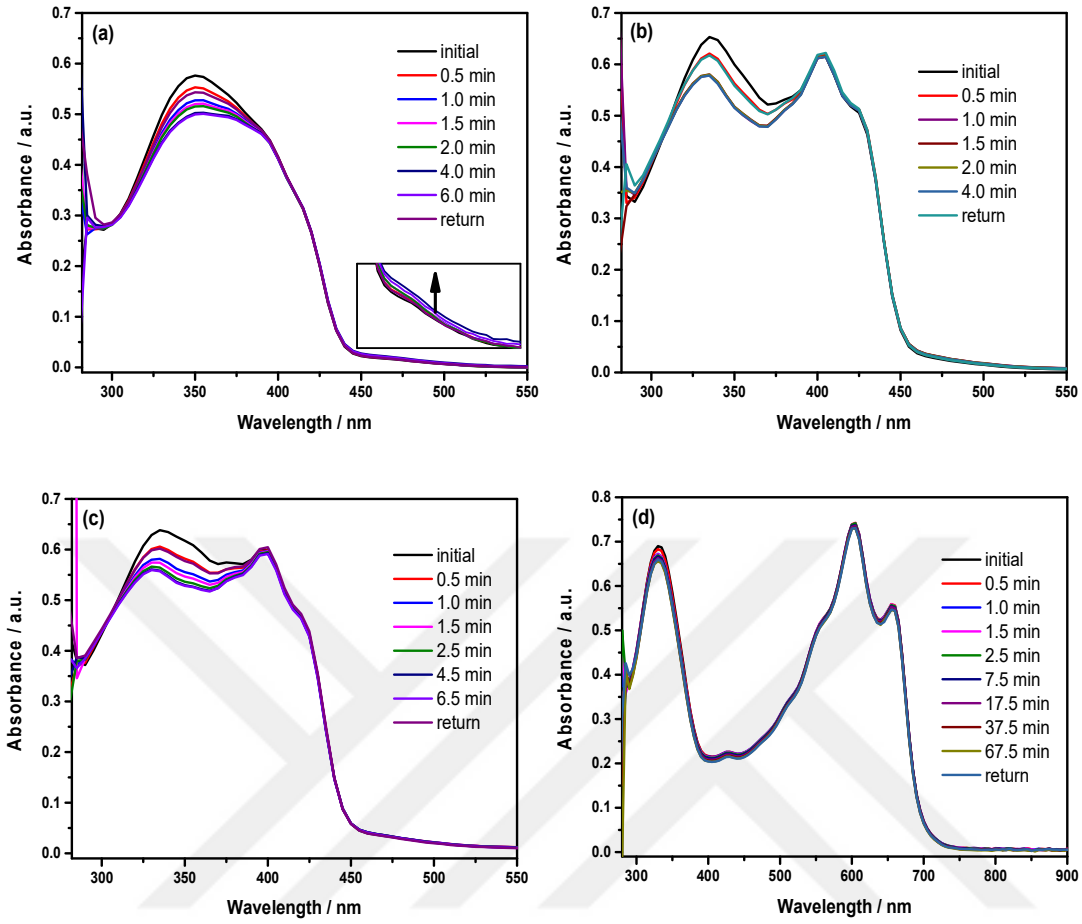

Figure 3.52. UV-Vis absorption spectra of (a) T(TPD-Azo)T, (b) E(TPD-Azo)E, (c) P(TPD-Azo)P and (d) PP(TPD-Azo)P before and after irradiation with Mercury UV light in toluene.

3.2.4 D-A-D Monomers Based on TPD-Fluo Acceptor Unit

In this part, TPD core unit is functionalized with a new substituent, fluorene to obtain a new kind acceptor unit. Then, two novel D-A-D monomers, E(TPD-Fluo)E and P(TPD-Fluo)P having this modified acceptor unit were synthesized by using EDOT and didecyl-ProDOT donors. Thiophene analogue was not synthesized due to the solubility and stability problems. (Scheme 3.6).

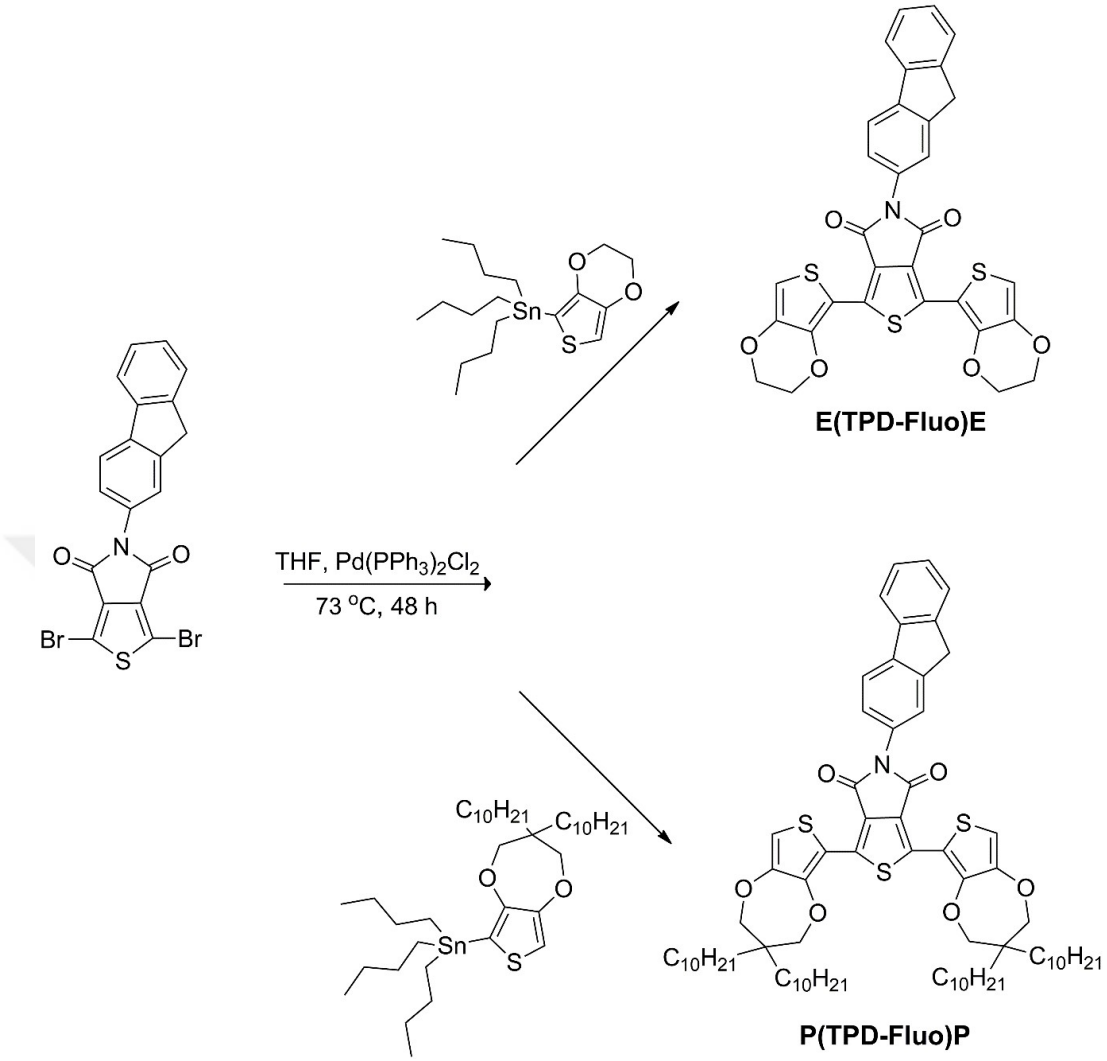

Scheme 3. 6. Synthesis route for the monomers.

3.2.4.1 Optical Properties of the Monomers

In order to investigate the optical behaviours of the monomers, firstly their electronic absorption and fluorescence emission spectra were recorded in DCM and the corresponding spectra are depicted in Figure 3.53. As shown in Figure 3.53 (a), the monomers exhibit three absorption bands and the highest energy band appeared nearly at the same wavelength (271 nm for E(TPD-Fluo)E and 272 nm for P(TPD-Fluo)P is observed due to the existence of fluorene unit on TPD core, which

exhibits a charasteristic absorption peak at about 270 nm[160]. The middle band in absorption spectra is originated from π-π* transition and appear at 305 nm for both monomers. The lowest energy bands of spectra resulted from the ICT between donor and acceptor exhibit the absorption maxima at 402 nm and 398 nm for E(TPD-Fluo)E and P(TPD-Fluo)P, respectively. The slight red shift in this band display the better conjugation between the acceptor and EDOT donor unit. The emission spectra of the monomers are depicted in Figure 3.53 (b), which exhibit emission peaks centered at 482 nm for E(TPD-Fluo)E and 477 nm for P(TPD-Fluo)P upon extication at 340 nm. The red shift in the emission spectrum of E(TPD-Fluo)E as compared to P(TPD-Fluo)P is observed due to stronger donor character of EDOT. All obtained results are given in Table 3.13.

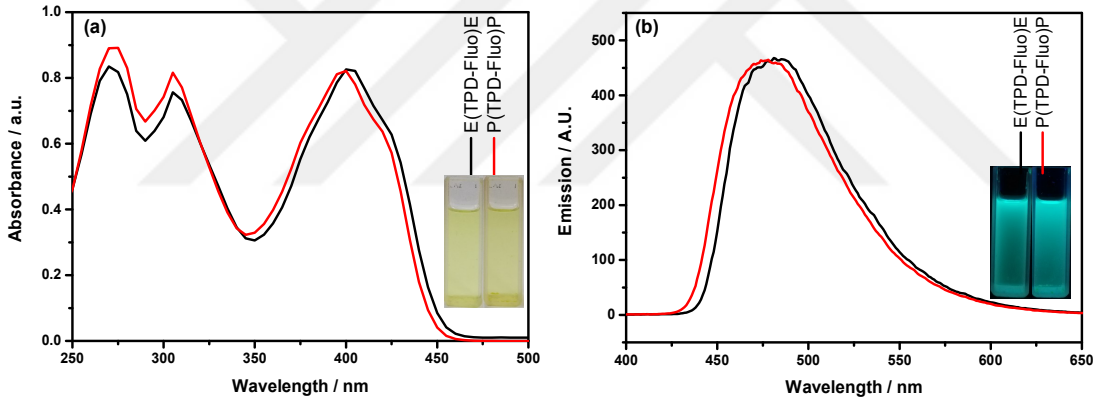

Figure 3.53. (a) Absorption and (b) emission spectra of the monomers in DCM. Inset: the colors of the monomers (a) in daylight and (b) under UV lamp at 365 nm.

3.2.4.2 Electrochemical Properties of the Monomers

In order to gain more insight into the redox properties of monomers, CV and DPV measurements were recorded in 0.1 M $TBAPF_6$/DCM electrolyte solution on Pt disc electrode and the resulting voltammograms are depicted in Figure 3.54. As

seen from the voltammograms (Figure 3.54 (a)), both E(TPD-Fluo)E and P(TPD-Fluo)P exhibit one irreversible oxidation peak, which is responsible from electropolymerization, at about 1.10 V and 1.19 V vs Ag/AgCl, respectively. The relatively lower oxidation potential of E(TPD-Fluo)E as compared to P(TPD-Fluo)P indicates the higher donor ability of EDOT as compared to ProDOT, which is in an agreement with previous results. On the other hand, the monomers display pseudo-reversible reduction peaks at -1.70 V and -1.64 V vs Ag/AgCl for E(TPD-Fluo)E and P(TPD-Fluo)P, respectively. The slight positive shift in the reduction potential from EDOT to ProDOT is not expected since the same acceptor unit is involved in two monomers and LUMO energy level is mainly controlled by the acceptor unit. However, in D-A-D type systems, LUMO energy levels can be affected in a different way from electronic nature of donor group, which is also correlated with previously reported results. The electrochemical band gaps of E(TPD-Fluo)E and P(TPD-Fluo)P were estimated from DPV data and found to be 2.52 eV and 2.62 eV, respectively. The lower E_g observed for E(TPD-Fluo)E is in accordance with aforementioned results obtained for the other D-A-D type monomers and can be explained in terms of higher donating character of EDOT unit as compared to ProDOT unit. The electrochemical data for the monomers are also listed in Table 3.13.

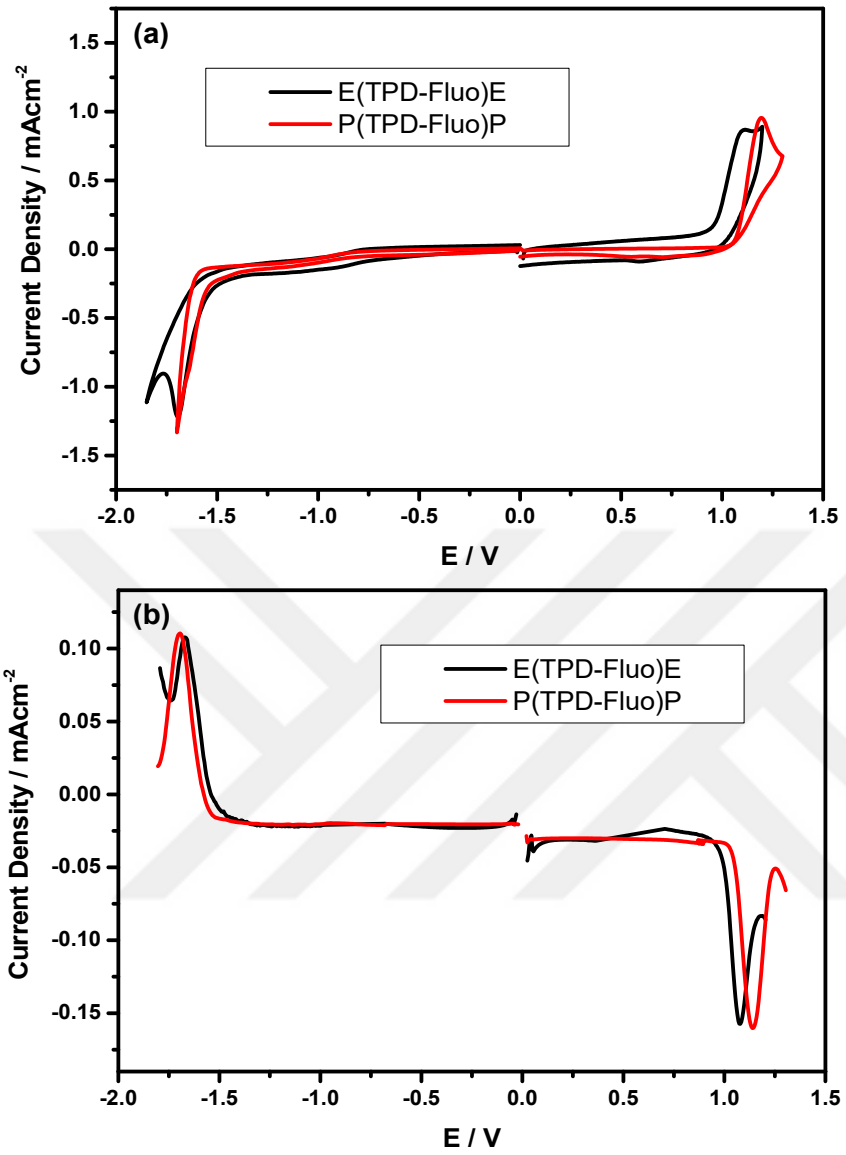

Figure 3.54. (a) Full scan cyclic voltammograms of the monomers on Pt electrode vs. Ag/AgCl in 0.1 M $TBAPF_6$ dissolved in DCM at a scan rate of 100 mVs^{-1} and (b) differential pulse voltammograms of the monomers on Pt electrode vs. Ag/AgCl in 0.1 M $TBAPF_6$ dissolved in DCM.

Table 3.13 Optical and electrochemical properties of the monomers

Monomer	E(TPD-Fluo)E	P(TPD-Fluo)P
$\lambda_{max,abs}$ (nm)	305, 402	305, 398
$\lambda_{max,em}$ (nm)	482	477
CV		
$E_{ox,m}$ (V)	1.10	1.19
$E_{red,m}$ (V)	-1.70	-1.64
$E_{ox,onset,m}$ (V)	0.96	1.07
$E_{red,onset,m}$ (V)	-1.56	-1.55
HOMO (eV)	-5.67	-5.78
LUMO (eV)	-3.15	-3.16
DPV		
$E_{ox,m}$ (V)	1.08	1.14
$E_{red,m}$ (V)	-1.67	-1.70
$E_{ox,onset,m}$ (V)	0.99	1.05
$E_{red,onset,m}$ (V)	-1.53	-1.57
HOMO (eV)	-5.70	-5.76
LUMO (eV)	-3.18	-3.14
$E_g^{electro}$ (eV)	2.52	2.62
E_g^{opt} (eV)	2.75	2.78
QY	0.0574	0.0719

3.2.4.3 Electropolymerization and Spectroelectrochemical Properties

The electrochemical polymerization of the monomers were carried out on Pt disc electrode vs Ag/AgCl via repetitive potential cycling from 0.0 V to +1.25 V for

E(TPD-Fluo)E and from 0.0 V to +1.3 V for P(TPD-Fluo)P to obtain their corresponding polymers as shown in Figure 3.55. The resulting voltammograms recorded during electropolymerization are given in Figure 3.56 (a) and (c). As seen from the voltammograms, new redox couples appear from +0.2 V to +1.0 V for PE(TPD-Fluo)E and at about +0.7 V for PP(TPD-Fluo)P and steadily intensify after each consecutive scan due to the formation of an electroactive polymer film on the working electrode surface.

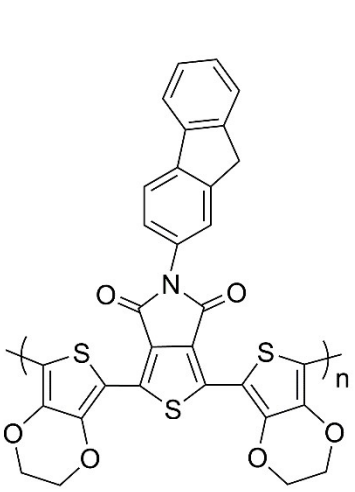

PE(TPD-Fluo)E

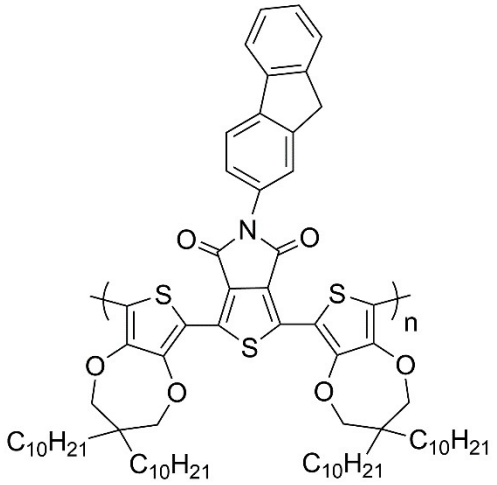

PP(TPD-Fluo)P

Figure 3.55. The structure of the polymer films.

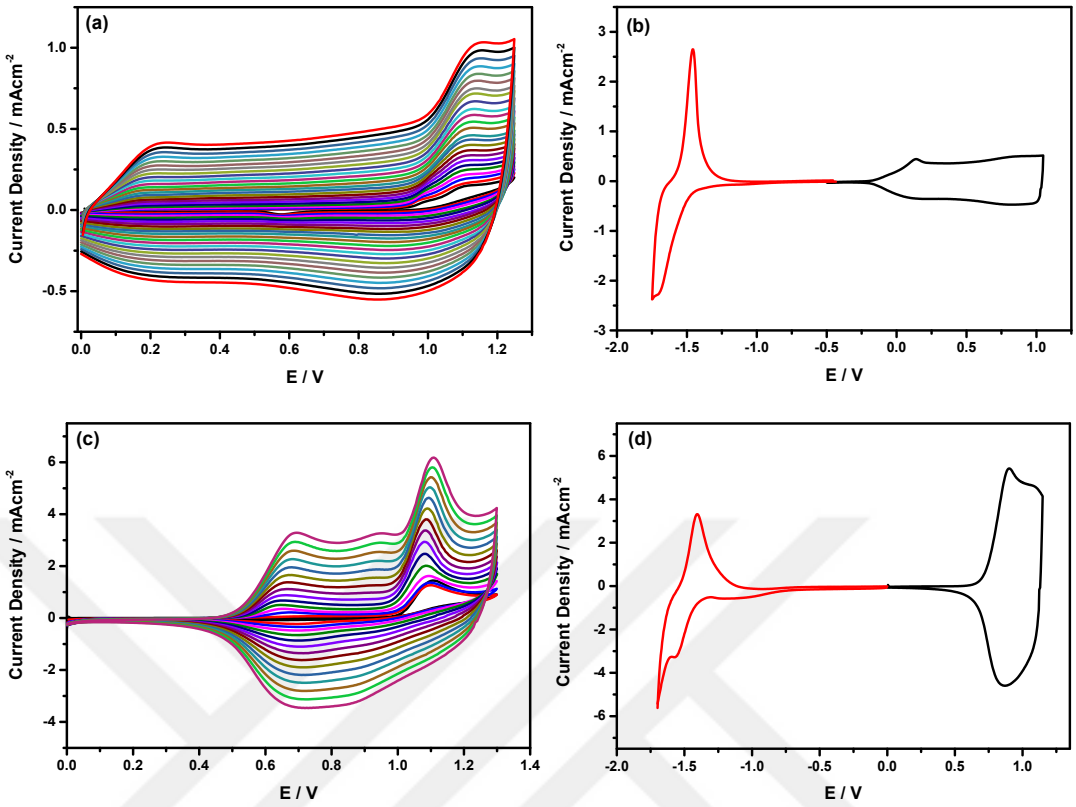

Figure 3.56. Repetitive cyclic voltammograms of (a) E(TPD-Fluo)E and (c) P(TPD-Fluo)P monomer recorded in 0.1 M $TBAPF_6$ in DCM for E(TPD-Fluo)E, in MeCN/DCM ((1/3: v/v) for P(TPD-Fluo)P and the cycling voltammograms of their corresponding polymer films (b) PE(TPD-Fluo)E and (d) PP(TPD-Fluo)P polymer films recorded in 0.1 M $TBAPF_6$ in DCM for PE(TPD-Fluo)E, in MeCN for PP(TPD-Fluo)P) on Pt disc electrode vs. Ag/AgCl at a scan rate of 100 mVs^{-1}.

The CVs and DPVs were recorded for the polymer films deposited on Pt disc electrode in a monomer-free electrolyte solution to comprehend electrochemical behaviour of the polymer films. Before the investigation, the polymer films were washed with the solvent to remove unreacted monomers and oligomeric species from the film surface. As it can be seen from the cyclic voltammograms depicted in Figure 3.56 (b) and (d), the polymer films exhibit reversible doping and

dedoping in both anodic and cathodic regions. During the anodic scan of the PE(TPD-Fluo)E, a rectangle shaped and very broad redox couple occurs between +0.2 V to +1.0 V, which shows the slow doping process because of the well-ordered polymer chains. In the case of PP(TPD-Fluo)P, a narrow redox couple is observed at about +0.9 V during p-doping. Moreover, during the cathodic region, the films exhibit a well-defined redox couple with a reduction peak at -1.71 V and -1.59 V for PE(TPD-Fluo)E and PP(TPD-Fluo)P, respectively. All the results together with the onset potentials obtained from both CV and DPV measurements are tabulated in Table 3.14. The corresponding DPVs of the polymer films are also given in Figure 3.57. HOMO/LUMO energy levels of the polymers were elucidated by utilizing the onset potentials from DPV measurements and noted in Table 3.14 together with the electrochemical band gap values. As seen from the table, as expected, PE(TPD-Fluo)E has a lower electrochemical band gap value than PP(TPD-Fluo)P, in an accordance with previous results.

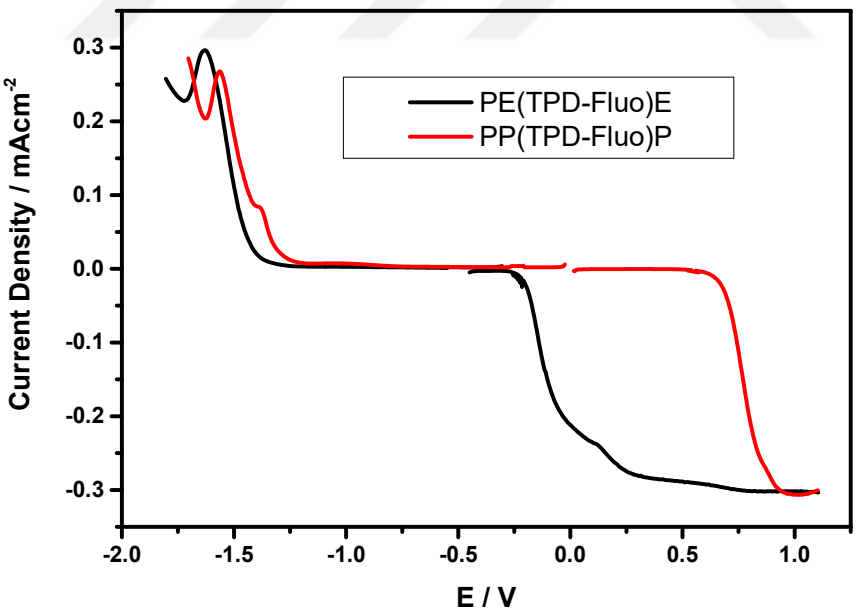

Figure 3.57. DPVs of polymer films recorded in 0.1 M $TBAPF_6$ in DCM for PE(TPD-Fluo)E, in MeCN for PP(TPD-Fluo)P on Pt disc electrode vs. Ag/AgCl.

Table 3.14 Electrochemical properties of the polymer films

Polymer	**PE(TPD-Fluo)E**	**PP(TPD-Fluo)P**
$E_{ox,p}$ (V)	0.14	0.90
$E_{red,p}$ (V)	-1.71	-1.59
$E_{ox,onset,p}$ (V)-CV	-0.11	0.72
$E_{red,onset,p}$ (V)-CV	-1.49	-1.41
$E_{ox,onset,p}$ (V)-DPV	-0.19	0.69
$E_{red,onset,p}$ (V)-DPV	-1.44	-1.38
HOMO (eV)	-4.52	-5.40
LUMO (eV)	-3.27	-3.33
$E_g^{electro}$ (eV)	1.25	2.07
E_g^{opt} (eV)	1.48	1.59

Furthermore, variations in the peak currents with the voltage scan rate during the anodic scan were examined by recording CVs at different scan rates ranging from 25 mVs^{-1} to 200 mVs^{-1} and the resulting voltammograms are given in Figure 3.58. The peak current increases linearly as a function of scan rate, which explicitly indicates the non-diffusional redox process.

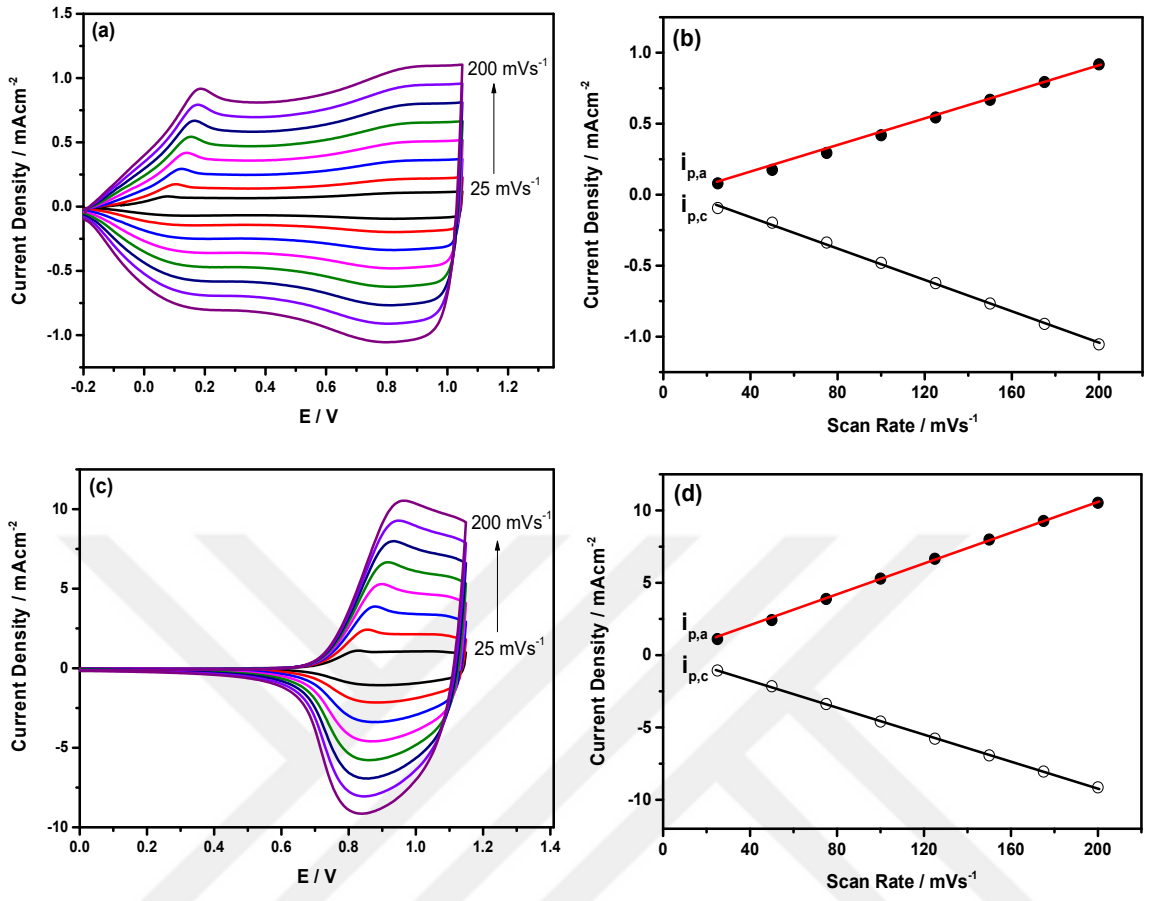

Figure 3.58. Scan rate dependence of the polymer films on Pt disc electrode recorded in 0.1 M $TBAPF_6$ solution (a) PE(TPD-Fluo)E in DCM and (c) PP(TPD-Fluo)P in MeCN at different scan rates from 25 mVs^{-1} to 200 mVs^{-1} with 25 mVs^{-1} increments. The relationship of anodic and cathodic current peaks as a function of scan rate for (b) PE(TPD-Fluo)E and (d) PP(TPD-Fluo)P polymer films.

For the inspection of electro-optical features such as optical band gap, percent transmittance change, response time and CE, etc., the polymer films were deposited on ITO-glass electrode by potentiodynamic method. After washing the polymer film on ITO electrode, the electronic absorption spectra of the neutral state films were recorded in monomer-free MeCN solution containing 0.1 M $TBAPF_6$ as

supporting electrolyte and the obtained spectra are given in Figure 3.59. As seen from the spectra, the neutral state polymer films on ITO exhibit absorption bands due to π-π* transitions. PE(TPD-Fluo)E exhibits one absorption band centered at 644 nm while PP(TPD-Fluo)P shows two well-seperated absorption bands at 609 nm and 668 nm as noted in Table 3.15. The vibronic coupling observed in the case of PP(TPD-Fluo)P is considered as a fingerprint of linear polymer chains[151,152]. The optical band gaps of the polymer films in their neutral states were calculated from the onsets of the low energy edge of π-π* transition and found to be 1.48 eV and 1.59 eV for PE(TPD-Fluo)E and PP(TPD-Fluo)P, respectively (see Table 3.15). The presence of EDOT donor group in PE(TPD-Fluo)E film leads to 0.11 eV decrease in the band gap as compared to PP(TPD-Fluo)P.

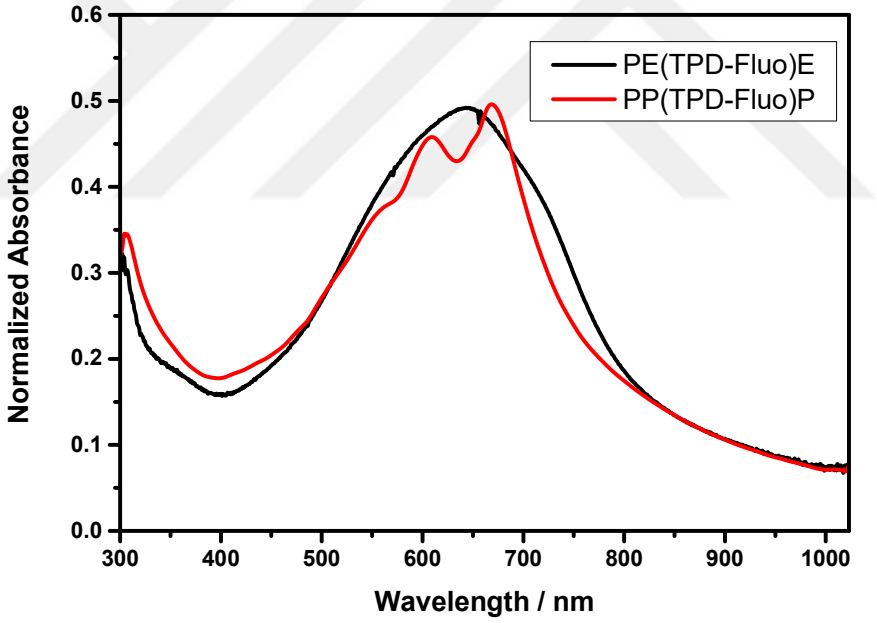

Figure 3.59. Neutral state absorption spectra of PE(TPD-Fluo)E and PP(TPD-Fluo)P films coated on ITO electrode in 0.1 M $TBAPF_6$/MeCN.

Under the applied external potential, the alterations in electro-optical behaviors of the polymer films on ITO were monitored and the resulting spectra are given in Figure 3.60. During the oxidation of each film, the intensity of π-π* transition band starts to diminish and a new absorption band, revealing the formation of polaron charge carriers, starts to appear. Upon further oxidation, this change is followed by a blue shift in the new absorption band, which is more pronounced in the case of PP(TPD-Fluo)P. In its fully oxidized form, π-π* transition band diminishes completely with a decrease in the polaron absorption band intensity. The color of the electrochromic polymer films changes from blue to gray for PE(TPD-Fluo)E and PP(TPD-Fluo)P upon oxidation. (see inset photos of Figure 3.60). L*, a*, b* values corresponding to the colors in two extreme states (neutral and oxidized) are noted in Table 3.15.

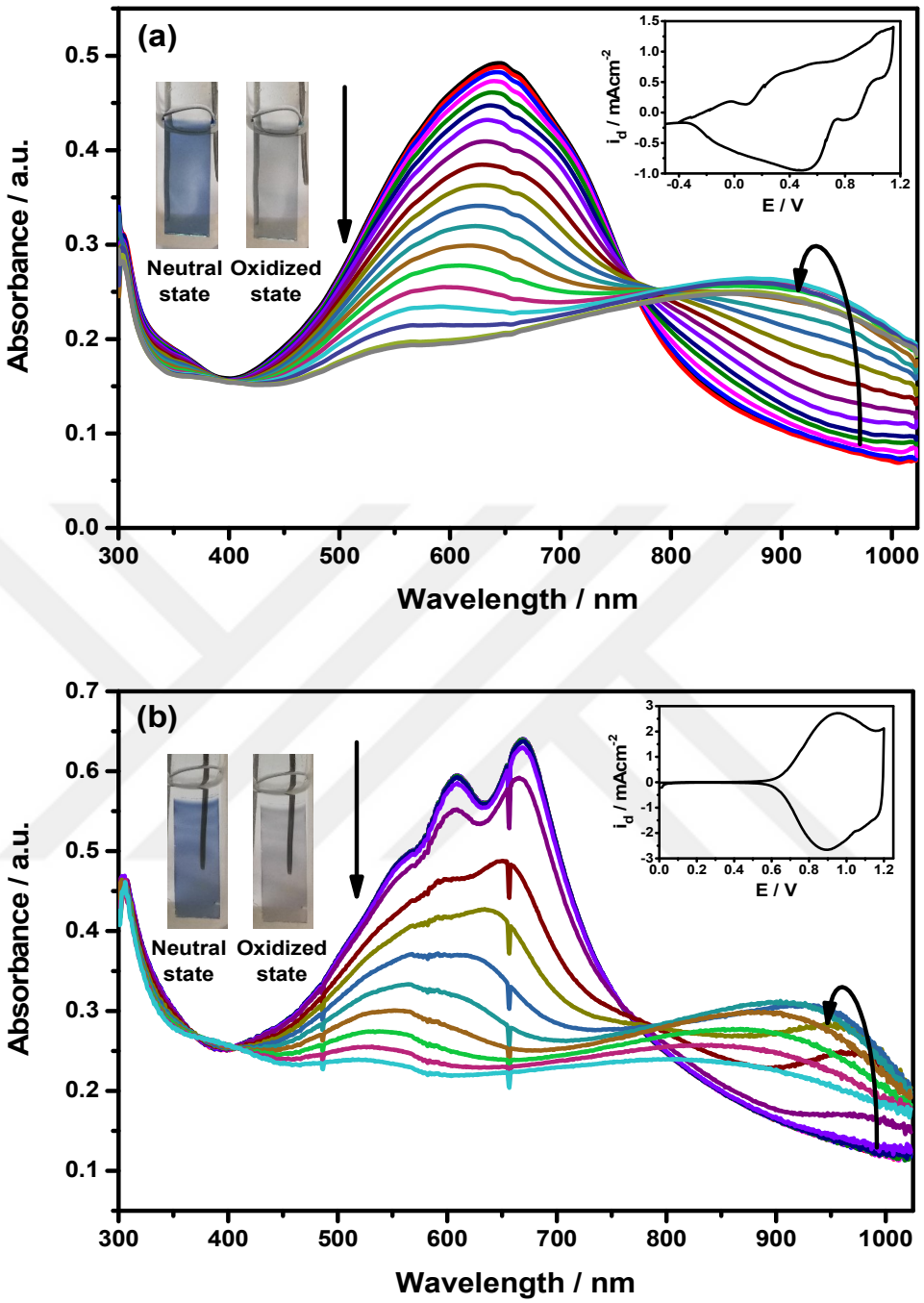

Figure 3.60. The changes in electronic absorption spectra of electrochemically deposited (a) PE(TPD-Fluo)E and (c) PP(TPD-Fluo)P films on ITO recorded at various applied potentials in 0.1 M $TBAPF_6$/MeCN. Insets: CVs of the films recorded with a scan rate of 20 mVs^{-1}. Inset: The colors of the films at neutral and oxidized states.

In order to investigate whether the polymer films are n-dopable or not, the alterations in their electronic absorption spectra were recorded under an externally applied potential in cathodic region as shown in Figure 3.61. As seen from the figure upon applied potential, the intensity of π-π* transition bands starts to diminish with the formation of new charge carrier bands at around 815 nm for PE(TPD-Fluo)E and 880 nm for PP(TPD-Fluo)P, which indicates that polymer films are n-dopable. The color changes during cathodic scan were also recorded and depicted in inset photos of Figure 3.61. The color coordinates of the polymer films in their neutral and reduced states were expressed as L*, a*, b* values and listed in Table 3.15.

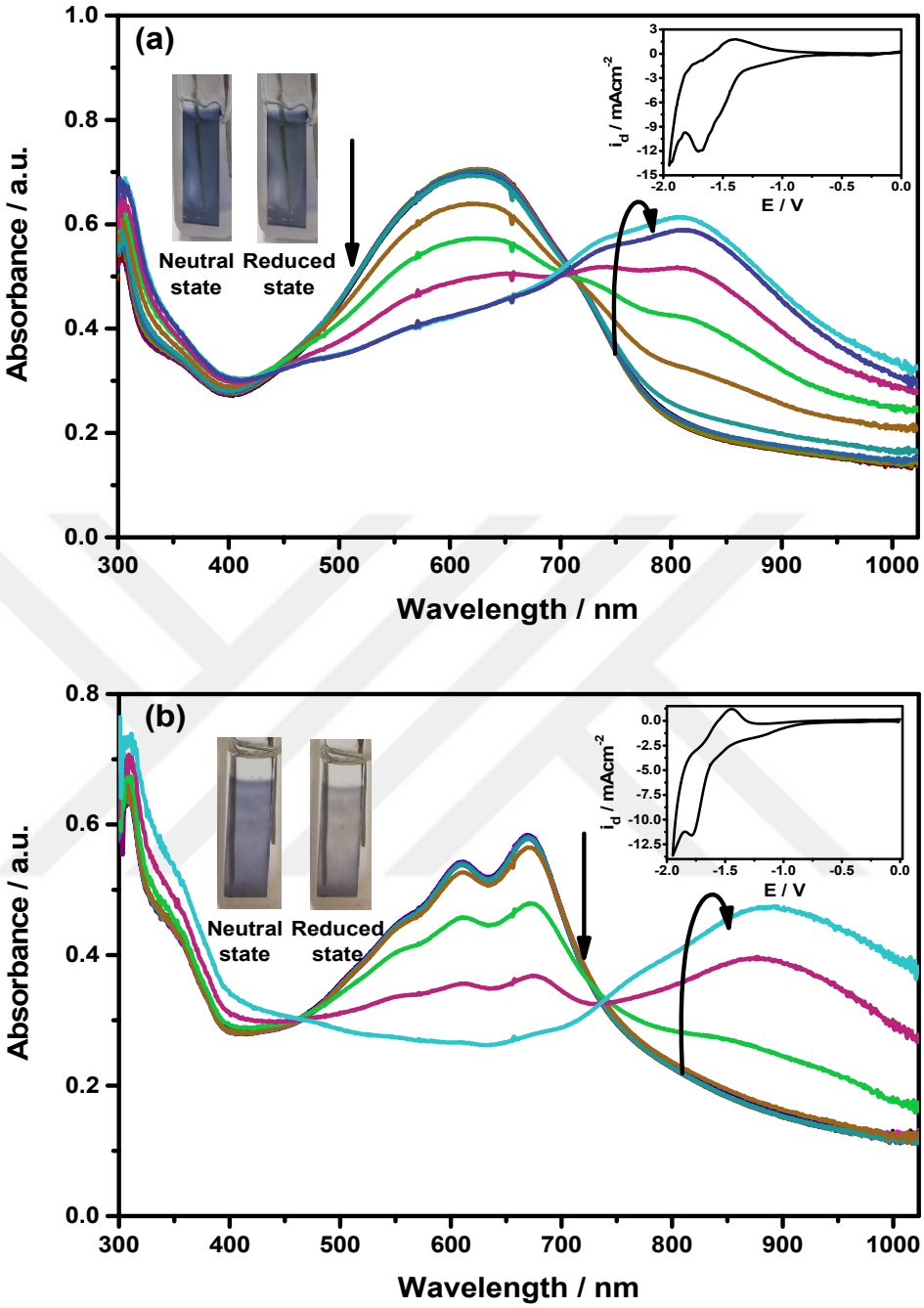

Figure 3.61. The changes in electronic absorption spectra of electrochemically deposited (a) PE(TPD-Fluo)E and (c) PP(TPD-Fluo)P films on ITO recorded at various applied potentials during n-doping in 0.1 M $TBAPF_6$/MeCN. Insets: CVs of the films recorded with a scan rate of 20 mVs^{-1}. Inset: The colors of the films at neutral and reduced states.

The chronoabsorptometry study of each polymer film was conducted by square wave potential method by applying potential difference between its redox states with a residence time of 10 s and depicted in Figure 3.62. The percent transmittance change from chronoabsorptometry study was found to be 32% at 644 nm for PE(TPD-Fluo)E and 34% at 609 nm and 36% at 668 nm for PP(TPD-Fluo)P. The corrresponding oxidation response time and CE at 95% full contrast were calculated as 0.4 s and 407 cm^2/C for PE(TPD-Fluo)E and 0.6 s and 501 cm^2/C at 609 nm, 0.5 s and 606 cm^2/C at 668 nm for PP(TPD-Fluo)P, respectively. The neutralization response time was calculated to be 0.2 s for both PE(TPD-Fluo)E and PP(TPD-Fluo)P polymer films. This fast response time for the neutralization of polymer films shows the fast removal of counter ions during neutralization due to electrostatic repulsion between polymer chain and counter ions All the results are also tabulated in Table 3.15.

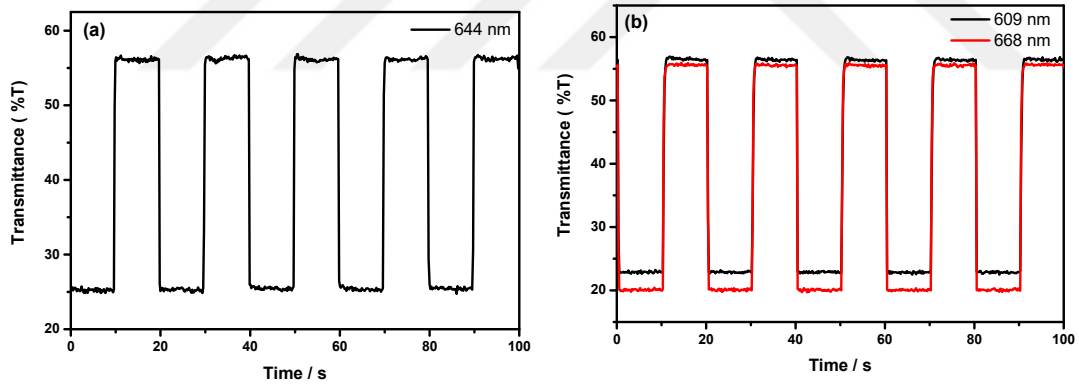

Figure 3.62. Chronoabsoptometry experiments for the polymer films on ITO in 0.1 M $TBAPF_6$/MeCN when the films were switched between redox states with an interval time of 10 s for (a) PE(TPD-Fluo)E (between -0.5 V and +1.2 V at 644 nm) and (b) PP(TPD-Fluo)P (between 0.0 V and +1.2 V at 609 nm and 668 nm).

Table 3.15 Optoelectronic properties of the polymer films on ITO in 0.1 M $TBAPF_6$/MeCN

Polymer	**PE(TPD-Fluo)E**	**PP(TPD-Fluo)P**
λ_{max} (nm)	644	609, 668
E_g^{opt} (eV)	1.48	1.59
Δ%T	32	34, 36
CE (cm^2/C)	407	501, 606
$t_{s,ox}$[a] (s)	0.4	0.6, 0.5
$t_{s,red}$[a] (s)	0.2	0.2, 0.2
Color at neutral state L*, a*, b*	71.19, -3.69, -18.14	68.75, -4.39, -17.24
Color at oxidized state L*, a*, b*	84.99, -0.95, -0.73	81.69, 2.14, 0.19
Color at neutral state L*, a*, b*	58.40, -2.07, -25.67	66.13, -2.88, -15.04
Color at reduced state L*, a*, b*	68.56, -2.45, -9.31	77.22, -3.35, 0.85

[a] 95% of full switch from colored to bleached states.

The long-term stability of fluorene-substituted polymer films were examined upon switching between their neutral and oxidized states via square wave potential

method. For this reason, the polymer films were switched between a potential range of -0.5 V and +1.1 V for PE(TPD-Fluo)P and 0.0 V and +1.1 V for PP(TPD-Fluo)P under ambient conditions. The obtained stability test results were depicted in Figure 3.63 to show the changes in optical and electrochemical activities of the polymer films after thousands of cycles. As seen from the Figure 3.63, PE(TPD-Fluo)P film exhibited a superior stability up to 20000 cyles by retaing 73% of its electroactivity and 75% of its optical activity. The high stability of PE(TPD-Fluo)P polymer film makes it very attractive for electrochromic applications. In the case of PP(TPD-Fluo)P, the polymer film also revealed high optical stability by preserving 89% of its optical activity with the loss of half of its electrochemical activity after 8000 cycles as shown in Figure 3.63.

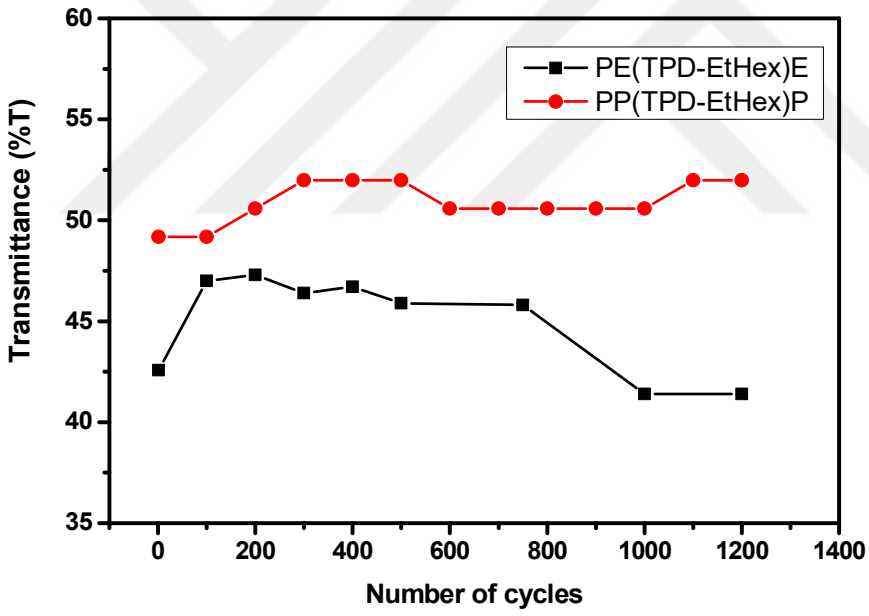

Figure 3.63. Electrochemical and optical stability tests for the polymer films on ITO in 0.1 M $TBAPF_6$/MeCN when the films switched between redox states (-0.5 V and +1.1 V) at 630 nm for (a) PE(TPD-Fluo)E and (0.0 V and +1.1 V) at 605 nm for (b) PP(TPD-Fluo)P with an interval of 1 s.

3.3 D-A-D Monomers Based on PH Type Acceptor Unit

In this part, PH unit was employed to be acceptor unit in the synthesis of a novel D-A-D monomer with the EDOT donor unit. The resulting trimeric monomer was named as E(PH)E. The pathway for the synthesis of E(PH)E was given in Scheme 3.7.

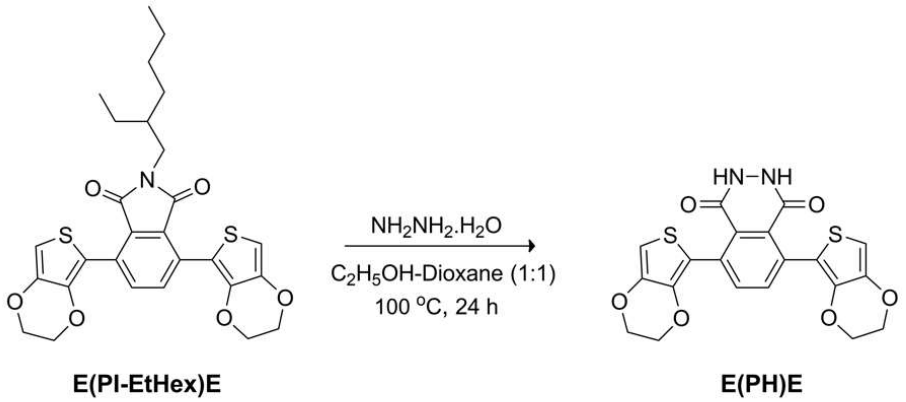

Scheme 3. 7. Synthetic route for the synthesis of E(PH)E.

3.3.1 Optical Properties of the Monomer

For the investigation of optical properties of trimeric structure, the electronic absorption and emission spectra of the monomer was recorded in DCM and the resulting spectrum is given in Figure 3.64. As shown in Figure 3.64 (a), one absorption band is detected at 318 nm for E(PH)E, corresponding to π-π* transition. Because the intramolecular interaction in this trimeric unit is negligible due to the very poor electron withdrawing nature of the PH structure, any sign for the formation of an ICT band cannot be observed in the case of E(PH)E.

The fluorescence emission spectrum of the monomer was also depicted in Figure 3.64 (b). As seen from the figure, E(PH)E displays characteristic emission band at

around 440 nm upon excitation at 300 nm. However, the fluorescence intensity of emission band is quite low as it is seen by naked eye from inset photo of Figure 3.64 (b). It is noteworthy that this trimeric monomer exhibits notably low fluorescence quantum efficiency due to the quenching effect of core structure. Table 3.16 tabulates all the absorption and emission maxima of the monomer. When this system was compared with previously synthesized terthienyl analog[122], the absorption and emission maxima of E(PH)E are shifted to a lower wavelength, which indicates the poor acceptor strength of PH unit as compared to its thiophene bearing analog.

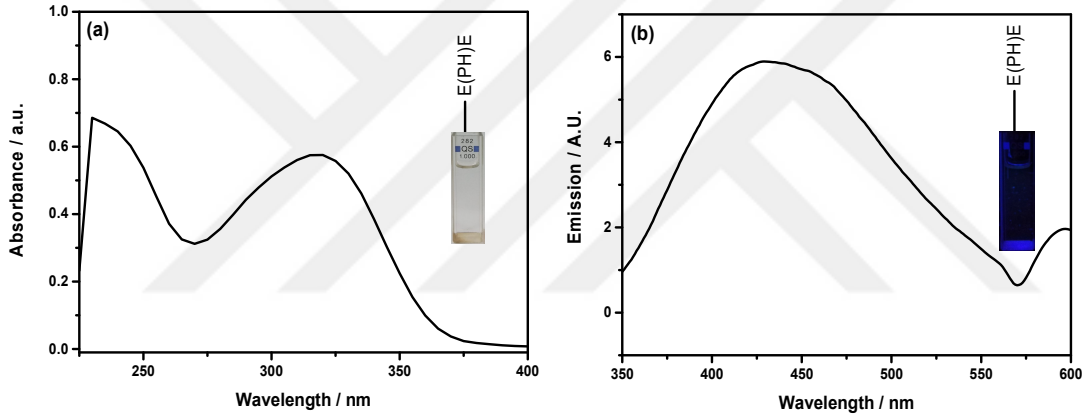

Figure 3.64. (a) Absorption and (b) emission spectra of the monomer in DCM. Inset: The color of the monomer (a) in daylight and (b) under UV lamp at 365 nm.

3.3.2 Electrochemical Properties of the Monomer

The electrochemical behavior of E(PH)E monomer bearing EDOT was investigated via both CV and square wave voltammetry (SWV) in order to reveal the effect of central acceptor moiety on the trimeric system and the results are given in Figure 3.65 for comparison sake. Both voltammograms of the trimeric system were recorded in 0.1 M $TBAPF_6$/MeCN solution containing 5% BF_3-Et_2O on Pt disc

electrode since the monomers are insoluble in MeCN. From the square wave voltammogram given in Figure 3.65 (b), one irreversible oxidation peak was observed at 1.36 V vs Ag/AgCl for E(PH)E vs Ag/AgCl. However, the voltammograms are not recorded in cathodic region due to the presence of BF_3-Et_2O in the electrolytic medium.

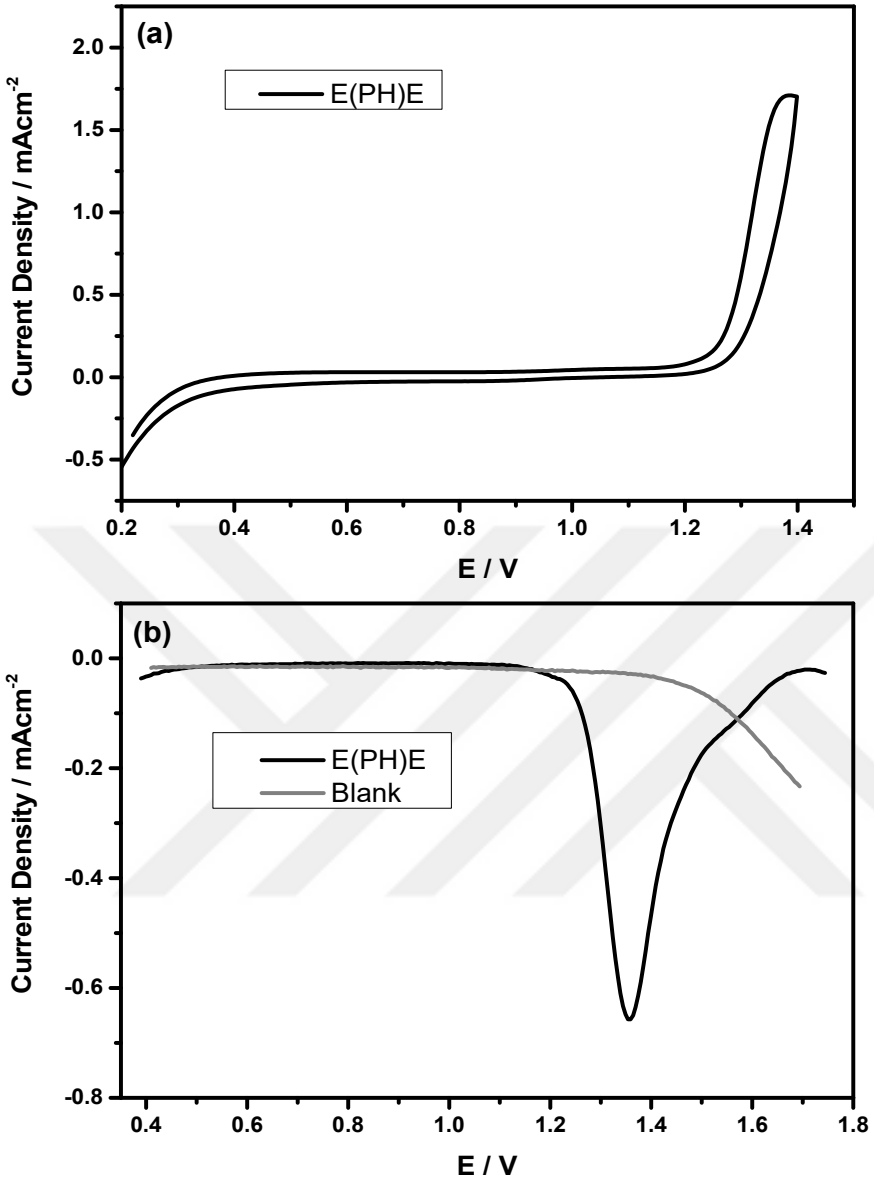

Figure 3.65. Cyclic voltammogram of E(PH)E on Pt electrode vs. Ag/AgCl in 0.1 M $TBAPF_6$ dissolved in MeCN containing 5% BF_3-Et_2O by volume at a scan rate of 100 mVs^{-1} and (b) square wave voltammogram of E(PH)E on Pt electrode vs. Ag/AgCl in 0.1 M $TBAPF_6$ dissolved in MeCN containing 5% BF_3-Et_2O by volume.

Moreover, the studies were also conducted for electropolymerization of electroactive E(PH)E system. Unfortunately, the electroactive E(PH)E system with PH core unit does not afford a successful electrochemical polymerization due to the lack of planarity in this trimeric system as observed in the case of PI-based systems. The computational studies revealed that the large dihedral angle at around 40° between benzene ring of PH with the adjacent EDOT unit distrupts the coplanarity of system and limits the electron delocalization and thereby prevents electropolymerization process. The comparison of this trimeric system with previosly synthesized terthienyl analog indicated that electropolymerization with the terthienyl system is possible unlike PH-based systems[122].

Table 3.16 Optical and electrochemical properties of the monomers

Monomers	**E(PH)E**	**E(PI-EtHex)E**
$\lambda_{max,abs}$ (nm)	318	235, 270, 335
$\lambda_{max,em}$ (nm)	440	506
$E_{ox,m}$ (V)-CV	1.38	1.39
$E_{ox,m}$ (V)-SWV	1.36	-

3.3.3 Chemiluminescence Properties of the Monomer

To investigate the chemiluminescence properties of E(PH)E system, two-syringes system, which is named as rapid mix system, was utilized. One of the syringes in the system contains oxidant and catalyst whereas the other one involves chemiluminescent compound dissolved in proper alkaline medium. The different type of catalysts (metal cations, blood or hemin) or oxidants (H_2O_2, $KMnO_4$ and $K_2Cr_2O_7$) can also be used in chemiluminescence measurements. When the blood

or hemin was used as catalyst, one of the syringes involves blood or hemin solutions together with chemiluminescent compound while the other syringe contains only oxidant. In chemiluminescence measurements, the concentration of reagents has also a priority as well as the types of reagents. For chemiluminescence measurements, the concentrations of reagents were generally adjusted to be 10^{-6} M for the target chemiluminescent compound, 10^{-3} M for oxidant and 10^{-3} M for catalyst. In order to understand the concentration effect on chemiluminescence intensity, the concentration of reagents can also be varied for chemiluminescence measurements. For this purpose, the reagents were diluted by distilled water or $NaOH_{(aq)}$ solution. While the chemiluminescent compound and hemin were diluted with 0.1 M $NaOH_{(aq)}$ solution, the blood, H_2O_2 and metal cations were diluted with distilled water. For comparison sake, chemiluminescence measurements were also carried out for luminol.

In order to determine the most efficient oxidant in chemiluminescence measurement, three different oxidizing agents, H_2O_2, $KMnO_4$ and $K_2Cr_2O_7$ were tested at the same concentrations. When the chemiluminescence radiation intensities of the oxidants were compared for both E(PH)E and luminol, it was found that H_2O_2 reveals the highest intensity among three oxidants as shown in Figure 3.66. Therefore, H_2O_2 was selected as oxidant for the following chemiluminescence measurements.

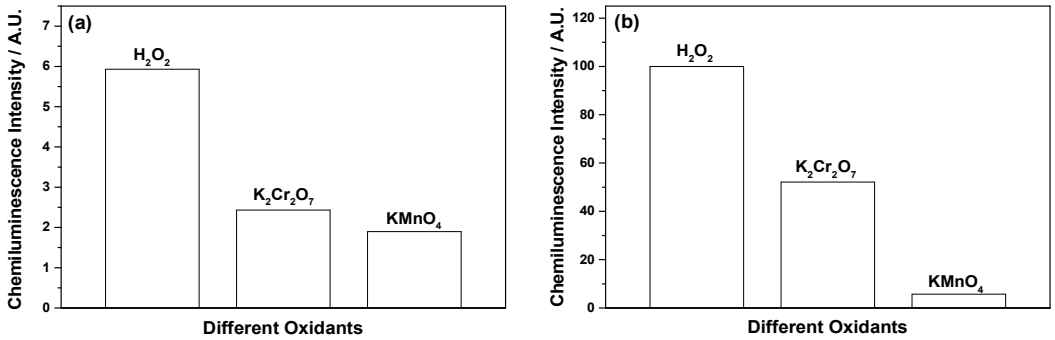

Figure 3.66. Chemiluminescence intensities of $1.0x10^{-6}$ M (a) E(PH)E and (b) luminol in 0.1 M $NaOH_{(aq)}$ with $1x10^{-3}$ M of various oxidants.

When taking into account the structural similarities between luminol and E(PH)E, a similar chemiluminescence mechanism can be suggested for E(PH)E system. In this mechanism, after the interaction of the oxidizing agent, H_2O_2 with E(PH)E, a bridge is formed between carbonyl groups via peroxide in pyridazine ring. This ring is irreversibly broken down due to the stretching in the bridge and the energy is released in the form light. Consequently, the blue-green light is emitted. The suggested mechanism is given in Scheme 3.8.

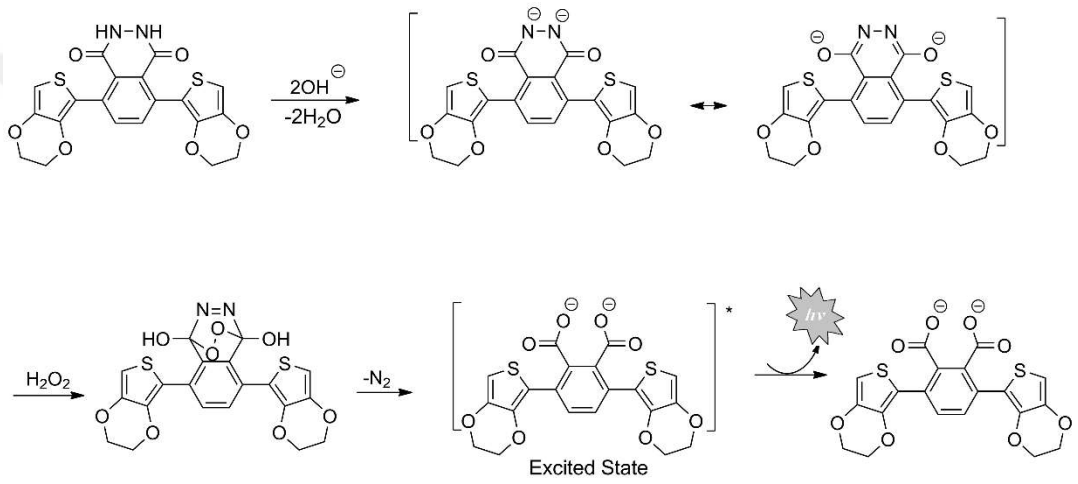

Scheme 3. 8. The suggested mechanism for E(PH)E.

In order to investigate the effect of H_2O_2 concentration on chemiluminescence reaction, the different concentrations of H_2O_2 was reacted with luminol in alkaline medium and the intensity of light emitted was recorded as a function of H_2O_2 concentration and depicted in Figure.3.67. It was found that the chemiluminescence intensity increases with increasing H_2O_2 concentration. Moreover, the chemiluminescence radiation can be detected even if the concentration of H_2O_2 is low as $1.0x10^{-6}$ M. However, chemiluminescence intensity is quite low to be seen by naked eye due to slow kinetics of chemiluminescence reaction in the absence of catalyst.

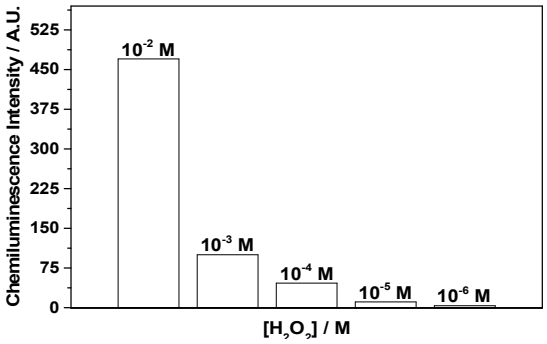

Figure 3.67. Chemiluminescence intensities of $1.0x10^{-6}$ M luminol in 0.1 M $NaOH_{(aq)}$ with different H_2O_2 concentrations.

The higher intensity of light can only be observed with the help of a catalyst which fasten the chemiluminescence reaction. In order to observe the effect of catalyst on the chemiluminescence reaction, Fe^{3+} ion was employed as catalyst in the reaction of E(PH)E and luminol with H_2O_2 in alkaline medium and the results are depicted in Figure 3.68. As it can be seen from the figure, the chemiluminescence emission intensity of E(PH)E and luminol compounds drastically increases with the addition of Fe^{3+} ion indicating the effect of catalyst on chemiluminescence reaction.

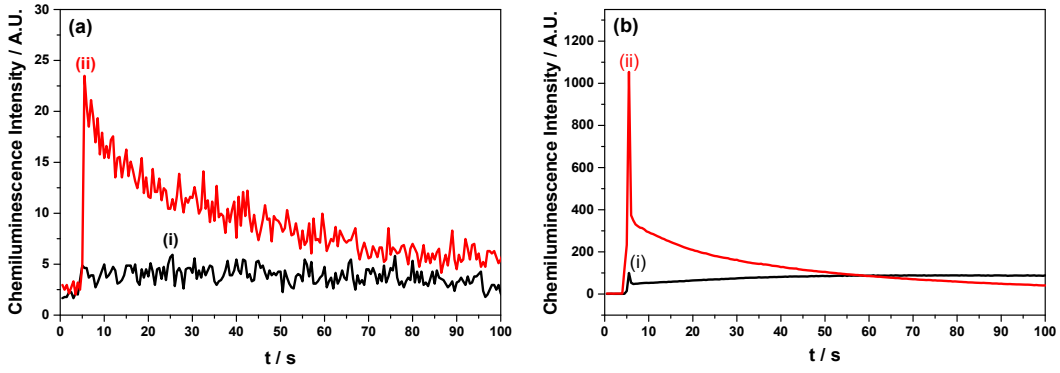

Figure 3.68. Chemiluminescence intensity of $1.0x10^{-6}$ M (a) E(PH)E and (b) luminol in 0.1 M $NaOH_{(aq)}$ with $1.0x10^{-3}$ M H_2O_2 (i) in the absence and (ii) in the presence of $1.0x10^{-3}$ M Fe^{3+} ion.

The different metallic cations can also catalyze the chemiluminescence reaction between luminol and H_2O_2 [161] .Thus, a variety of different metal ions (Ag^+, Al^{3+}, Cd^{2+}, Co^{2+}, Cu^{2+}, Fe^{3+}, Mg^{2+}, Mn^{2+}, Ni^{2+}, Pb^{2+}, Zn^{2+}) were also analyzed to detect the catalytic effect of these metal ions on chemiluminescence reaction of E(PH)E and luminol. As shown in Figure 3.69, E(PH)E compound exhibits high selectivity towards Cu^{2+}, Zn^{2+}, Pb^{2+} and Fe^{3+} ions while luminol shows high sensitivity towards Al^{3+}, Cu^{2+} and Fe^{3+} ions. Among these ions, the highest catalytic activity on chemiluminescence reaction of E(PH)E and luminol was detected for Cu^{2+} and Al^{3+} ions, respectively. These properties of E(PH)E and luminol make them ameable for both blood detection and ion sensing applications in the field of analytical chemistry.

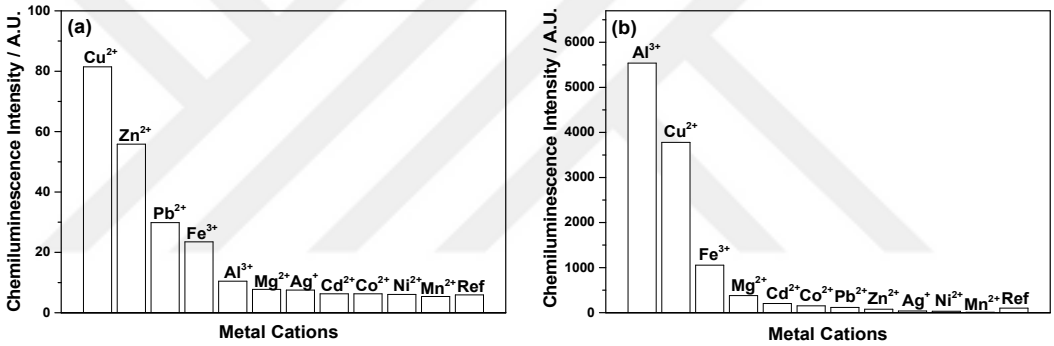

Figure 3.69. Chemiluminescence intensity of $1.0x10^{-6}$ M of (a) E(PH)E and (b) luminol in 0.1 M $NaOH_{(aq)}$ with $1.0x10^{-3}$ M H_2O_2 in the presence of $1.0x10^{-3}$ M of different metal ions.

In order to the evaluate the potential use of E(PH)E compound for ion sensing or blood detection applications, the response of E(PH)E compound towards different concentrations of metal ions was also investigated. Only a few metal ions were selected for the investigation of concentration effect of metal ions on chemiluminescence reaction. Firstly, the effect of Fe^{3+} ion concentration was investigated. For this purpose, five-different concentrations of Fe^{3+} were applied for chemiluminescence reaction of E(PH)E and chemiluminescence intensity was recorded as a function of metal ion concentration.(Figure 3.70). It was found that

chemiluminescence intensity is still detectable at 10^{-3} M Fe^{3+}. The same study was also conducted for Cu^{2+} ion since it exhibits the highest catalytic activity towards chemiluminescence reaction of E(PH)E and it was observed that chemiluminescence radiation intensity increases as a function of increased Cu^{2+} ion concentration. Also, more enhanced response was observed for Cu^{2+} ions as compared to that of Fe^{3+} even at a concentration level of 10^{-4} M. (Figure 3.70)

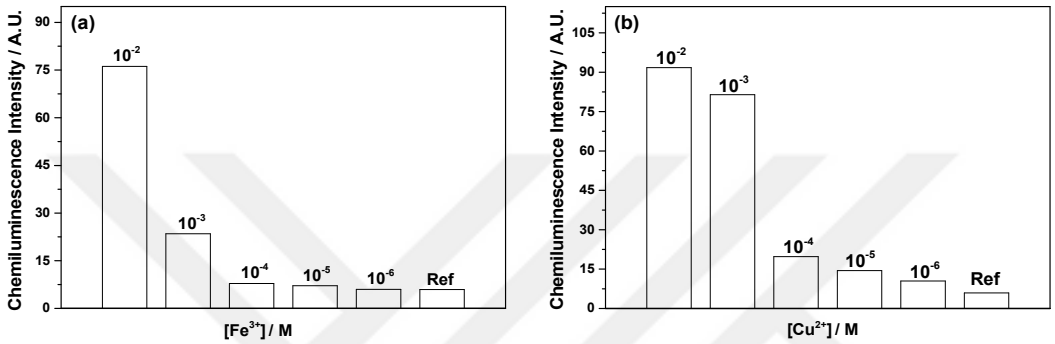

Figure 3.70. Chemiluminescence intensity of $1.0x10^{-6}$ M of E(PH)E in 0.1 M $NaOH_{(aq)}$ with $1.0x10^{-3}$ M H_2O_2 in the presence of different concentrations of (a) Fe^{3+} and (b).Cu^{2+} ions.

A similar study was also conducted for hemin to reveal the effect of hemin concentration on chemiluminescence emission intensity for both E(PH)E and luminol and the obtained results were given in Figure 3.71. As shown in Figure 3.71 (a), hemin can catalyze the chemiluminescence reaction of E(PH)E even at a low concentration of 10^{-7} M. In the case of luminol depicted in Figure 3.71 (b), chemiluminescence intensity can be detected even at a lower hemin concentration, which is about 10^{-10} M.

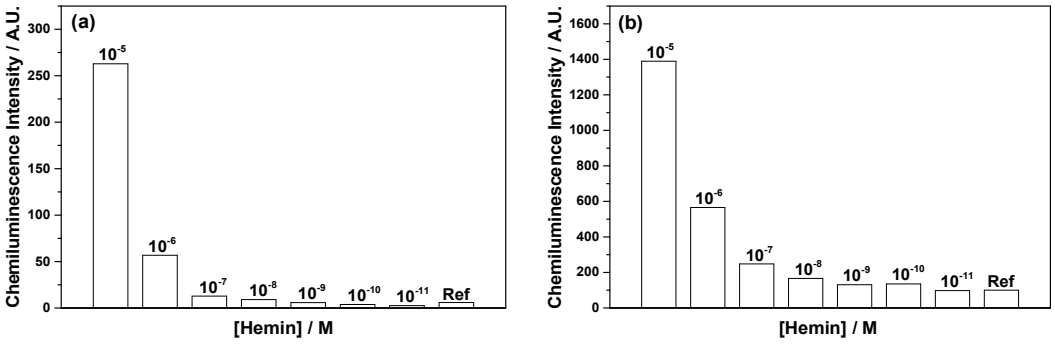

Figure 3.71. Chemiluminescence intensity of $1.0x10^{-6}$ M of (a) E(PH)E and (b) luminol in 0.1 M $NaOH_{(aq)}$ with $1.0x10^{-3}$ M H_2O_2 in the presence of different hemin concentrations.

The chemiluminescence emission profile of the compound E(PH)E was also investigated in the presence of blood sample instead of Fe^{3+} ion in order to determine the potential use of E(PH)E for blood detection in forensic science. For these measurements, the blood samples were diluted by water in different proportions to determine the lowest detection limit. The obtained results were depicted for both E(PH)E and luminol in Figure 3.72 for comparison sake. It was observed that light intensity still can be detected even at 100,000 fold dilution level for E(PH)E.

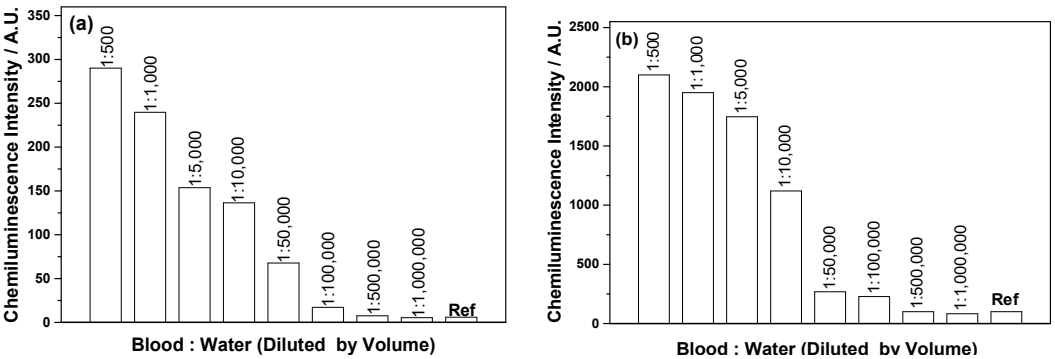

Figure 3.72. Chemiluminescence intensity of $1.0x10^{-6}$ M of (a) E(PH)E and (b) luminol in 0.1 M $NaOH_{(aq)}$ with $1.0x10^{-3}$ M H_2O_2 in the presence of blood samples diluted with water in different proportions.

CHAPTER 4

CONCLUSION

In the previous sections, an extensive study has been presented so as to reveal optical, electronic and optoelectronic features of new D-A-D type trimeric monomer systems and their corresponding polymers. With the goal of exploring such kind of properties, different kinds of donors, acceptor and the substituents are involved in this study. In order to elucidate the effect of donor, acceptor and the substituent on the acceptor, D-A-D type sytems have been created with three series of acceptor units involving different substituents. Thiophene and alkylene dioxythiophene-based donor units are used for the synthesis of D-A-D monomers.

In the first section, two PI based acceptor units with propyl- and POSS propyl-substituents were coupled with thiophene and EDOT donor units and four new PI based analogues were synthesized and characterized. When the results are examined, it is noted that the substituents have very little effect on the absorption and emission profiles of monomers, whereas the donor group has a more pronounced effect on absorption and emission bands that red shift with increased donor strength. Moreover, the electrochemical data shows that the oxidation potentials of POSS-substituted monomers were found to be slightly more positive and the reduction potentials were found to be more negative than their propyl-substituted analogues. The effect of POSS substituent on the oxidation potential seems quite negligible, whereas it is more pronounced in the reduction potential. This change is due to lowering of LUMO. Also, it was found that POSS-substituted monomers have the potential of electrochemical polymerization unlike their propyl-substituted analogues. Although there exist some studies based on PI acceptor unit in the literature, there are few examples with different functional groups. The studies based on PI acceptor unit was already reported in literature, but with the limited number of functional groups. Our studies show that PI can be

modified by any functional group other than common alky chains. Furthermore, it is noteworthy that PI is a poorer acceptor unit as compared to the other acceptors in the literature without being dependent on the type of substituent.

In the second section, a similar type of acceptor with the N-functionalization center, TPD, was involved in the synthesis of new D-A-D type monomers. Four series of D-A-D monomers, each containing TPD core unit with a different substituent, have been synthesized and characterized to reveal the precise effect of the substituent concerning optical and electrochemical properties of the monomers and polymers synthesized in this work. In addition, both the effect of different donor groups and structural modifications in the acceptor unit as changed from PI to TPD have been investigated as well. Several important conclusions were drawn according to the data presented in this section.

Firstly, the factors affecting the photophysical properties of TPD based monomers were evaluated and it was found that alky type substitution (ethyl hexyl or POSS propyl) on TPD acceptor unit has no appreciable effect on the photophysical properties of the monomers, whereas aryl substituents result in a change in electronic absorption profile of the monomers due to the absorption of aryl substituents (azobenzene and fluorene) in the relevant range. On the contrary, photophysical properties of the monomers were found to exhibit more pronounced variations depending on the type of donor unit rather than the substituent. The trend observed for varying donor units in each serie containing the same substituent was similar. When the effects of these factors on the properties of corresponding polymers were investigated, it was found that donor and acceptor units play key roles on the electrochemical and optical behaviors such as band gap, neutral state color, and electrochromic performance while the substituent does not significantly change optoelectronic properties of polymers. Accordingly, it was found that the optoelectronic behavior of each serie containing the same substituent was comparable. For example, E_g values evaluated from optical data follows the same trend for each series (i.e. $E_{g,\ Thiophene} > E_{g,\ ProDOT} > E_{g,\ EDOT}$) but each substituent contributes its own properties into polymer backbone. For example, all POSS

propyl appended polymer films exhibit solubility in common organic solvents and greater thermal stability in contrast to ethyl hexyl-substituted ones. Similarly, both azobenzene-substituted monomers and their polymers adopt photoswitching property.

Secondly, when the effect of both alky or aryl substituents on electrochemical behaviours of the monomers were examined, it was found that all monomers exhibit similar pattern with one oxidation peak and one reduction peak. Detailed examination of peak potentials from all series of TPD based monomers shows that the substituent on the acceptor unit does not appreciably affect the oxidation potential except for POSS propyl substituent which results in slight anodic shift in the oxidation potential of all three POSS propyl appended monomers. This trend is also observed in POSS propyl appended PI based monomers. The reason for this anodic shift is not clear yet. Moreover, when the effect of donor groups on the oxidation peak and onset potentials are examined in all TPD based monomers, it was found that the oxidation peak and onset potentials exhibits more pronounced variations and decrease drastically when moving from thiophene unit to EDOT donor unit in each monomer series without being dependent on the subtituent on the acceptor unit. This trend is explained by the strength of donor group. By taking all these results into account, it can be concluded that the trend observed in the oxidation potentials is solely determined by the strength of donor group. On the other hand, detailed inspection and comparison of reduction potential of the TPD based monomers revealed that the reduction potentials show variations depending on aryl or alky substituents on the acceptor unit. For example, the reduction potentials of POSS propyl-substituted D-A-D monomers were found to be more negative than their ethyl hexyl analogues. This is because reduction potentials are related to LUMO energy levels of the monomers and LUMO energy levels can be tuned by any structural change in the acceptor units. Furthermore, it was found that the reduction potentials of all azobenzene-substituted monomers are drastically shifted to more positive values as compared to all other substituted analogs. This drastic change in reduction potentials also originates from the substituent effect on

the acceptor unit since azobenzene as an electron withdrawing functional group increases the electron deficiency of the acceptor unit, thereby the D-A-D system and as a result reduction potentials shift to more positive values. When the effect of donor moiety on the reduction behavior of all TPD based monomers were taken into account, the reduction potentials of EDOT derivatives were found to be more negative due to higher electron density of D-A-D systems with the EDOT donor unit as compared to thiophene or ProDOT analogues. This result is also correlated for PI based D-A-D systems. When the effects of these factors on the electrochemical properties of corresponding polymers were investigated, it was found that the effect of donor and acceptor units on the electrochemical band gap is concrete while the effect of substituent is quite negligible. Also, the effect of donor units on the electrochemical and optical band gap values of polymers were investigated, it was found that each serie follows the same trend depending on the strength of donor unit (i.e. $E_{g,Thiophene} > E_{g,ProDOT} > E_{g,EDOT}$).

Lastly, in order to understand the structure-property relationships that occur with the replacement of PI core with TPD core unit in a D-A-D system, PI based monomers were directly compared with TPD containing ones having the same substituent and donor units. As a result, it was found that both absorption and emission spectra of D-A-D monomers with PI core unit are significantly blue-shifted relative to their TPD based counterparts. This shift can be explained by higher electron affinity of the TPD core unit than PI unit and the better coplanarity of TPD based system than PI based ones as supported by theoretical calculations. The better coplanarity enhances the conjugation and ICT, which explains the bathochromic shift of TPD based system as compared to their PI based counterparts. Moreover, the examination of electrochemical data indicated that the oxidation potentials of the PI based monomer systems are drastically shifted to more positive values as compared to their TPD based counterparts. This shift is also ascribed to the strength of acceptor group which is the only variable in both D-A-D systems. Although HOMO energy levels are independent of identity of acceptor unit, in this case a noticeable shift was observed in HOMO energy levels

of D-A-D systems depending on the change in acceptor unit. In literature, it was declared that the nature of acceptor unit can lead to HOMO energy level to become deeper. More electronegative acceptor unit can lower both the HOMO and LUMO energy levels of a conjugated system, but not at the same level. This explains the low lying HOMO levels of PI based systems as compared to TPD based ones, both having the same donor unit. It can be concluded that the acceptor unit has a slight impact on the HOMO energy level in addition to LUMO. Furthermore, when the reduction potentials of the same monomer systems were examined, it was found that PI based monomers exhibit less negative reduction peak and onset potentials as compared to their TPD based counterparts. Since the reduction potentials are directly related to the LUMO energy level, it can be stated that the monomers with the PI acceptor unit result in a lower LUMO energy level than their TPD counterparts. However, in literature, it was reported that a stronger acceptor unit results in a lower LUMO energy level. According to this information, it is expected that TPD based monomers have lower lying LUMO energy level since TPD is a stronger electron deficient unit than PI acceptor unit. However, in our study, the obtained results indicated that all TPD based monomers have more negative reduction potentials, thereby higher LUMO levels as compared to PI based ones, which is not correlated to the literature knowledge. When the effect of acceptor units on the optoelectronic properties of corresponding polymers were investigated, it was found that more improved results such as low band gap, high optical contrast, fast switching time etc., were observed for TPD-based polymers as compared to PI-based polymer. This study also shows that both PI and TPD acceptors can be modified by any functional group to impart new functionalities without altering their optoelectronic properties.

In the third and last section, a novel D-A-D system with the chemiluminescent property was synthesized in a two-step pathway. Firstly, the optical and electrochemical properties of this PH-based system was investigated and compared with the terthienyl analog. According to this, PH structure is not able to afford coplanarity in this trimeric conjugated system, which explains hypsochromic shift

and ineffective polymerization observed in the PH-based systems. This results show that PH unit with the benzene ring is weaker acceptor unit as compared to its thiophene bearing analog. Moreover, chemiluminescence quantum efficiency of PH based system is not high as much as luminol.

In summary, this work experimentally evaluates the electrochemical and optoelectronic properties of some novel D-A-D type monomers containing PI and TPD acceptor which can be functionalized with a variety of alky or aryl groups. The effect of substituent, donor and acceptor were directly compared to elucidate the structure-property relationship.

REFERENCES

1. Moore, J. W. & Stanitski, C. L. Lengthening the Chain: Polymers in General Chemistry. *J. Chem. Educ.* **94**, 1603–1606 (2017).
2. Kumar, R., Singh, S. & Yadav, B. C. Conducting Polymers : Synthesis , Properties and Applications. *IARJSET* **2**, 110–124 (2016).
3. Hiroki, K. What conductive polymers have taught us about the meaning of education: Education before innovation. *IOP Conf. Ser. Mater. Sci. Eng.* **54**, 1–8 (2014).
4. Kumar, D. & Sharma, R. C. Advances in conductive polymers. *Eur. Polym. J.* **34**, 1053–1060 (1998).
5. Yi, N. & Abidian, M. R. Conducting polymers and their biomedical applications. in *Biosynthetic Polymers for Medical Applications* 243–276 (Elsevier, 2016).
6. Çakal, D., Ertan, S., Cihaner, A. & Önal, A. M. Synthesis and electrochemical polymerization of D-A-D type monomers with thieno[3,4-c]pyrrole-4,6-dione acceptor unit. *Dye. Pigment.* **158**, 175–182 (2018).
7. Someya, T., Bao, Z. & Malliaras, G. G. The rise of plastic bioelectronics. *Nature* **540**, 379–385 (2016).
8. Soloducho, J. & Cabaj, J. Conducting Polymers in Biological Systems. *Med. Chem. (Los. Angeles).* **6**, 531–540 (2016).
9. Epstein, A. J. Electrical conductivity in conjugated polymers. in *Conductive Polymers and Plastics in Industrial Applications* vol. 2 1–9 (1999).
10. Shirakawa, H. The discovery of polyacetylene film: The dawning of an era of conducting polymers. *Reports Prog. Polym. Phys. Japan* **43**, 1–19 (2000).
11. Harun, M. H., Saion, E., Kassim, A., Yahya, N. & Mahmud, E. Conjugated Conducting Polymers : A Brief Overview. *Sensors Peterbrgh. NH* **2**, 63–68 (2007).
12. Reddinger, J. L. & Reynolds, J. R. Molecular Engineering of π-conjugated Polymers. in *Advances in Polymer Science* 57–112 (Springer, Berlin, Heidelberg, 1999).
13. Chiang, C. K. *et al.* Electrical Conductivity in Doped Polyacetylene. *Phys. Rev. Lett.* **39**, 1098–1101 (1977).
14. Salaneck, W. R., Friend, R. H. & Brédas, J. L. Electronic structure of conjugated polymers: Consequences of electron-lattice coupling. *Phys. Rep.* **319**, 231–251 (1999).

15. Rasmussen, S. Low-Bandgap Polymers. in *Encyclopedia of Polymeric Nanomaterials* 1–13 (Springer, 2013).

16. Roncali, J. Molecular engineering of the band gap of π-conjugated systems: Facing technological applications. *Macromol. Rapid Commun.* **28**, 1761–1775 (2007).

17. Le, T. H., Kim, Y. & Yoon, H. Electrical and electrochemical properties of conducting polymers. *Polymers (Basel).* **9**, 150 (2017).

18. Bakhshi, A. K., Kaur, A. & Arora, V. Molecular engineering of novel low band gap conducting polymers. *Indian J. Chem. -Sect. A* **51**, 57–68 (2012).

19. Brédas, J. L. Relationship between band gap and bond length alternation in organic conjugated polymers. *J. Chem. Phys.* **82**, 3808–3811 (1985).

20. Jacquemin, D. & Adamo, C. Bond length alternation of conjugated oligomers: Wave function and DFT Benchmarks. *J. Chem. Theory Comput.* **7**, 369–376 (2011).

21. Gieseking, R. L., Risko, C. & Brédas, J. L. Distinguishing the effects of bond-length alternation versus bond-order alternation on the nonlinear optical properties of conjugated chromophores. *J. Phys. Chem. Lett.* **6**, 2158–2162 (2015).

22. *Handbook of Advanced Electronic and Photonic Materials and Devices: Conducting polymers*. (Academic Press, 2001).

23. Kwon, O. & McKee, M. L. Theoretical calculations of band gaps in the aromatic structures of polythieno[3,4-b]benzene and polythieno[3,4-b]pyrazine. *J. Phys. Chem. A* **104**, 7106–7112 (2000).

24. Skotheim, T. A. & Reynolds, J. R. *Conjugated polymers: Theory, synthesis, properties, and characterization*. (CRC Press, 2007).

25. Roncali, J., Thobie-Gautier, C. & Brisset, H. The rigidification of the π-conjugated system: An efficient new strategy towards small bandgap semi-conductors. *Phosphorus. Sulfur. Silicon Relat. Elem.* **95**, 513–514 (1994).

26. Wu, K. Y., Chiu, C. C., Chuang, W. T., Wang, C. L. & Hsu, C. S. The backbone rigidity and its influence on the morphology and charge mobility of FBT based conjugated polymers. *Polym. Chem.* **6**, 1309–1315 (2015).

27. Wijsboom, Y. H. *et al.* Controlling Rigidity and Planarity in Conjugated Polymers: Poly(3,4-ethylenedithioselenophene). *Angew. Chemie* **121**, 5551–5555 (2009).

28. Salzner, U. & Kiziltepe, T. Theoretical analysis of substituent effects on building blocks of conducting polymers: 3,4'-Substituted bithiophenes. *J. Org. Chem.* **64**, 764–769 (1999).

29. Bakhshi, A. K. Electronic structure of conducting polymers. *Annu. Reports Prog. Chem. - Sect. C* **89**, 147–178 (1992).

30. Saravanan, C., IS, N. & SD, M. Electron Withdrawing Substituent that Control Band Gap and Planar Conformation in Push-Pull Molecules Through Non-Covalent Interactions : Density Functional Theory Study. *Res. Rev. J. Chem.* **7**, 20–30 (2018).

31. Swager, T. M. 50th Anniversary Perspective: Conducting/Semiconducting Conjugated Polymers. A Personal Perspective on the Past and the Future. *Macromolecules* **50**, 4867–4886 (2017).

32. Tarkuç, S. Tuning the Optoelectronic Properties Of Conjugated Polymers via Donor-Acceptor-Donor Architectures. (METU, 2010).

33. Malhotra, B. D. Defects in conducting polymers. *Bull. Mater. Sci.* **10**, 85–96 (1988).

34. Chiang, C. K. *et al.* Synthesis of Highly Conducting Films of Derivatives of Polyacetylene, (CH)x. *J. Am. Chem. Soc.* **100**, 1013–1015 (1978).

35. Nigrey, P. J., MacDiarmid, A. G. & Heeger, A. J. Electrochemistry of polyacetylene, (CH)x: Electrochemical doping of (CH)x films to the metallic state. *J. Chem. Soc. Chem. Commun.* 594–595 (1979).

36. MacInnes, D. *et al.* Organic batteries: Reversible n- and p-type electrochemical doping of polyacetylene, (CH)x. *J. Chem. Soc. Chem. Commun.* 317–319 (1981).

37. *Encyclopedia of Polymer Applications, 3 Volume Set*. (CRC Press, 2018).

38. Bakhshi, A. K. Electrically conducting polymers: from fundamental to applied research. *Bull. Mater. Sci.* **18**, 469–495 (1995).

39. Agobi, A. U., Louis, H., Magu, T. O. & Dass, P. M. A Review on Conducting Polymers-Based Composites for Energy Storage Application. *J. Chem. Rev.* **1**, 19–34 (2019).

40. Saravanan, C., Shekhar, R. C. & Palaniappan, S. Synthesis of polypyrrole using benzoyl peroxide as a novel oxidizing agent. *Macromol. Chem. Phys.* **207**, 342–348 (2006).

41. Chitte, H. K., Shinde, G. N., Bhat, N. V. & Walunj, V. E. Synthesis of Polypyrrole Using Ferric Chloride (FeCl3) as Oxidant Together with Some Dopants for Use in Gas Sensors. *J. Sens. Technol.* **1**, 47–56 (2011).

42. Kiebooms, R., Menon, R. & Lee, K. Synthesis, electrical, and optical properties of conjugated polymers. in *Handbook of Advanced Electronic and Photonic Materials and Devices* 1–102 (Academic Press, 2001).

43. Street, G. B. *et al.* Preparation and Characterization of Neutral and Oxidized

Polypyrrole Films. *Mol. Cryst. Liq. Cryst.* **83**, 253–264 (1981).

44. Filimon, A. Perspectives of Conductive Polymers Toward Smart Biomaterials for Tissue Engineering. in *Conducting Polymers* 119–143 (IntechOpen, 2016).

45. Cheng, Y. J. & Luh, T. Y. Synthesizing optoelectronic heteroaromatic conjugated polymers by cross-coupling reactions. *J. Organomet. Chem.* **689**, 4137–4148 (2004).

46. Bao, Z., Chan, W. K. & Yu, L. Exploration of the Stille Coupling Reaction for the Syntheses of Functional Polymers. *J. Am. Chem. Soc.* **117**, 12426–12435 (1995).

47. Tappe, F. M. J., Trepohl, V. T. & Oestreich, M. Transition-metal-catalyzed C-P cross-coupling reactions. *Synthesis (Stuttg).* 3037–3062 (2010).

48. Mark, H. F. *Encyclopedia of Polymer Science and Technology*. (John Wiley & Sons Inc., 2014).

49. Kumar, S. Conducting polymers and their characterization. *Int. Res. J. Eng. Technol.* **3**, 479–482 (2016).

50. Inzelt, G. *Conducting polymers book: A New Era in Electrochemistry*. (Springer, 2012).

51. Sandler, S., Karo, W., Bonesteel, J. & Pearce, E. *Polymer Synthesis and Characterization: A Laboratory Manual*. (Academic Press, 1998).

52. Diehl, B. Principles in NMR spectroscopy. in *NMR Spectroscopy in Pharmaceutical Analysis* 1–41 (Elsevier, 2008).

53. Sandler, S. R., Karo, W., Bonesteel, J. & Pearce, E. M. Nuclear magnetic resonance. in *Polymer Synthesis and Characterization: A Laboratory Manual* 83–97 (Academic Press, 1998).

54. French, D., Cook-Botelho, J. C. & Bachmann, L. M. Chapter 10 - Steroid hormones. in *Mass Spectrometry for the Clinical Laboratory* 205–230 (Academic Press, 2017).

55. Pleil, J. D. & Isaacs, K. K. High-resolution mass spectrometry: Basic principles for using exact mass and mass defect for discovery analysis of organic molecules in blood, breath, urine and environmental media. *J. Breath Res.* **10**, 1–10 (2016).

56. Stock, N. L. Introducing Graduate Students to High-Resolution Mass Spectrometry (HRMS) Using a Hands-On Approach. *J. Chem. Educ.* **94**, 1978–1982 (2017).

57. Shono, T. Oxidation by Electrochemical Methods. in *Comprehensive Organic Synthesis* 789–813 (Pergamon Press, 1991).

58. Parsons, R. Cyclic voltammetry and the frontiers of electrochemistry. *J. Electroanal. Chem. Interfacial Electrochem.* **305**, 164–166 (1991).

59. Skoog, D. A. & West, D. M. *Fundamentals of Analytical Chemistry*. (New York : Holt, Rinehart, and Winsto, 1976).

60. Creager, S. Solvents and supporting electrolytes. in *Handbook of Electrochemistry* 57–72 (Elsevier B.V., 2007).

61. Elgrishi, N. *et al.* A Practical Beginner's Guide to Cyclic Voltammetry. *J. Chem. Educ.* **95**, 197–206 (2018).

62. Evans, D. H., O'Connell, K. M., Petersen, R. A. & Kelly, M. J. Cyclic voltammetry. *J. Chem. Educ.* **60**, 290–293 (1983).

63. Brajter-Toth, A. Electroanalytical methods: Guide to experiments and applications. *J. Am. Chem. Soc.* **125**, 3398 (2003).

64. Wang, J. *Analytical Electrochemistry*. (John Wiley & Sons Inc., 2006).

65. Carbó, A. D. Electrochemical dictionary. Allen J. Bard, György Inzelt, Fritz Scholz (eds). *J. Solid State Electrochem.* 505–506 (2009).

66. Bard, A. J. & Mayell, J. S. Secondary reactions in controlled potential coulometry. II. Secondary electrode reactions. *J. Phys. Chem.* **66**, 2173–2179 (1962).

67. Perkowitz, S. *Optical Characterization of Semiconductors : Infrared, Raman, and Photoluminescence Spectroscopy.* (Elsevier Science & Technology, 1993).

68. Perkampus, H.-H. *UV-VIS Spectroscopy and Its Applications*. (Springer, 1992).

69. Kothekar, V. Basic UV-Vis Theory, Concepts and Applications Basic UV-Vis Theory, Concepts and Applications. *Protocol* 1–28 (2012).

70. *Principles of fluorescence spectroscopy*. (Springer, 2006).

71. Fery-Forgues, S. & Lavabre, D. Are fluorescence quantum yields so tricky to measure? A demonstration using familiar stationery products. *J. Chem. Educ.* **76**, 1260–1264 (1999).

72. Jarosz, T., Krukiewicz, K., Lapkowski, M. & Domagala, W. Spectroelectrochemical techniques as modern tools for investigating charge transfer processes in conjugated polymers. *Chemik* **69**, 485–490 (2015).

73. Jarosz, T., Data, P. & Lapkowski, M. In Situ Spectroelectrochemical Techniques as Tools for Investigating the Properties of Electroactive Systems. *Disp. Imaging* **2**, 229–248 (2016).

74. Zhai, Y., Zhu, Z., Zhou, S., Zhu, C. & Dong, S. Recent advances in

spectroelectrochemistry. *Nanoscale* **10**, 3089–3111 (2018).

75. Chen, K. C., Hsu, C. Y., Hu, C. W. & Ho, K. C. A complementary electrochromic device based on Prussian blue and poly(ProDOT-Et2) with high contrast and high coloration efficiency. *Sol. Energy Mater. Sol. Cells* **95**, 2238–2245 (2011).

76. Krishnamoorthy, K., Ambade, A. V., Kanungo, M., Contractor, A. Q. & Kumar, A. Rational design of an electrochromic polymer with high contrast in the visible region: Dibenzyl substituted poly(3,4-propylenedioxythiophene). *J. Mater. Chem.* **11**, 2909–2911 (2001).

77. Lakshmanan, R., Raja, P. P., Shivaprakash, N. C. & Nair, S. S. Specroelectrochemical, switching kinetics, and chronoamperometric studies of dibenzyl derivative of poly(3,4-propylenedioxythiophene) thin-film-based electrochromic device. *J. Appl. Polym. Sci.* **131**, 40717 (2014).

78. Özkut, M. I., Atak, S., Önal, A. M. & Cihaner, A. A blue to highly transmissive soluble electrochromic polymer based on poly(3,4-propylenedioxyselenophene) with a high stability and coloration efficiency. *J. Mater. Chem.* **21**, 5268–5272 (2011).

79. Beaujuge, P. M. & Reynolds, J. R. Color control in π-conjugated organic polymers for use in electrochromic devices. *Chem. Rev.* **110**, 268–320 (2010).

80. Argun, A. A. *et al.* Multicolored electrochromisin in polymers: Structures and devices. *Chem. Mater.* **16**, 4401–4412 (2004).

81. Amb, C. M., Dyer, A. L. & Reynolds, J. R. Navigating the color palette of solution-processable electrochromic polymers. *Chem. Mater.* **23**, 397–415 (2011).

82. Algar, W. R., Jong, C. A. G. De, Maxwell, E. J. & Atkins, C. G. Demonstration of the Spectrophotometric Complementary Color Wheel Using LEDs and Indicator Dyes. *J. Chem. Educ.* **93**, 162–165 (2016).

83. Dyer, A. L., Thompson, E. J. & Reynolds, J. R. Completing the color palette with spray-processable polymer electrochromics. *ACS Appl. Mater. Interfaces* **3**, 1787–1795 (2011).

84. Ohta, N. & Robertson, A. R. *Colorimetry: Fundamentals and Applications*. (John Wiley & Sons Inc., 2005).

85. *Introduction to organic electronic and optoelectronic materials and devices: Second edition*. (CRC Press, 2016).

86. Bard, A. & Faulkner, L. *Electrochemical Methods: fundamentals and applications*. (John Wiley & Sons Inc., 2000).

87. Fereja, T. H., Hymete, A. & Gunasekaran, T. A Recent Review on

Chemiluminescence Reaction, Principle and Application on Pharmaceutical Analysis. *ISRN Spectrosc. Int. Sch. Res. Not.* **2013**, 1–12 (2013).

88. García-Campaña, A. M. & Baeyens, W. R. G. Principles and recent analytical applications of chemiluminescence. *Analusis* **28**, 686–698 (2000).

89. Elbanowski, M., Staniński, K. & Kaczmarek, M. Chemiluminescence Used in Biochemical Investigations. An Application of the Lanthanide Ions as a Chemiluminescent Probe. *Acta Phys. Pol. A* **84**, 993–1002 (1993).

90. *Chemiluminescence and Bioluminescence: Past, Present and Future*. (Royal Society of Chemistry, 2010).

91. Baeyens, W. R. G. *et al.* Chemiluminescence-based detection: Principles and analytical applications in flowing streams and in immunoassays. *J. Pharm. Biomed. Anal.* **17**, 941–953 (1998).

92. Xu, G., Zhang, J. & Dong, S. Chemiluminescent determination of glucose with a modified carbon paste electrode. *Microchem. J.* **62**, 259–265 (1999).

93. Yuan, J. & Shiller, A. M. Determination of subnanomolar levels of hydrogen peroxide in seawater by reagent-injection chemiluminescence detection. *Anal. Chem.* **71**, 1975–1980 (1999).

94. Sakura, S. Electrochemiluminescence of hydrogen peroxide-luminol at a carbon electrode. *Anal. Chim. Acta* **262**, 49–57 (1992).

95. Stuart H. James, Paul E. Kish, T. P. S. Introduction to Bloodstain Pattern Analysis: Theory and Practice. in *Principles of Bloodstain Pattern Analysis* (CRC Press, 2005).

96. Brundrett, R. B. & White, E. H. Synthesis and Chemiluminescence of Derivatives of Luminol and Isoluminol. *J. Am. Chem. Soc.* **96**, 7497–7502 (1974).

97. Albrecht, H. O. Über die Chemiluminescenz des Aminophthalsäurehydrazids. *Zeitschrift für Phys. Chemie* **136U**, 321–330 (1928).

98. Rauhut, M. M., Semsel, A. M. & Roberts, B. G. Reaction Rates, Quantum Yields, and Partial Mechanism for the Chemiluminescent Reaction of 3-Aminophthalhydrazide with Aqueous Alkaline Hydrogen Peroxide and Persulfate. *J. Org. Chem.* **31**, 2431–2436 (1966).

99. Barni, F., Lewis, S. W., Berti, A., Miskelly, G. M. & Lago, G. Forensic application of the luminol reaction as a presumptive test for latent blood detection. *Talanta* **72**, 896–913 (2007).

100. Smith, Z. M., Adcock, J. L., Barnett, N. W. & Francis, P. S. Chemiluminescence | liquid-phase. in *Encyclopedia of Analytical Science* (Oxford Academic Press, 2019).

101. Gundermann, K., Horstmann, W. & Bergmann, G. Konstitution und Chemilumineszenz, II. Synthese und Chemilumineszenz-Verhalten von 7-Dialkylamino-naphthalindicarbonsäure-(1.2)-hydraziden. *Liebig's Ann Chem* **684**, 127–141 (1965).

102. Wei, C. C. & White, E. H. An efficient chemiluminescent hydrazide: benzo(ghi)perylene-1,2-dicarboxylic acid hydrazide. *Tetrahedron Lett.* **12**, 3559–3562 (1971).

103. Panoutsou, P. & Economou, A. Rapid enzymatic chemiluminescent assay of glucose by means of a hybrid flow-injection/sequential-injection method. *Talanta* **67**, 603–609 (2005).

104. Li, B., Zhang, Z. & Jin, Y. Plant tissue-based chemiluminescence flow biosensor for determination of unbound dopamine in rabbit blood with on-line microdialysis sampling. *Biosens. Bioelectron.* **17**, 585–589 (2002).

105. Zhao, S., Yuan, H., Xie, C. & Xiao, D. Determination of folic acid by capillary electrophoresis with chemiluminescence detection. *J. Chromatogr. A* **1107**, 290–293 (2006).

106. Navas, M. J. & Jiménez, A. M. Review of chemiluminescent methods in food analysis. *Food Chem.* **55**, 7–15 (1996).

107. Sigsby, J. E., Black, F. M., Bollar, T. A. & Klosterman, D. L. Chemiluminescent method for analysis of nitrogen compounds in mobile source emissions nitric oxide, nitrogen dioxide, and ammonia. *Environ. Sci. Technol.* **7**, 51–54 (1973).

108. Kushwaha, N. & Kaushik, D. Recent advances and future prospects of phthalimide derivatives. *J. Appl. Pharm. Sci.* **6**, 159–171 (2016).

109. Lee, J. Y., Song, K. W., Ku, J. R., Sung, T. H. & Moon, D. K. Development of DA-type polymers with phthalimide derivatives as electron withdrawing units and a promising strategy for the enhancement of photovoltaic properties. *Sol. Energy Mater. Sol. Cells* **95**, 3377–3384 (2011).

110. Chen, D. *et al.* Effect of polymer chain conformation on field-effect transistor performance: Synthesis and properties of two arylene imide based D-A copolymers. *J. Mater. Chem.* **22**, 14639–14644 (2012).

111. Pérez-Mayoral, E., Calvino-Casilda, V., Godino, M., López-Peinado, A. J. & Martín-Aranda, R. M. Porous Catalytic Systems in the Synthesis of Bioactive Heterocycles and Related Compounds. in *Green Synthetic Approaches for Biologically Relevant Heterocycles* 377–408 (Elsevier Inc., 2015).

112. Liu, F., Zhang, Y., Wang, H. & Zhang, S. Novel conjugated polymers prepared by direct (hetero) arylation: An eco-friendly tool for organic electronics. *Molecules* **23**, 408 (2018).

113. Joule, J. A. *Heterocyclic Chemistry in the 21st Century - A Tribute to Alan Katritzky*. *Advances in Heterocyclic Chemistry* vol. 119 (2016).

114. Geng, S. Z. *et al.* Non-fullerene Acceptors with a Thieno[3,4-c]pyrrole-4,6-dione (TPD) Core for Efficient Organic Solar Cells. *Chinese J. Polym. Sci.* **37**, 1005–1014 (2019).

115. Guo, X. *et al.* Bithiopheneimide-dithienosilole/dithienogermole copolymers for efficient solar cells: Information from structure-property-device performance correlations and comparison to thieno[3,4- c]pyrrole-4,6-dione analogues. *J. Am. Chem. Soc.* **134**, 18427–18439 (2012).

116. Berrouard, P., Dufresne, S., Pron, A., Veilleux, J. & Leclerc, M. Low-cost synthesis and physical characterization of thieno[3,4-c]pyrrole-4, 6-dione-based polymers. *J. Org. Chem.* **77**, 8167–8173 (2012).

117. Ghahremani, M., Davarpanah, J., Rezaee, P. & Davoodi, G. Synthesis of phthalazine compounds using heterogeneous base catalyst based on silica nanoparticles obtained from rice husk. *Res. Chem. Intermed.* **46**, 2683–2704 (2020).

118. Makarem, S., Fakhari, A. R. & Mohammadi, A. A. Electro-organic synthesis: An efficient method for the preparation of nanosized particles of phthalazine derivatives via one-pot multicomponent reactions. *Anal. Bioanal. Chem. Res.* **2**, 85–89 (2015).

119. Kealy, T. J. The chemistry of diazaquinones. 3,6-pyridazinedione and 1,4-phthalazinedione. **84**, 966–973 (1962).

120. Vaughan, W. R. The Chemistry of the Phthalazines. *Chem. Rev.* **43**, 447–508 (1948).

121. Tominaga, Y., Sasaki, K. & Castle, R. N. Synthesis of polycyclic pyridazinediones as chemiluminescent compounds. *J. Heterocycl. Chem.* **35**, 1219–1234 (1998).

122. Atılgan, N., Algı, F., Önal, A. M. & Cihaner, A. Synthesis and properties of a novel redox driven chemiluminescent material built on a terthienyl system. *Tetrahedron* **65**, 5776–5781 (2009).

123. Asil, D., Cihaner, A. & Önal, A. M. Electropolymerization and ion sensitivity of chemiluminescent thienyl systems. *Electrochim. Acta* **54**, 6740–6746 (2009).

124. Zhou, H., Ye, Q. & Xu, J. Polyhedral oligomeric silsesquioxane-based hybrid materials and their applications. *Mater. Chem. Front.* **1**, 212–230 (2017).

125. Gnanasekaran, D., Madhavpan, K. & Reddy, R. S. R. Developments of polyhedral oligomeric silsesquioxanes (POSS), POSS nanocomposites and

their applications: A review. *J. Sci. Ind. Res. (India).* **68**, 437–464 (2009).

126. Kuo, S. W. & Chang, F. C. POSS related polymer nanocomposites. *Prog. Polym. Sci.* **36**, 1649–1696 (2011).

127. Zhang, W. & Müller, A. H. E. Architecture, self-assembly and properties of well-defined hybrid polymers based on polyhedral oligomeric silsequioxane (POSS). *Prog. Polym. Sci.* **38**, 1121–1162 (2013).

128. Bandara, H. M. D. & Burdette, S. C. Photoisomerization in different classes of azobenzene. *Chem. Soc. Rev.* **41**, 1809–1825 (2012).

129. Merino, E. & Ribagorda, M. Control over molecular motion using the cis-trans photoisomerization of the azo group. *Beilstein J. Org. Chem.* **8**, 1071–1090 (2012).

130. Yager, K. G. & Barrett, C. J. Azobenzene Polymers as Photomechanical and Multifunctional Smart Materials. in *Intelligent Materials* 424–446 (Royal Society of Chemistry, 2008).

131. Beharry, A. A. & Woolley, G. A. Azobenzene photoswitches for biomolecules. *Chem. Soc. Rev.* **40**, 4422–4437 (2011).

132. Shaya, J. Fluorene-based fluorescent markers : new insights in synthesis and applications into labeling of nucleic acids and imaging of cell membranes. (Nice-Sophia Antipolis University, 2016).

133. Abbel, R., Schenning, A. P. H. J. & Meijer, E. W. Fluorene-based materials and their supramolecular properties. *J. Polym. Sci. Part A Polym. Chem.* **47**, 4215–4233 (2009).

134. Inaoka, S. & Advincula, R. Synthesis and oxidative cross-linking of fluorene-containing polymers to form conjugated network polyfluorenes: Poly(fluoren-9,9-diyl-alt-alkan-α,ω-diyl). *Macromolecules* **35**, 2426–2428 (2002).

135. Çakal, D., Ertan, S., Cihaner, A. & Önal, A. M. Electrochemical and optical properties of substituted phthalimide based monomers and electrochemical polymerization of 3,4-ethylenedioxythiophene-polyhedral oligomeric silsesquioxane (POSS) analogue. *Dye. Pigment.* **161**, 411–418 (2019).

136. Lee, J. Y., Lee, S. M., Song, K. W. & Moon, D. K. Synthesis and photovoltaic property of polymer semiconductor with phthalimide derivative as a promising electron withdrawing material. *Eur. Polym. J.* **48**, 532–540 (2012).

137. Guo, X., Kim, F. S., Jenekhe, S. A. & Watson, M. D. Phthalimide-Based Polymers for High Performance Organic Thin-Film Transistors. *J. Am. Chem. Soc.* **131**, 7206–7207 (2009).

138. Griffi, G. *et al.* Long-Term Thermal Stability of High-Efficiency Polymer

Solar Cells Based on Photocrosslinkable Donor-Acceptor Conjugated Polymers. *Adv. Mater.* **23**, 1660–1664 (2011).

139. Cornelis, D. *et al.* A Chiroptical Study of Chiral Λ- and X- Type Oligothiophenes Toward Modelling the Interchain Interactions of Chiral Conjugated Polymers. *Chem. Mater.* **20**, 2133–2143 (2008).

140. Degirmenci, A. & Algi, F. Synthesis, chemiluminescence and energy transfer efficiency of 2,3-dihydrophthalazine-1,4-dione and BODIPY dyad. *Dye. Pigment.* **140**, 92–99 (2017).

141. Zhang, Z. G. & Wang, J. Structures and properties of conjugated Donor–Acceptor copolymers for solar cell applications. *J. Mater. Chem.* **22**, 4178–4187 (2012).

142. Yasutani, Y., Honsho, Y., Saeki, A. & Seki, S. Polycarbazoles: Relationship between intra- and intermolecular charge carrier transports. *Synth. Met.* **162**, 1713–1721 (2012).

143. Zhao, H. *et al.* Structure and electronic properties of triphenylamine-substituted indolo[3,2-b]carbazole derivatives as hole-transporting materials for organic light-emitting diodes. *Chem. Phys. Lett.* **439**, 132–137 (2007).

144. Pamuk, M., Algi, F., Onal, A. M. & Cihaner, A. Donor-Acceptor Polymer Electrochromes with Tunable Colors and Performance. *Chem. Mater.* **22**, 4034–4044 (2010).

145. Ha, J. *et al.* Thieno[3,4-c]pyrrole-4,6-dione-Based Small Molecules for Highly Efficient Solution-Processed Organic Solar Cells. *Chem. An Asian J.* **6**, 1045–1053 (2014).

146. Wang, E. *et al.* Donor Polymers Containing Benzothiadiazole and Four Thiophene Rings in Their Repeating Units with Improved Photovoltaic Performance. *Macromolecules* **42**, 4410–4415 (2009).

147. İçli- Özkut, M., İpek, H., Karabay, B., Cihaner, A. & Önal, A. M. Furan and benzochalcogenodiazole based multichromic polymers via a donor–acceptor approach. *Polym. Chem.* **4**, 2457–2463 (2013).

148. Thompson, M., Davis, J. & Compton, R. G. Theory of cyclic voltammetry in tubular electrodes under no flow conditions. *J. Electroanal. Chem.* **587**, 56–59 (2006).

149. Lane, R. F. & Hubbard, A. T. Electrochemistry of Chemisorbed Molecules. *Electrochem. Chemisorbed Mol.* **77**, 1401–1410 (1973).

150. Laviron, E. Theoretical Study of a Reversible Reaction Followed by a Chemical Reaction in Thin Layer Linear Potential Sweep Voltammetry. *Electroanal. Chem. Interfacial Electrochem.* **39**, 1–23 (1972).

151. Li, M., Patra, A., Sheynin, Y. & Bendikov, M. Hexyl-Derivatized Poly(3,4-

ethylenedioxyselenophene): Novel Highly Stable Organic Electrochromic Material with High Contrast Ratio, High Coloration Efficiency, and Low-Switching Voltage. *Adv. Mater.* **21**, 1707–1711 (2009).

152. Roncali, J. Synthetic Principles for Bandgap Control in Linear π-Conjugated Systems. *Chem. Rev.* **97**, 173–205 (1997).

153. Magdaline, J. D. & Chithambarathanu, T. Vibrational Spectra (FT-IR, FT-Raman), NBO and HOMO, LUMO Studies of 2-Thiophene Carboxylic Acid Based on Density Functional Method. *IOSR J. Appl. Chem.* **8**, 6–14 (2015).

154. Koren, A. B., Curtis, M. D., Francis, A. H. & Kampf, J. W. Intermolecular Interactions in π-Stacked Conjugated Molecules. Synthesis, Structure, and Spectral Characterization of Alkyl Bithiazole Oligomers. *J. Am. Chem. Soc.* **125**, 5040–5050 (2003).

155. Yuan, M., Chiu, M., Liu, S., Chen, C.-M. & Wei, K.-H. A Thieno[3,4-c]pyrrole-4,6-dione-Based Donor-Acceptor Polymer Exhibiting High Crystallinity for Photovoltaic Applications. *Macromolecules* **43**, 6936–6938 (2010).

156. García-Amorós, J. & Velasco, D. Recent advances towards azobenzene-based light- driven real-time information-transmitting materials. *Beilstein J. Org. Chem.* **8**, 1003–1017 (2012).

157. Griggs, S., Marks, A., Bristow, H. & Mcculloch, I. n-Type organic semiconducting polymers: stability limitations, design considerations and applications. *J. Mater. Chem. C* **9**, 8099–8128 (2021).

158. Lu, Y., Wang, J. & Pei, J. Achieving Efficient n-Doping of Conjugated Polymers by Molecular Dopants. *Acc. Chem. Res.* **54**, 2871−2883 (2021).

159. Liu, M. *et al.* Synthesis of Discrete Conjugated Fluorene-Azo Oligomers for the Investigation of Azobenzene Position-Dependent Physical Properties and Photoresponsive Behavior. *Macromol. Chem. Phys.* **222**, 2100092(1–9) (2021).

160. Correia, F. C., Santos, T. C. F., Garcia, J. R., Peres, L. O. & Wang, S. H. Synthesis and Characterization of a New Semiconductor Oligomer Having Quinoline and Fluorene Units. *J. Brazil Chem. Soc.* **26**, 84–91 (2015).

161. García-Campaña, A. M. Baeyens, W. R. G. *Chemiluminescence in Analytical Chemistry*. (Marcel Dekker, Inc., 2001).

APPENDICES

A. NMR Spectra of Monomers and Polymers

NMR was recorded by Bruker Spectrospin Avance DPX-400 Spectrometer. TMS was used as internal reference.

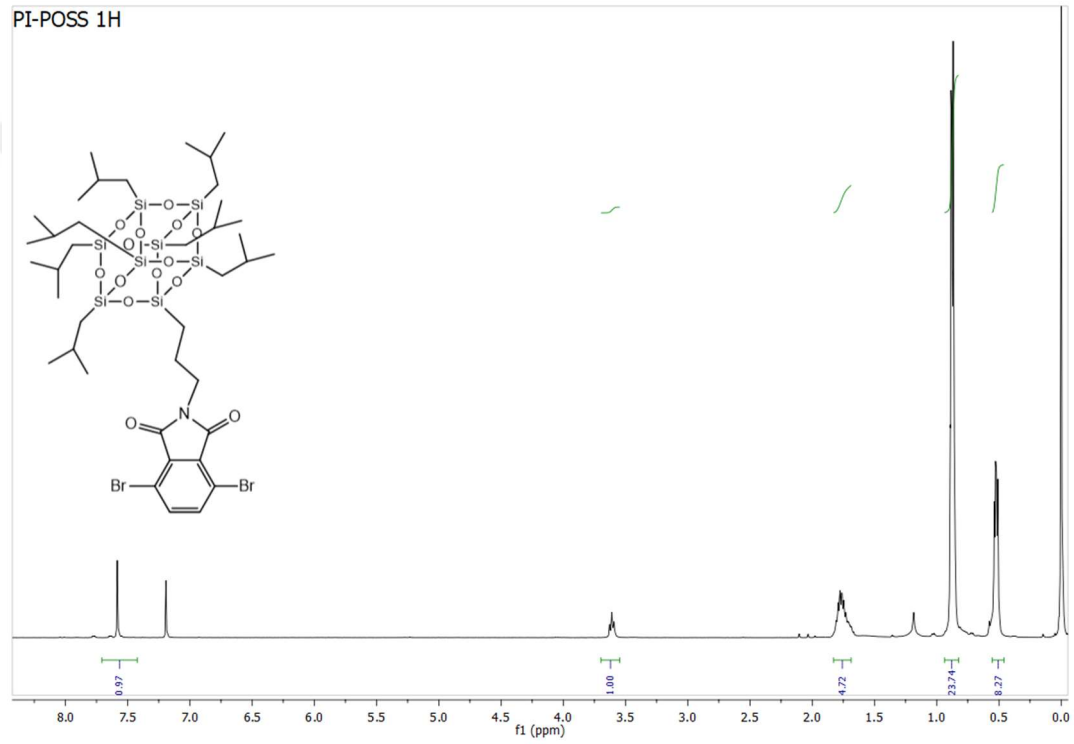

Figure A.1. ^{1}H NMR spectrum of PI-POSS in $CDCl_3$.

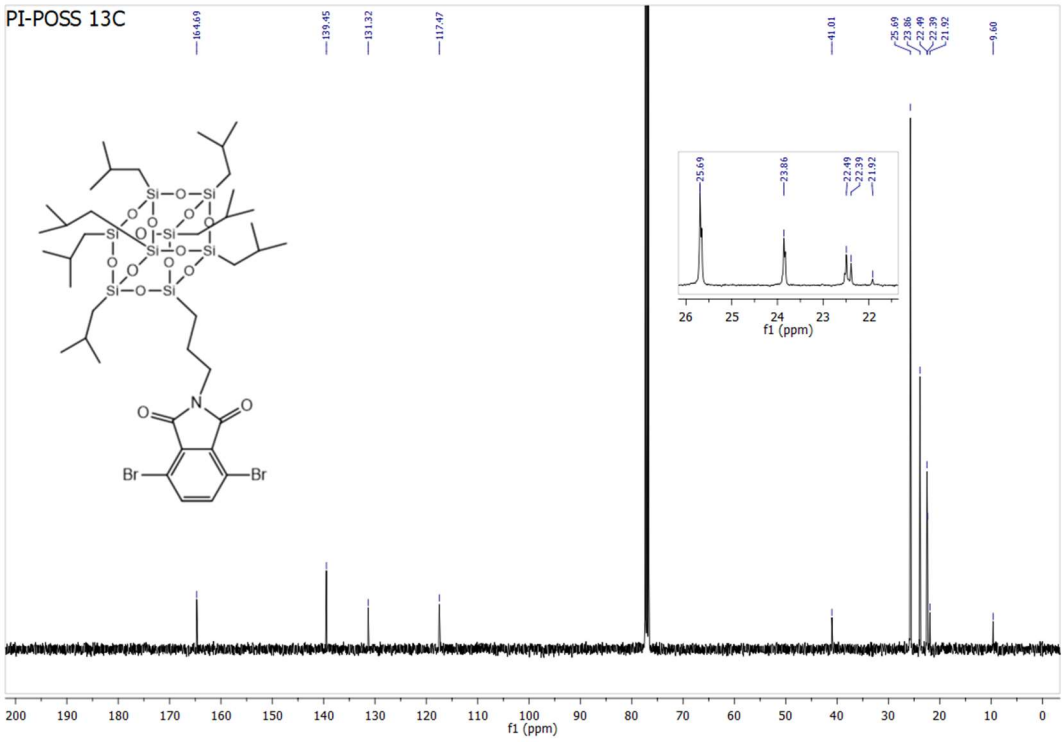

Figure A.2. ^{13}C NMR spectrum of PI-POSS in $CDCl_3$.

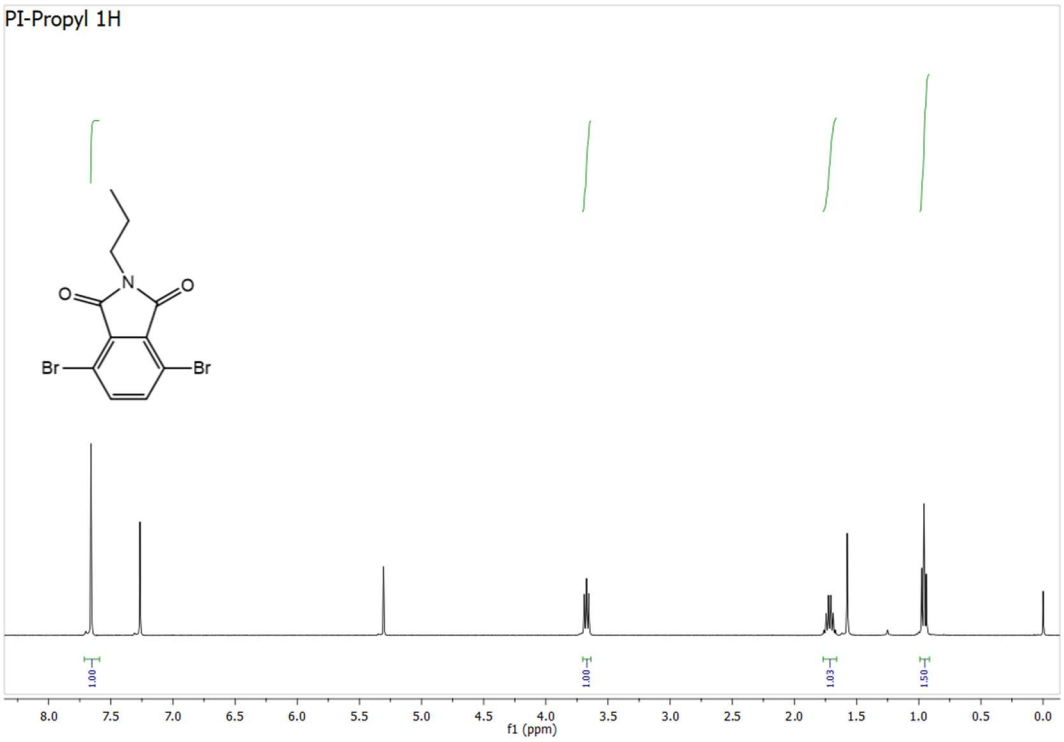

Figure A.3. ^{1}H NMR spectrum of PI-Pro in $CDCl_3$.

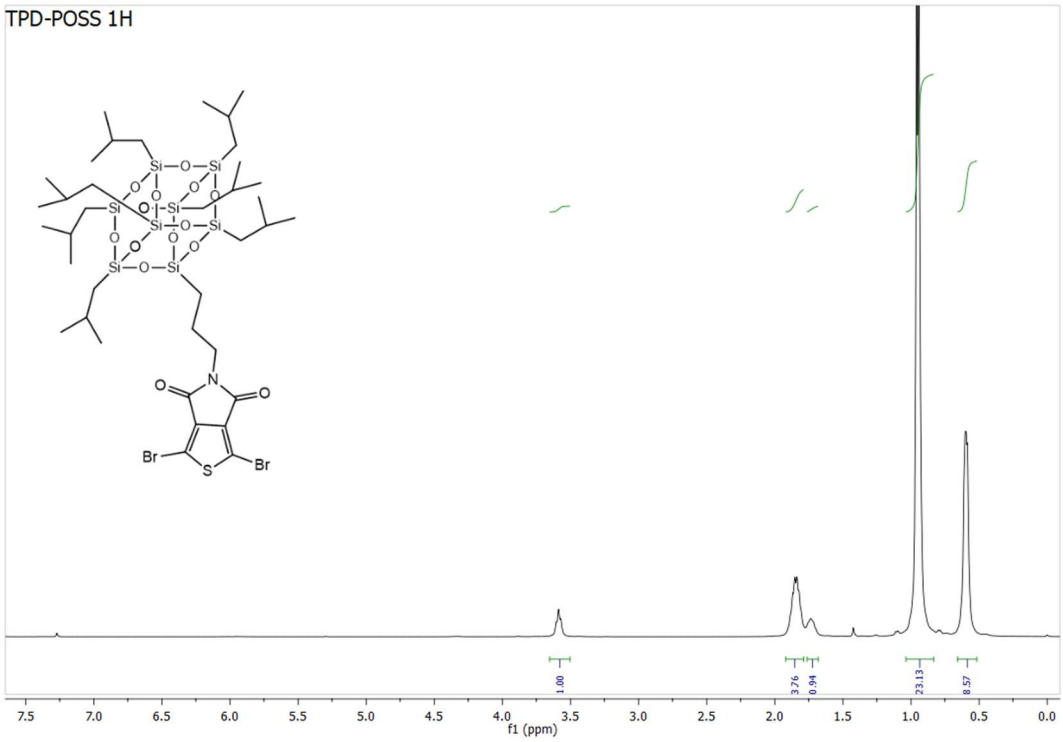

Figure A.4. ^{1}H NMR spectrum of TPD-POSS in $CDCl_3$.

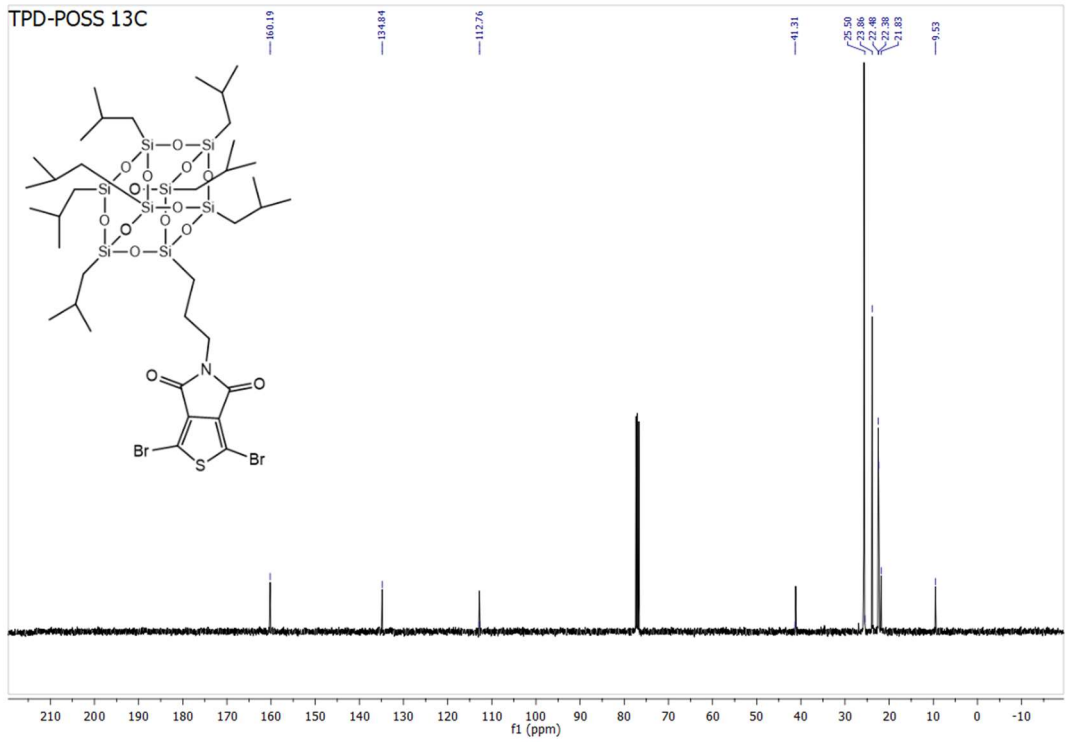

Figure A.5. ^{13}C NMR spectrum of TPD-POSS in $CDCl_3$.

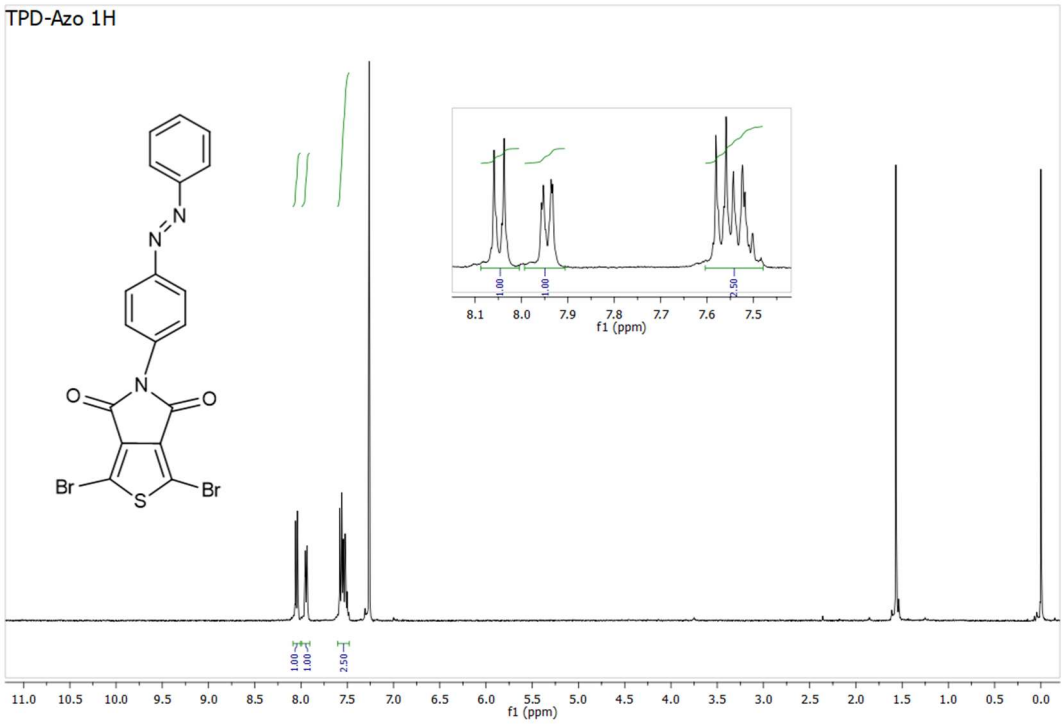

Figure A.6. ^{1}H NMR spectrum of TPD-Azo in $CDCl_3$.

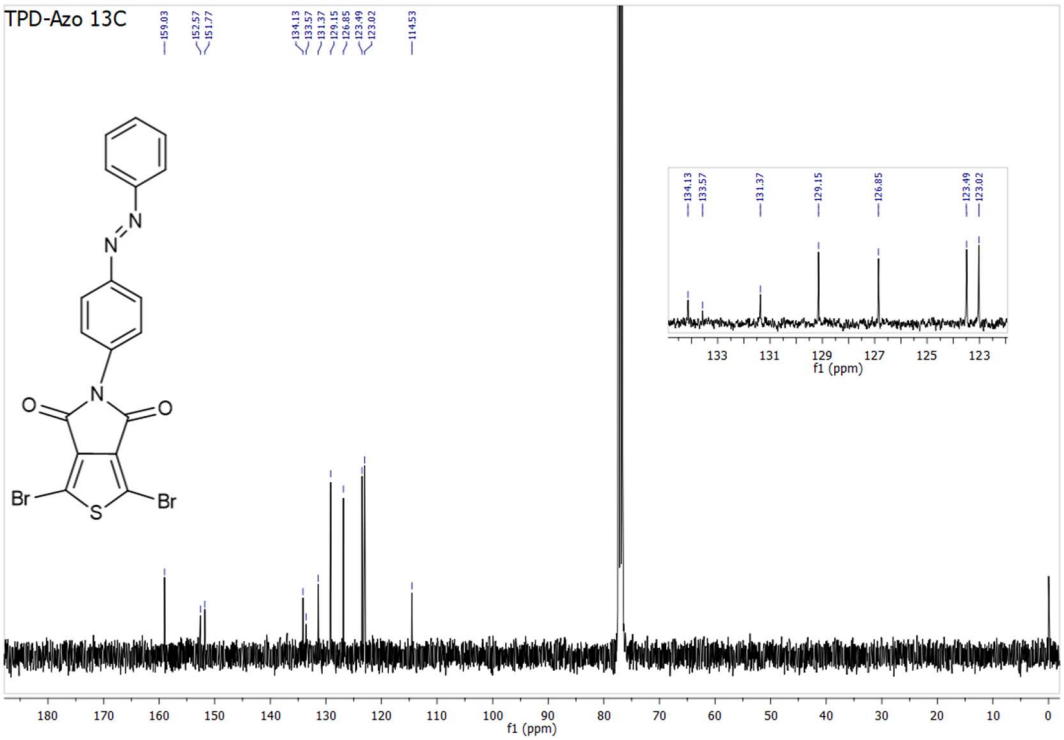

Figure A.7. ^{13}C NMR spectrum of TPD-Azo in $CDCl_3$.

1

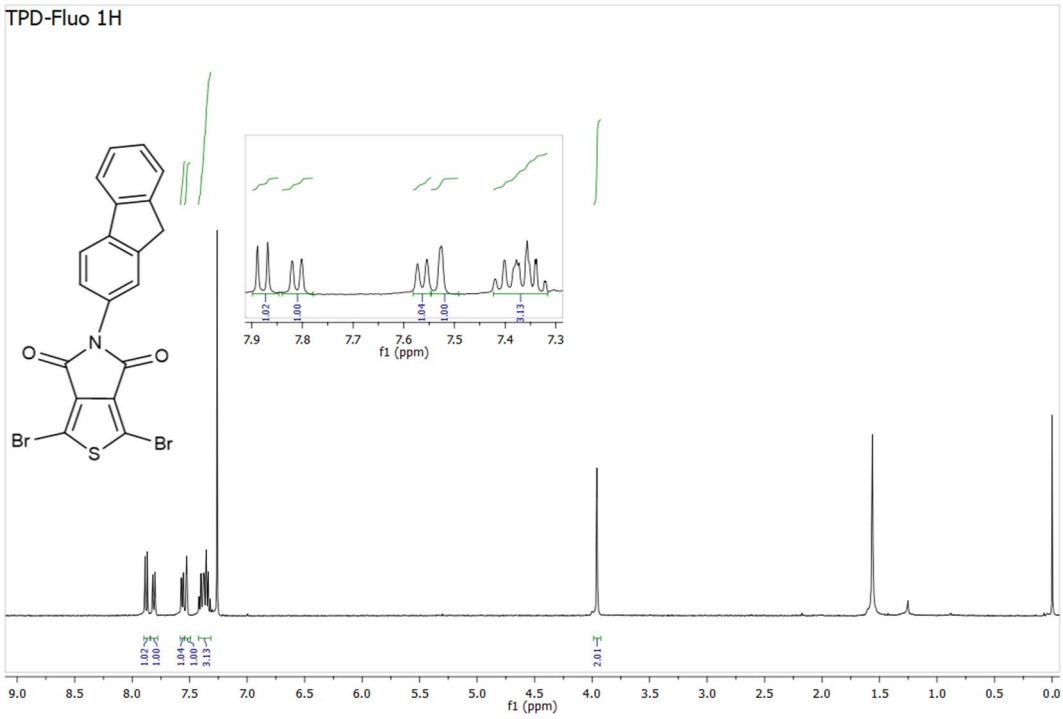

Figure A.8. ^{1}H NMR spectrum of TPD-Fluo in $CDCl_3$.

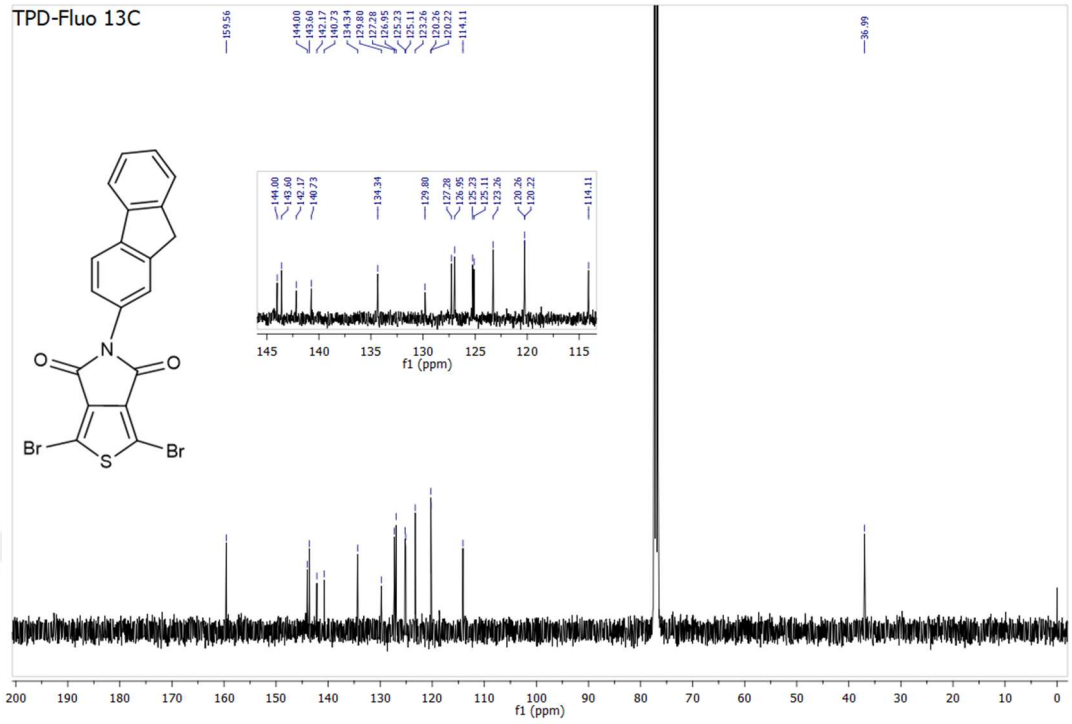

Figure A.9. ^{13}C NMR spectrum of TPD-Fluo in $CDCl_3$.

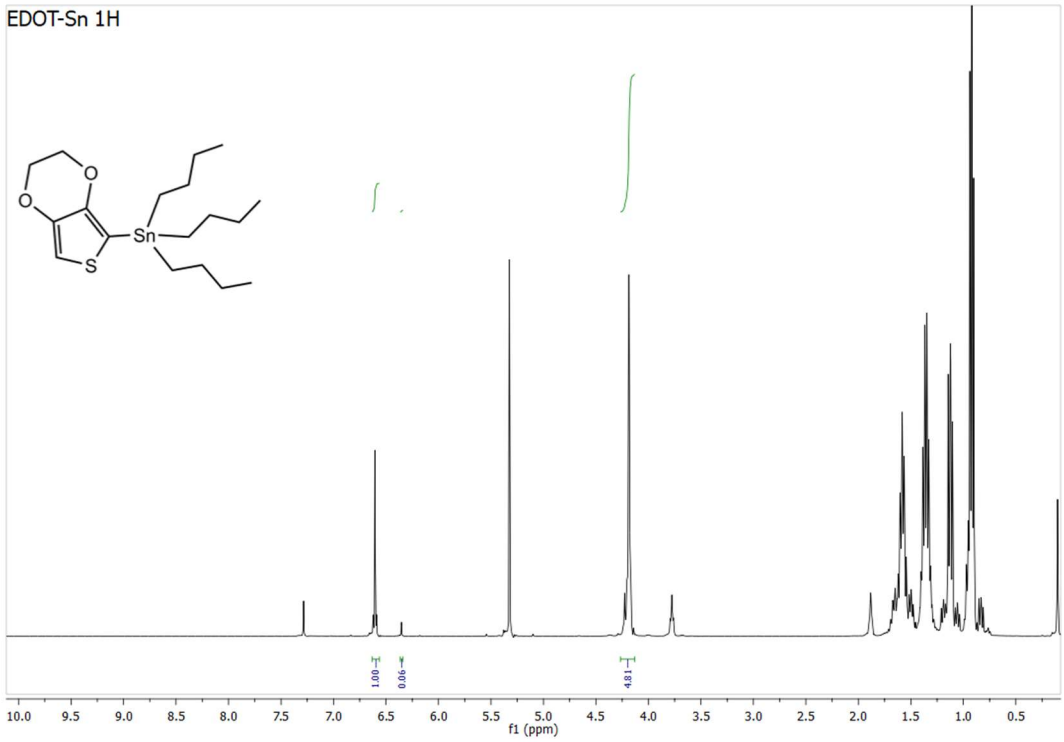

Figure A.10. ^{1}H NMR spectrum of EDOT-Sn in $CDCl_3$.

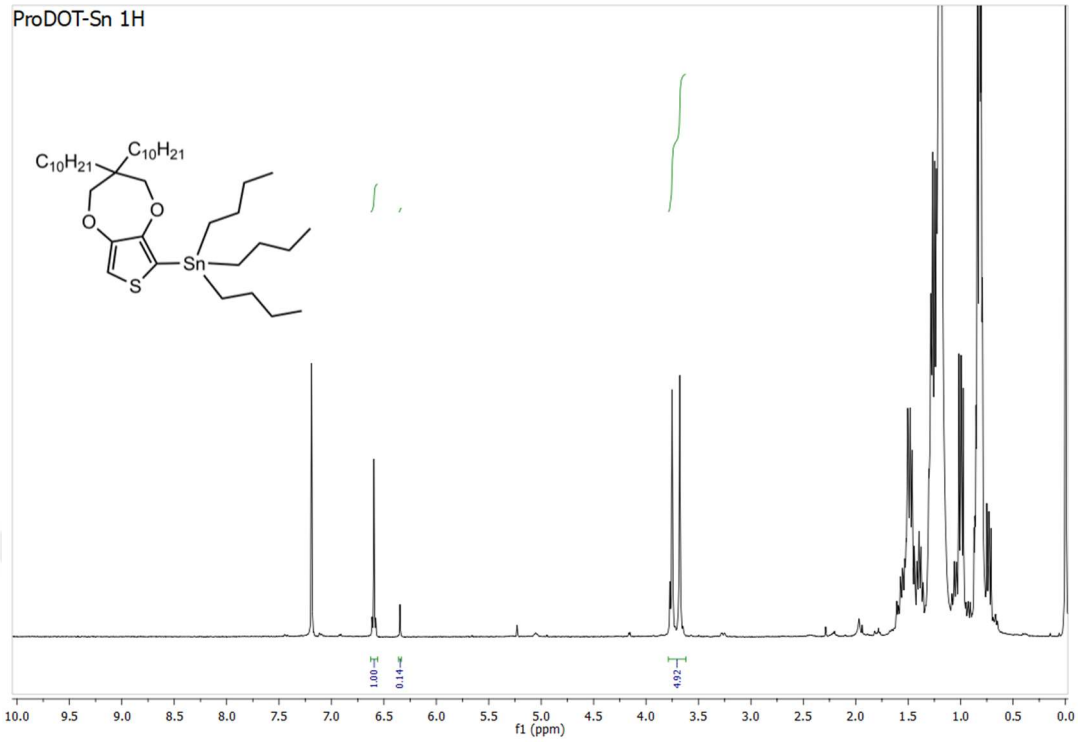

Figure A.11. ^{1}H NMR spectrum of ProDOT-Sn in $CDCl_3$.

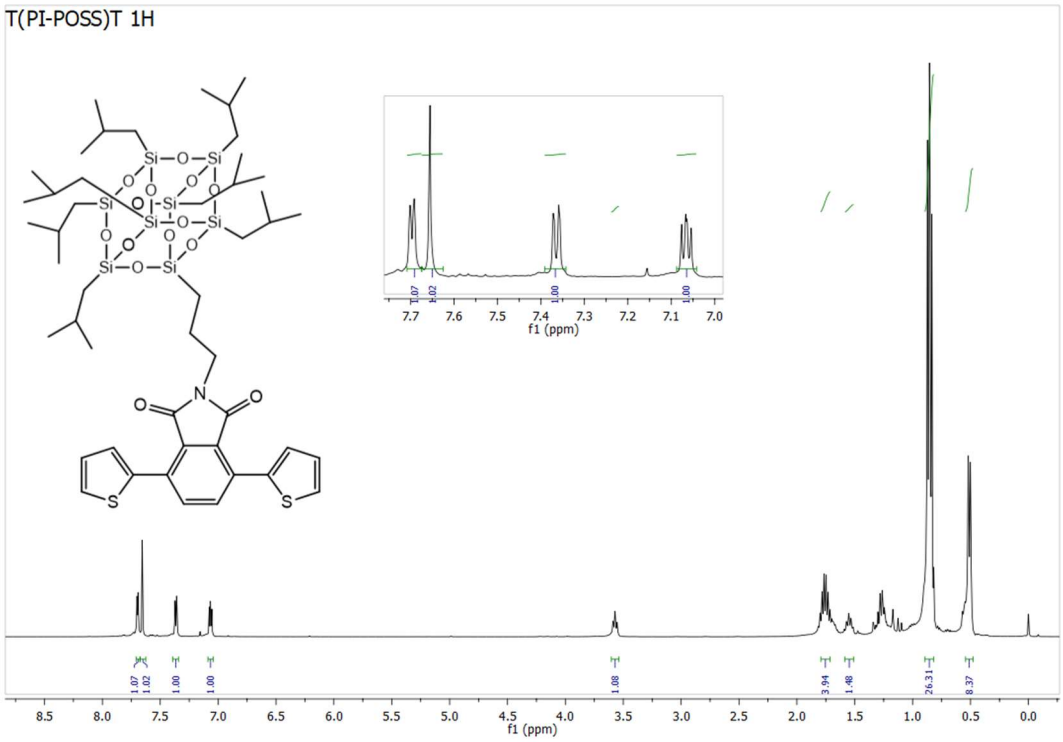

Figure A.12. ^{1}H NMR spectrum of T(PI-POSS)T in $CDCl_3$.

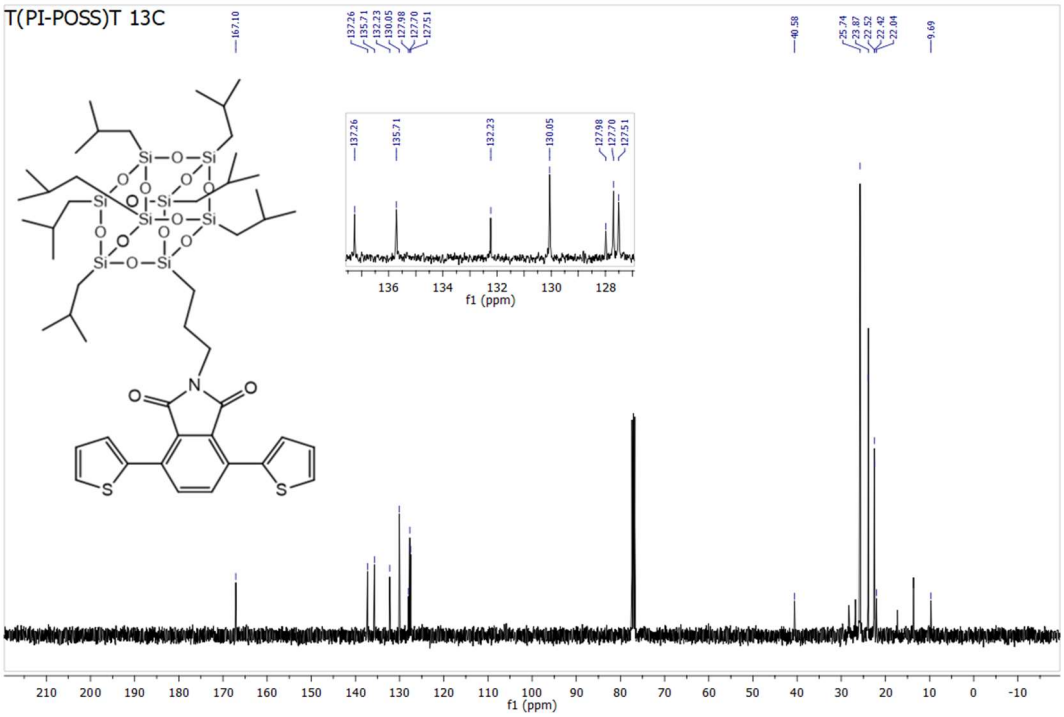

Figure A.13. ^{13}C NMR spectrum of T(PI-POSS)T in $CDCl_3$.

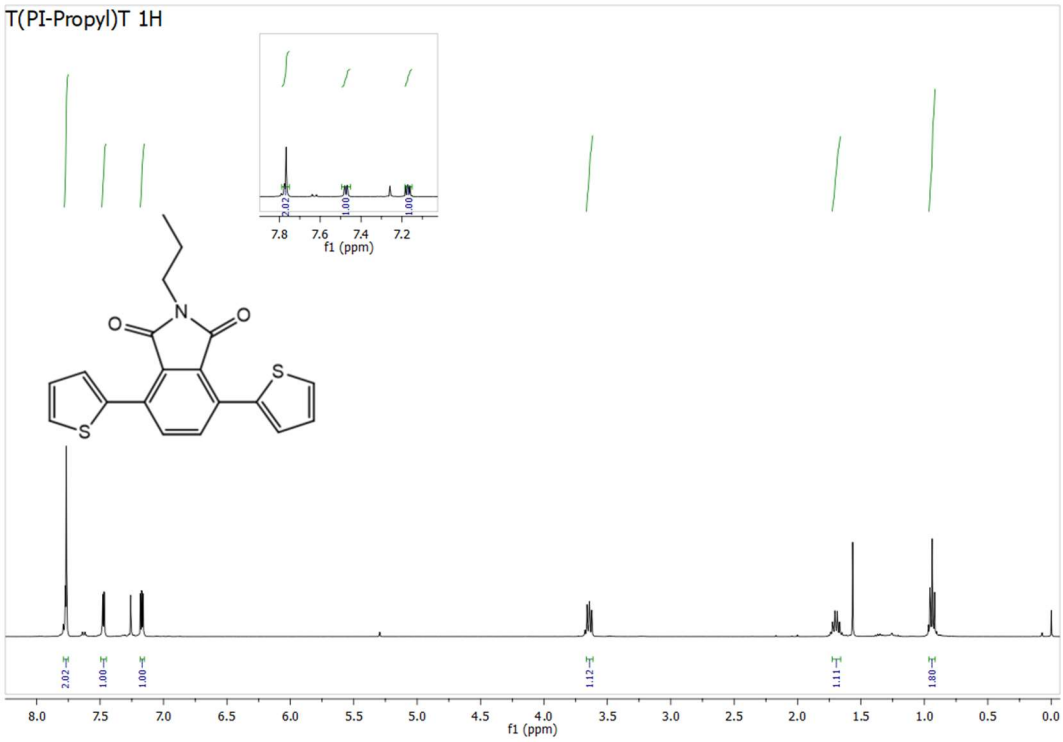

Figure A.14. ^{1}H NMR spectrum of T(PI-Propyl)T in $CDCl_3$.

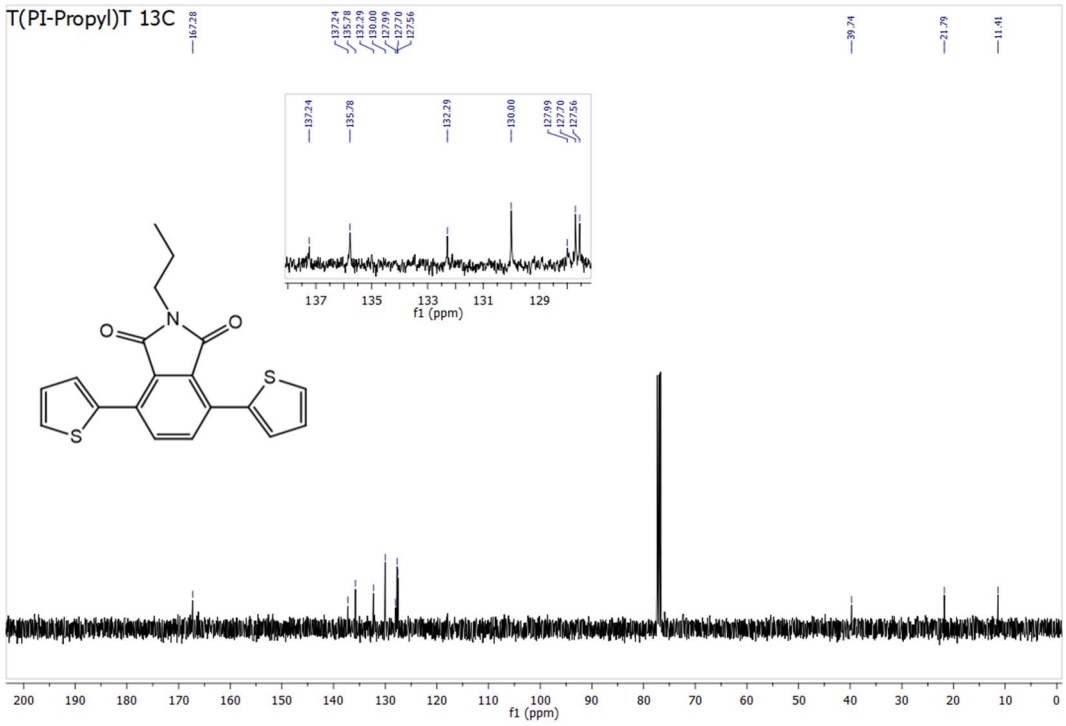

Figure A.15. ^{13}C NMR spectrum of T(PI-Propyl)T in $CDCl_3$.

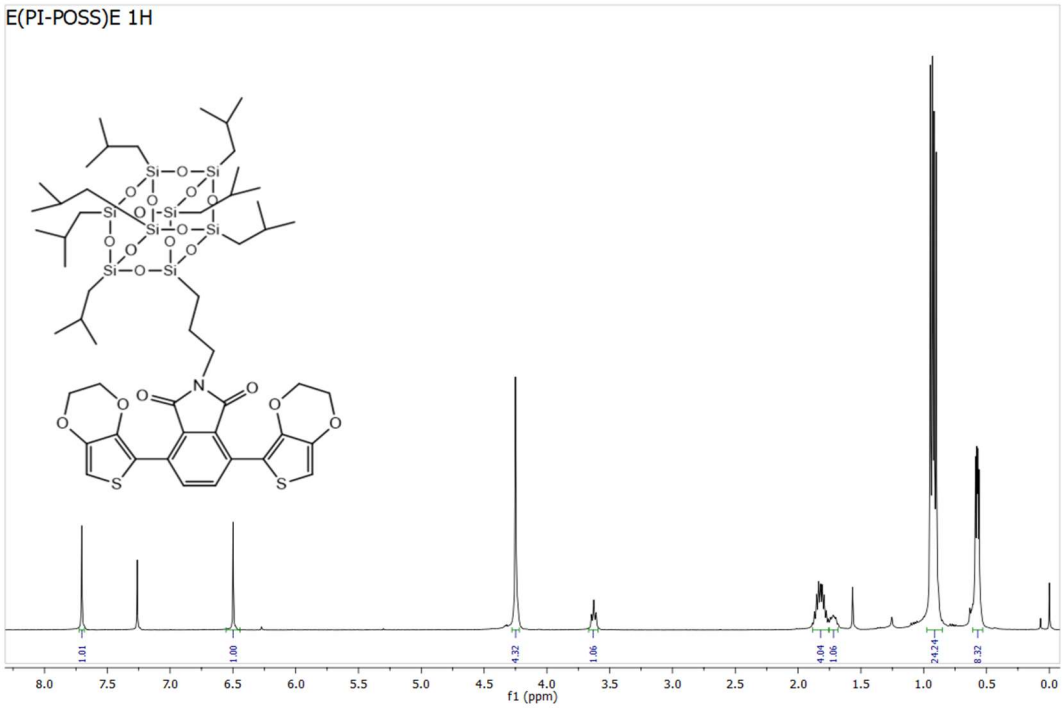

Figure A.16. ^{1}H NMR spectrum of E(PI-POSS)E in $CDCl_3$.

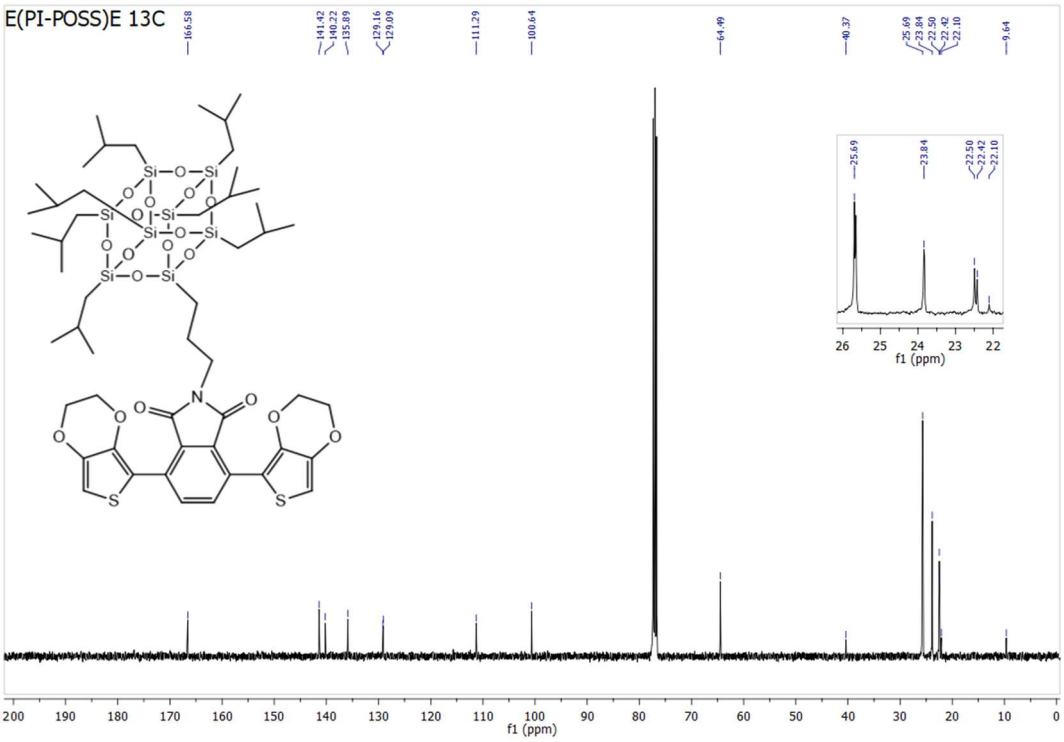

Figure A.17. ^{13}C NMR spectrum of E(PI-POSS)E in $CDCl_3$.

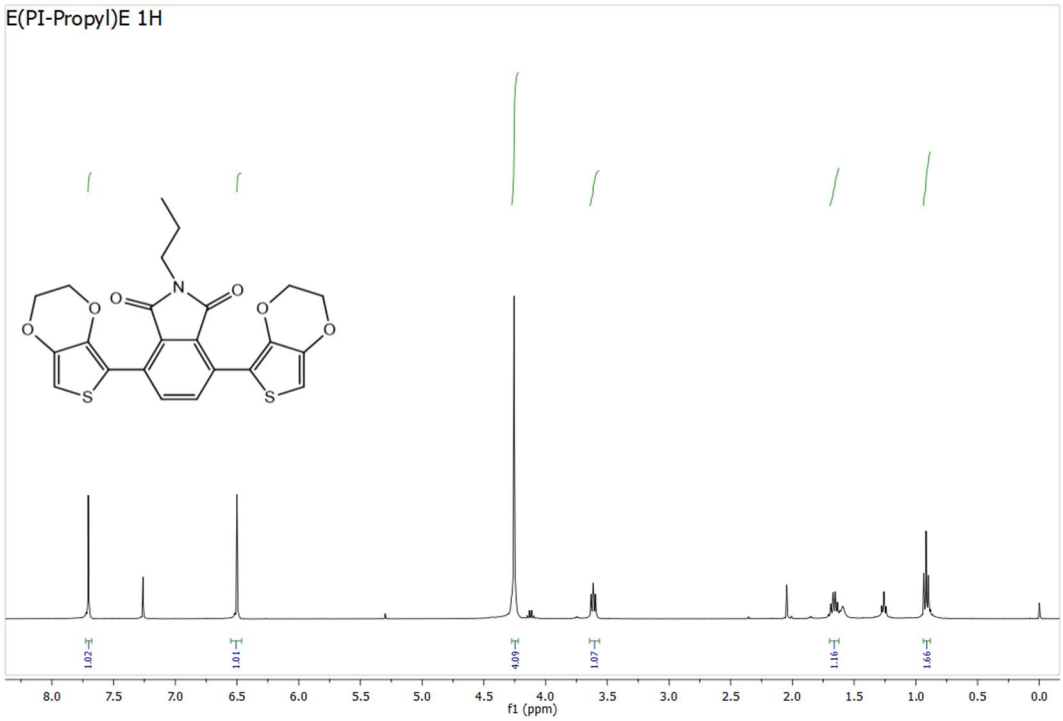

Figure A.18. ^{1}H NMR spectrum of E(PI-Propyl)E in $CDCl_3$.

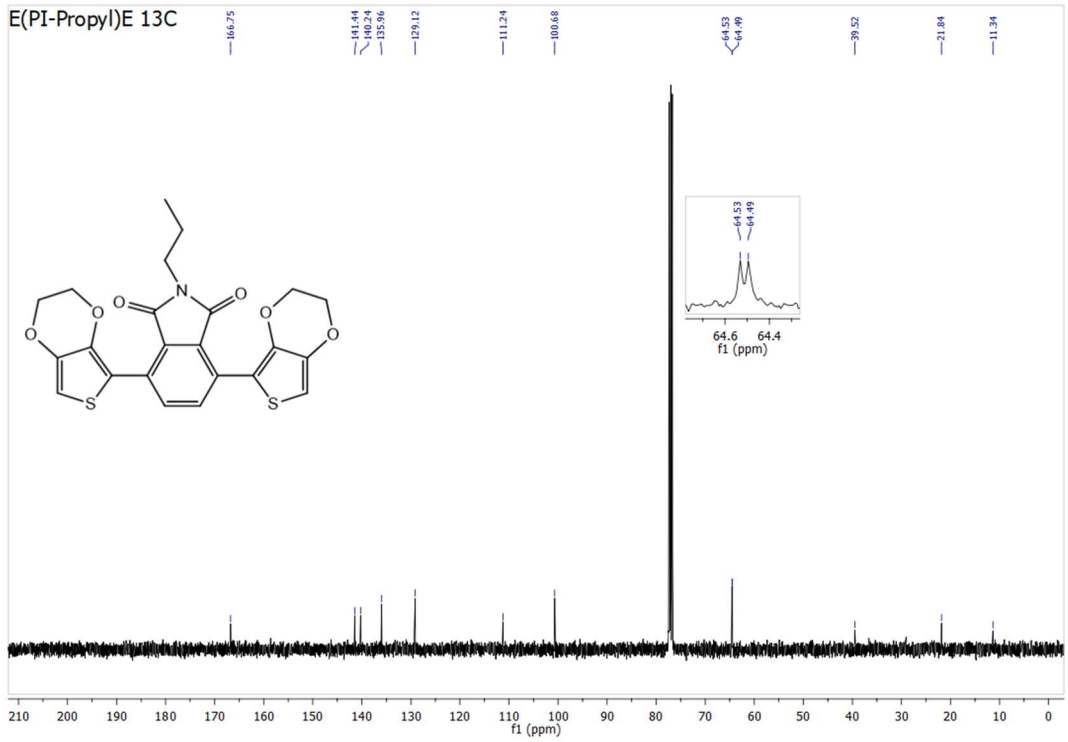

Figure A.19. ^{13}C NMR spectrum of E(PI-Propyl)E in $CDCl_3$.

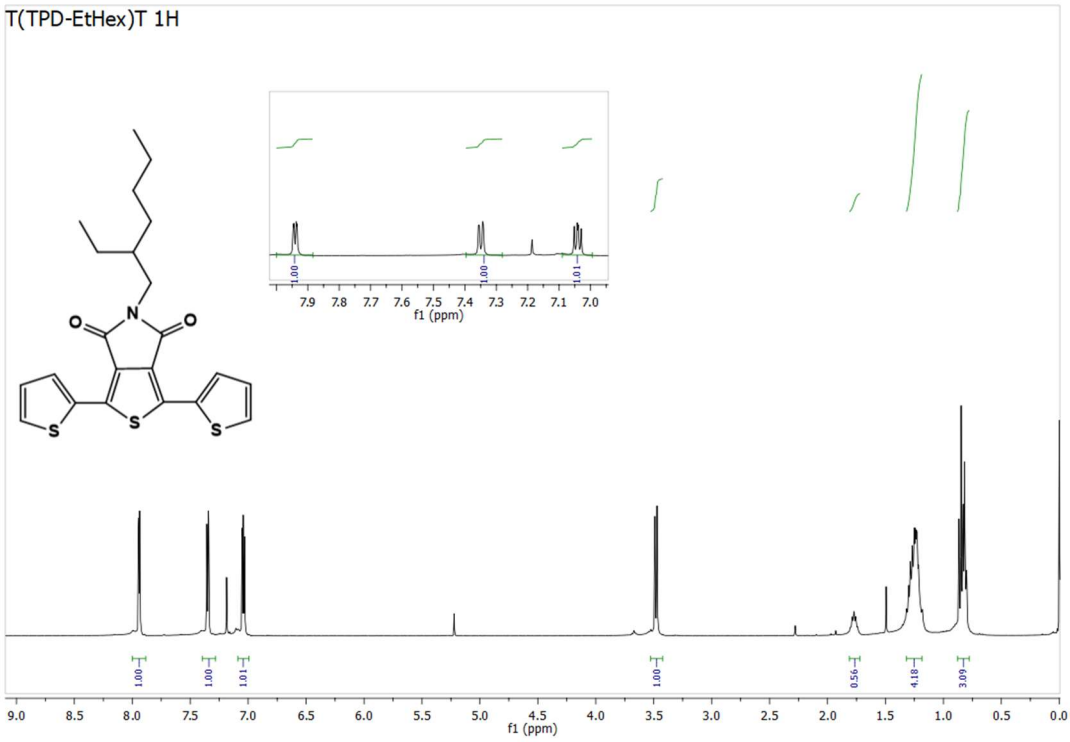

Figure A.20. ^{1}H NMR spectrum of T(TPD-EtHex)T in $CDCl_3$.

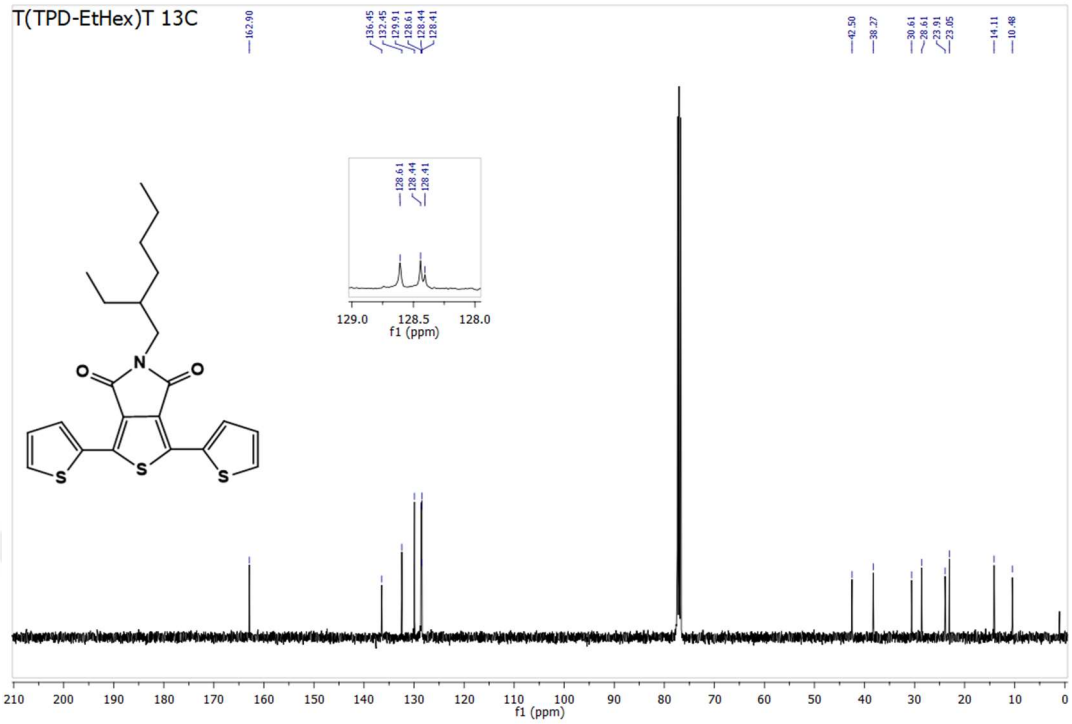

Figure A.21. ^{13}C NMR spectrum of T(TPD-EtHex)T in $CDCl_3$.

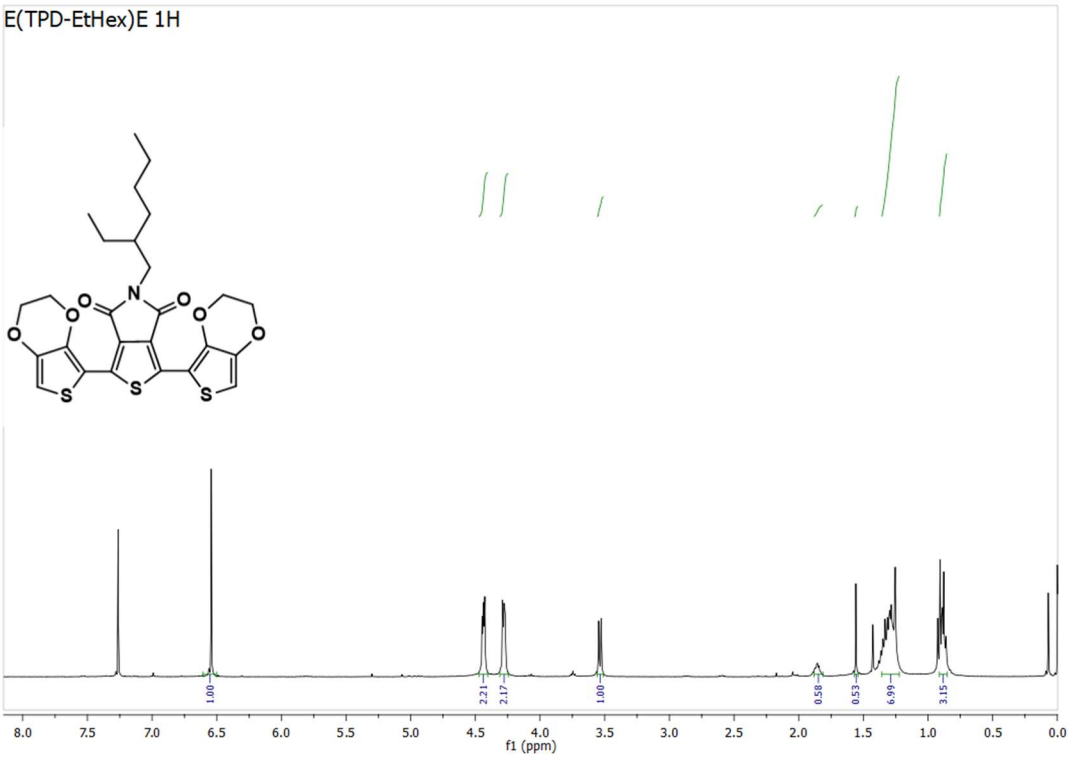

Figure A.22. ^{1}H NMR spectrum of E(TPD-EtHex)E in $CDCl_3$.

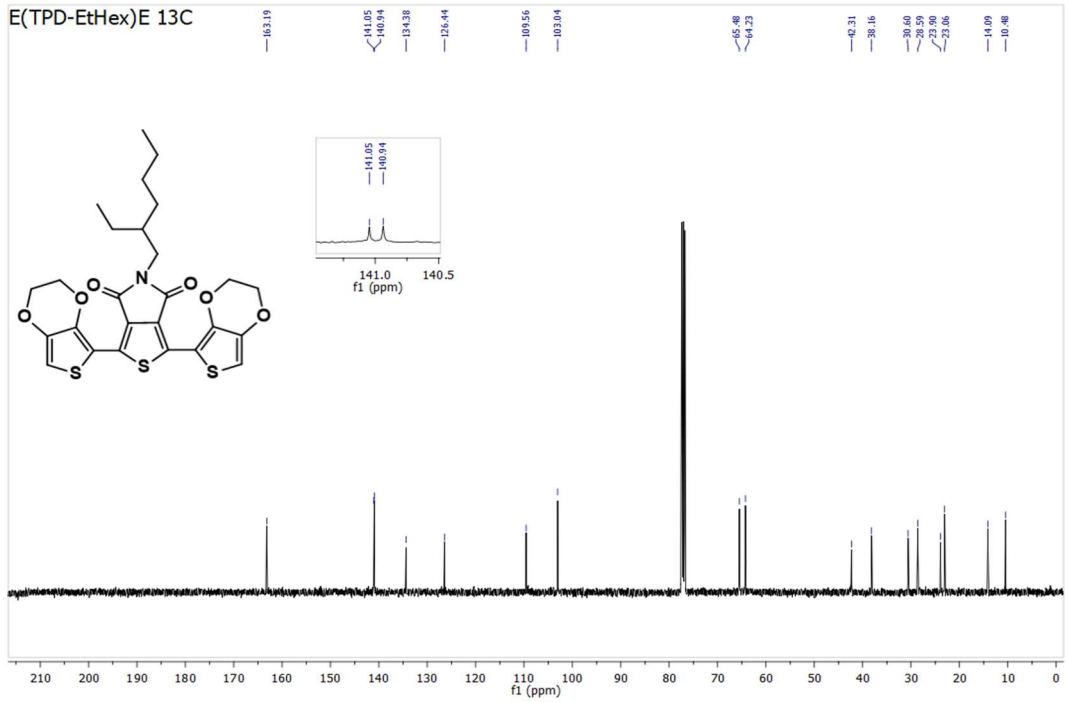

Figure A.23. ^{13}C NMR spectrum of E(TPD- EtHex)E in $CDCl_3$.

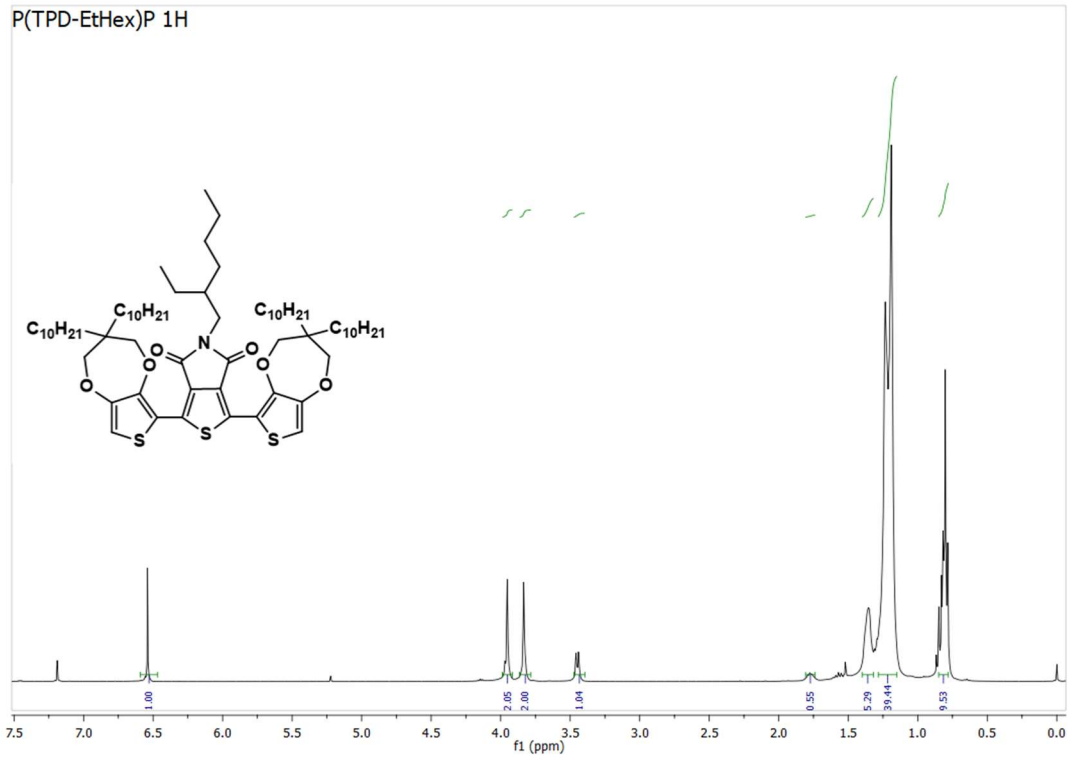

Figure A.24. ^{1}H NMR spectrum of P(TPD-EtHex)P in $CDCl_3$.

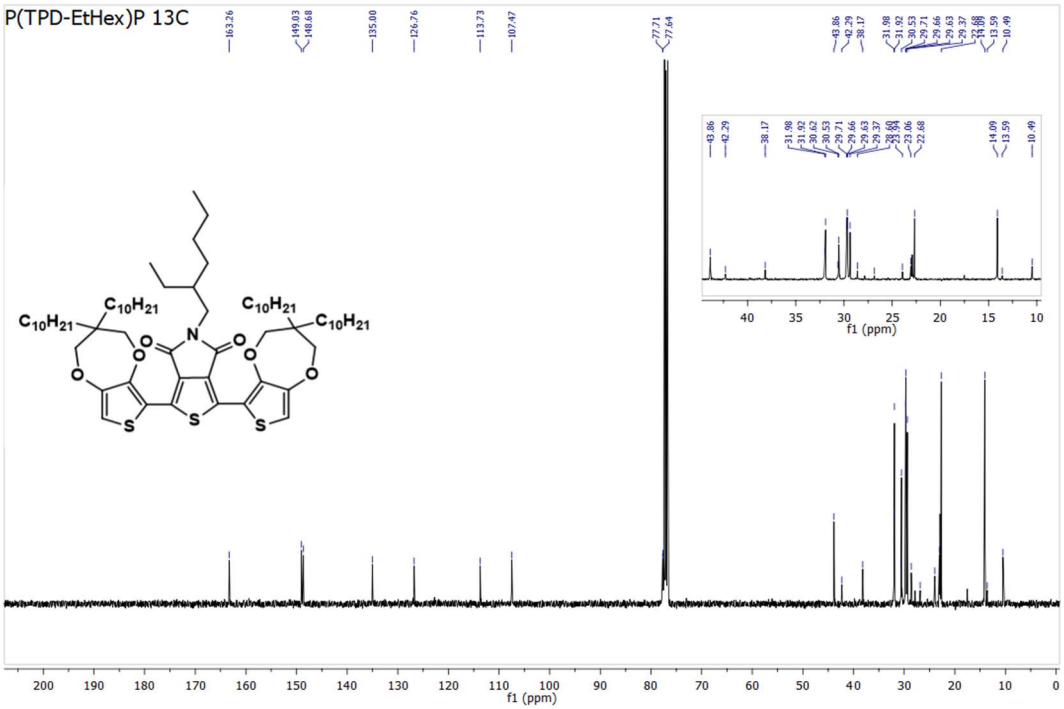

Figure A.25. ^{13}C NMR spectrum of P(TPD-EtHex)P in $CDCl_3$.

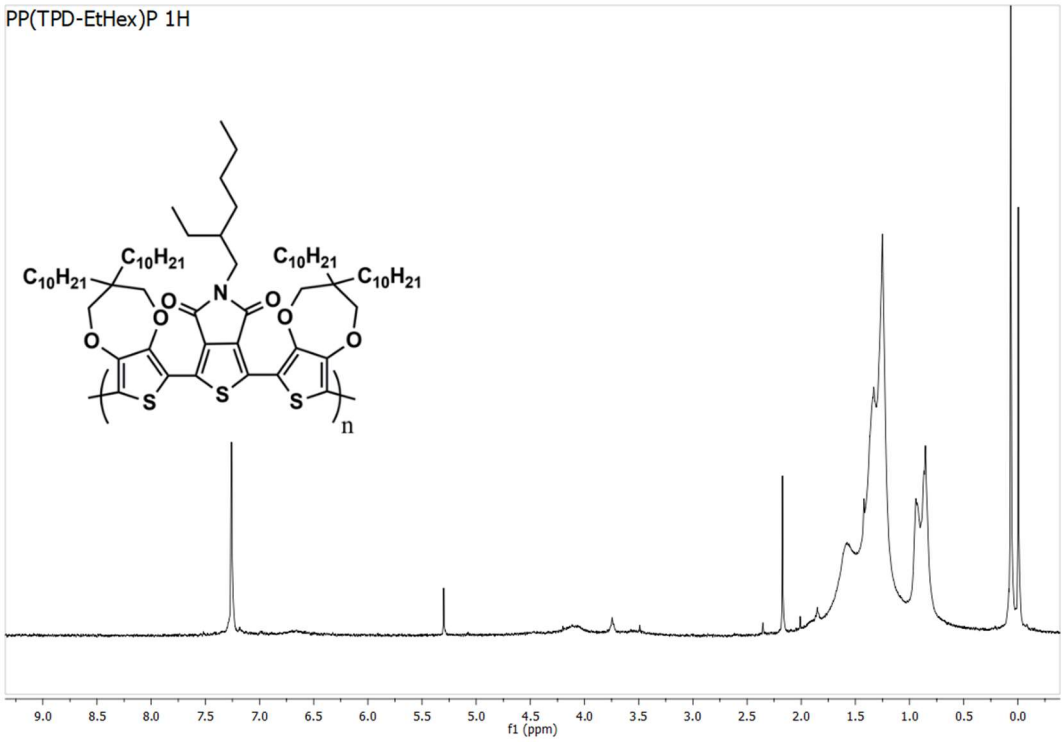

Figure A.26. ^{1}H NMR spectrum of PP(TPD-EtHex)P in $CDCl_3$.

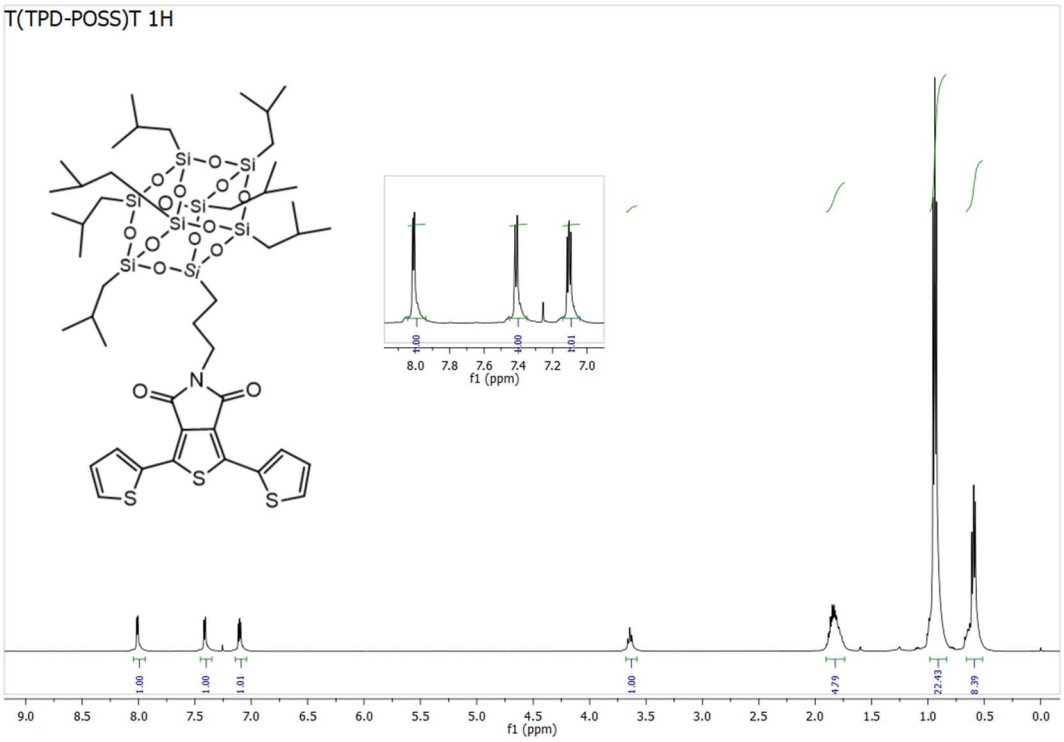

Figure A.27. ^{1}H NMR spectrum of T(TPD-POSS)T in $CDCl_3$.

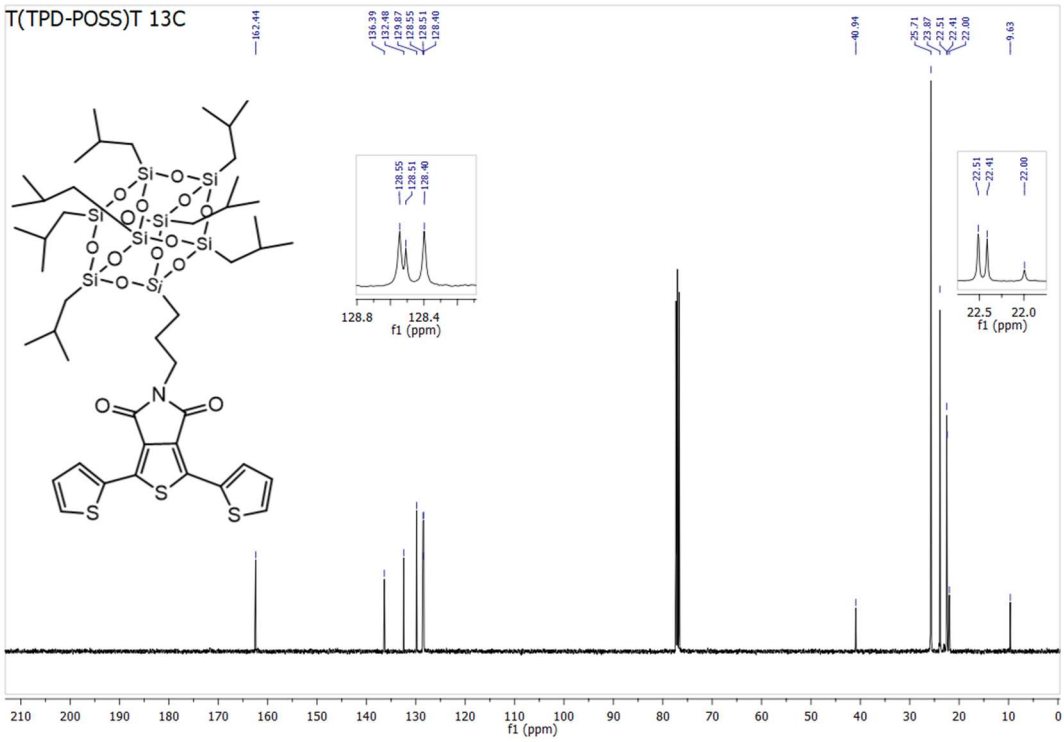

Figure A.28. ^{13}C NMR spectrum of T(TPD-POSS)T in $CDCl_3$.

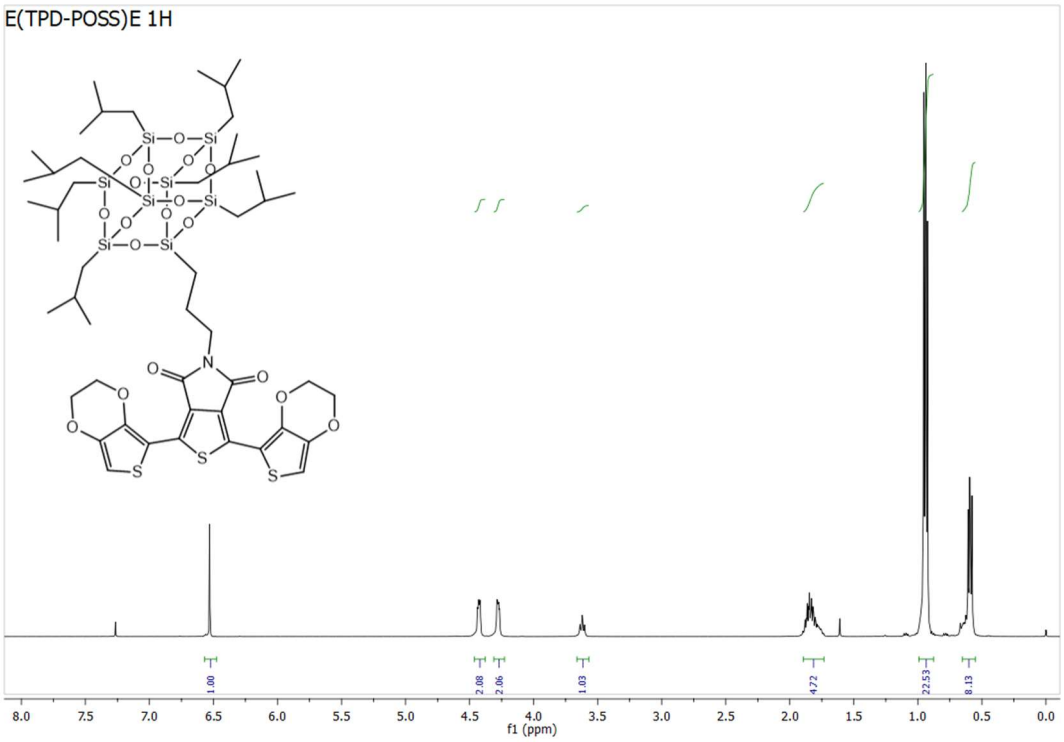

Figure A.29. ^{1}H NMR spectrum of E(TPD-POSS)E in $CDCl_3$.

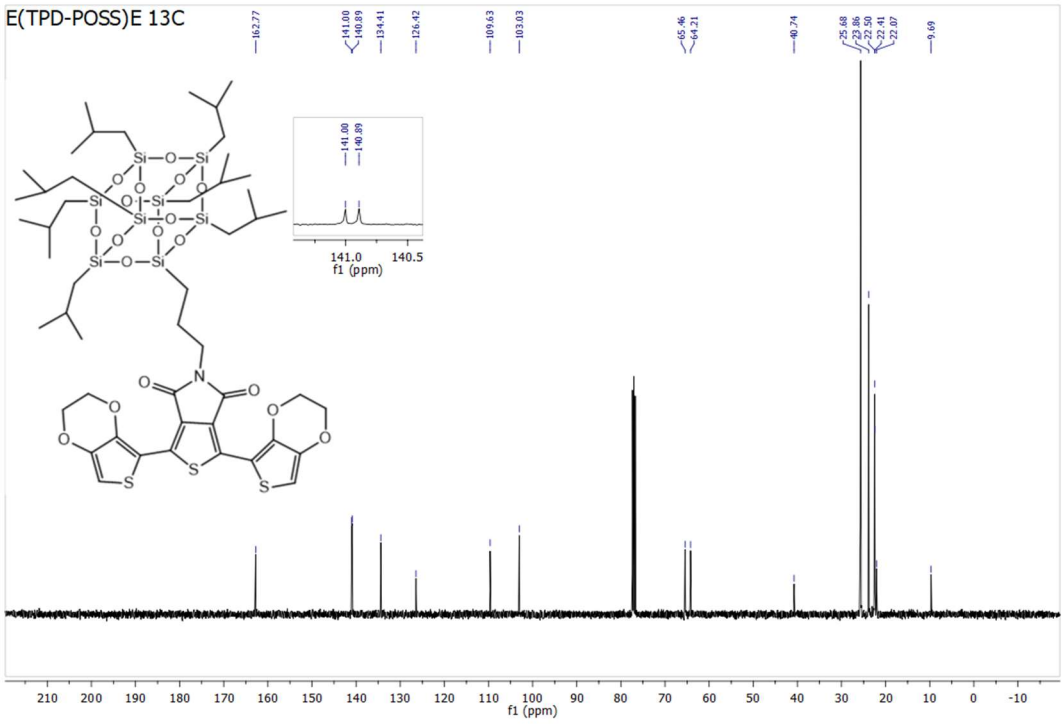

Figure A.30. ^{13}C NMR spectrum of E(TPD-POSS)E in $CDCl_3$.

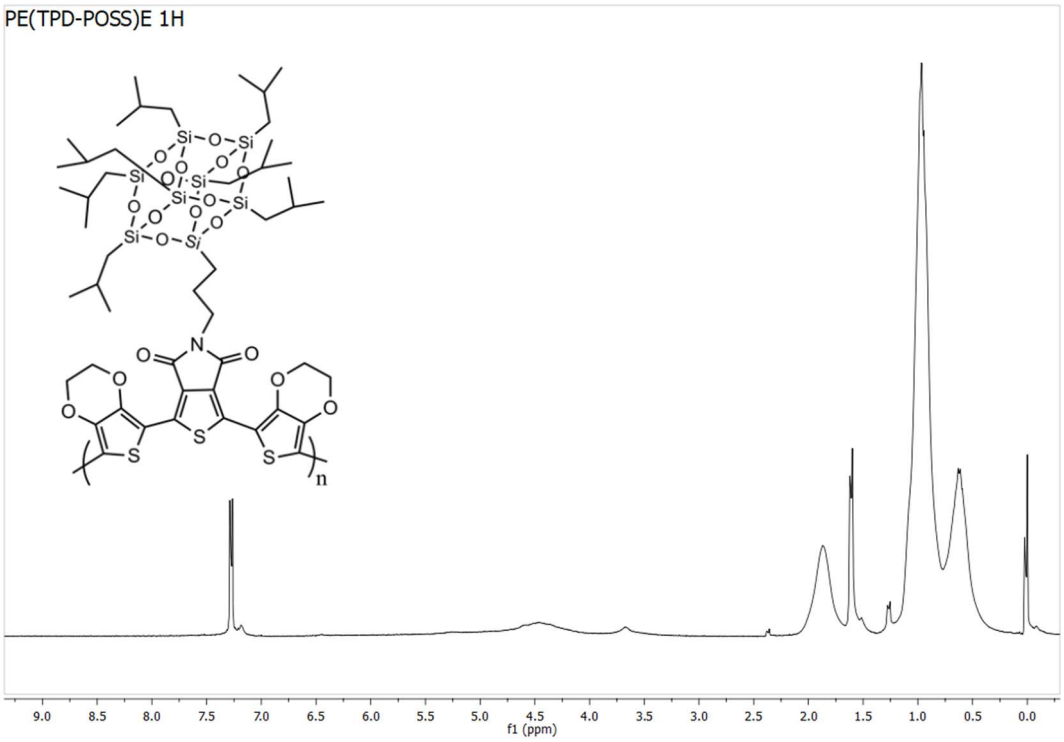

Figure A.31. ^{1}H NMR spectrum of PE(TPD-POSS)E in $CDCl_3$.

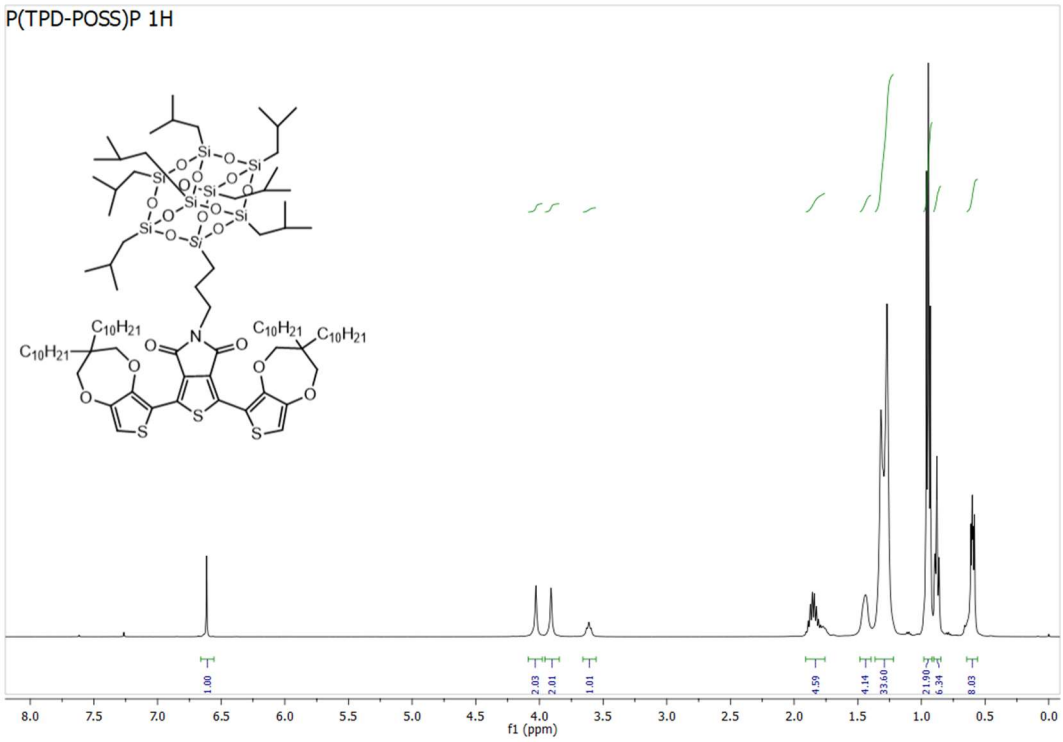

Figure A.32. ^{1}H NMR spectrum of P(TPD-POSS)P in $CDCl_3$.

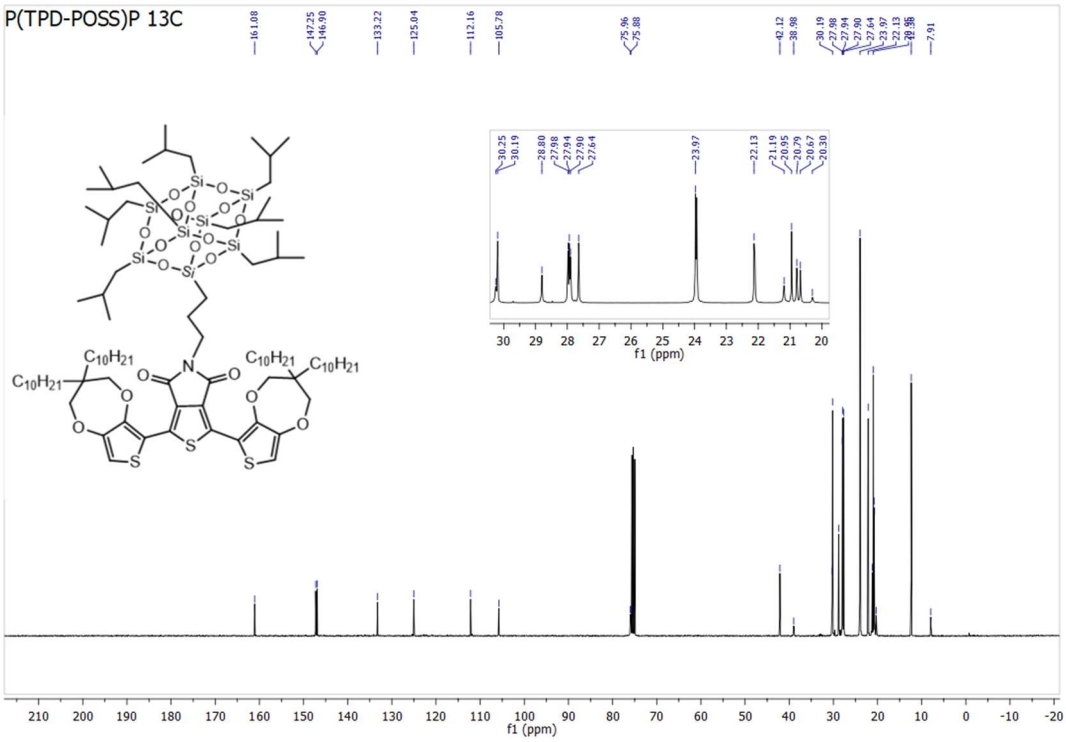

Figure A.33. ^{13}C NMR spectrum of P(TPD-POSS)P in $CDCl_3$.

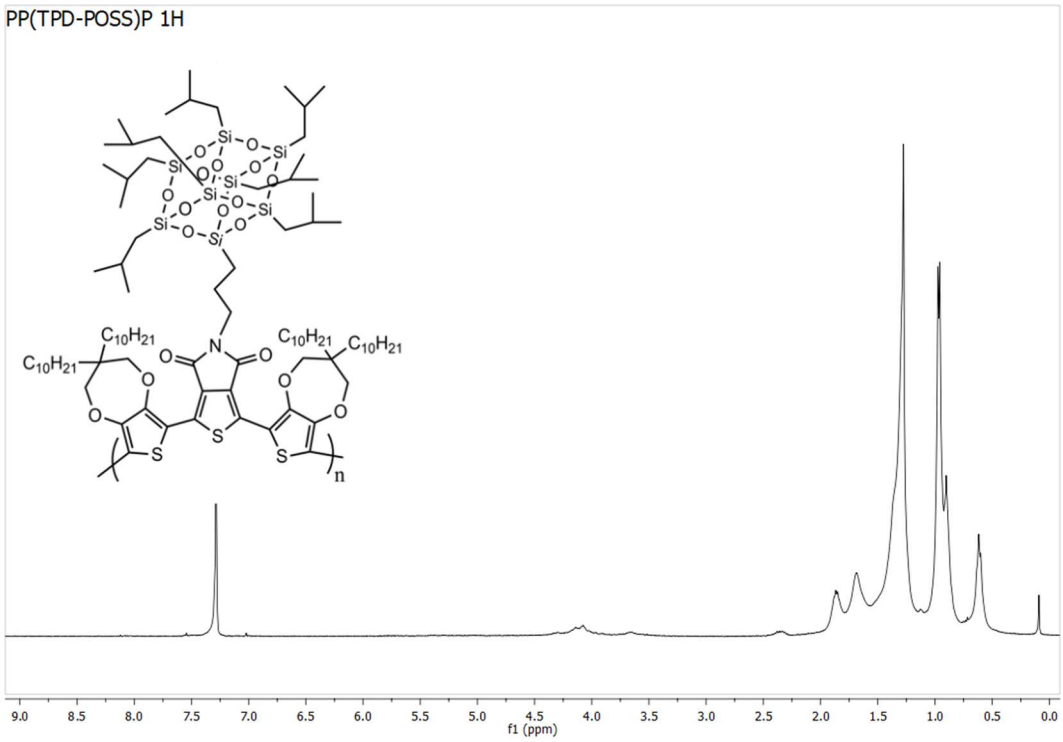

Figure A.34. ^{1}H NMR spectrum of PP(TPD-POSS)P in $CDCl_3$.

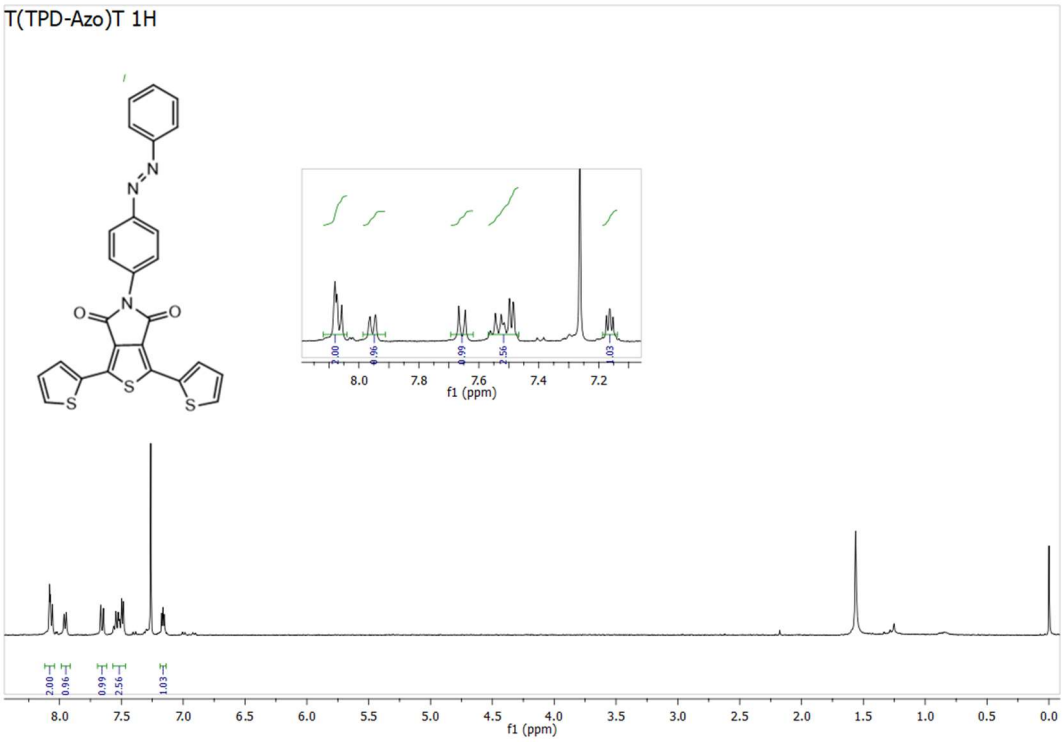

Figure A.35. ^{1}H NMR spectrum of T(TPD-Azo)T in $CDCl_3$.

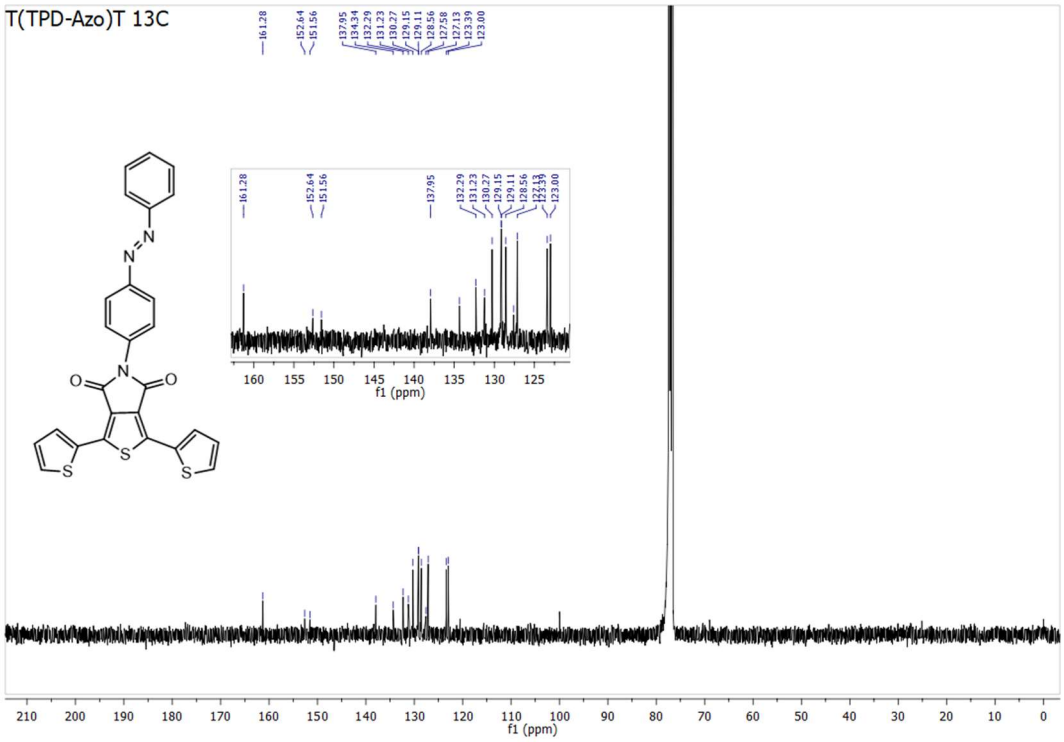

Figure A.36. ^{13}C NMR spectrum of T(TPD-Azo)T in $CDCl_3$.

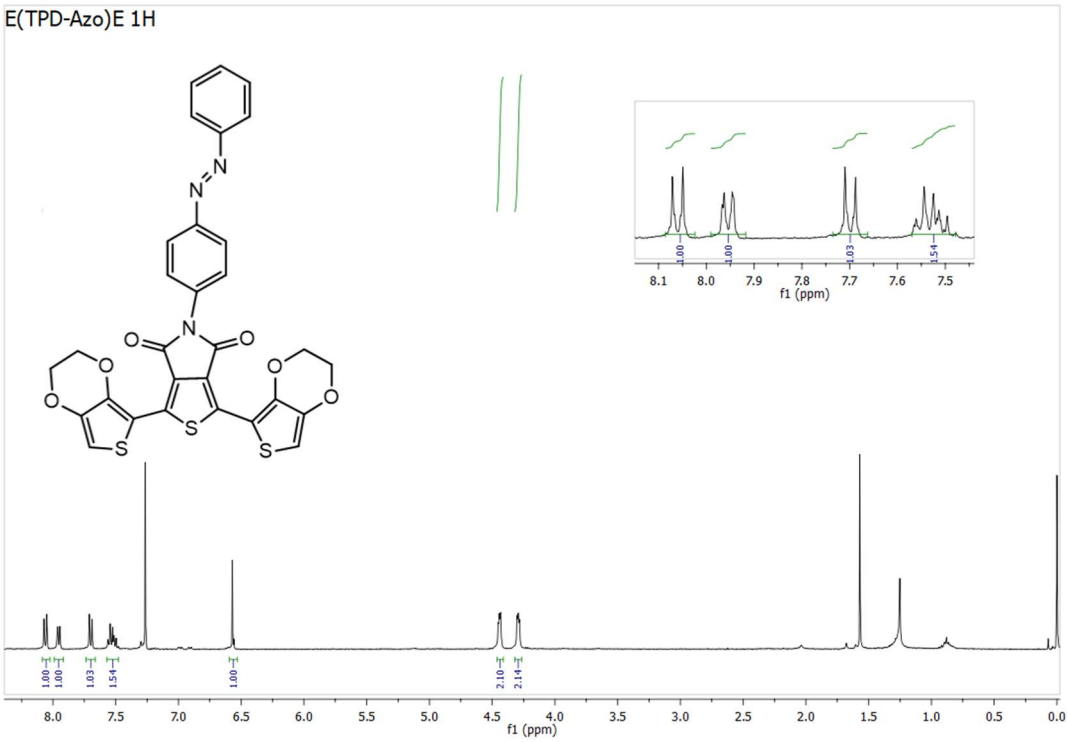

Figure A.37. ^{1}H NMR spectrum of E(TPD-Azo)E in $CDCl_3$.

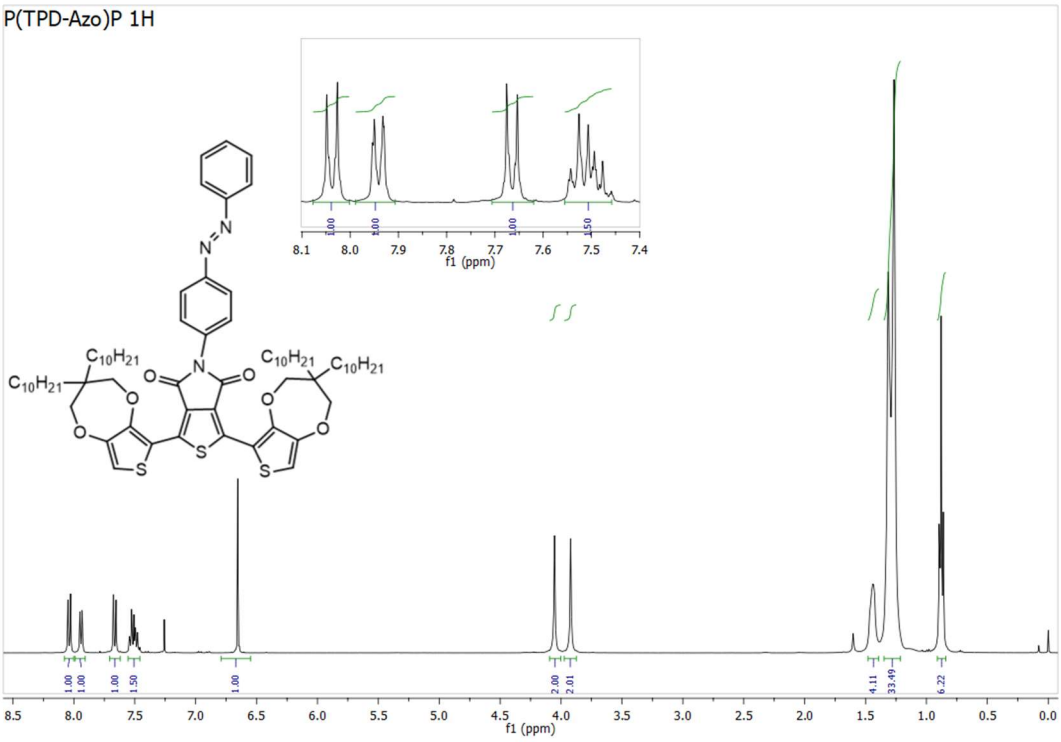

Figure A.38. ^{1}H NMR spectrum of P(TPD-Azo)P in $CDCl_3$.

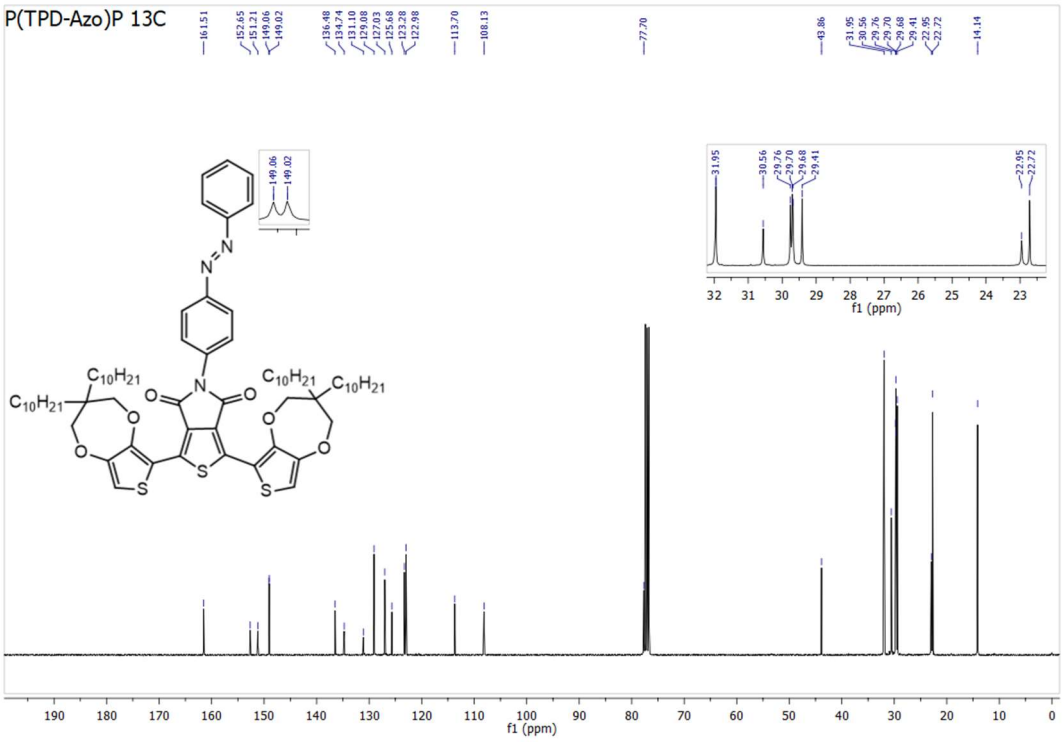

Figure A.39. ^{13}C NMR spectrum of P(TPD-Azo)P in $CDCl_3$.

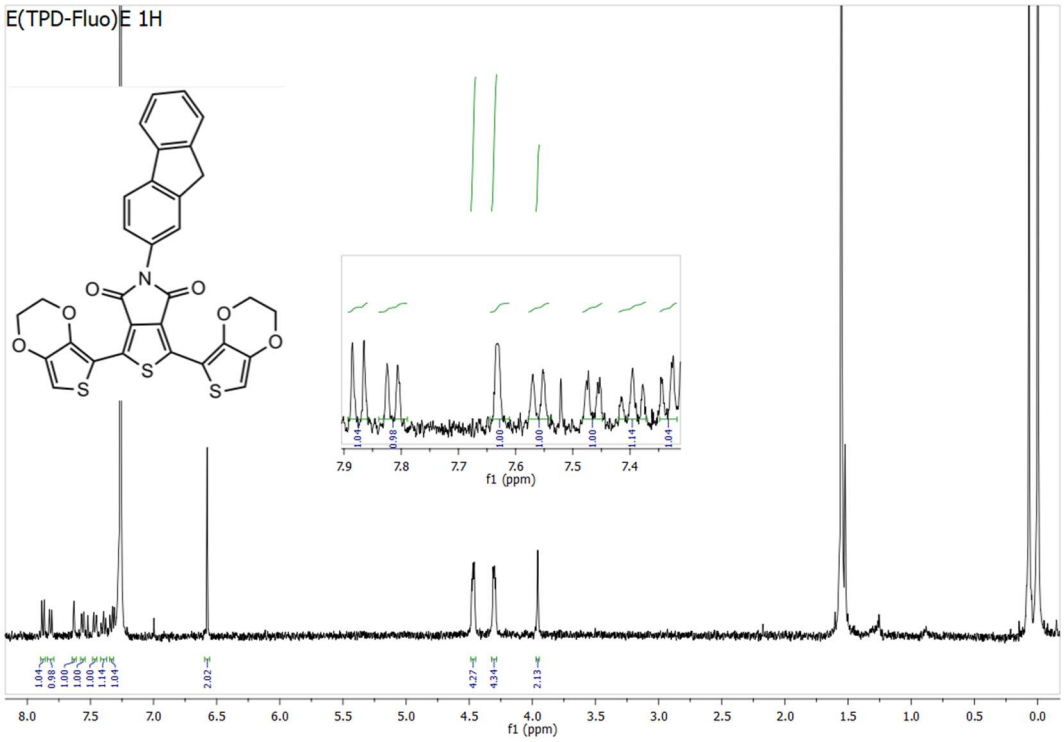

Figure A.40. ^{1}H NMR spectrum of E(TPD-Fluo)E in $CDCl_3$.

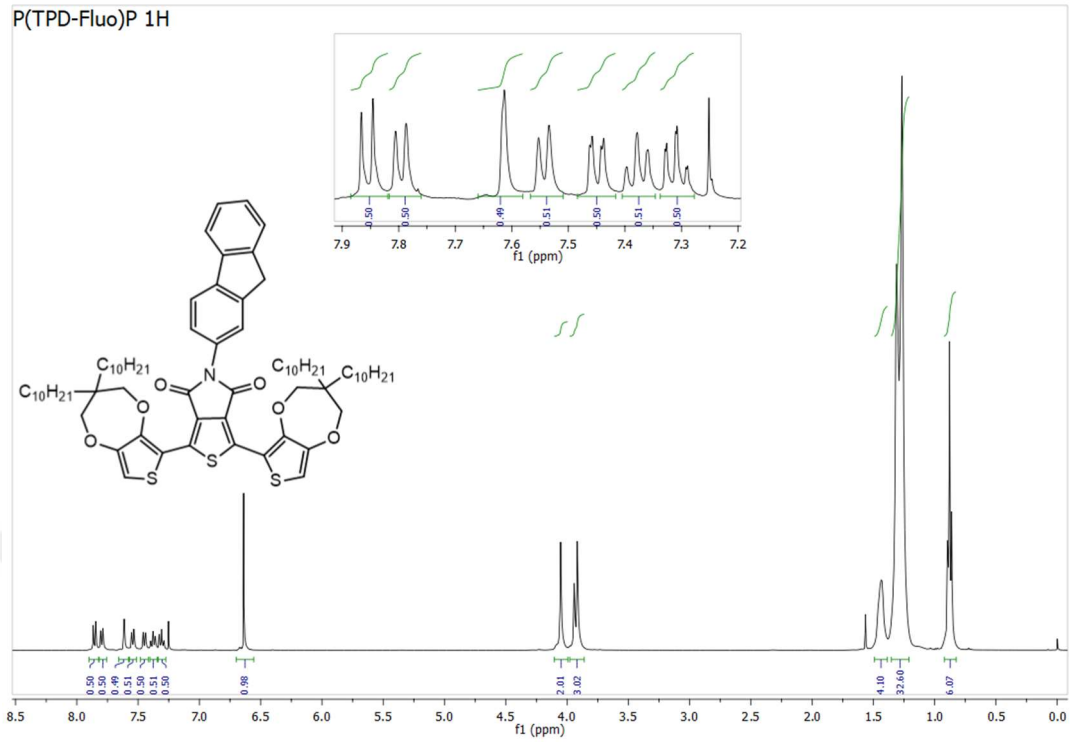

Figure A.41. ^{1}H NMR spectrum of E(TPD-Fluo)E in $CDCl_3$.

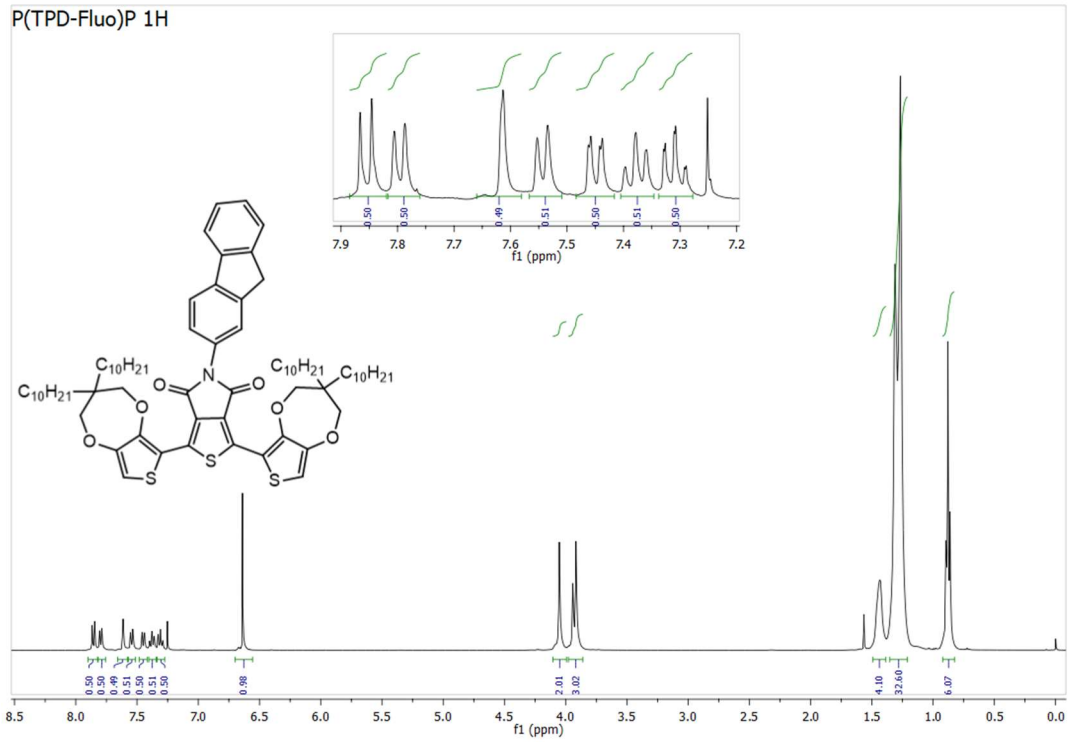

Figure A.42. ^{1}H NMR spectrum of P(TPD-Fluo)P in $CDCl_3$.

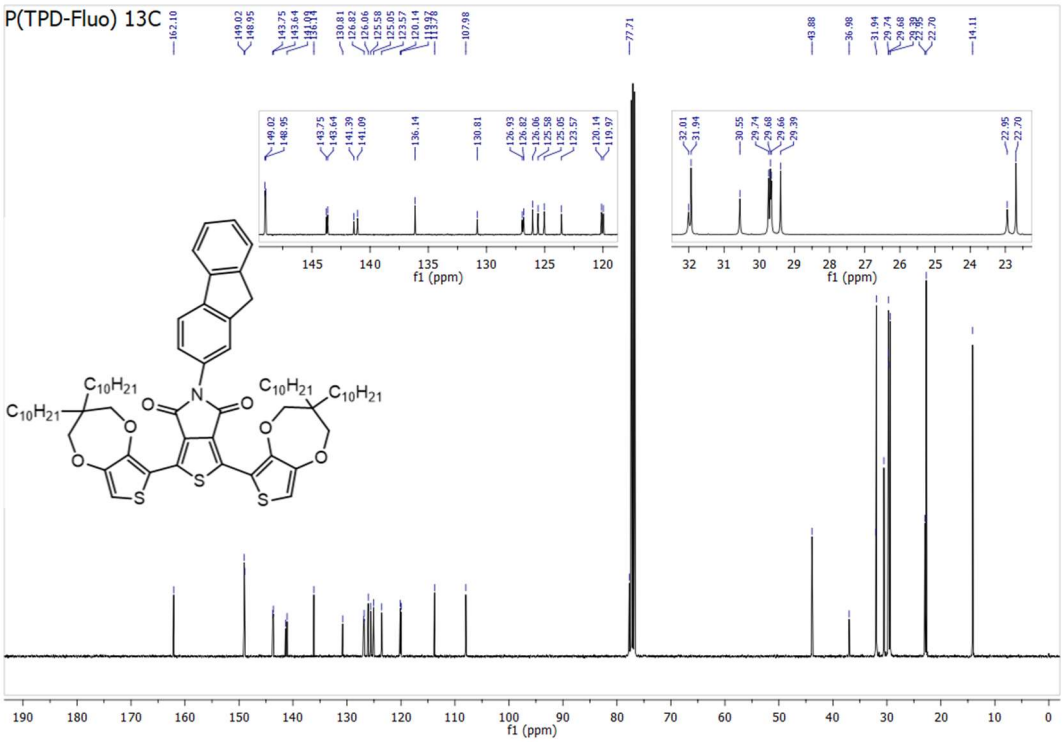

Figure A.43. ^{13}C NMR spectrum of P(TPD-Fluo)P in $CDCl_3$.

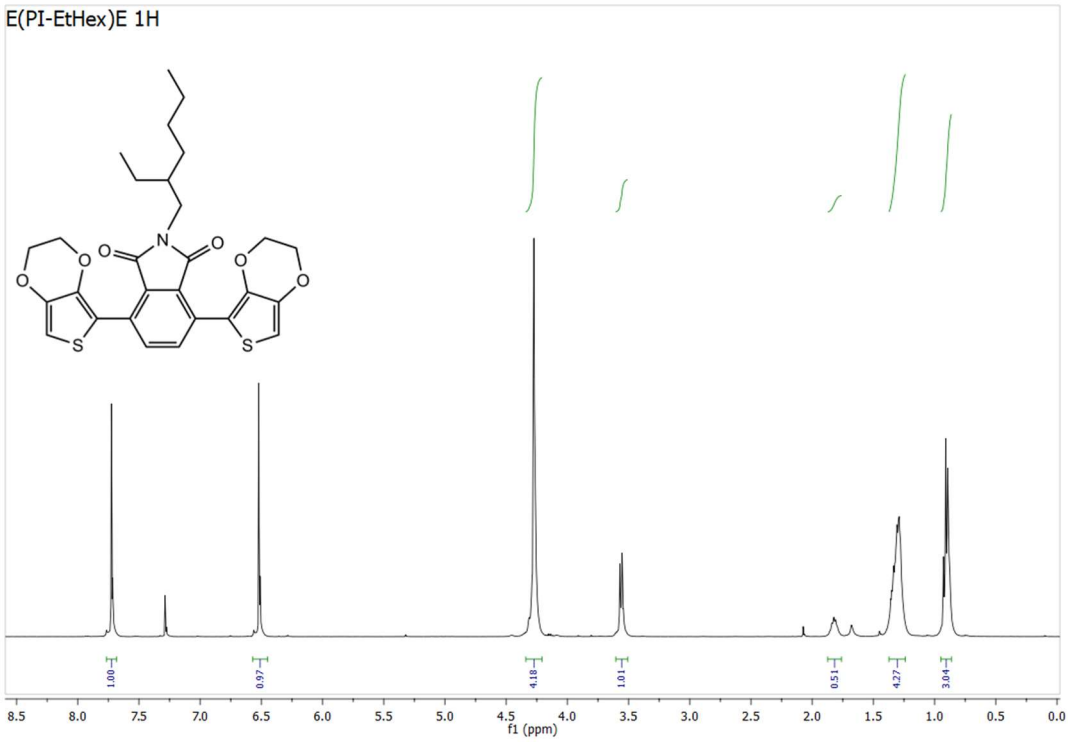

Figure A.44. ^{1}H NMR spectrum of E(PI-EtHex)E in $CDCl_3$.

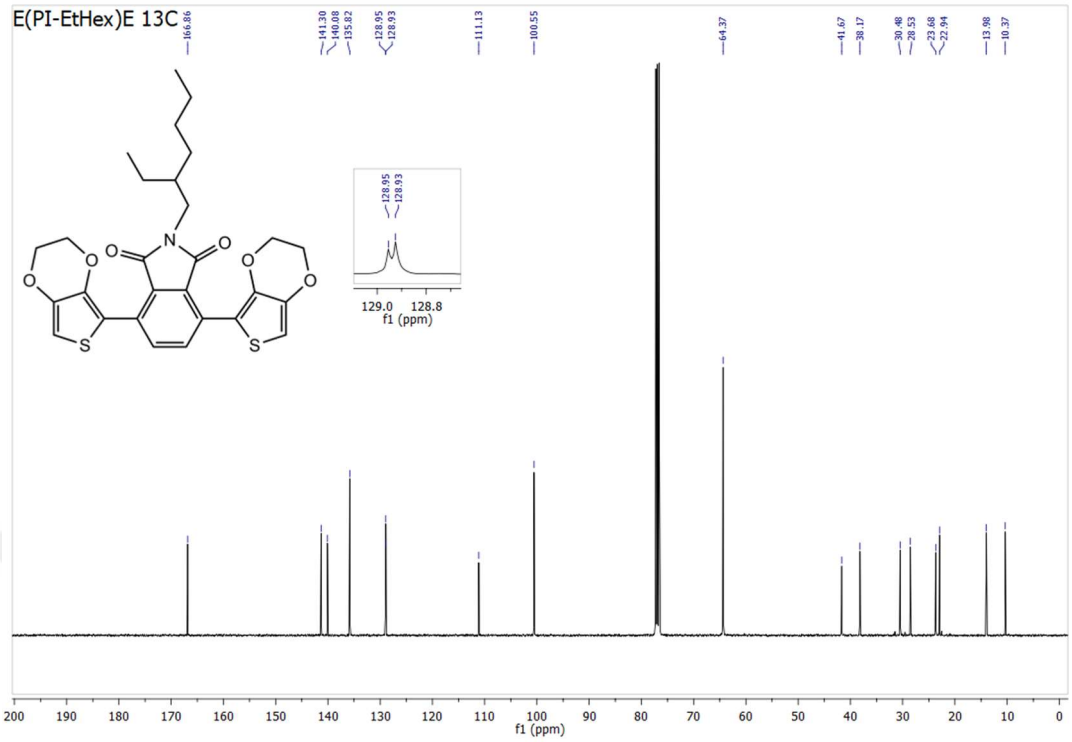

Figure A.45. ^{13}C NMR spectrum of E(PI-EtHex)E in $CDCl_3$.

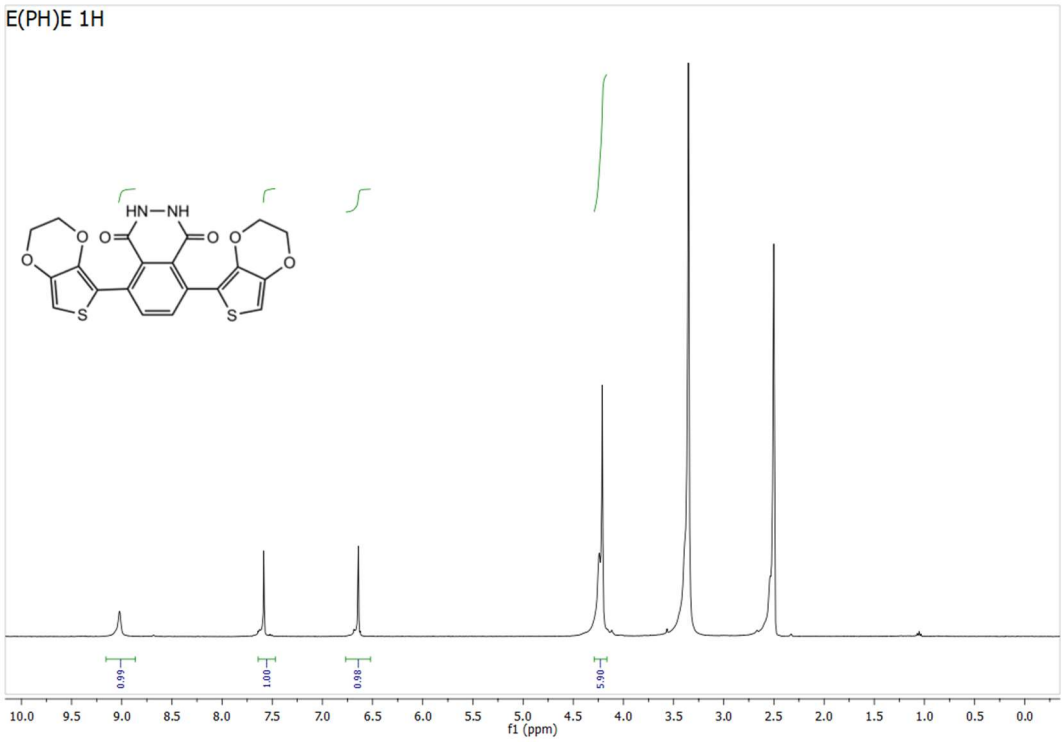

Figure A.46. ^{1}H NMR spectrum of E(PH)E in d-DMSO.

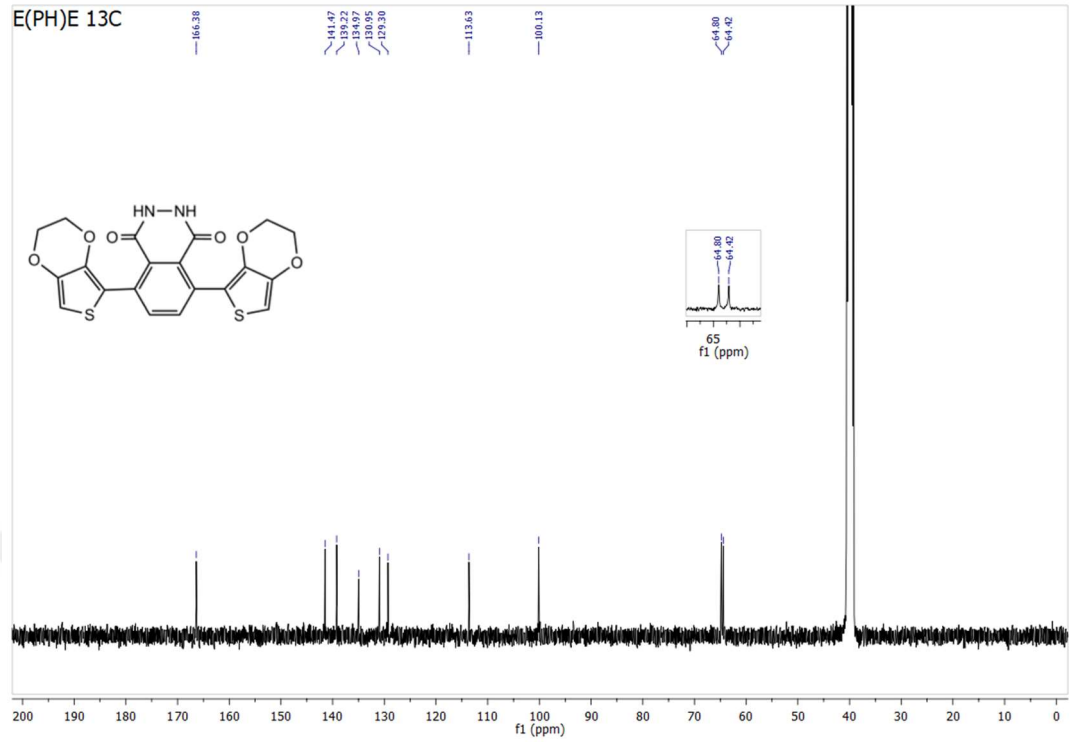

Figure A.47. ^{13}C NMR spectrum of E(PH)E in d-DMSO.

B. HRMS Data of Monomers

HRMS was performed by Waters SYNAPT G1 MS System under the electron impact mode at METU Central Laboratory.

Single Mass Analysis
Tolerance = 5000.0 PPM / DBE: min = -5.5, max = 1000.0
Element prediction: Off
Number of isotope peaks used for i-FIT = 3

Monoisotopic Mass, Even Electron Ions
6 formula(e) evaluated with 1 results within limits (all results (up to 1000) for each mass)
Elements Used:
C: 11-11 H: 9-10 N: 1-1 O: 2-2 79Br: 0-2 81Br: 0-2

Ahmet Onal
28093_20191024_02-02 8 (0.328) Cm (1:10)

1: TOF MS ES+
2.67e+004

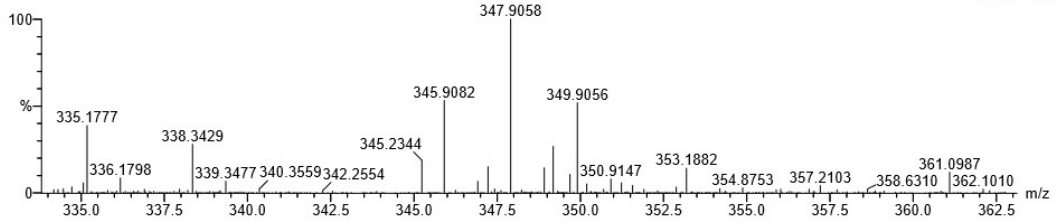

Minimum:				-5.5			
Maximum:		1000.0	5000.0	1000.0			
Mass	Calc. Mass	mDa	PPM	DBE	i-FIT	i-FIT (Norm)	Formula
347.9058	347.9058	0.0	0.0	6.5	359.8	0.0	C11 H10 N O2 79Br 81Br

Figure B.1. HRMS spectrum of PI-Propyl.

Single Mass Analysis
Tolerance = 5000.0 PPM / DBE: min = -5.5, max = 1000.0
Element prediction: Off
Number of isotope peaks used for i-FIT = 3

Monoisotopic Mass, Even Electron Ions
4 formula(e) evaluated with 1 results within limits (all results (up to 1000) for each mass)
Elements Used:
C: 18-18 H: 8-10 N: 3-3 O: 2-2 S: 1-1 79Br: 0-1 81Br: 0-1

Ahmet Onal
25158_20181220_01-04 10 (0.396) Cm (5:11)

1: TOF MS ES+
4.96e+005

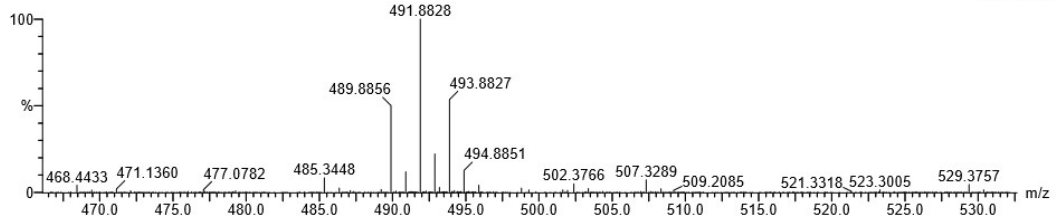

Minimum:				-5.5			
Maximum:		1000.0	5000.0	1000.0			
Mass	Calc. Mass	mDa	PPM	DBE	i-FIT	i-FIT (Norm)	Formula
491.8828	491.8840	-1.2	-2.4	14.5	479.8	0.0	C18 H10 N3 O2 S 79Br 81Br

Figure B.2. HRMS spectrum of TPD-Azo.

Single Mass Analysis
Tolerance = 5000.0 PPM / DBE: min = -5.5, max = 1000.0
Element prediction: Off
Number of isotope peaks used for i-FIT = 3

Monoisotopic Mass, Even Electron Ions
7 formula(e) evaluated with 1 results within limits (all results (up to 1000) for each mass)
Elements Used:
C: 19-19 H: 9-10 N: 1-1 O: 2-2 S: 1-1 79Br: 0-2 81Br: 0-2

Ahmet Onal
288853_20200116_04-04 9 (0.362) Cm (1:10)

1: TOF MS ES+
1.20e+004

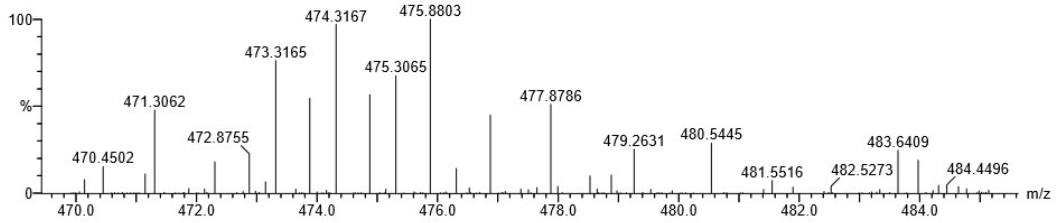

Minimum:				-5.5			
Maximum:		1000.0	5000.0	1000.0			
Mass	Calc. Mass	mDa	PPM	DBE	i-FIT	i-FIT (Norm)	Formula
475.8803	475.8779	2.4	5.0	14.5	182.2	0.0	C19 H10 N O2 S 79Br 81Br

Figure B.3. HRMS spectrum of TPD-Fluo.

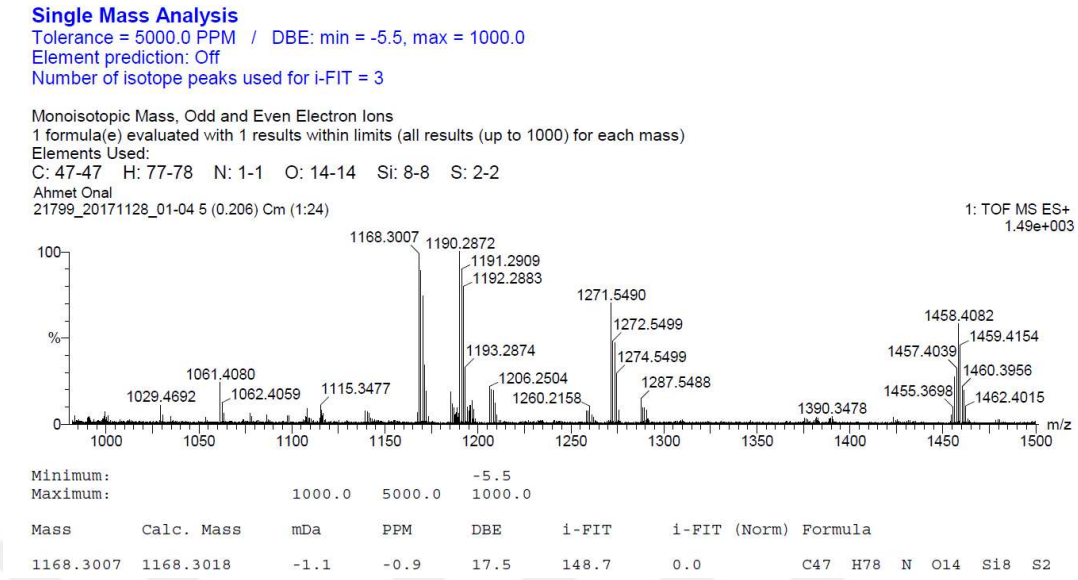

Figure B.4. HRMS spectrum of T(PI-POSS)T.

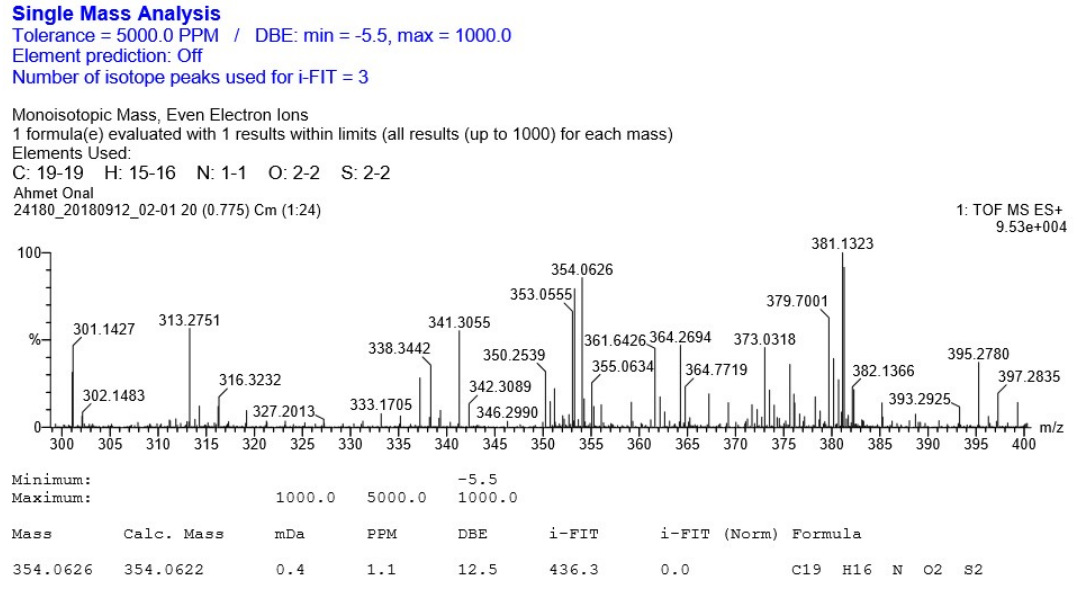

Figure B.5. HRMS spectrum of T(PI-Propyl)T.

Single Mass Analysis
Tolerance = 5000.0 PPM / DBE: min = -5.5, max = 1000.0
Element prediction: Off
Number of isotope peaks used for i-FIT = 3

Monoisotopic Mass, Even Electron Ions
1 formula(e) evaluated with 1 results within limits (all results (up to 1000) for each mass)
Elements Used:
C: 51-51 H: 82-83 N: 1-1 O: 18-18 Si: 8-8 S: 2-2
Ahmet Onal
21799_20171128_02-01 21 (0.829) Cm (1:25)

1: TOF MS ES+
2.48e+004

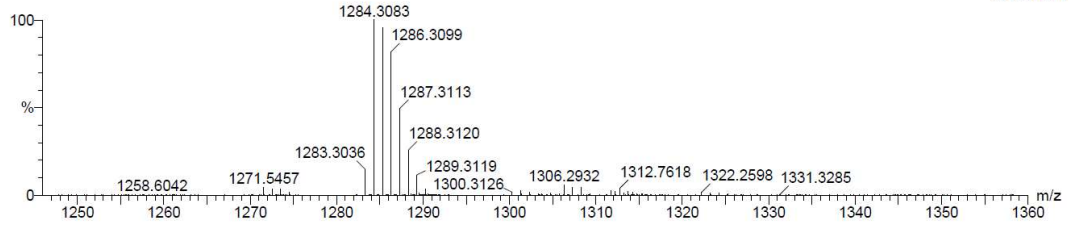

Minimum:				-5.5			
Maximum:		1000.0	5000.0	1000.0			
Mass	Calc. Mass	mDa	PPM	DBE	i-FIT	i-FIT (Norm)	Formula
1284.3083	1284.3128	-4.5	-3.5	19.5	161.7	0.0	C51 H82 N O18 Si8 S2

Figure B.6. HRMS spectrum of E(PI-POSS)E.

Single Mass Analysis
Tolerance = 5000.0 PPM / DBE: min = -5.5, max = 1000.0
Element prediction: Off
Number of isotope peaks used for i-FIT = 3

Monoisotopic Mass, Even Electron Ions
1 formula(e) evaluated with 1 results within limits (all results (up to 1000) for each mass)
Elements Used:
C: 23-23 H: 19-20 N: 1-1 O: 6-6 S: 2-2
Ahmet Onal
24180_20180913_01-02 16 (0.639) Cm (1:16)

1: TOF MS ES+
6.75e+004

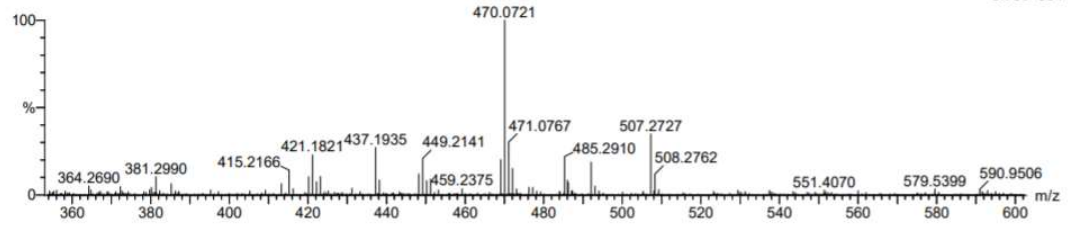

Minimum:				-5.5			
Maximum:		1000.0	5000.0	1000.0			
Mass	Calc. Mass	mDa	PPM	DBE	i-FIT	i-FIT (Norm)	Formula
470.0721	470.0732	-1.1	-2.3	14.5	378.0	0.0	C23 H20 N O6 S2

Figure B.7. HRMS spectrum of E(PI-Propyl)E.

Single Mass Analysis
Tolerance = 50.0 PPM / DBE: min = -5.5, max = 1000.0
Element prediction: Off
Number of isotope peaks used for i-FIT = 3

Monoisotopic Mass, Even Electron Ions
28 formula(e) evaluated with 1 results within limits (all results (up to 1000) for each mass)
Elements Used:
C: 22-22 H: 10-27 N: 1-2 O: 1-3 Na: 0-1 S: 3-3 I: 0-3
Ahmet Onal
22323_20180208_01-01 4 (0.172) Cm (1:11)

1: TOF MS ES+
7.19e+004

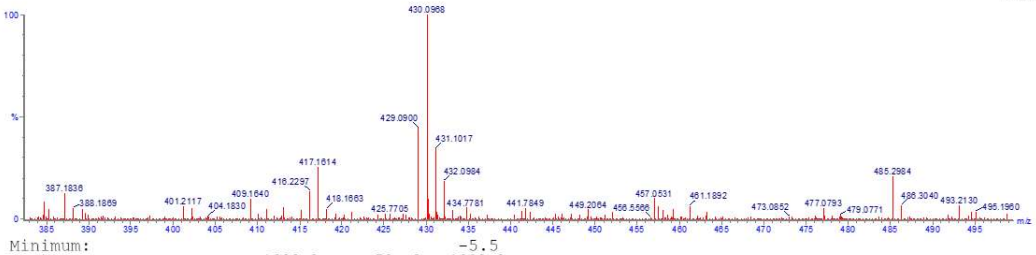

Minimum:				-5.5		
Maximum:		1000.0	50 .0	1000.0		

Mass	Calc. Mass	mDa	PPM	DBE	i-FIT	i-FIT (Norm)	Formula
430.0968	430.0969	-0.1	-0.2	11.5	413.6	0.0	C22 H24 N O2 S3

Figure B.8. HRMS spectrum of T(TPD-EtHex)T.

Single Mass Analysis
Tolerance = 10000.0 PPM / DBE: min = -5.5, max = 1000.0
Element prediction: Off
Number of isotope peaks used for i-FIT = 3

Monoisotopic Mass, Even Electron Ions
3 formula(e) evaluated with 1 results within limits (all results (up to 1000) for each mass)
Elements Used:
C: 26-26 H: 26-28 N: 1-1 O: 6-6 Na: 0-1 S: 3-3 K: 0-1
Ahmet Onal
22223_20180122_01-04 15 (0.586) Cm (10:21)

1: TOF MS ES+
3.16e+003

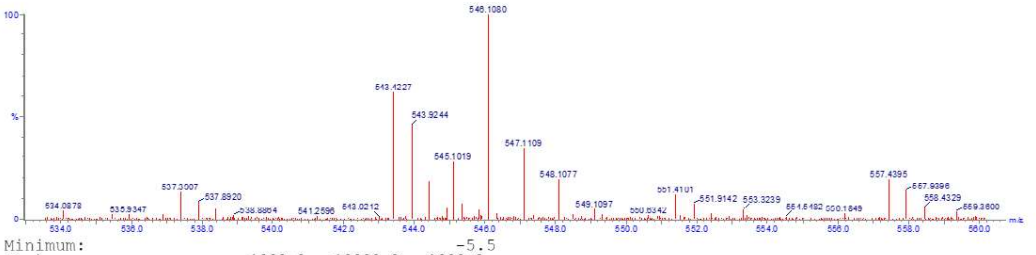

Minimum:				-5.5		
Maximum:		1000.0	10000.0	1000.0		

Mass	Calc. Mass	mDa	PPM	DBE	i-FIT	i-FIT (Norm)	Formula
546.1080	546.1079	0.1	0.2	13.5	200.1	0.0	C26 H28 N O6 S3

Figure B.9. HRMS spectrum of E(TPD-EtHex)E.

Single Mass Analysis
Tolerance = 10000.0 PPM / DBE: min = -5.5, max = 1000.0
Element prediction: Off
Number of isotope peaks used for i-FIT = 3

Monoisotopic Mass, Even Electron Ions
1 formula(e) evaluated with 1 results within limits (all results (up to 1000) for each mass)
Elements Used:
C: 68-68 H: 111-112 N: 1-1 O: 6-6 Na: 0-1 S: 3-3 K: 0-1
Ahmet Onal
22223_20180122_02-01 23 (0.897) Cm (17:25)

1: TOF MS ES+
3.02e+003

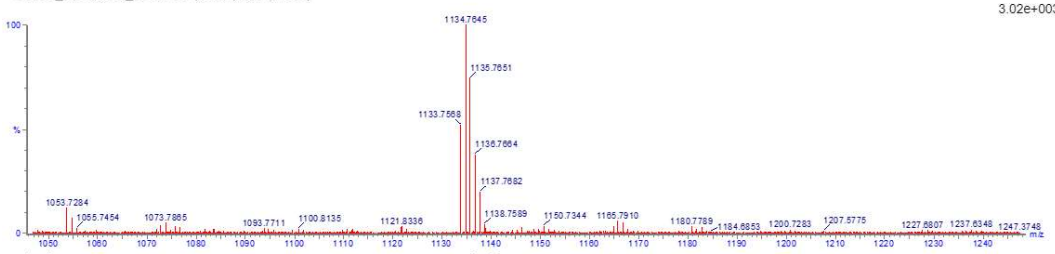

Minimum: -5.5
Maximum: 1000.0 10000.0 1000.0

Mass	Calc. Mass	mDa	PPM	DBE	i-FIT	i-FIT (Norm)	Formula
1134.7645	1134.7652	-0.7	-0.6	13.5	99.0	0.0	C68 H112 N O6 S3

Figure B.10. HRMS spectrum of P(TPD-EtHex)P.

Single Mass Analysis
Tolerance = 5000.0 PPM / DBE: min = -5.5, max = 1000.0
Element prediction: Off
Number of isotope peaks used for i-FIT = 3

Monoisotopic Mass, Odd and Even Electron Ions
1 formula(e) evaluated with 1 results within limits (all results (up to 1000) for each mass)
Elements Used:
C: 45-45 H: 75-76 N: 1-1 O: 14-14 Si: 8-8 S: 3-3
Ahmet Onal
29233_20200219_01-01 16 (0.639) Cm (15:24)

1: TOF MS ES+
3.85e+003

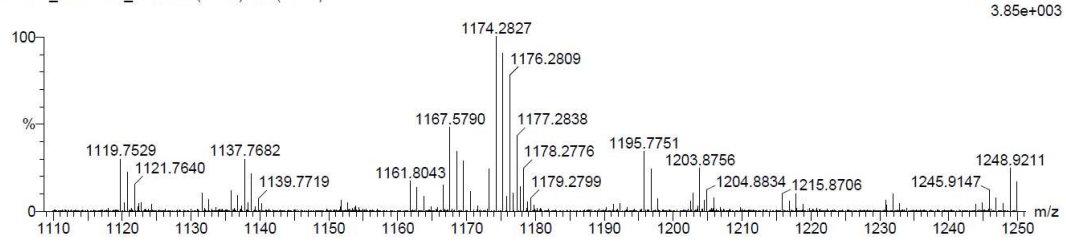

Minimum: -5.5
Maximum: 1000.0 5000.0 1000.0

Mass	Calc. Mass	mDa	PPM	DBE	i-FIT	i-FIT (Norm)	Formula
1174.2827	1174.2582	24.5	20.9	16.5	61.2	0.0	C45 H76 N O14 Si8 S3

Figure B.11. HRMS spectrum of T(TPD-POSS)T.

Single Mass Analysis
Tolerance = 5000.0 PPM / DBE: min = -5.5, max = 1000.0
Element prediction: Off
Number of isotope peaks used for i-FIT = 3

Monoisotopic Mass, Even Electron Ions
1 formula(e) evaluated with 1 results within limits (all results (up to 1000) for each mass)
Elements Used:
C: 49-49 H: 79-80 N: 1-1 O: 18-18 Si: 8-8 S: 3-3
Ahmet Onal
288854_20200117_02-05 21 (0.829) Cm (16:25)

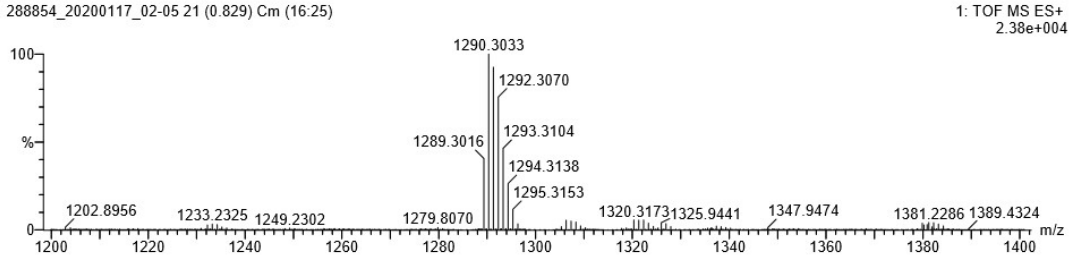

Minimum:				-5.5								
Maximum:		1000.0	5000.0	1000.0								
Mass	Calc. Mass	mDa	PPM	DBE	i-FIT	i-FIT (Norm)	Formula					
1290.3033	1290.2692	34.1	26.4	18.5	115.5	0.0	C49	H80	N	O18	Si8	S3

Figure B. 12.HRMS spectrum of E(TPD-POSS)E.

Single Mass Analysis
Tolerance = 5000.0 PPM / DBE: min = -5.5, max = 1000.0
Element prediction: Off
Number of isotope peaks used for i-FIT = 3

Monoisotopic Mass, Even Electron Ions
1 formula(e) evaluated with 1 results within limits (all results (up to 1000) for each mass)
Elements Used:
C: 91-91 H: 162-165 N: 1-1 O: 18-18 Si: 8-8 S: 3-3
Ahmet Onal
288854_20200117_01-03 4 (0.172) Cm (1:24)

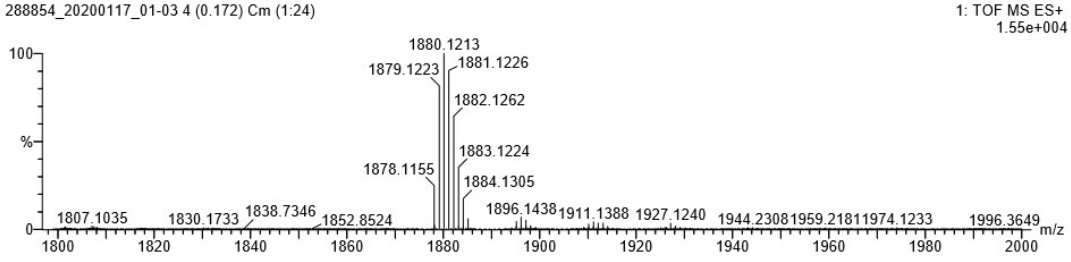

Minimum:				-5.5								
Maximum:		1000.0	5000.0	1000.0								
Mass	Calc. Mass	mDa	PPM	DBE	i-FIT	i-FIT (Norm)	Formula					
1879.1223	1878.9265	195.8	104.2	18.5	108.8	0.0	C91	H164	N	O18	Si8	S3

Figure B.13. HRMS spectrum of P(TPD-POSS)P.

Single Mass Analysis
Tolerance = 5000.0 PPM / DBE: min = -5.5, max = 1000.0
Element prediction: Off
Number of isotope peaks used for i-FIT = 3

Monoisotopic Mass, Even Electron Ions
1 formula(e) evaluated with 1 results within limits (all results (up to 1000) for each mass)
Elements Used:
C: 26-26 H: 15-16 N: 3-3 O: 2-2 S: 3-3
Ahmet Onal
288853_20200116_02-04 19 (0.741) Cm (1:24)

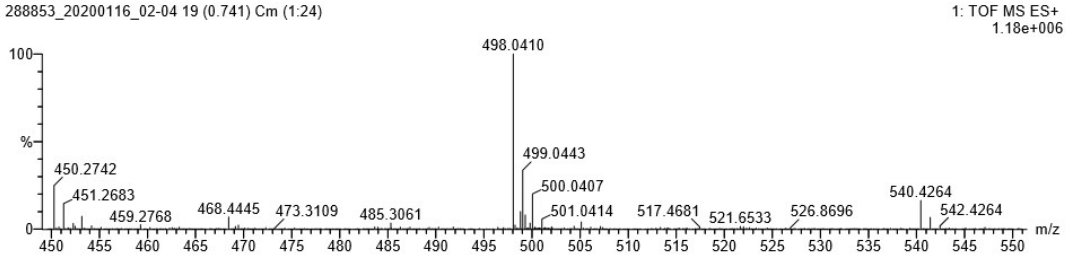

Minimum:				-5.5			
Maximum:		1000.0	5000.0	1000.0			
Mass	Calc. Mass	mDa	PPM	DBE	i-FIT	i-FIT (Norm)	Formula
498.0410	498.0405	0.5	1.0	20.5	493.2	0.0	C26 H16 N3 O2 S3

Figure B.14. HRMS spectrum of T(TPD-Azo)T.

Single Mass Analysis
Tolerance = 5000.0 PPM / DBE: min = -5.5, max = 1000.0
Element prediction: Off
Number of isotope peaks used for i-FIT = 3

Monoisotopic Mass, Even Electron Ions
1 formula(e) evaluated with 1 results within limits (all results (up to 1000) for each mass)
Elements Used:
C: 30-30 H: 19-20 N: 3-3 O: 6-6 S: 3-3
Ahmet Onal
288853_20200116_01-03 5 (0.206) Cm (1:21)

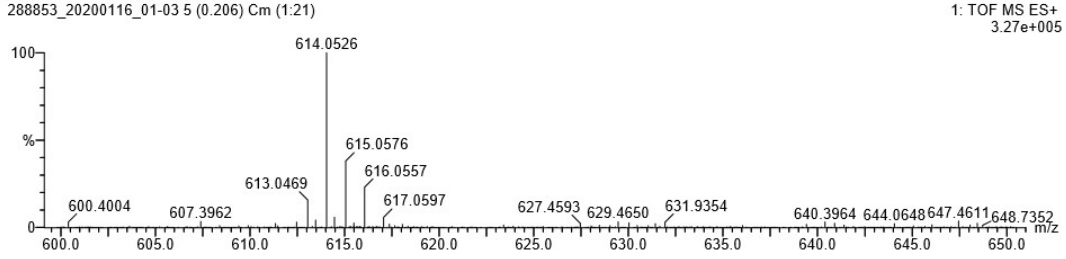

Minimum:				-5.5			
Maximum:		1000.0	5000.0	1000.0			
Mass	Calc. Mass	mDa	PPM	DBE	i-FIT	i-FIT (Norm)	Formula
614.0526	614.0514	1.2	2.0	22.5	404.2	0.0	C30 H20 N3 O6 S3

Figure B.15. HRMS spectrum of E(TPD-Azo)E.

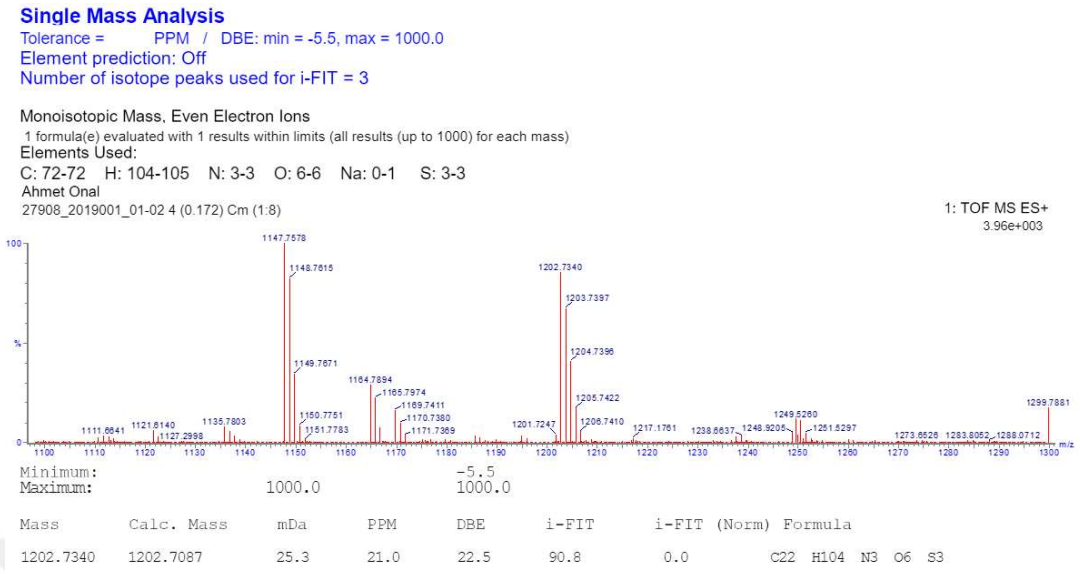

Figure B.16. HRMS spectrum of P(TPD-Azo)P.

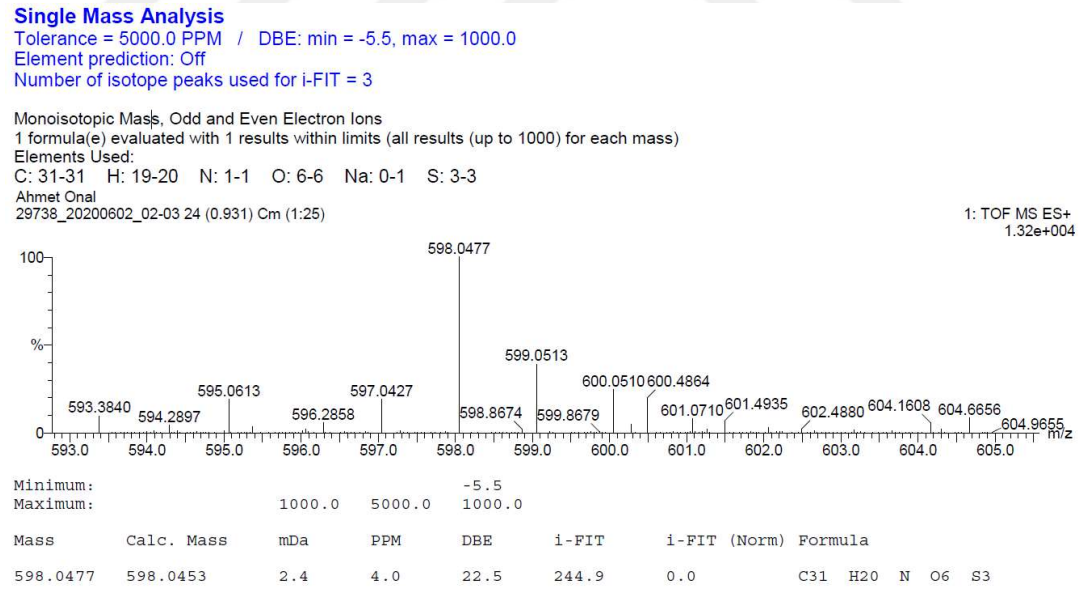

Figure B.17. HRMS spectrum of E(TPD-Fluo)E.

Single Mass Analysis
Tolerance = 5000.0 PPM / DBE: min = -5.5, max = 1000.0
Element prediction: Off
Number of isotope peaks used for i-FIT = 3

Monoisotopic Mass, Even Electron Ions
1 formula(e) evaluated with 1 results within limits (all results (up to 1000) for each mass)
Elements Used:
C: 73-73 H: 102-104 N: 1-1 O: 6-6 S: 3-3
Ahmet Onal
288853_20200117_03-04 6 (0.260) Cm (1:9)

1: TOF MS ES+
5.60e+002

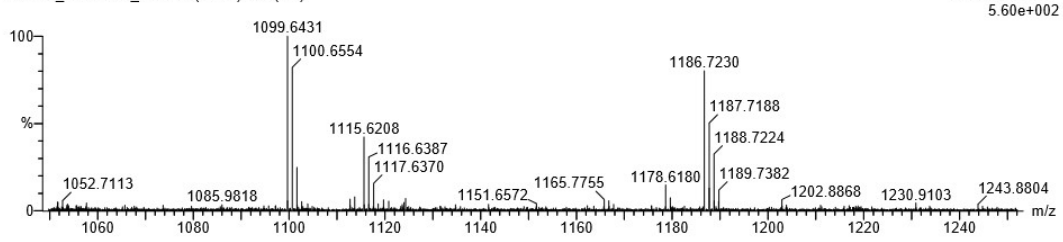

Minimum:				-5.5			
Maximum:		1000.0	5000.0	1000.0			
Mass	Calc. Mass	mDa	PPM	DBE	i-FIT	i-FIT (Norm)	Formula
1186.7230	1186.7026	20.4	17.2	22.5	82.4	0.0	C73 H104 N O6 S3

Figure B.18. HRMS spectrum of P(TPD-Fluo)P.

Single Mass Analysis
Tolerance = 1000.0 PPM / DBE: min = -5.5, max = 1000.0
Element prediction: Off
Number of isotope peaks used for i-FIT = 3

Monoisotopic Mass, Odd and Even Electron Ions
1 formula(e) evaluated with 1 results within limits (all results (up to 1000) for each mass)
Elements Used:
C: 28-28 H: 29-30 N: 1-1 O: 6-6 S: 2-2
Ahmet Onal
31999_20210309_04-01 13 (0.518) Cm (12:24)

1: TOF MS ES+
1.30e+005

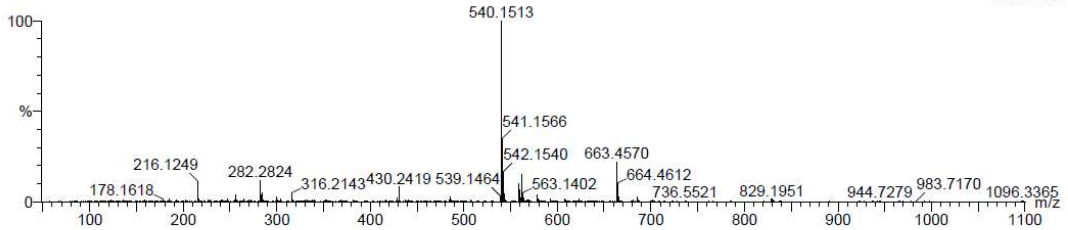

Minimum:				-5.5			
Maximum:		1000.0	1000.0	1000.0			
Mass	Calc. Mass	mDa	PPM	DBE	i-FIT	i-FIT (Norm)	Formula
540.1513	540.1515	-0.2	-0.4	14.5	306.3	0.0	C28 H30 N O6 S2

Figure B.19. HRMS spectrum of E(PI-EtHex)E.

Single Mass Analysis
Tolerance = 1000.0 PPM / DBE: min = -5.5, max = 1000.0
Element prediction: Off
Number of isotope peaks used for i-FIT = 3

Monoisotopic Mass, Even Electron Ions
1 formula(e) evaluated with 1 results within limits (all results (up to 1000) for each mass)
Elements Used:
C: 20-20 H: 14-15 N: 2-2 O: 6-6 S: 2-2
Ahmet Onal
31145_20210106_01-03 22 (0.863) Cm (15:24)

1: TOF MS ES+
1.25e+006

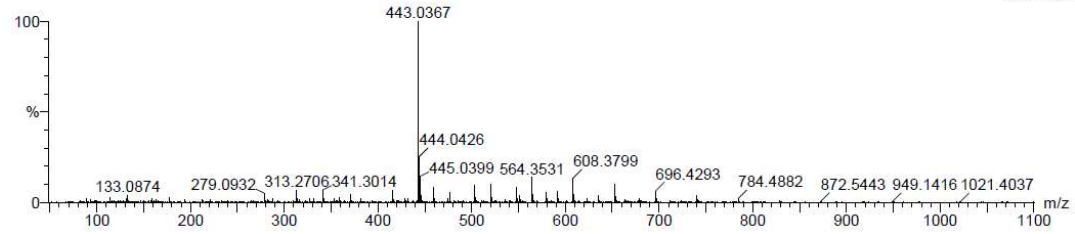

Minimum:				-5.5			
Maximum:		1000.0	1000.0	1000.0			
Mass	Calc. Mass	mDa	PPM	DBE	i-FIT	i-FIT (Norm)	Formula
443.0367	443.0372	-0.5	-1.1	14.5	629.2	0.0	C20 H15 N2 O6 S2

Figure B.20. HRMS spectrum of E(PH)E.

C. GPC Data of Polymers

Gel Permeation Chromatography analysis was performed on Malvern Omnisec GPC system.

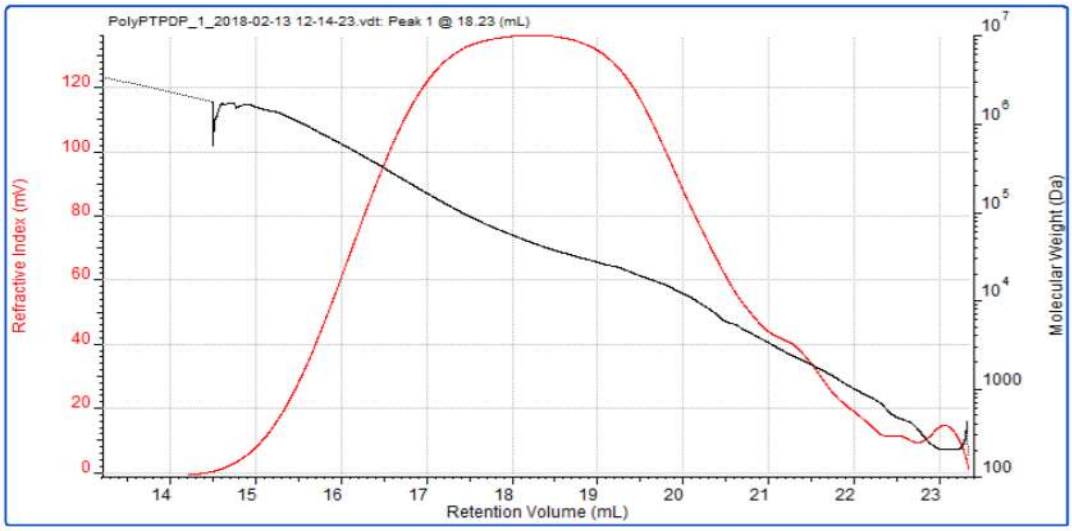

Figure C.1. GPC chromatogram of PP(TPD-EtHex)P-C in THF.

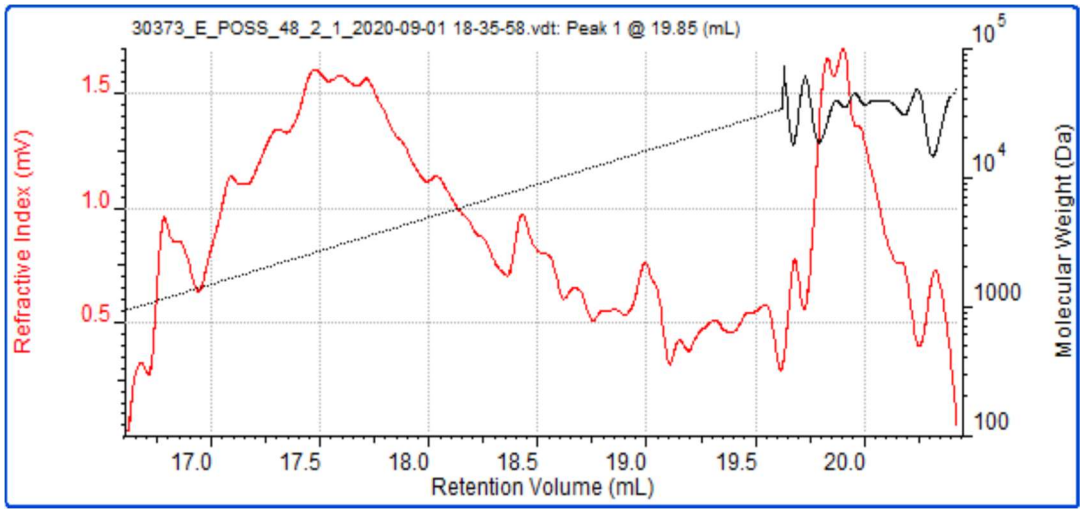

Figure C.2. GPC chromatogram of PE(TPD-POSS)E-C in THF.

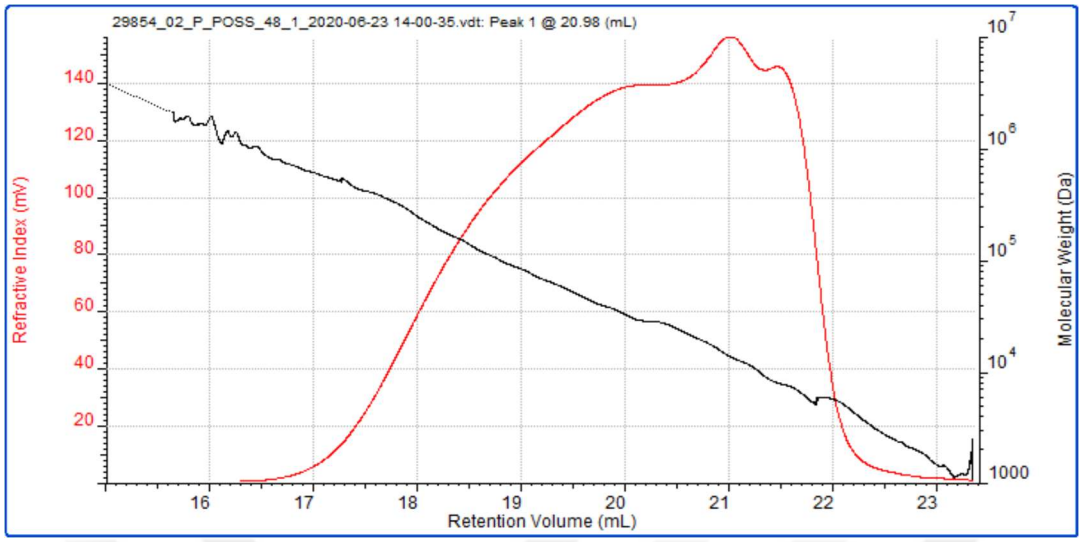

Figure C.3. GPC chromatogram of PP(TPD-POSS)P-C in THF.

D. TGA Data of Polymers

TGA measurements were performed using Perkin Elmer Pyris 1 TGA instrument.

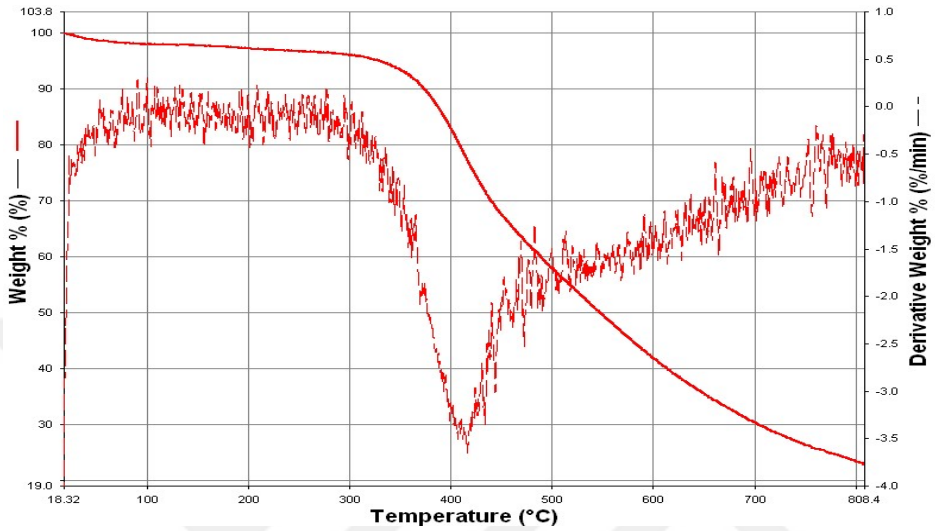

Figure D.1. TGA analysis of chemically obtained PE(TPD-EtHex)E-C.

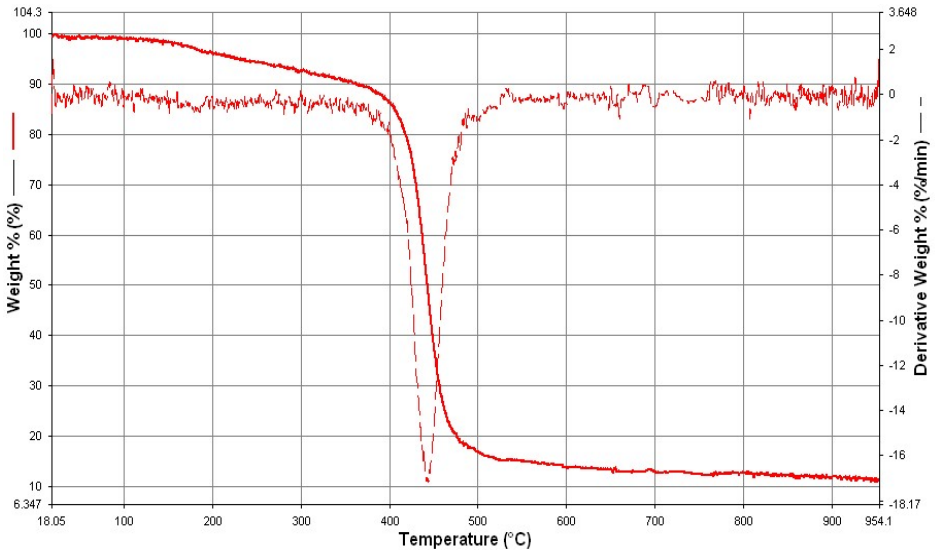

Figure D.2. TGA analysis of chemically obtained PP(TPD-EtHex)P-C.

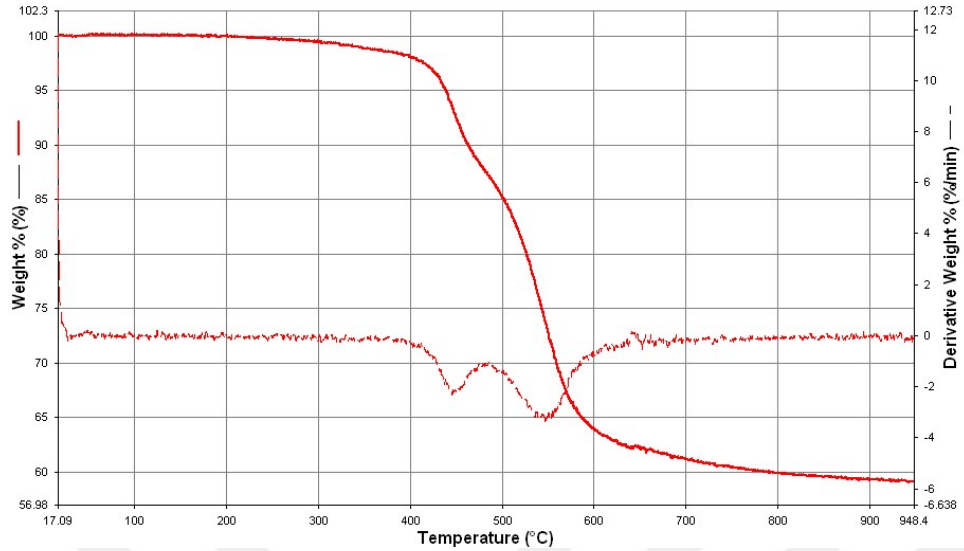

Figure D.3. TGA analysis of chemically obtained PE(TPD-POSS)E-C.

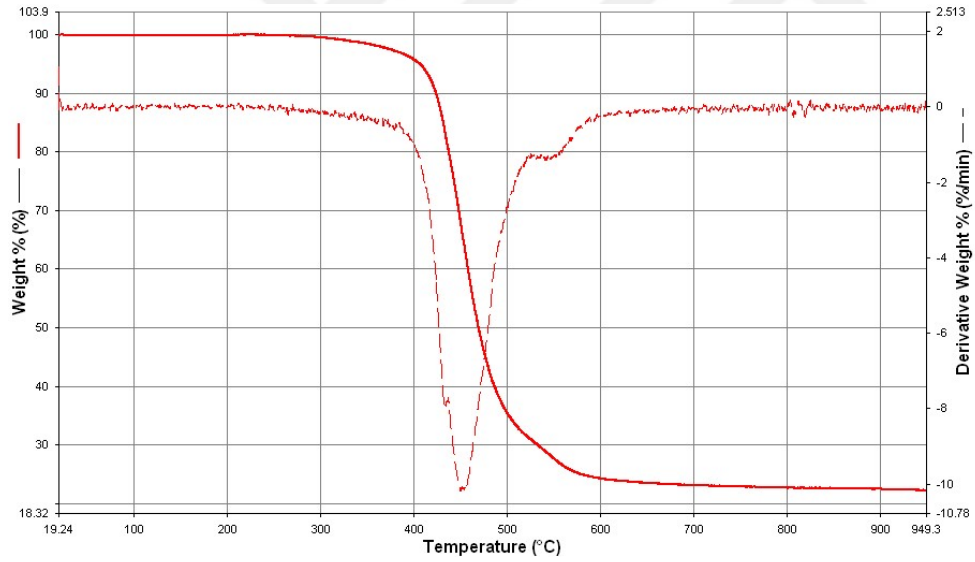

Figure D.4. TGA analysis of chemically obtained PP(TPD-POSS)P-C.

E. FTIR Spectra of Monomer and Polymer

FTIR spectra were recorded on an Thermo Scientific Nicolet iS10 FTIR spectrometer with an attenuated total reflectance.

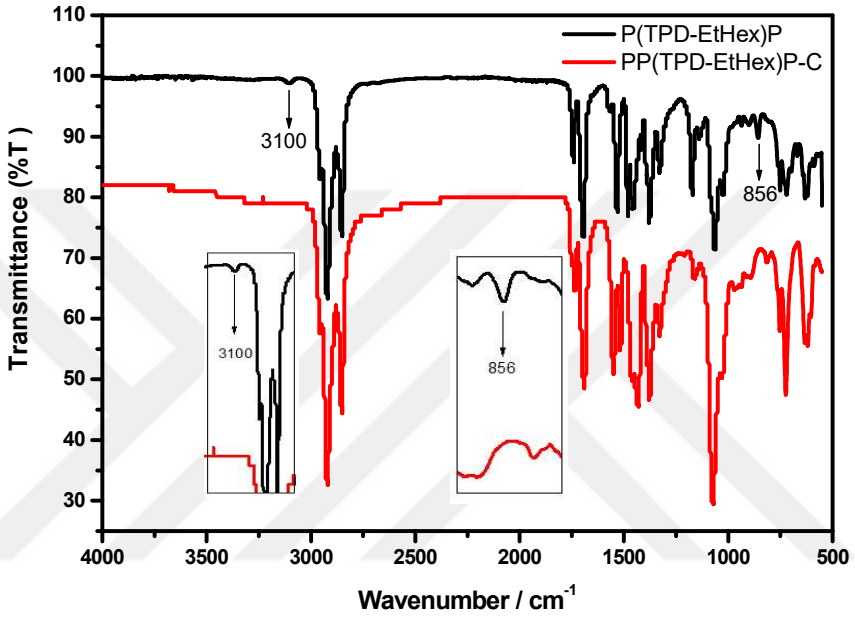

Figure E.1. FTIR spectra of P(TPD-EtHex)P monomer and chemically obtained PP(TPD-EtHex)P-C polymer.

CURRICULUM VITAE

PERSONAL INFORMATION

Surname, Name : Çakal, Deniz

EDUCATION

Degree	Institution	Year of Graduation
PhD	METU Chemistry	2021
MS	METU Chemistry	2014
BS	METU Chemistry	2011
High School	Bayburt Anadolu High School, Bayburt	2006

WORK EXPERIENCE

Year	Place	Enrollment
2014-2021	METU Chemistry	Teaching Assistant
2010 July	TAI – Turkish Aerospace Industries	Intern

FOREIGN LANGUAGES

Advanced English, Intermediate German

PUBLICATIONS

1. Çakal D., Cihaner A. and Önal A. M. "Electrochemical and optical properties of dicyclohexylmethyl substituted poly (3, 4-propylenedioxythiophene) analogue", Journal of Applied Polymer Science, 135(18), 46214 (2018)

2. Çakal D., Ertan S., Cihaner A. and Önal A. M. "Synthesis and electrochemical polymerization of DAD type monomers with thieno [3, 4-*c*] pyrrole-4, 6-dione acceptor unit", Dyes and Pigments, 158, 175-182 (2018)

3. Çakal D., Ertan S., Cihaner A. and Önal A. M. "Electrochemical and optical properties of substituted phthalimide based monomers and electrochemical polymerization of 3, 4-ethylenedioxythiophene-polyhedral oligomeric silsesquioxane (POSS) analogue", Dyes and Pigments, 161, 411-418 (2019)

4. Çakal D., Boztaş Y., Cihaner A. and Önal A. M. "Investigation of Fluorine Atom Effect on Benzothiadiazole Acceptor Unit in Donor Acceptor Donor Systems", Journal of The Electrochemical Society, 166(12), G141 (2019)

5. Çakal D., Cihaner A. and Önal A. M. "Synthesis and electropolymerization of thieno [3, 4-c] pyrrole-4, 6-dione based donor-acceptor-donor type monomers", Journal of Electroanalytical Chemistry, 862, 114000 (2020)

6. Çakal D., Boztaş Y., Cihaner A. and Önal A. M. "Effect of fluorine substituted benzothiadiazole on electro-optical properties of donor-acceptor-donor type monomers and their polymers", Dyes and Pigments, 182, 108622 (2020)

7. Çakal D., Akdag A., Cihaner A. and Önal A. M. "Effect of the donor units on the properties of fluorinated acceptor based systems", Dyes and Pigments, 185, 108955 (2021)

8. Çakal D., Cihaner A. and Önal A. M. "Polyhedral Oligomeric Silsesquioxanes Appended Conjugated Soluble Polymers Based on Thieno[3,4-c]pyrrole-4,6-dione Acceptor Unit", Electrochimica Acta, 377, 138064 (2021)

9. Çakal D., Cihaner A. and Önal A. M. "Synthesis and Electropolymerization of Donor-Acceptor-Donor Type Monomers based on Azobenzene-substituted thieno[3,4-c]pyrrole-4,6-dione Acceptors", Electrochimica Acta, 398, 139325 (2021)

PATENT

1. Önal A. M., Cihaner A., Balcı B., Kesimal B. and Çakal D. "Electroactive Chemiluminescence Compounds for Blood Detection in Forensic Science", Patent application in examination process.

PROJECTS

Year	Institution	Project
2019-2020	Atılım University	Tübitak Project (118Z067)- Researcher

2013-2014	METU	Tübitak Project (111T162)- Researcher

CONFERENCE PRESENTATIONS

1. Çakal D. and Gökağaç G. " Electrochemical Oxidation of Methanol by Carbon-Supported Platinum Nanoparticles Prepared by Different Reducing Agents and Surfactants", Turkish-German Conference on Energy Technologies, Ankara, Turkey, Poster presentation (13.10.2014-15.10.2014)

2. Çakal D., Cihaner A. and Önal A.M. "Synthesis and Electropolymerization of D-A-D Monomers with New Acceptor Units Based on Phthalic Anhydride", International Congress on Semiconductor Materials and Devices, Konya, Turkey, Poster presentation (17.08.2017-19.08.2017)

3. Çakal D., Cihaner A. and Önal A.M. "Fitalik anhidrit Alıcı Grubu İçeren, Alıcı-Verici Düzeninde Yeni Monomer(ler)in Sentezi ve Elektropolimerizasyonu", 29th National Chemistry Congress, Ankara, Turkey, Oral presentation (10.09.2017-14.09.2017)

4. Çakal D., Cihaner A. and Önal A.M. "Synthesis and electrochemical polymerization of D-A-D monomers based on Thieno[3,4-c]pyrrole-4,6-dione Acceptor Unit", 69th Annual Meeting of the International Society of Electrochemistry, Bologna, Italy, Oral Presentation (02.09.2018-07.09.2018)

5. Çakal D., Cihaner A. and Önal A.M. "Synthesis and electrochemical polymerization of D-A-D monomers based on Thieno[3,4-c]pyrrole-4,6-dione Acceptor Unit", 7th Polymer Science and Technology Conference, Eskisehir, Turkey, Poster presentation (09.09.2018-12.09.2018)

6. Çakal D., Boztaş A. and Önal A.M. "Synthesis and Electrochemical Polymerization of New D-A-D Monomers Based on Fluorinated Benzothiadiazole Acceptor Unit", 12th Electrochemistry Congress of Turkey, İstanbul, Turkey, Oral presentation-Presented by Ahmet M. Önal (30.09.2019-02.10.2019)

RESEARCH INTERESTS

Material Science
Material Characterization
Conjugated Polymers & Electroactive Materials
Electrochromic Materials
Chemiluminescent Compounds

HOBBIES

Swimming
Reading Novels
Travelling & Seeing Natural Places
Movies